

**FLUORINATED 2-NITROIMIDAZOLES:
NON-INVASIVE PROBES FOR DETECTING
THERAPEUTICALLY RELEVANT TUMOUR HYPOXIA BY
MAGNETIC RESONANCE SPECTROSCOPY**

b y

**Eric Ofori Aboagye
B.Pharm. (Hons.), M.Sc., MPSGh**

**A Thesis Submitted for the Degree of
Doctor of Philosophy
t o**

The University of Glasgow

From Research Conducted in

**The CRC Department of Medical Oncology
CRC Beatson Laboratories
University of Glasgow**

a n d

**The CRC Biomedical Magnetic Resonance Group
Department of Biochemistry
St. George's Hospital Medical School
University of London
September 1995**

© E.O. Aboagye, 1995.

ProQuest Number: 13834047

All rights reserved

INFORMATION TO ALL USERS

The quality of this reproduction is dependent upon the quality of the copy submitted.

In the unlikely event that the author did not send a complete manuscript and there are missing pages, these will be noted. Also, if material had to be removed, a note will indicate the deletion.



ProQuest 13834047

Published by ProQuest LLC (2019). Copyright of the Dissertation is held by the Author.

All rights reserved.

This work is protected against unauthorized copying under Title 17, United States Code
Microform Edition © ProQuest LLC.

ProQuest LLC.
789 East Eisenhower Parkway
P.O. Box 1346
Ann Arbor, MI 48106 – 1346

Ther
10223
Copy 1

ABSTRACT

Tumour hypoxia is a well described phenomenon which is primarily created by an inadequate and non-uniform vascular network. Importantly, hypoxia within certain solid tumours has been linked to the failure of conventional therapy, including radiotherapy and chemotherapy. For this reason, many attempts have been made to identify, characterise, and quantify hypoxic cells within these tumours as a prelude to the design of rational therapies aimed to kill all the cancer cells present within tumours. The use of 2-nitroimidazoles containing appropriate labels as markers for the detection of hypoxic cells, is based on the ability of these compounds to undergo selective nitroreduction and adduct formation within hypoxic cells.

The fluorinated 2-nitroimidazole, SR-4554, was rationally designed as a non-invasive hypoxia probe with low toxicity and high sensitivity for detection by magnetic resonance spectroscopy (MRS) and imaging (MRI). SR-4554 was demonstrated to be enzymatically reduced by mouse liver microsomes, SCCVII tumour homogenates and purified rat and human NADPH: cytochrome P450 reductase under hypoxia. In this regard, NADPH: cytochrome P450 reductase was found to be the major enzyme involved in this bioreduction of SR-4554. In a panel of murine and human tumour xenografts, only a 3 fold variation in NADPH: cytochrome P450 reductase activities was observed. These differences in NADPH: cytochrome P450 activities are unlikely to significantly influence SR-4554 adduct formation *in vivo*. Importantly, the reduction of SR-4554 by mouse liver microsomes showed a characteristic oxygen dependence with a half-maximal inhibition of 0.48%. Using a high resolution ^{19}F nuclear magnetic resonance (NMR) technique, soluble hypoxia-dependent metabolites of various fluorinated 2-nitroimidazoles, including SR-4554, were identified. The chemical shifts of these metabolites were found to be less than those required to give resolved peaks in *in vivo* MRS studies. Determination of the possible regions of SR-4554 adduct formation within A2780 human ovarian multicellular spheroids was achieved by electron energy loss spectroscopic imaging. Using this technique, an 8 fold differential between the fluorinated probe levels retained in the inner hypoxic regions of the spheroid vs the outer more aerobic regions was observed. SR-4554 was localised mainly to the nuclear periphery, nucleus and cytoplasm within cells from the hypoxic region of the spheroids.

The toxicity and pharmacokinetics of SR-4554 was studied in mice as a prelude to non-invasive ^{19}F MRS/MRI studies. SR-4554 was found to be non-toxic in mice up to a dose of 1300 mg/kg. Pharmacokinetics of SR-4554 fitted either a one compartment or two

compartment open model depending on the route of administration. The probe was characterised by a relatively short half-life, linear kinetics, high urinary excretion, high oral bioavailability and low plasma protein binding. Importantly, the brain to plasma ratio of SR-4554 was lower than previously reported trends in the literature, thus confirming its potentially low toxicity.

As a consequence of the low toxicity and favourable pharmacokinetic properties of SR-4554, a non-invasive multi-tuned ^{19}F MRS technique was implemented to detect this compound in tissues. Using this MRS technique, SR-4554 was found to be selectively retained in both murine and human tumour xenografts. Importantly the ^{19}F retention index was found to correlate with the reported radiobiological hypoxic fraction of the tumours used. This ^{19}F retention index was also found to be higher in larger tumours but, interestingly, did not correlate with the bioenergetic status of the tumours, as determined by ^{31}P MRS. Manipulation of tumour microenvironment to affect the degree of hypoxia within these tumours was studied *in vivo*. In mouse tumours for instance, the ^{19}F retention index increased 2 fold compared to control values, following hydralazine pre-treatment, and decreased by 6 fold compared to control values, following carbogen breathing. Important to the clinical development of SR-4554, ^{19}F MRI techniques showed localisation of SR-4554 in the bladder, tumour and liver of mice. This technique was, however, limited by low sensitivity due to the extremely short transverse relaxation time of the probe in tissues.

Finally this thesis has demonstrated that SR-4554 has suitable metabolic, pharmacological and MRS properties for its use in the quantification of critical levels of hypoxia within human tumours. As a consequence, this compound has been approved by CRC phase I/II committee for clinical development.

DEDICATION

To Mum, Dad and Nancy

DECLARATION

The work described in this thesis was performed personally unless otherwise acknowledged.

Eric. O. Aboagye,
September, 1995.

ACKNOWLEDGEMENT

I would like to take this opportunity to thank all those who have in one way or the other been associated with this project. In particular, I would like to thank my current supervisor, Dr. Alex Lewis (Glasgow University, Glasgow), for the enormous assistance he has given to me to enable me complete this thesis. I would also like to extend this appreciation to my co-supervisor, Prof. John Griffiths (St. George's Hospital, London), who has also been of great help from the start of my thesis.

This project would not have come this far without the great help and encouragement from my previous supervisors, who inspite of their busy schedules, have continued to assist me in this project. In this regard, I will like to thank Prof. Paul Workman (Zeneca Pharmaceuticals, Macclesfield), Prof. Ross Maxwell (Skejby Hospital, Aarhus), and Dr. Martin Graham (Sanofi Research, Alnwick) for their assistance.

This is also an opportunity to express my appreciation to members of the two groups with whom I performed this project, at Glasgow (Clinical and Molecular Pharmacology) and London (Biomedical MRS). Its been great working with you. Two of my collaborators at SRI International (California), including Dr. Mike Tracy and Dr. Andy Kelson also deserve thanks for the provision of SR-4554 which has proved to be a 'winner'.

I would like to acknowledge collaborative work reported in this thesis. The electron energy loss spectroscopic experiments described in chapter 4, was carried out with Dr. Max Huxhum at the E.M. centre, Division of Molecular and Cellular Biology, University of Glasgow. The comparative oxygen needle electrode vs ^{19}F MRS studies reported in chapter 6, was carried out with Dr. Ross Maxwell and Dr. Mike Horsman at the Skejby University Hospital and the Department of Experimental Clinical Oncology, University of Aarhus, Denmark.

My final thanks go to my parents and Nancy for their moral support and to the Cancer Research Campaign and Overseas Research Studentship, for funding my research. To all I say "AYEKOOOOOO".

CONTENTS

	PAGE
Abstract	i
Dedication	iii
Declaration	iv
Acknowledgements	v
Contents	vi
List of Tables	xi
List of Figures	xiii
Abbreviations	xvi
Chapter 1 INTRODUCTION	1
1.1 The nature of cancer	1
1.2 Physiological properties of tumours	2
1.2.1 Tumour hypoxia	2
1.2.2 Cell cycle regulation of hypoxic cells	3
1.2.3 Molecular response of cancer cells to hypoxia	3
1.3 Therapeutic importance of tumour hypoxia	4
1.3.1 Radio- and chemoresistance of hypoxic cells	4
1.3.2 Treatment of hypoxic cells	5
1.3.3 Reoxygenation of hypoxic cells	6
1.4 Measurement of tumour hypoxia	6
1.5 Physicochemical and biological properties of 2-nitroimidazoles	8
1.5.1 Structure of 2-nitroimidazoles	8
1.5.2 Metabolism of 2-nitroimidazoles	8
1.6 Theory of MRS and MRI	11
1.6.1 Magnetic properties of atomic nuclei	11
1.6.2 Relaxation	12
1.6.3 Spin echoes, pulse sequences and MR-imaging	13
1.7 Aims of thesis	14
1.8 Layout of thesis	14
Chapter 2 Development of a high performance liquid chromatographic assay for SR-4554 in plasma and tissues	16

2.1	Introduction	16
2.2	Materials and methods	17
2.2.1	Chemicals and reagents	17
2.2.2	Preparation of calibration and validation standards	17
2.2.3	Extraction efficiency	18
2.2.4	Preparation of quality control (QC) samples	18
2.2.5	Within and between day variability, freeze/thaw stability and long term stability studies	18
2.2.6	Extraction of plasma and tissue samples and standards	19
2.2.7	HPLC methodology	19
2.2.8	Mass spectral (MS) analysis	21
2.2.9	Statistical analysis	21
2.3	Results	21
2.3.1	Chromatography	21
2.3.2	Mass spectral (MS) analysis	22
2.3.3	Validation	22
2.4	Discussion	23
Chapter 3	Metabolism of 2-nitroimidazoles	26
3.1	Introduction	26
3.2	Materials and methods	27
3.2.1	Chemicals and reagents	27
3.2.2	Experimental animals and tumours	28
3.2.3	Preparation of mouse liver microsomes, S9 fraction and tumour samples	28
3.2.4	Protein and enzyme assay	29
3.2.5	Characteristics of the reductive metabolism of SR-4554	29
3.2.6	Identification of reductive metabolites of 2-nitroimidazoles by high resolution ^{19}F NMR	30
3.2.7	<i>In vivo</i> reductive metabolism of SR-4554	31
3.2.8	Statistical analysis	32
3.3	Results	32
3.3.1	Enzyme activity	32
3.3.2	Characteristics of reductive metabolism	32
3.3.3	Identification of reductive metabolites	34
3.3.4	<i>In vivo</i> reductive metabolism of SR-4554	35

3.4	Discussion	35
Chapter 4	Localisation of SR-4554 in multicellular spheroids as measured by electron energy loss spectroscopic imaging	40
4.1	Introduction	40
4.4.1	Subcellular localisation of 2-nitroimidazoles	40
4.1.2	Electron energy loss spectroscopy (EELS) and electron spectroscopic imaging (ESI)	41
4.2	Materials and methods	42
4.2.1	Chemicals and reagents	42
4.2.2	Reductive metabolism of SR-4554 by A2780 cells	42
4.2.3	Preparation of A2780 multicellular spheroids	43
4.2.4	Incubation of A2780 spheroids with SR-4554	43
4.2.5	Electron energy loss spectroscopic analysis	43
4.2.6	Statistical analysis	44
4.3	Results	45
4.3.1	Metabolism of SR-4554 by A2780 cells	45
4.3.2	Growth characteristics of A2780 spheroids	45
4.3.3	Sub-cellular localisation of SR-4554 in A2780 spheroids	45
4.3.4	Semi-quantitative localisation of SR-4554 in A2780 spheroids	46
4.4	Discussion	47
Chapter 5	Toxicity and pharmacokinetics of SR-4554 in mice	51
5.1	Introduction	51
5.2	Materials and methods	53
5.2.1	Chemicals and reagents	53
5.2.2	Experimental animals and tumour implantation	53
5.2.3	Partition coefficient of SR-4554	54
5.2.4	Toxicity studies	55
5.2.5	Plasma and tissue pharmacokinetic studies	55
5.2.6	Bioavailability studies	56
5.2.7	Elimination of SR-4554	56
5.2.8	Pharmacokinetic analysis	59
5.2.9	Plasma protein binding studies	58

5.3	Results	59
5.3.1	Partition coefficient studies	59
5.3.2	Toxicity studies	59
5.3.3	Pharmacokinetic studies	60
5.3.4	Bioavailability studies	61
5.3.5	Elimination of SR-4554	61
5.3.6	Plasma protein binding studies	61
5.4	Discussion	61
Chapter 6	<i>In vivo</i> magnetic resonance spectroscopy and imaging of SR-4554	67
6.1	Introduction	67
6.2	Materials and methods	70
6.2.1	Chemicals and reagents	70
6.2.2	Experimental animals and tumour models	70
6.2.3	Development of an MRS method for the absolute quantitation of ^{19}F levels	70
6.2.4	Drug administration	72
6.2.5	<i>In vivo</i> MRS protocol	72
6.2.6	Retention of ^{19}F in tumours	73
6.2.7	Correlation between ^{19}F retention index and the oxygenation status of mouse tumours	74
6.2.8	Effect of agents that modulate tumour blood flow and/or oxygenation on the ^{19}F retention index	74
6.2.9	<i>In vivo</i> MRI protocol	75
6.3	Results	76
6.3.1	MRS studies	76
6.3.2	Retention of ^{19}F signals in mouse tumours	76
6.3.3	Correlation between ^{19}F retention index and the oxygenation status of mouse tumours	78
6.3.4	Effect of agents that modulate tumour blood flow and/or oxygenation on the ^{19}F retention index	78
6.3.5	MRI studies	79
6.4	Discussion	80
Chapter 7	Summary and conclusions	88
	References	94

Appendices	117
A Synthesis of SR-4554	118
B Molecular models of SR-4554, etanidazole and misonidazole	119
C A list of publications arising from this thesis	120

LIST OF TABLES

- 1.1 A summary of methods used to measure tumour hypoxia.
- 2.1 Recovery of SR-4554 from tissue homogenates using different clean-up techniques.
- 2.2 Within and between day variability of the HPLC assay for SR-4554 at six different drug concentration.
- 2.3 Freeze-thaw and long-term stability of SR-4554 in mouse plasma.
- 3.1 Sources and characteristics of cell lines.
- 3.2 NADPH: cytochrome P450 reductase activities in a panel of murine and human tumour xenografts.
- 3.3 Characteristics of the metabolism of SR-4554 by mouse liver microsomes.
- 3.4 Reduction of SR-4554 by purified rat and human NADPH cytochrome P450 reductase.
- 4.1 Rate of loss of SR-4554 incubated with A2780 cells.
- 4.2 The relative average fluorine and fluorine/nitrogen elemental ratios for six intracellular domains of both outer and inner cells from A2780 multicellular spheroids following a 'chase' culture.
- 5.1 Pharmacokinetic parameters for SR-4554 following i.p. administration of 162 mg/kg to mice bearing the EMT6 tumour.
- 5.2 Pharmacokinetic parameters for SR-4554 following i.p. administration of 180 and 337 mg/kg to mice bearing the EMT6 tumour.
- 5.3 Pharmacokinetic parameters for SR-4554 following i.v., i.p., and p.o. administration at a dose of 90 mg/kg in non-tumour bearing female Balb/c mice.
- 5.4 Urinary excretion of SR-4554 in non-tumour bearing female Balb/c mice.
- 5.5 *In vitro* plasma protein binding studies with SR-4554 and compared to misonidazole.
- 5.6 Pharmacokinetic parameters for selected 2-nitroimidazoles in Balb/c mice.
- 6.1 T₁ values of fluorinated and deuterated compounds measured in both phantom (*in vitro*) experiments, as well as, following the injection of SR-4554 (*in vivo* experiments).

- 6.2 Retention of ^{19}F signals from SR-4554 in RIF-1 tumours.
- 6.3 Hypoxic fraction of solid tumours as measured by radiobiological assays.
- 6.4 The effect of SR-4554 and anaesthesia on the oxygenation of C3H mammary foot tumours implanted in female CDF₁ mice.
- 6.5 Detection of changes in tumour microenvironment using ^{19}F MRS. Studies with hydralazine, carbogen and carbon monoxide.

LIST OF FIGURES

- 1.1 A schematic representation of the two types of hypoxia present within solid tumours.
- 1.2 Molecular structure of some bioreductive agents.
- 1.3 General structure of 2-nitroimidazoles and constitution of the R-side chain.
- 1.4 Nitroreductive bioactivation of 2-nitroimidazoles.
- 1.5 Formation of glyoxal from the reactive hydroxylamine derivative of 2-nitroimidazoles.
- 1.6 The classical precession of a magnetic nucleus with a nuclear magnetic moment (μ) in a magnetic field (B_0).
- 1.7 The effect of a radiofrequency (RF) 90° pulse.
- 1.8 Three important pulse sequences used in medicine.
- 2.1 A typical chromatogram obtained from a plasma extract.
- 2.2 UV-spectra of SR-4554 and internal standard (Ro 07-0269) in HPLC mobile phase using photodiode array detection.
- 2.3 Typical chromatograms of SR-4554 (4 $\mu\text{g}/\text{ml}$) and internal standard (I.S.; Ro 07-0269) obtained from 0.1 M Tris-HCl buffer (pH 7.4) and 10% tumours homogenates.
- 2.4 Chromatograms of SR-4554 (4 $\mu\text{g}/\text{ml}$) and internal standard (I.S.; Ro 07-0269) obtained by silver nitrate extraction of 10% liver (a), and brain (b) homogenates spiked with SR-4554.
- 2.5 Positive ion chemical ionisation spectrum of SR-4554.
- 2.6 Recovery of SR-4554 from mouse plasma.
- 3.1 Typical HPLC chromatograms of extracts obtained from the hypoxic incubation of SR-4554 at zero time (a), and 15 min (b).
- 3.2 The effect of microsomal protein concentration on the rate of reduction of SR-4554 under hypoxia.
- 3.3 The kinetics of reductive metabolism of SR-4554 by mouse liver microsomes, showing the classical V vs [S] plot (a), and the corresponding Hanes Woolf plot (b).
- 3.4 The reduction rate of SR-4554 by mouse liver microsomes at various oxygen concentrations.
- 3.5 Reductive metabolism of SR-4554 by mouse liver microsomes.
- 3.6 Hypoxia-dependent metabolism of SR-4554.
- 3.7 Reductive metabolism of CCI-103F by mouse liver microsomes.
- 3.8 Reductive metabolism of Ro 07-2044 by mouse liver

microsomes.

- 3.9 Reductive metabolism of KU-2285 by mouse liver microsomes.
- 3.10 Reductive metabolism of fluoromisonidazole (Ro 07-0741) by mouse liver microsomes.
- 3.11 SR-4554 (vertical arrow) and its metabolites in EMT6 tumours excised from drug treated mice at (a) 15 min, (b) 2 hr, (c) 4 hr, and (d) 6 hr post-injection.
- 3.12 SR-4554 (vertical arrow) and its metabolites in liver (a) and (b), and brain (c) and (d), of Balb/c mice.
- 3.13 SR-4554 (vertical arrow) and its metabolites in non-tumour bearing mouse urine collected over 24 hr.
- 4.1 Elastically (a) and inelastically (b) scattered electrons produced by the interaction of the incident electron beam with specimen nuclei and electrons respectively.
- 4.2 Typical energy loss spectrum showing a continuously decreasing background and an elemental edge.
- 4.3 Typical HPLC plot of SR-4554 after incubation with A2780 cells for 30 min under (a) Aerobic and (b) Hypoxic conditions.
- 4.4 Energy filtered image of a portion of a heavy metal free A2780 cell within SR-4554 treated multicellular spheroids after a 'chase' culture, recorded at $\Delta E = 150$ eV, showing enhanced contrast in phosphorus-rich regions.
- 4.5 Reference image of a section from an inner A2780 cell within SR-4554 treated multicellular spheroids after a 'chase' culture, recorded $\Delta E = 150$ eV.
- 4.6 Histograms showing the mean \pm standard deviation of fluorine/nitrogen (F/N) elemental ratios for cytoplasmic domains.
- 5.1 HPLC retardation of a series of 2-nitroimidazoles (10 $\mu\text{g/ml}$) on C_{18} column.
- 5.2 HPLC retardation of a series of 2-nitroimidazoles on C_{18} column (15% methanol-water mobile phase) vs partition coefficient.
- 5.3 Pilot toxicity studies with SR-4554.
- 5.4 Typical chromatograms of plasma extracts obtained from (a) control, and (b) SR-4554 treated mice.
- 5.5 Plasma pharmacokinetics of SR-4554 at 162 mg/kg body weight in EMT6 tumour bearing female Balb/c mice.

- 5.6 Biodistribution of SR-4554 (162 mg/kg) in tumour (□), liver (O) and brain (Δ) of tumour bearing mice.
- 5.8 Linear relationship between i.p. dose of SR-4554 injected and the corresponding area under the concentration vs time curve AUC in female Balb/c mice ($r = 0.99$).
- 5.9 Intravenous (i.v.; □), intraperitoneal (i.p.; O) and oral (p.o.; Δ) plasma pharmacokinetics of SR-4554 (at 90 mg/kg) in female Balb/c mice.
- 6.1 A model for studying hypoxia in tumours using ^{19}F MRS.
- 6.2 A typical fluorine (a) and deuterium (b) spectra obtained from a RIF-1 tumour (and reference bulb) after the injection of 180 mg/kg of SR-4554.
- 6.3 Quantitation of SR-4554 in 100 mM saline solution using a double tuned ($^{19}\text{F}/^2\text{H}$) MRS circuit at 4.7 Tesla.
- 6.4 Typical ^{19}F spectra obtained from a tumour (SCCVII) bearing mouse after the co-injection of fluoromisonidazole (Ro 07-0741) (1 mmol/kg), SR-4554 (0.32 mmol/kg) and CCI-103F (0.125 mmol/kg).
- 6.5 The retention of ^{19}F signals from SR-4554 in murine and human xenografts.
- 6.6 Relationship between ^{19}F retention index and tumour weight in RIF-1 tumours.
- 6.7 A localised ^{31}P spectra obtained from a KHT tumour by means of an ISIS sequence.
- 6.8 Relationship between ^{19}F retention index and pO_2 parameters.
- 6.9 Typical tumour ^{19}F spectra obtained from control [(a) and (b)] and carbogen breathing [(c) and (d)] CDF₁ mice at 45 min [(a) and (c)] and 6 hr [(b) and (d)] after the injection of SR-4554.
- 6.10 Typical 1-D and 2-D CSI of SR-4554 in RIF-1 tumour showing drug signals from tumour and bladder regions.
- 6.11 The ^1H spin echo images obtained from a tumour (SCCVII) bearing mouse.
- 6.12 A ^{19}F spin echo image superimposed on the corresponding ^1H image of a tumour (SCCVII) bearing C3H mouse.
- 6.13 A T_2 curve obtained from a RIF-1 tumour bearing mouse at 3 hr after the injection of 180 mg/kg SR-4554.
- 7.1 Design features of the fluorinated 2-nitroimidazole SR-4554.

ABBREVIATIONS

AcOH- <i>d</i>	Acetic acid- <i>d</i> .
ATP	Adenosine triphosphate.
AUC	Area under the concentration time curve.
B ₀	External magnetic field.
B ₁	Radiofrequency field (or pulse).
CNS	Central nervous system.
CSI	Chemical shift imaging.
CV	Coefficient of variation.
DMSO	Dimethyl sulfoxide.
DNA	Deoxyribonucleic acid.
$E \frac{1}{2}$	Half-wave reduction potential.
EELS	Electron energy loss spectroscopy.
ELISA	Enzyme-linked immunosorbent assay.
EPR	Electron paramagnetic resonance.
ESI	Electron spectroscopic imaging.
ESR	Electron spin resonance.
FACS	Fluorescence activated cell sorting.
FID	Free induction decay.
F/N	Fluorine to nitrogen ratio.
5-FTP	5-Fluorotryptophan.
HOD	Natural abundance deuterium in water.
HPLC	High performance liquid chromatography.
i.p.	Intraperitoneal.
i.v.	Intravenous.
ISIS	Image-selected <i>in vivo</i> spectroscopy.
LD ₁₀	Lethal dose (to kill 10% of experimental animals).
LD ₅₀	Lethal dose (to kill 50% of experimental animals).
MQL	Minimum quantifiable limit.
MRI	Magnetic resonance imaging.
MRS	Magnetic resonance spectroscopy.
MS	Mass spectra (or spectroscopy).
NADPH	Nicotinamide adenine dinucleotide phosphate (reduced).
NMR	Nuclear magnetic resonance.
NTP	Nucleotide triphosphate.
p.o.	per oral.

PBS	Phosphate buffered saline.
PCR	Polymerase chain reaction.
PCr	Phosphocreatine.
PDE	Phosphodiester.
PET	Positron emission tomography.
Pi	Inorganic phosphate.
PME	Phosphomonoester.
pO ₂	Oxygen tension.
ppm	Parts per million.
QC	Quality control.
RF	Radiofrequency.
RNA	Ribonucleic acid.
SPECT	Single photon emission computed tomography.
T	Tesla.
T ₁	Longitudinal (or spin-lattice) relaxation time.
T ₂	Transverse (or spin-spin) relaxation time.
T ₂ *	Effective transverse (spin-spin) relaxation time.
TE	Echo time.
TR	Repetition time.
UV	Ultra-violet.
v / v	Volume in volume.
w / v	Weight in volume.

Phases of Cell cycle

G ₁	Gap 1 (Interval between M- and S-phases).
G ₂	Gap 2 (Interval between S- and M-phases).
M	Mitosis.
S	DNA synthesis.

CHAPTER 1

Introduction

1.1 NATURE OF CANCER

A cancer can be defined as a group of cells within the body that escapes from normal, orderly homeostatic control, and multiplies until, unless treated, it leads to organ dysfunction or death of the host. Normal cells proliferate in a controlled fashion due to the presence of feedback mechanisms which stimulate or inhibit cell division (Pera, 1995). In contrast, however, cancer cells lose this regulation of cell proliferation leading to the formation of a tumour mass and, in addition, may also lose the ability to differentiate (Pera, 1995).

A tumour may be classified as being benign or malignant. In this regard, malignant tumours differ from benign tumours in their ability to spread from their primary sites to distant tissues from where they can grow into new tumours (metastasis) (Tarin, 1995). Importantly, in most cases, it is this metastasis which causes the progression of tumours resulting in death of the host.

The annual incidence rates of cancer (crude and age standardised) and also the numbers of new cases of 18 different cancers have been estimated, for the year 1985, in 24 areas of the world (Parkin *et al.*, 1993). The total number of new cases was 7.6 million, 52% of which occurred in developing countries (Parkin *et al.*, 1993). Lung cancer is the most common cancer, followed by stomach cancer and then breast cancer (Parkin *et al.*, 1993). The trends in cancer mortality in different parts of the world have also been reported (Franceschi *et al.*, 1994; La Vecchia *et al.*, 1993a; La Vecchia *et al.*, 1993b; La Vecchia *et al.*, 1992; Parkin *et al.*, 1993). For instance, the overall age-standardised rates for breast cancer in the late 1980's in most European countries, were between 20 and 30 per 100,000 (La Vecchia *et al.*, 1992).

In spite of recent advances in the treatment of cancers, there are still a lot of obstacles. One of the most important of these obstacles is the resistance of tumours to conventional therapy, in particular chemotherapy and radiotherapy. One such resistance mechanism, tumour hypoxia, which is a result of the physiological status of the tumour, is the basis of this thesis and will be described in more detail in section 1.2.

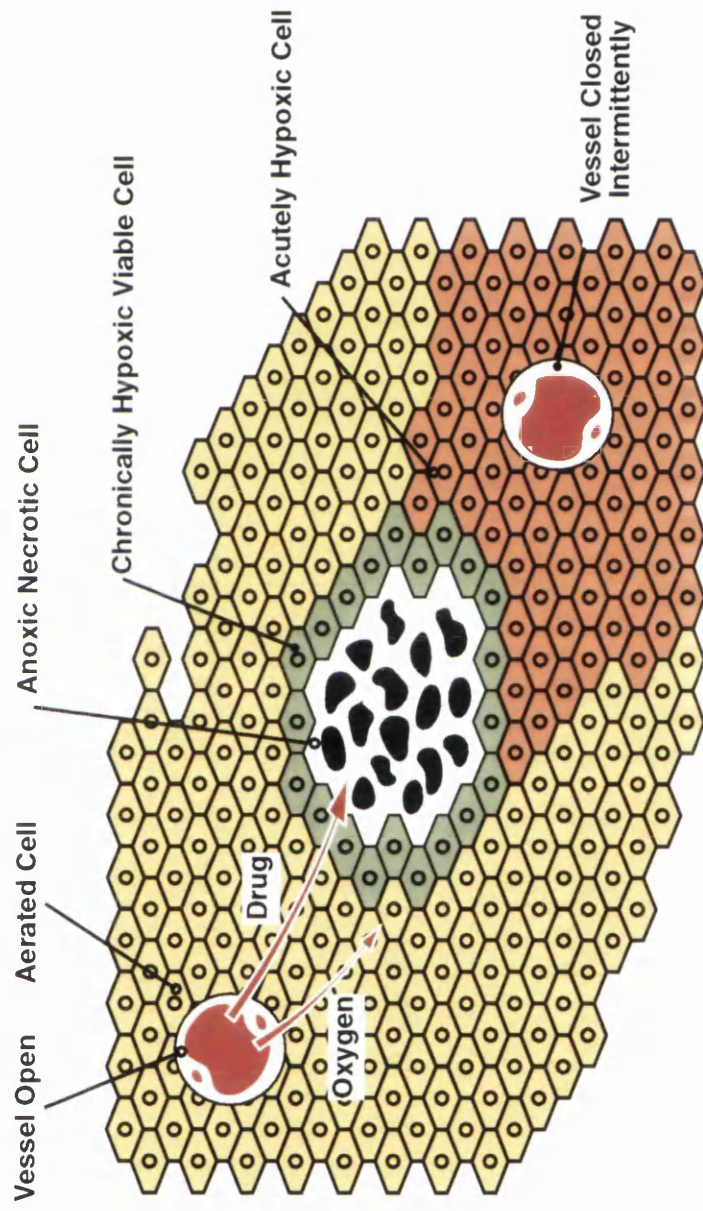
1.2 PHYSIOLOGICAL PROPERTIES OF TUMOURS

1.2.1 Tumour hypoxia

Oxygen provides cells with their major source of cellular energy through oxidative phosphorylation. Tissue hypoxia results from an inhibition of oxygen supply to cells and may occur in vascular disease, such as during a stroke, or in tumours. Structural and functional abnormalities of the tumour vasculature may account for the existence of hypoxic cells within tumours (Vaupel *et al.*, 1989). Generally, tumour cells adjacent to capillaries are adequately oxygenated and capable of normal aerobic metabolism and cell division. Since oxygen must be carried to distant cells by diffusion, however, cell respiration reduces the oxygen tension with increasing distance from capillaries. Thus hypoxic cells may be defined as cells existing at an intermediate oxygen tension between well oxygenated cells (oxic population) and those cells with insufficient oxygen to support viability (anoxic or necrotic population). Cells existing under an oxygen tension (pO_2) of 0.1% or less are specifically referred to as radiobiologically hypoxic cells, due to the resistance of such cells to radiation treatment (see section 1.3).

Tumour hypoxia may present as an irreversible diffusion limited (chronic) (Thomlinson & Gray, 1955) or a reversible perfusion limited (acute) (Brown, 1979; Chaplin *et al.*, 1987) form. These two forms of hypoxia are illustrated in Fig. 1.1. Chronic hypoxia which is the classical model of tumour hypoxia occurs when solid tumours out-grow their supportive vasculature (Thomlinson & Gray, 1955; Vaupel, 1992). The diffusion distance of molecular oxygen is limited, by metabolic consumption, to 150-200 μm from the nearest capillary. Beyond this diffusion distance, cells are non-viable and become necrotic. Immediately proximal to the necrotic zone is a layer of hypoxic cells which are oxygen deprived and yet viable. These cells which are a result of the diffusion limitation of oxygen, remain hypoxic until they become reoxygenated or die, and hence are referred to as chronically hypoxic cells. Such cells are also characterised by their low rate of metabolism, low levels of glucose and adenosine triphosphate (ATP), and high levels of catabolites such as lactate (Vaupel, 1992).

Fig.1.1. A schematic representation of the two types of hypoxia present within solid tumours. Chronic hypoxia, as described by Tomlinson and Gray (1955), results from the exhaustion of oxygen by metabolism as it diffuses from the supportive vasculature. Acute hypoxia is a more transient effect and results from the intermittent closing and reopening of tumour vessels. Taken from Workman (1992).



The second type of hypoxia occurs when blood flowing through a vessel is transiently stopped, resulting in oxygen deprivation of all the normally oxic cells down-stream of the occlusion (Brown, 1979; Chaplin *et al.*, 1987; Trotter *et al.*, 1989). These cells are considered acutely hypoxic because they only remain hypoxic as long as the occlusion continues, becoming oxygenated again when blood flow resumes. Prolonged vascular occlusion can, however, lead to decreased cell survival and death (Denekamp *et al.*, 1983). Current literature indicates that significant variations in the oxygenation status of tumours can occur, between different locations within a tumour, and between tumours of the same grading and clinical staging (Vaupel, 1992).

1.2.3 Cell cycle regulation of hypoxic cells

Reduced oxygenation can affect the processes of cell growth and cell cycle control. There is evidence to suggest that in some tumours cells can arrest in G₂ or M-phase under hypoxia (Shrieve & Begg, 1985; Shrieve *et al.*, 1983). In general, however, existing data indicate that cells in S-phase immediately arrest following exposure to extreme hypoxia, while cells in other phases of the cell cycle proceed through the cell cycle and become arrested in late G₁ (Amellem & Pettersen, 1993; Bedford & Mitchell, 1974; Koch *et al.*, 1973). This oxygen-dependent G₁ check-point is certainly different from the quiescent G₀ phase exhibited by non-cycling aerobic cells and may act to protect cells from the lethal effect of extreme hypoxia in S-phase (Amellem & Pettersen, 1991; Spiro *et al.*, 1984). In addition, although hypoxia can induce the tumour suppressor protein p53, the hypoxia induced G₁-checkpoint is independent of p53 status (Graeber *et al.*, 1994). More recently, hypoxia and reoxygenation of hypoxic tumour cells (section 1.3.3) have also been demonstrated to act as signals for the programmed cell death (apoptosis) of these cells (Yao *et al.*, 1995).

1.2.4 Molecular response of cancer cells to hypoxia

In recent years, the response of cancer cells to hypoxia and reoxygenation has been evaluated at the molecular level. The transcriptional activation and expression of various genes and proteins are considered as adaptive response of these cells to the

hypoxic stress. Genes and proteins shown to be modulated by hypoxia include oxygen regulated proteins (Heacock & Sutherland, 1986), glucose regulated proteins (Koong *et al.*, 1994a), heat shock proteins (Giaccia *et al.*, 1992), vascular endothelial growth factor (Shweiki *et al.*, 1992), erythropoietin (Madan & Curtin, 1993), lactate dehydrogenase (Firth *et al.*, 1994), phosphoglycerate kinase 1 (Firth *et al.*, 1994), and also the enzyme DT-diaphorase (Robertson *et al.*, 1994). Transcriptional factors regulated by hypoxia include the hypoxia inducible factor 1 (Wang *et al.*, 1995), the bifunctional redox protein/endonuclease Ref-1 (Yao *et al.*, 1994), the proto-oncogenes jun and fos (AP-1) (Yao *et al.*, 1994), the nuclear transcription factor kB (Koong *et al.*, 1994b), and the tumour suppressor gene p53 (Graeber *et al.*, 1994). In addition, it also appears that reduced *de novo* synthesis of deoxynucleotides may play a part in the cell cycle regulation of hypoxic cells (Ameltem *et al.*, 1994).

1.3. THERAPEUTIC IMPORTANCE OF TUMOUR HYPOXIA

1.3.1 Radioresistance and chemoresistance of hypoxic cells

The presence within tumours of hypoxic cells has long been considered as a problem in cancer therapy due to the radio- and chemoresistance of hypoxic cells (Bush *et al.*, 1978; Coleman, 1988; Gatenby *et al.*, 1988; Hall, 1988; Workman, 1983a). Following therapy, these cells can repopulate and cause relapse of the cancer. For instance, hypoxic cells are 2-3 times more resistant to cell killing by radiation compared to well oxygenated or aerobic cells (Coleman, 1988; Hall, 1988). Unlike hypoxic cells, oxic cells are sensitive to radiation because molecular oxygen is capable of interacting with radiation-induced radicals in DNA, leading to irreversible fixation of the damage (Hall, 1988). In addition, oxygen competes with reducing species present within cells, such as thiols, which can restore the target molecule to the original undamaged form (Hall, 1988). As a consequence, the lower levels of oxygen within hypoxic cells make them more resistant to radiation.

Hypoxic cells are also resistant to certain chemotherapeutic agents, including bleomycin and some alkylating agents (Workman, 1983a). Chemoresistance may arise within these cells through the

impairment of drug delivery, non-cycling cell kinetic status of the cells due to reduced oxygen levels, involvement of molecular oxygen in the mechanism of action of the drug, as well as changes in the pH of hypoxic regions and its subsequent effect on the drug ionisation state (Wilson, 1992). It could also be envisaged that, the up- or down-regulation of certain proteins (including potential drug metabolising enzymes) during exposure to hypoxia and/or reoxygenation may affect response to therapy. For example, cell lines containing high levels of DT-diaphorase were found to be more sensitive to the bioreductive drugs mitomycin C and EO9, compared to low diaphorase expressing cell lines (Fitzsimmons *et al.*, 1995). In addition, relatively transient hypoxia can lead to an enhanced frequency of dihydrofolate reductase gene amplification and hence to methotrexate resistance (Rice *et al.*, 1986).

1.3.2 Treatment of hypoxic cells

Due to the co-existence of both aerobic and hypoxic cells within tumours, rational therapies devised to deal with hypoxic tumours will involve the combination of hypoxic cell-targeted strategies, alongside those aimed to eradicate the oxic population such as radiotherapy. Some of such approaches are summarised below:

1. Increased oxygen delivery

Various methods have been employed to manipulate oxygen delivery to tissues as a means of increasing radiosensitivity. These methods have been reviewed by Coleman (1988), and include altering the oxygen carrying capacity by the use of blood transfusion and the administration of perfluorochemicals or hyperbaric oxygen. In addition, the administration of nicotinamide and carbogen can lead to improved radiosensitization by overcoming acute and chronic hypoxia respectively (Horsman *et al.*, 1994).

2. Bioreductive agents

The use of electron affinic drugs to sensitize tumour cells to radiation or alternatively as hypoxia-selective cytotoxins, has received a lot of attention in recent times (Wilson, 1992; Workman, 1989; Workman & Stratford, 1993). These drugs, collectively referred to as bioreductive agents, are pro-drugs often containing nitro, N-oxide and quinone groups, which are selectively activated under hypoxia. Typical examples of clinically used and investigational

bio-reductive agents are illustrated in Fig. 1.2. Enhanced anti-tumour effect can also be achieved by a combination of these bio-reductive agents with vasoactive agents, such as hydralazine (Chaplin & Acker, 1987), which decrease tumour blood flow and increase tumour hypoxia.

1.3.3 Reoxygenation of hypoxic cells

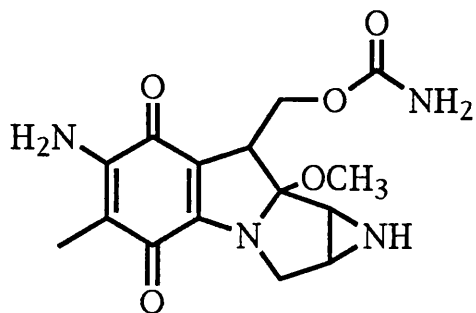
There is experimental evidence to suggest that the oxygenation of surviving hypoxic tumour cells can be improved after irradiation (Hall, 1988). The term reoxygenation was introduced to describe the reacquisition of tumour radiosensitivity due to such oxygenation of hypoxic cells, and is believed to be a major reason why fractionated radiotherapy leads to better clinical results than single dose radiotherapy (Kallman, 1972). Depending on the tumour type, this process may take from only a few minutes to several hours (Grau & Overgaard, 1990; Javed Afzal *et al.*, 1991; Kallman, 1972; Rofstad, 1989). Factors which may be responsible for this reoxygenation of hypoxic cells include: removal of radiation damaged (oxic) cells so that hypoxic cells become closer to functional blood vessels; reduced oxygen utilisation by radiation damaged cells and; increase or redistribution of blood flow to hypoxic cells caused by reduced intratumour pressure (Rofstad, 1989). It is also possible that reoxygenation of acutely hypoxic cells may arise from resumption of blood flow in transiently non-functioning vessels, a process which is independent of therapy (Chaplin *et al.*, 1987).

Since the measurement of the degree of hypoxia within tumours is important to the design of appropriate therapeutic schedules for these particular tumours, the next section will focus on methods used to evaluate tumour hypoxia.

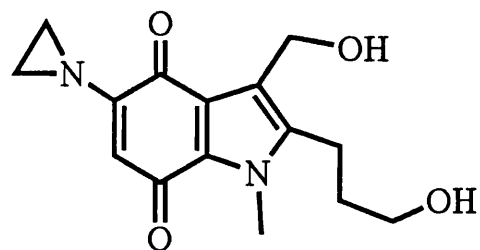
1.4 MEASUREMENT OF TUMOUR HYPOXIA

The association of tumour hypoxia with treatment failure has led to the search for clinically relevant detection techniques to enable the selection of patients who will benefit from manoeuvres aimed at circumventing the hypoxic effect. The pO_2 of venous blood is approximately 5%, thus providing nearly full radiation sensitivity. The oxygen tension at which cells display sensitivity midway between nitrogen and air or oxygen (K_m value), however, falls between 0.3

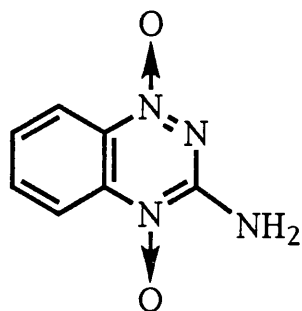
Fig. 1.2. Chemical structure of some bioreductive agents. These compounds undergo selective activation under hypoxia to potential cytotoxic species.



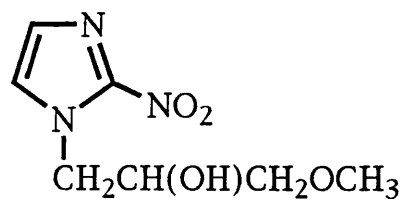
(a) Mitomycin C



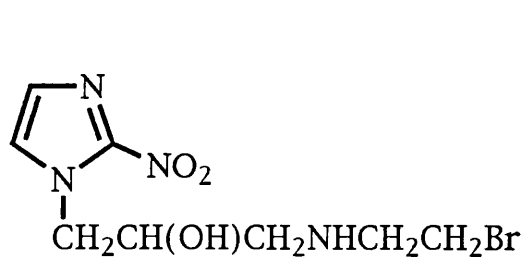
(b) EO9



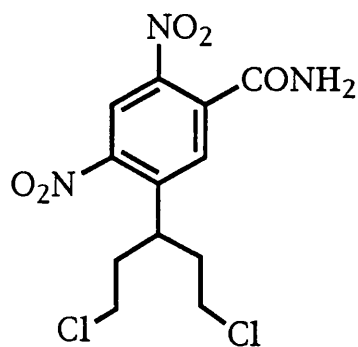
(c) Tirapazamine



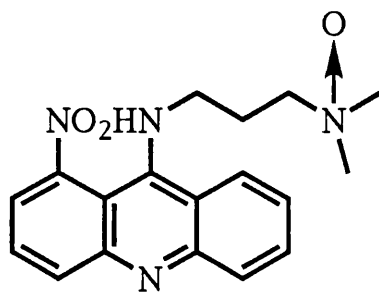
(d) Misonidazole



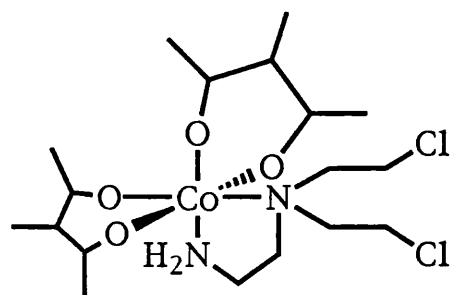
(e) RB 6145



(f) SN 23862



(g) Nitracrine N-oxide



(h) SN 24771

and 0.5% (Hall, 1988; Koch *et al.*, 1984). This implies that oxygen levels far below those encountered in normal tissues need to be measured. Apart from dynamic range limitations, the ability to measure hypoxia on a cell to cell basis is also important, since histological evaluation of solid tumours has suggested that significant changes in cellular oxygen levels can occur over dimensions of a few cell diameters (Urtasun *et al.*, 1986a). Other factors such as degree of invasiveness of the technique, resolution, the measurement parameters used (and their relationship with the oxygen tension), the toxicity and the stability of probes used and finally cost considerations, are all relevant to the development of clinically appropriate techniques to detect hypoxia *in vivo*. Table 1.1 summarises some of the techniques designed to measure hypoxia within tumours which have been investigated to date. Techniques that measure nitroimidazole binding act as, 'no oxygen detectors', i.e. they show maximal response under complete anoxia (no oxygen), and a lowering of response with increasing pO₂. The binding of these agents, therefore, mimics radioresistance of tumour cells and has a suitable dynamic range for measuring hypoxia within tumours (Koch *et al.*, 1984). Since 2-nitroimidazole binding is sensitive to differences in cellular reductive enzymes (Joseph *et al.*, 1994; Walton & Workman, 1987; Workman & Walton, 1990), however, these probes may be more suited to the measurement of changes in tumour oxygenation or providing a predictive index which can be used in the selection of patients likely to benefit from bioreductive therapy, rather than the measurement of absolute tumour pO₂. Interestingly, nitroimidazoles may be detected by both invasive or non-invasive methods (Table 1.1). In both cases, however, the results represent measurement of oxygenation at the cell to cell level (heterogeneity), including discrimination between tumour and adjacent vascularised stromal tissue (Franko *et al.*, 1987; Urtasun *et al.*, 1986b). Nitroimidazole probes are also relatively cheap to produce and have a fairly predictable pharmacokinetic and toxicity profile (Stone *et al.*, 1993; Workman & Brown, 1981).

Since most of the measurement techniques described to date (Table 1.1) are based on nitroimidazole binding, the physicochemical properties of these agents, as well as their use as hypoxia probes, will be described in section 1.5.

Table 1.1. Summary of methods used to measure tumour hypoxia
(a) *Invasive techniques*

Technique	Parameter	Comments	References
Radiobiologic hypoxic fraction	Radiosensitivity	The bulk of existing data on hypoxic fraction of animal tumours have been generated by this technique. Measures clonogenic radiobiological hypoxic cells. Unsuitable clinically.	(Moulder & Rockwell, 1984)
Double label fluorescent microscopy	Perivascular cell staining	Measures acute hypoxia in accessible tumours, with a resolution of about 1 mm ³ . Clinical usefulness may be limited by toxicity of currently available probes.	(Chaplin <i>et al.</i> , 1987) (Minchinton <i>et al.</i> , 1993)
Polarographic oxygen electrodes	pO ₂	Direct pO ₂ measurement with a resolution of about 50 to 100 cells. Accuracy at low pO ₂ is questionable. Necrosis can influence data. Only suitable for accessible tumours.	(Vaupel <i>et al.</i> , 1991) (Gatenby <i>et al.</i> , 1988) (Horsman <i>et al.</i> , 1993)
Phosphorescence imaging	Phosphorescence quenching by oxygen	'No oxygen detector'; suitable for accessible superficial tumours with a resolution of about 50-100 mm ³ . The probes are not yet suitable for clinical use.	(Rumsey <i>et al.</i> , 1988)
Comet assay	Radiosensitivity (DNA damage)	Measures clonogenic radiobiological hypoxic fraction of accessible tumours at the level of single cells. It has an assay time of about 5 hr.	(Olive <i>et al.</i> , 1990) (Olive <i>et al.</i> , 1993) (Olive, 1995)

Technique	Parameter	Comments	References
Immu- histochemistry	Nitroimidazole binding	'No oxygen detector'; suitable for accessible tumours. Depending on the exact technique, the resolution may vary from single cells (FACS analysis) to about 1 mm ³ biopsy samples (ELISA). Differences in tumour enzyme levels may influence the measurements.	(Olive & Durand, 1983) (Raleigh et al., 1994) (Lord et al., 1993)
Electron energy loss spectroscopy (EELS)	Nitroimidazole binding	'No oxygen detector'; suitable for accessible tumours. Measures hypoxia with a resolution of single cells. Differences in tumour enzyme levels may influence the measurements.	(Chapter 4 of this thesis)
Intrinsic tumour markers	Protein and mRNA	Measures hypoxia regulated proteins and mRNA of accessible tumours. Resolution varies from single cells to about 1 mm ³ biopsy samples. The relationship between hypoxia/reoxygenation and protein/mRNA levels has not been well characterised.	(Heacock & Sutherland, 1990)
¹⁴ C-/ ³ H- misonidazole	Nitroimidazole binding	'No oxygen' detector suitable for accessible tumours, with a resolution of about 1 mm ³ . Labels may be unstable. Radiation exposure. Differences in tumour enzyme levels may influence the measurements.	(Chapman, 1984) (Chapman, 1991)

(b) Non-invasive techniques

Technique	Parameter	Comments	References
¹⁹ F Magnetic resonance spectroscopy (¹⁹ F MRS)	Nitroimidazole binding	'No oxygen detector'; suitable for all tumours; with a resolution of about 100 mm ³ . Differences in tumour enzyme levels may influence the measurements. Has imaging capabilities	(Maxwell <i>et al.</i> , 1988) (Kwock <i>et al.</i> , 1992) (Chapter 6 of this thesis)
¹⁹ F Magnetic resonance imaging (¹⁹ F MRI)	Spin-lattice relaxation rates of perfluoro-carbons	Imaging technique suitable for all tumours, with a resolution of about 100 mm ³ . Mechanism of uptake is unclear. Poor diffusion of probe limits this technique to the detection of acutely hypoxic cells. Highly sensitive to tumour blood flow and temperature.	(Sotak <i>et al.</i> , 1993)
¹⁸ F Positron emission tomography (¹⁸ F PET)	Nitroimidazole binding	'No oxygen detector' suitable for all tumours, with a resolution of about 50 million cells. It has imaging capabilities. Differences in tumour enzyme levels may influence the measurements. Radiation exposure. The label has a very short half life.	(Koh <i>et al.</i> , 1991)
³¹ P Magnetic resonance spectroscopy (³¹ P MRS)	Bioenergetic status	Relationship with hypoxia is not very clear. Strongly influenced by other factors such as glucose concentration and necrosis. It has a resolution of about 100 mm ³ .	(Negendank, 1992) (Tozer & Griffiths, 1992)

Technique	Parameter	Comments	References
Electron paramagnetic resonance (EPR)	pO ₂ at site of paramagnetic probe	Direct measurement of pO ₂ with a resolution of about 50 - 100 mm ³ . Suitable for all tumours. The probes have not been approved for routine clinical use.	(Glockner & Swartz, 1992)
[¹²³ I]IAZA Single photon emission computed tomography (SPECT)	Nitroimidazole binding	'No oxygen detector' suitable for all tumours. Oxygenation of the whole tumour is detected. Has imaging capabilities. Measurements may be influenced by enzyme levels. The probe may be taken up into thyroid. Radiation exposure.	(Groshar <i>et al.</i> , 1993)

1.5 PHYSICOCHEMICAL AND BIOLOGICAL PROPERTIES OF 2-NITROIMIDAZOLES

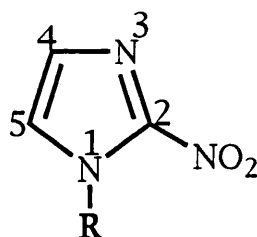
1.5.1 Structure of 2-nitroimidazoles

Fig. 1.3 shows the general structure of 2-nitroimidazoles, together with specific 2-nitroimidazoles and their side chain substituents. Although the structures of most of these compounds are based on the prototype 2-nitroimidazole, misonidazole, the structures of some recently synthesised 2-nitroimidazoles are centred on the amide nitroimidazole etanidazole. Various misonidazole analogues containing radioisotopic forms of hydrogen, halogens, and carbon exist and have been widely used particularly as hypoxia probes. The list is by no means exhaustive and it continues to increase with the search for 2-nitroimidazoles that are less lipophilic than misonidazole.

1.5.2 Metabolism of 2-nitroimidazoles

The metabolism and hypoxia selective binding of 2-nitroimidazoles has been investigated extensively with misonidazole (Franko, 1986). Misonidazole can be metabolised under aerobic or hypoxic conditions. Under aerobic conditions misonidazole undergoes both O-demethylation of the terminal methoxy group, as well as glucuronidation of the side chain hydroxyl group predominantly in the liver (Workman, 1983b). Misonidazole can also be metabolised by cellular electron donors, and enzymes, to the nitro radical anion (Fig. 1.4.) (Biaglow *et al.*, 1986; Mason & Holtzman, 1975; Wardman & Clarke, 1976). In the presence of molecular oxygen, the nitro radical anion (1-electron reduced product) is back-oxidised to form the original parent compound and superoxide (and resulting toxic species, such as hydroxyl radicals). This establishes a futile cycle in aerobic cells with no net nitroreduction of the parent compound. Under hypoxia, however, the radical anion can be further reduced to the hydroxylamine (4-electron product) and amine (6-electron product) presumably via the nitroso intermediate (2-electron) (Rauth, 1984). Other products including mercapturic acid and glutathione adducts have also been identified (Smith & Born, 1984; Varghese, 1983). In addition, fragmentation products such as glyoxal (Fig. 1.5), as well as species obtained from the reaction of the hydroxylamine intermediate with water have been identified and may partly account for the

Fig. 1.3. General structure of 2-nitroimidazoles and constitution of the R-side chain. The 2-nitroimidazoles can be grouped into two main classes: misonidazole analogues and etanidazole analogues depending on the side chain composition at the N-1 position. Misonidazole analogues have a hydroxypropyl side chain, whilst etanidazole analogues possess an amide side chain. The fluorinated 2-nitroimidazole developed pre-clinically in this thesis as a hypoxia probe **SR-4554** (shown in bold letters), is an etanidazole analogue.




<u>R-group</u>	<u>Compound</u>
<i>Misonidazole analogues</i>	
—CH ₂ CH(OH)CH ₂ OMe	Misonidazole (Ro 07-0528)
—CH ₂ CH(OH)CH ₂ OEt	Ethylmisonidazole (Ro 07-0913)
—CH ₂ CH(OH)CH ₂ OH	Desmethylnisonidazole (Ro 05-9963)
—CH ₂ CH(OH)CH ₂ Cl	Chloromisonidazole (Ro 07-0269)
—CH ₂ CH(OH)CH ₂ N ₂ 	Pimonidazole (Ro 03-8799)
—CH ₂ CH(OH)CH ₂ F	Fluoromisonidazole (Ro 07-0741)
—CH ₂ CH(OH)CH ₂ OCH ₂ CF ₃	Trifluoropropanal (Ro 07-2044)
—CH ₂ CH(OH)CH ₂ OCH(CF ₃) ₂	CCI-103F
<i>Etanidazole analogues</i>	
—CH ₂ CONHCH ₂ CH ₂ OH	Etanidazole (SR-2508)
—CH ₂ CON(CH ₂ OH) ₂	SR-2555
—CH ₂ CONHCH ₂ CH(OH)CH ₂ OH	SR-2530
—CH ₂ CONHCH ₂ CH ₂ Ph	Benznidazole (Ro 07-1051)
—CH ₂ CF ₂ CONHCH ₂ CH ₂ OH	KU-2285
—CH ₂ CONHCH ₂ CH ₂ CF ₂ CF ₃	EF5
—CH ₂ CONHCH ₂ CH(OH)CF ₃	SR-4554

Fig. 1.4. Nitroreductive bioactivation of 2-nitroimidazoles. **a, b, c, d, e, and f,** represent the parent nitro compound, nitro anion radical, nitroso compound, hydronitroxide radical, hydroxylamine and primary amine derivatives respectively. The reactive intermediates are capable of forming covalent adducts under hypoxia. The figure also illustrates the phenomenon of futile recycling, a competing reaction within aerobic cells which leads to the formation of the toxic superoxide anion.

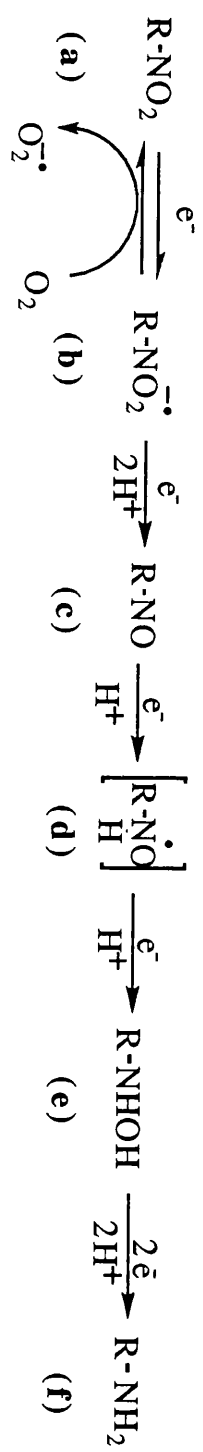
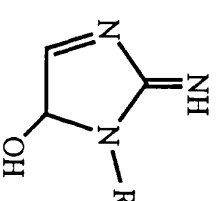
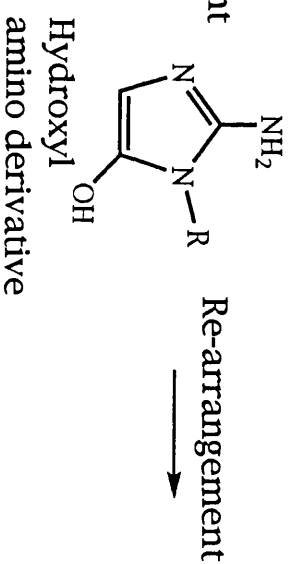
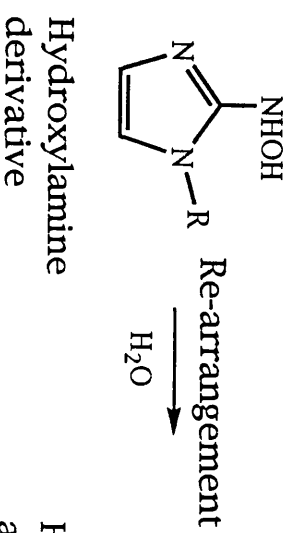
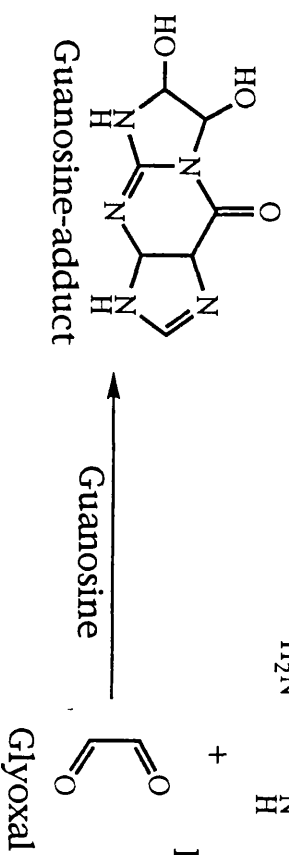
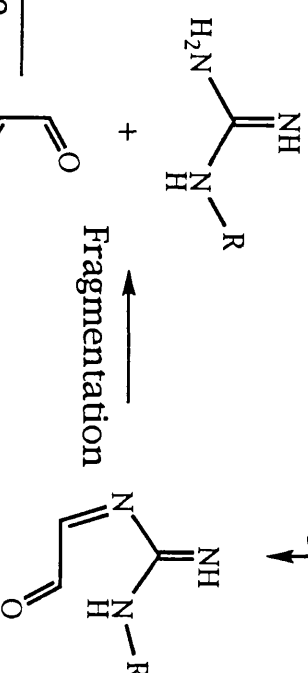


Fig. 1.5. Formation of glyoxal from the reactive hydroxylamine derivative of 2-nitroimidazoles. The ability of glyoxal to form guanine-adducts, may partly explain the cytotoxicity of 2-nitroimidazoles.



Ring
Cleavage

\downarrow



toxicity of 2-nitroimidazoles (Franko, 1986; Raleigh & Liu, 1984; Varghese & Whitmore, 1984b; Varghese & Whitmore, 1984c).

The ease of reduction of these compounds depend on both their electron affinities (or reduction potential) and their ability to act as substrates for the various reductases present within cells (Adams *et al.*, 1979; Adams *et al.*, 1980). Essentially all nitro(hetero)cycles with reduction potentials more positive than -500 mV are reduced metabolically at appreciable rates (Adams, 1992; Wilson, 1992). It is worth noting, however, that reduction of the compounds also depends on the degree of oxygenation (Franko *et al.*, 1987), as well as non-oxygen dependent factors, such as temperature (Chapman *et al.*, 1983), 2-nitroimidazole concentration (Chapman *et al.*, 1983), and the levels of various cellular reductase enzymes (Joseph *et al.*, 1994).

Misonidazole has often been used as the prototype 2-nitroimidazole to investigate the characteristics of metabolism induced binding. Research in the early 1980's indicated that reductive products of misonidazole can bind covalently to cellular macromolecules and localise selectively within hypoxic cells (Chapman *et al.*, 1981; Chapman *et al.*, 1983; Miller *et al.*, 1982). In addition, misonidazole binding was shown to decrease with increasing oxygen concentration, resulting in characteristic labelling of cells further away from blood vessels in tumours and near the necrotic region of spheroids (Urtasun *et al.*, 1986a; Urtasun *et al.*, 1986b; Garrecht & Chapman, 1983; Franko *et al.*, 1982; Franko *et al.*, 1987; Franko *et al.*, 1992). The oxygen concentration which inhibits misonidazole binding by 50%, between that in nitrogen and air, was reported to vary between 0.1 and 0.6% in tumours (Franko, 1986; Franko *et al.*, 1987). In addition, the pO₂ required for full radiosensitivity (2.5% (Koch *et al.*, 1984)) has been shown to inhibit misonidazole binding by 90% (Franko *et al.*, 1987). It therefore appears that the inhibition of misonidazole binding by oxygen mimics the effect of oxygen on radioresistance. This is relevant with regard to the use of 2-nitroimidazoles to predict radiosensitivity. These experiments have also demonstrated that the compounds can reach, and be metabolically activated within hypoxic cells. Hence this preferential metabolism or adduct formation within hypoxic cells can provide an indirect measure of the degree of hypoxia present within tumours.

The protocols currently being employed for the detection of nitroimidazole binding, are based on experiments conducted by Garrecht & Chapman (1983), and by Chapman *et al.* (1983), which demonstrated that ^{14}C labelled misonidazole adducts were cleared less rapidly compared to the original drug in EMT6 tumours and cells. These experiment have prompted the determination of the acid insoluble adducts (Miller *et al.*, 1982) of misonidazole observed 24 hr post-injection as a measure of hypoxia within tumours (Garrecht & Chapman, 1983; Hirst *et al.*, 1985; Sasai & Brown, 1994). It is believed that this 24 hr period was used to assure complete removal of the original parent misonidazole compound. Of interest, however, were experiments performed by Olive and Durand with SCCVII tumours (Olive & Durand, 1989) which demonstrated firstly, that the use of acid soluble and acid insoluble adducts of misonidazole predicted hypoxia equally well up to 16 hr post-injection. Secondly, the detection of adduct formation at earlier time points was thought to minimise the problems associated with cell turnover and hypoxic cell lysis, which undoubtedly do occur during the 24 hr experiments, and still provide misonidazole binding characteristics similar to those obtained at later time points (Olive & Durand, 1989).

With regard to the prediction of acute hypoxia with 2-nitroimidazoles, Olive and Durand (1989) have suggested that, provided blood vessels in tumours remained closed for 30 min or more, then misonidazole binding should be seen in acutely hypoxic cells. In addition, misonidazole binding should occur within acutely hypoxic cells, if vessels remained closed for a few minutes at a time, but the same vessels opened and closed several times over an hour (Olive & Durand, 1989).

The use of 2-nitroimidazoles as markers of hypoxia measures the biochemical process of adduct formation, rather than oxygen tension (pO_2) directly. The role of the non-oxygen dependent factors mentioned above, and therefore the susceptibility of a particular 2-nitroimidazole to these non-oxygen dependent factors, are important in the design and choice of a hypoxia marker. Misonidazole is more susceptible to non-oxygen dependent factors than etanidazole, although the rate of adduct formation is higher in the case of misonidazole (Koch, 1990; Koch *et al.*, 1993). As suggested by Chapman *et al.* (1983), the rate of adduct formation is probably

related to the differences in lipophilicity between the two compounds and hence their delivery to possible reductive sites. This implies that etanidazole analogues designed to have similar lipophilicities to misonidazole will be superior with regard to a combination of high reduction rates and minimal non-oxygen dependent binding. For instance, SR-4554 (this thesis) and EF5 (Fig. 1.3) (Lord *et al.*, 1993) are etanidazole analogues which have been designed to have appreciable rates of reduction comparable to misonidazole, while retaining the oxygen dependent property characteristic of etanidazole. In addition, SR-4554 was designed to have three magnetically equivalent fluorine atoms, thus making it sensitive for detection by non-invasive techniques such as magnetic resonance spectroscopy (MRS) and imaging (MRI). The theory of detecting fluorinated 2-nitroimidazoles by MRS and MRI will be described in more detail in section 1.6.

1.6 THEORY OF MRS AND MRI

Nuclear magnetic resonance (NMR) was discovered in 1946 by Bloch *et al.* and by Purcell *et al.*, and has proved to be a very versatile tool. Although it was initially applied to physics and chemistry, NMR has now been extended to physiology and medicine. In medicine, the terms magnetic resonance spectroscopy (MRS) and magnetic resonance imaging (MRI) have been used to describe the same phenomenon (i.e. NMR). In oncology, the application of NMR has grown since the observation by Damadian (1971) that ^1H properties of rat tumours differed from those of normal tissues. Although some NMR principles require quantum mechanical formulation, in most cases as shown in this section, a simple diagrammatic illustration can be employed.

1.6.1 Magnetic properties of atomic nuclei

Atomic nuclei are made up of neutrons and protons collectively called nucleons. Protons carry a charge which determines the electric charge of the nucleus. Many atomic nuclei possess an intrinsic angular momentum or spin. Only nuclei with an odd number of neutrons and/or protons have a resultant angular momentum. A spinning object which possesses a charge constitutes a circulation of electric current and therefore has an equivalent nuclear magnetic

moment (μ). Nuclei of potential interest in physiology and medicine include, ^1H , ^{13}C , ^{15}N , ^{19}F and ^{31}P all of which have a spin of $\frac{1}{2}$. Other nuclei such as ^2H and ^{14}N have a spin of 1 and have an electric quadrupolar moment, i.e. departure of the nuclei from a spherical shape, and are also important in medicine.

When placed in a magnetic field (B_0), a spinning nucleus behaves like a tiny bar magnet precessing about its long axis (Fig. 1.6). The angular frequency of precession (ω) is proportional to the applied magnetic field as shown in the Larmor equation below (Larmor, 1900):

$$\omega = \gamma B_0$$

where γ is the gyromagnetic ratio i.e. the ratio of the nuclear magnetic moment to its angular momentum, and is characteristic of each nucleus; the Larmor frequency is defined as $\omega/2\pi$. The Larmor precession of magnetic nuclei is a resonance phenomenon i.e. nuclei will absorb the most energy at its resonance frequency. The net magnetization (M) of a population of atomic nuclei (Fig. 1.7) is therefore made up of an ensemble of individual nuclear magnetic moments, each precessing about the magnetic field B_0 , which is by convention oriented along the z-axis. In NMR experiments a radiofrequency field or pulse (B_1) of appropriate frequency is introduced to flip the magnetization away from the z-axis. For instance the application of an appropriate 90° pulse results in a decrease in longitudinal magnetization and the generation of a new magnetization (the transverse magnetization) in the xy-plane in which all nuclei are in phase. When the radiofrequency field is removed, the magnetization decays back to the z-axis generating an NMR signal or free induction decay (FID), which can be amplified and displayed. FID's can be summed to give an enhanced signal to noise ratio. The NMR spectrum (or image) can be obtained by mathematical transformation of FID's (Fourier transform) in one or more dimensions.

1.6.2 Relaxation

The return of magnetization to equilibrium is called relaxation. In practice, this is found to be exponential and characterised by two

Fig. 1.6. The classical precession of a magnetic nucleus with a nuclear magnetic moment (μ) in a magnetic field (B_0).

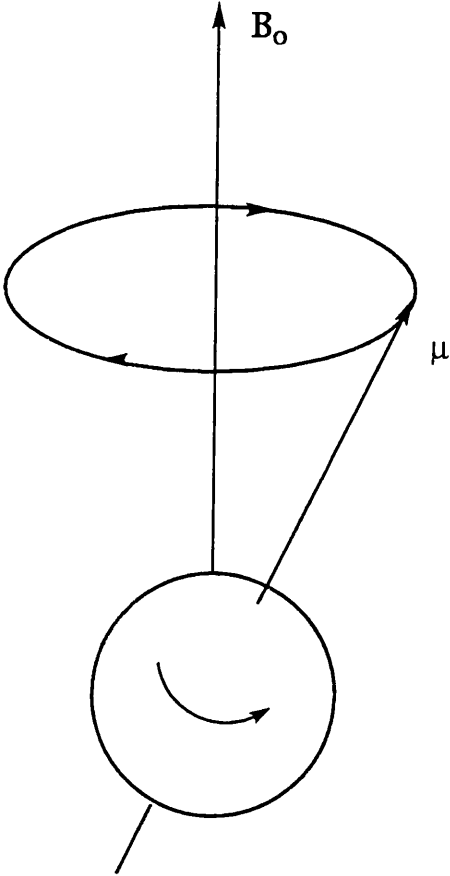
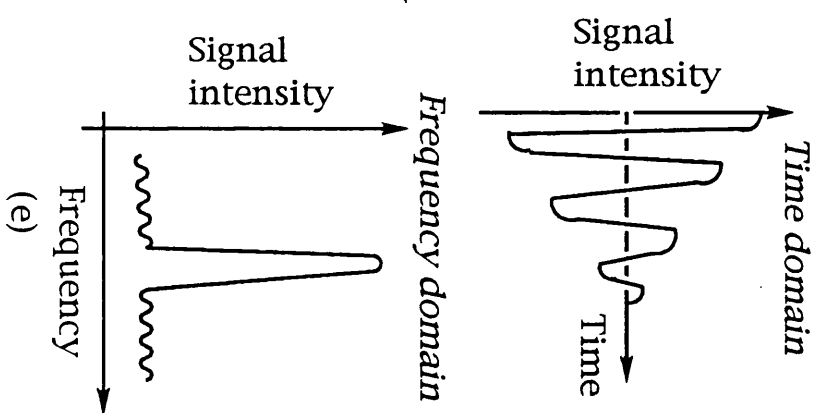
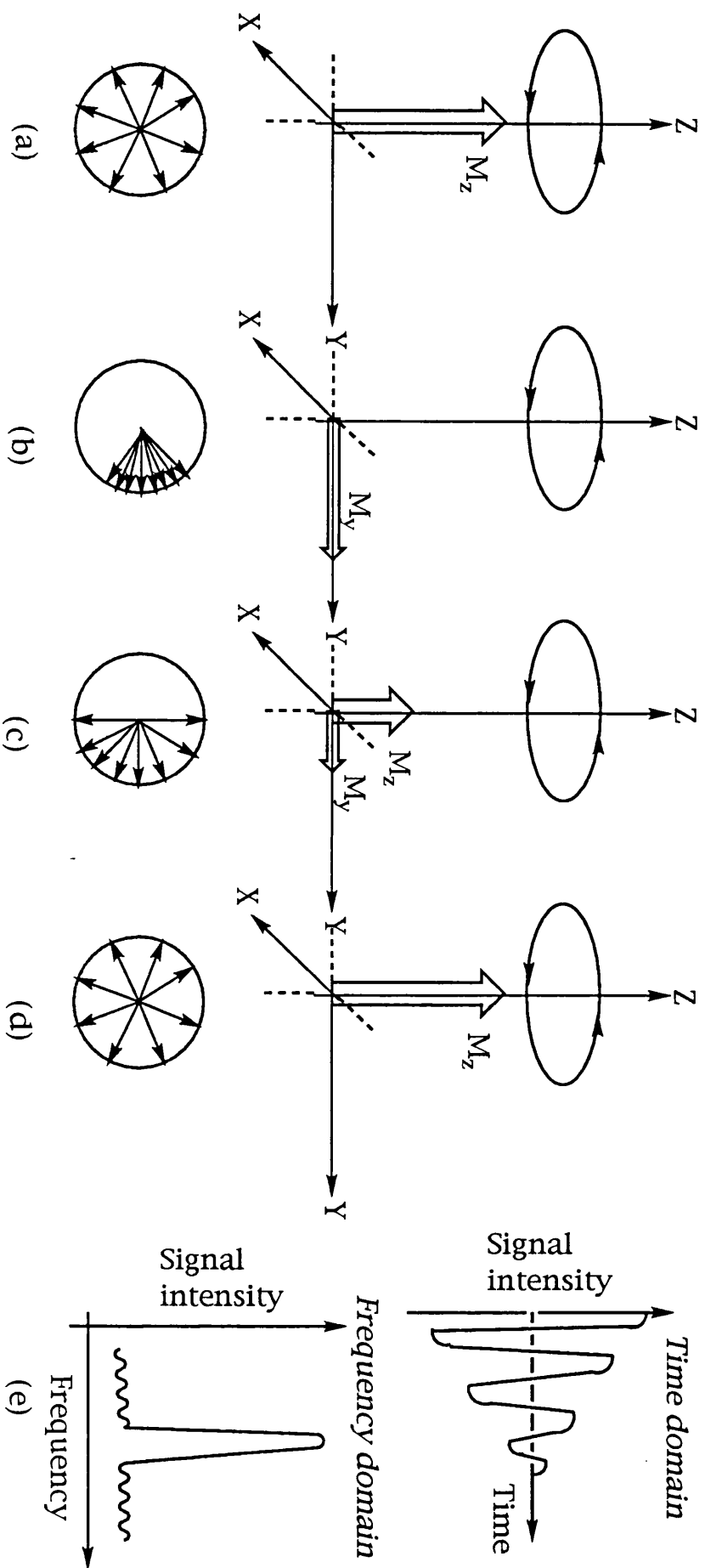


Fig. 1.7. The effect of a radiofrequency (RF) 90° pulse. (a) In equilibrium, the net magnetisation (M) representing the sum vector of magnetic moments is longitudinal and lies along the z -axis (M_z). (b) A 90° pulse flips the magnetisation into the xy -plane generating a new transversal magnetisation (M_y). This process is also associated with phase coherence of magnetic spins. (c and d). When the RF pulse is switched off, relaxation occurs with loss of phase coherence and transversal magnetisation. Relaxation also results in the regeneration of longitudinal magnetisation, as well as the generation of the free induction decay (FID) in the time domain which can be Fourier transformed into the frequency domain (e).



time constants. The first of these time constant is called T_1 (longitudinal relaxation or spin-lattice relaxation time) and is due to return of magnetization along the z-axis which occurs through loss of energy to the surrounding environment. This time constant is important with regard to time to repeat measurements (TR) for summation of FID's. Maximum signal intensity for subsequent FID measurements is only achieved when magnetization completely returns to equilibrium. Short TR's can therefore lead to incomplete return to equilibrium or 'saturation' of NMR signals. The second of these time constants is called T_2 (transverse relaxation or spin-spin relaxation time) and is due to loss of phase coherence between magnetic nuclei and subsequent decay of the NMR signal. T_2 is important in determining the linewidth in NMR experiments according to the equation:

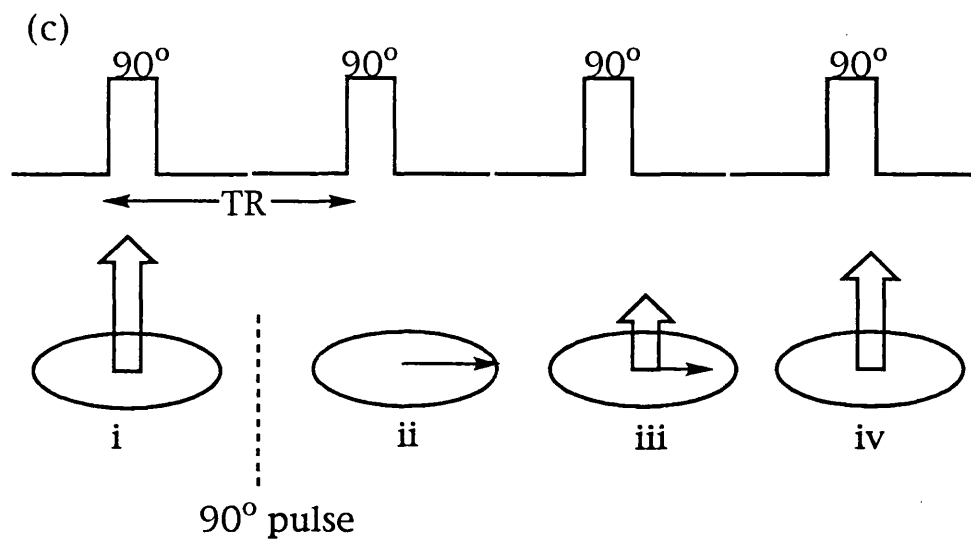
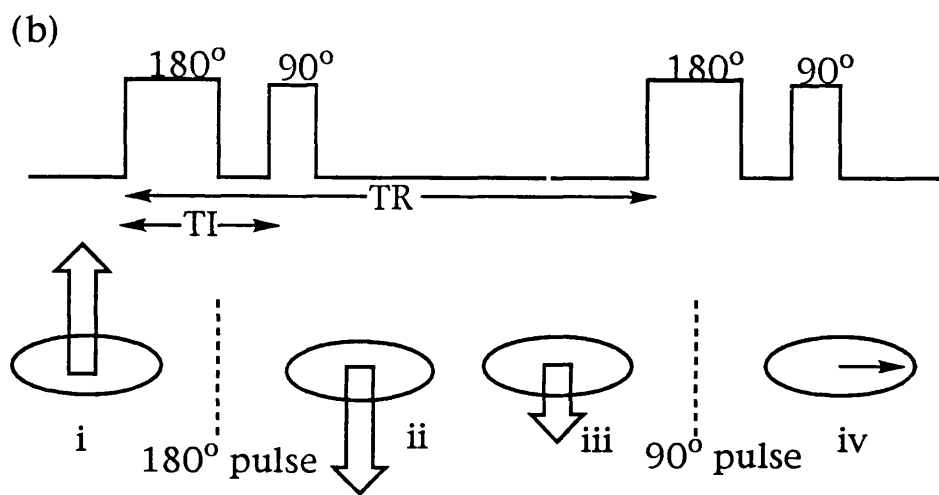
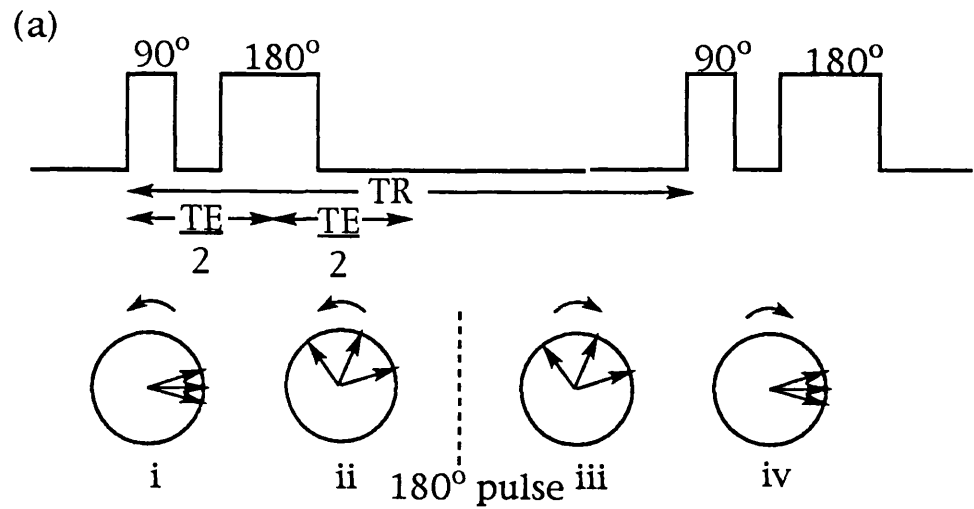
$$V_{\frac{1}{2}} = \frac{1}{\pi T_2}$$

where $V_{\frac{1}{2}}$ is the natural linewidth at half peak height. The magnetic field over a whole sample is not uniform resulting in a spread of magnetic fields (δB) or Larmor precession frequencies ($\delta \omega$) within various domains within the sample. This instrumental artefact is expressed in a new parameter T_2^* , which results from the dephasing of the various domains. T_2^* is often shorter than T_2 and dominates the transversal decay. In practice this effect can be minimised in high resolution NMR and *in vivo* MR-spectroscopic experiments by sample spinning and 'shimming' respectively.

1.6.3 Spin echoes, pulse sequences and MR-imaging

The phenomenon of spin echo is very important in MR-studies (Hahn, 1950). The spin echo pulse sequence is described in Fig. 1.8. This consists of a 90° pulse followed by a (series of) 180° pulse(s). After the 90° pulse, spins dephase resulting in the FID which lasts for approximately $2T_2^*$. However, the application of a 180° pulse at a time $TE/2$ (where TE is the echo time) rephases the dephasing protons and produces a strong signal (the spin echo) at time TE . The spins dephase after the echo and can be rephased again with another 180° pulse and so on. Spin echoes refocus dephasing due to chemical shift, J-coupling and B_0 inhomogeneities (i.e. what makes $T_2^* < T_2$). Due to

Fig. 1.8. Three important pulse sequences used in medicine. (a) The spin echo sequence can be used to obtain T₂-weighted spectra or images. (b) The inversion recovery sequence gives spectra or images which are T₁-weighted whilst, (c) a partial saturation sequence gives spin density-weighted spectra or images. The figure also shows the effect of the 90° and 180° pulses on the magnetisation of the spins. TR, TE, and TI represent the repetition time, echo time, and time to invert respectively.



T₂ relaxation, however, spin echoes show loss of signal intensity with time. This T₂-weighted sequence can therefore be used to determine the T₂ of a sample and is also important in imaging. Fig. 1.8 also shows an inversion recovery sequence which is T₁-weighted and can be used to determine the T₁ of a sample. These, as well as other important sequences have been recently described by Andrew (1994).

Unlike spectroscopy, MRI deals with localisation of spin distribution within a sample. In conventional MRI, different combinations of three important gradients are used to define the region of interest. These include the slice selection, phase encoding and read-out gradients (Andrew, 1994). Construction of both planar and 3-dimensional images can be obtained with the magnetic nucleus of interest.

1.7 AIMS OF THESIS

The aims of this thesis were two-fold. The first aim was to study the *in vitro* and *in vivo* pharmacological properties and toxicity of the novel, rationally designed, fluorinated 2-nitroimidazole SR-4554. In particular this has involved investigation into SR-4554 drug localisation, drug tolerability studies, pharmacokinetics and metabolism.

Using this information, the second aim of this project was to assess the ability of ¹⁹F MRS (of SR-4554) to detect and quantify hypoxia within tumours. This has involved the development and validation of both MRS and MRI techniques, to quantify the selective retention of SR-4554 within hypoxic tumours. Both aims have been met and the results outlined in the following chapters of the thesis.

1.8 LAYOUT OF THESIS

Several studies have either directly or indirectly demonstrated the presence of hypoxia within rodent and human tumours, and also how this can affect conventional therapy for cancers. As a consequence, this has led to the development of clinically relevant markers for hypoxia. The development of one of such markers, SR-4554, is described in this thesis.

In order to detect SR-4554 in bio-fluids and tissues, a sensitive high performance liquid chromatographic (HPLC) technique has been

developed and validated (chapter 2). This method is used in subsequent chapters to measure SR-4554 levels.

The *in vitro* and *in vivo* metabolism of SR-4554, as well as the enzymology of reductive activation of this compound necessary for the use of SR-4554 as a hypoxia probe have been investigated in chapter 3. In addition, both HPLC and high resolution NMR have been used to characterise the metabolic properties of a series of fluorinated 2-nitroimidazoles including SR-4554.

The selective reduction and localisation of SR-4554 within multicellular spheroids is described in chapter 4. In this chapter a sensitive technique called electron energy loss spectroscopy (EELS) has been employed to directly detect fluorine atoms in SR-4554 in cells within the spheroids. The subcellular localisation of SR-4554 has also been investigated with this technique in order to define the interaction of SR-4554 with cellular macromolecules.

For the continued use of SR-4554 in *in vivo* MRS studies, toxicity studies are required. In chapter 5, a preliminary toxicity study with this compound was performed. In addition, the HPLC technique developed in chapter 2 has been used to evaluate the pharmacokinetics of SR-4554 in mice. Various aspects of SR-4554 pharmacokinetics are described and comparisons made with other 2-nitroimidazoles.

In vivo ^{19}F MRS and MRI techniques are developed and employed to detect the selective retention of SR-4554 in murine and human tumour xenografts in chapter 6. This ^{19}F MRS technique has been used as a quantitative measure of hypoxia within these tumours. The relationship between the ^{19}F MRS technique and direct measurement of tumour oxygen tension by oxygen electrodes is also described.

Finally, the work carried out in this thesis is summarised and conclusions made in chapter 7. In addition, future directions for the development of superior probes for tumour hypoxia are elaborated.

CHAPTER 2

Development of a high performance liquid chromatographic assay for SR-4554 in plasma and tissues

2.1 INTRODUCTION

Substituted nitroimidazoles have a number of structural and chemical properties which are important with regard to the development of methods required to assay their levels in body fluids and pharmaceutical preparations (Grimmett, 1980; Wardman, 1985). Levels of 2-nitroimidazoles, and some of their stable metabolites, have previously been assessed by techniques such as ultraviolet spectroscopy (De Silva *et al.*, 1970), gas chromatography (Flockhart *et al.*, 1978a), high performance liquid chromatography (HPLC) (Chacon *et al.*, 1988; Flockhart *et al.*, 1978a; Flockhart *et al.*, 1978b; Middlestadt & Rauth, 1982; Workman *et al.*, 1978), polarography (De Silva *et al.*, 1970) and various radiochemical techniques (Flockhart *et al.*, 1978b; Middlestadt & Rauth, 1982; Prekeges *et al.*, 1991). Limited studies on unstable metabolites of 2-nitroimidazoles have also been carried out using electron spin resonance (ESR) techniques (Wardman, 1985).

Some of the previously reported techniques in the literature, however, are limited by sensitivity or selectivity, while others are not suitable for routine analysis. For instance, in spite of the high sensitivity associated with radiochemical methods, which employ liquid scintillation, these methods lack selectivity and will not distinguish between the parent drug and any metabolites. Radiochemical methods which employ HPLC are, however, superior to HPLC with ultraviolet (UV) detection since such techniques may still detect non-UV absorbing metabolites. Chromatographic techniques which employ mass spectroscopy detection are also useful since they provide additional information on the structure of the analytes. It should be noted, however, that radiochemical techniques (which employ liquid scintillation) lack specificity and are limited by their requirement for radiolabelled compound, whilst chromatographic techniques employing mass spectral detection are not suitable for routine analysis.

This chapter describes a sensitive and selective method for the routine detection of SR-4554 in mouse plasma and tissues as a prelude to studying the pharmacokinetics of this compound in mice. A full validation for plasma and a working method for tissues are described.

2.2 MATERIALS AND METHODS

2.2.1 Chemicals and reagents

N-(2-Hydroxy-3,3,3-trifluoropropyl)-2-(2-nitro-1-imidazolyl) acetamide (SR-4554), was synthesized (see Appendix A) and supplied by SRI International, Menlo Park, CA, USA. The internal standard used in the HPLC assay described in this chapter, 1-(2-nitro-1-imidazolyl)-3-chloro-2-propanol (Ro 07-0269), was synthesized and supplied by Roche products, Welwyn Garden City, Herts, UK. The compounds (Fig 1.3.) were assessed for chromatographic purity and used without further purification. All other reagents were HPLC or analytical reagent grade. Female Balb/c mouse plasma was obtained from Harlan Olac, Oxon, UK.

2.2.2 Preparation of calibration curve and validation standards

SR-4554 was weighed and dissolved in 1 mM Tris-HCl buffer (pH 7.4) to give a 2 mg/ml solution. Other standard stock solutions (1000, 500, 125, 50, 12.5, 5, 2.5, 1.25, 0.625, 0.3125, 0.15625, and 0.0625 $\mu\text{g/ml}$) were prepared by serial dilution in the same buffer.

The internal standard solution was prepared by dissolving Ro 07-0269 in methanol to give a 1 mg/ml solution. For the analysis of plasma samples, an aliquot (0.5 ml) of this solution was made up to 500 ml in 1 mM Tris-HCl buffer (pH 8.5) to give a final concentration of 1 $\mu\text{g/ml}$. For the analysis of tissue samples, however, an aliquot (1.25 ml) of the 1 mg/ml solution was made up to 100 ml in 0.1 M Tris-HCl buffer (pH 7.4) to give a concentration of 12.5 $\mu\text{g/ml}$.

Calibration standards were prepared by adding 20 μl of the standard stock solutions to 230 μl of mouse plasma or 10% tissue homogenates to give final drug concentrations of between 0.025 and 160 $\mu\text{g/ml}$ in plasma and 40 $\mu\text{g/ml}$ in tissues. Each concentration ($n = 13$) was prepared as a single sample, except for the lowest (0.025

µg/ml), intermediate (10 µg/ml) and highest (160 or 40 µg/ml) concentrations which were prepared in triplicate.

2.2.3 Extraction efficiency

Efficiency of the extraction process for SR-4554 from plasma and tissues were evaluated using recovery standards prepared in 1 mM Tris-HCl buffer (pH 7.4). The recovery standards contained 1 µg/ml of the internal standard (Ro 07-0269). The recovery standards (0.025 to 160 µg/ml for plasma or to 40 µg/ml for tissues) were also prepared as single samples except for the lowest (0.025 µg/ml), intermediate (10 µg/ml) and highest (160 or 40 µg/ml) concentrations which were prepared in triplicate. The overall extraction efficiency was calculated as the ratio of the slope of the plasma or tissue standard to recovery standard calibration curves.

2.2.4 Preparation of quality control (QC) samples

Quality control (QC) samples containing SR-4554 were prepared in mouse plasma as follows: QC1 blank; QC2 0.025 µg/ml; QC3 0.1 µg/ml; QC4 10 µg/ml; QC5 100 µg/ml; QC6 160 µg/ml. Aliquots (250 µl) of the QC sample were stored at -70°C until analysis.

2.2.5 Within and between day variability, freeze/thaw stability and long term stability studies.

Six quality control samples at each concentration level were thawed and analysed together with the calibration standards on day 1, to assess the within-assay (day) variability at the various levels. The between-day variability was evaluated on five separate occasions by assaying single QC samples from all the concentration levels together with fresh calibration standards. Within-day and between day variability were calculated as the percentage coefficient of variation (C.V) of the QC samples.

In addition, triplicates of freshly prepared QC samples, as well as, those subjected up to three cycles of freezing (-70°C) and thawing, were analysed to determine the ability of SR-4554 to withstand multiple cycles of freezing and thawing. The long-term stability of SR-4554 in mouse plasma was also assessed by analysing QC samples on day 1 and after storage for 32 days at -70°C.

2.2.6 Extraction of plasma and tissue samples and standards

Plasma: Aliquots (250 μ l) of 1 mM Tris-HCl buffer (pH 8.5) containing 1 μ g/ml of the internal standard (Ro 07-0269) were added to plasma samples or standards (250 μ l) and vortexed. The buffered plasma samples and standards were then applied to Bond Elut C₁₈ cartridges (100 mg, 1 ml capacity; Varian, Harbor City, CA, USA), pre-conditioned with 1 ml of methanol and 2 ml of 1 mM Tris-HCl buffer (pH 8.5). The samples were drawn through the cartridges under vacuum using a Vac Elut SPS24 (Varian) system. Plasma contaminants were eluted to waste with 1 ml of 1 mM Tris-HCl buffer (pH 8.5) and the columns dried for 5 min under vacuum. The analytes were then eluted with 1 ml of methanol-HCl (199:1).

The extracts were taken to dryness under vacuum using a vortex-evaporator (Haakebuehler Instruments, Saddle Brook, NJ, USA), at a temperature of 50°C. The dried extracts were reconstituted in 250 μ l of HPLC mobile phase, clarified by centrifugation to remove any contaminating silica resin (8 min, 2500 \times g, at 20°C) and transferred into autosampler glass inserts. Aliquots (200 μ l) of these samples were then injected into the chromatograph. All solvents used for the extraction of the plasma samples and standards were filtered (0.45 μ m Teflon PTFE-polypropylene filter membranes) and degassed with helium.

Tissues: As part of method development, 30% w/v silver nitrate (AgNO₃; 1:10), ice cold methanol (1:1) and ice cold acetonitrile (1:1) were tested as protein precipitants for SR-4554 containing tissue homogenates. The precipitants were added to 250 μ l of the tissue samples, containing standards and 20 μ l of the internal standard solution (12.5 μ g/ml). The samples were then vortexed and centrifuged (2000 \times g) for 5 min. Aliquots (50 μ l) of the supernatant obtained from these samples were then analysed by HPLC.

2.2.7 HPLC methodology

All extracts were analysed using a Walters chromatographic system (Millipore, Milford, MA, USA) consisting of a WISP Model 712 autosampler, a Model 660 gradient controller with a quaternary HPLC pump, a Model 991 photodiode-array detector and a NEC Powermate

SX/16 personal computer running the Walters 991 photodiode array software.

Separation of analytes were performed on a μ -Bondapak C₁₈ (10 μ m, 300 \times 3.9 mm) analytical column (Millipore) at ambient temperature. The analytical column was protected from contamination by a pellicular ODS pre-column (Anachem, Luton, UK). The mobile phase which comprised methanol-water (15:85), was filtered through a 0.45 μ m Teflon PTFE-polypropylene filter membrane, degassed with helium, and delivered isocratically at a flow-rate of 2 ml/min. Column effluents were monitored by UV-photodiode-array detection at 324 nm and the peak area ratio of SR-4554 to internal standard (Ro 07-0269) used for conversion of the detector response to concentration estimates. The column performance in the assay was determined by measuring the efficiency or height equivalent to a theoretical plate (HTEP), the symmetry factor (SF), and the resolution (R) between drug and internal standard using the standard equations below (Davidson, 1988):

$$HTEP = \frac{L}{5.54(t_R/W_{1/2})^2}$$

$$SF = \frac{y_x}{2A}$$

$$R = \frac{2(t_{Rb} - t_{Ra})}{W_a - W_b}$$

where L , t_R , $W_{1/2}$, y_x , A , t_{Rb} , t_{Ra} , W_a , and W_b are defined as length of column, retention time, peak width at half peak height, peak width at one-twentieth of the peak height, distance between the perpendicular dropped from the peak maximum and the leading edge of the peak at one-twentieth of the peak height, retention time of second peak, retention time of the first peak, peak width of the first peak, and peak width of the second peak respectively (Davidson, 1988).

2.2.8 Mass spectral (MS) analysis

Prior to analysis by MS, plasma samples containing SR-4554 were separated on a column as above, and the peak corresponding to SR-4554 collected using a Walters fraction collector (Millipore). Both the SR-4554 fractions which were evaporated to dryness under nitrogen gas, as well as authentic samples of SR-4554, were dissolved in a minimum amount of dichloromethane-methanol mixture (5:1). Aliquots (20 μ l) were injected into a JEOL JMS-AX505HA (JEOL, Tokyo, Japan) MS in direct inlet mode. The mass spectrometer was operated at an accelerating potential of 3 kV (voltage 200 eV) in the positive ion chemical ionisation mode using methane gas.

2.2.9 Statistical analysis

The statistical analysis of the results were generated using Minitab Release 9 (Minitab, State College, PA, USA) and Microsoft Excel Version 4.0 (Microsoft, Redmond, WA, USA). The assay precision was defined as the coefficient of variation C.V. (%) for each concentration level. This was calculated as the ratio of the standard deviation to the mean expressed as a percentage. The accuracy was defined as the mean % difference (% deviation) from the given or nominal concentration. The minimum quantifiable level (MQL) was defined as the lowest concentration of analyte which could be accurately and reproducibly measured.

The following acceptance criteria were used to evaluate the data:

1. p -values for all statistical tests be < 0.05 .
2. the within/between assay variability be within 15%.
3. 75% of all QC samples analysed be within 15% of their respective nominal values.
4. the correlation coefficient (r) of calibration curves be ≥ 0.98 .
5. the C.V. for the lowest, intermediate and highest levels within individual calibrations be within 15%.

2.3 RESULTS

2.3.1 Chromatography

Plasma: Analysis of plasma samples and standards showed that the assay which was developed in this thesis was suitable for the detection and quantitation of SR-4554. A typical chromatogram of

SR-4554 and internal standard is illustrated in Fig. 2.1. No drug-related metabolites or interfering peaks were observed on analysis of the plasma samples and standards. The chromatographic analysis was rapid allowing separation of SR-4554 and internal standard (Ro 07-0269) within 10 min. The retention times of these compounds were 5.8 and 7.4 min, respectively, and the two peaks were completely resolved (resolution, $R = 1.4$). Typical column efficiencies (HETP) were 0.28 mm and 0.14 mm for SR-4554 and internal standard (Ro 07-0269), respectively. In addition symmetry factors were calculated to be 1.09 and 1.12, respectively. Both SR-4554 and the internal standard (Ro 07-0269) had similar UV-spectral properties with a λ_{\max} (for both compounds) of 324 nm (Fig. 2.2).

Tissues: Similar chromatograms as for plasma were obtained when tissue samples were analysed. Fig. 2.3 shows the chromatograms obtained by extracting 10% tumour homogenates with different precipitants. All precipitants showed good recovery (Table 2.1) and low background interference. Silver nitrate precipitation was, however, twice as sensitive as the other two methods tested. The optimal volume of silver nitrate (30% w/v) used was 25 μ l per 250 μ l of tissue homogenates (1:10). Fig. 2.4 illustrates a typical chromatogram of SR-4554 the extracted from liver and brain homogenates using the conditions described in section 2.2.6. The recovery of SR-4554 from these tissues is also presented in Table 2.1.

2.3.2 Mass spectral (MS) analysis

In addition to UV-spectra, the identity of SR-4554 extracted from plasma was also confirmed by MS in positive ion chemical ionisation mode (Fig. 2.5). As indicated in Fig. 2.5, the most intense m/z ratios were obtained from the protonated molecular ion ($M + 1$) peak and another peak corresponding to ($M - \text{NO}_2$). Methane adducts such as ($M + \text{C}_2\text{H}_5$) were also observed.

2.3.3 Validation

The assay of SR-4554 in mouse plasma using solid phase extraction and HPLC was reproducible at all concentration levels (Table 2.2), with all C.V.'s within the accepted limit of 15%. The MQL was validated at 25 ng/ml (on-column concentration of 5 ng) with a C.V. of 6.0%.

Fig. 2.1. A typical chromatogram obtained from a plasma extract. Aliquots (250 μ l) of plasma samples containing SR-4554 (4 μ g/ml) were extracted with internal standard (I.S.; Ro 07-0269) using a C₁₈ solid phase cartridge and analysed by HPLC as described in section 2.2.7.

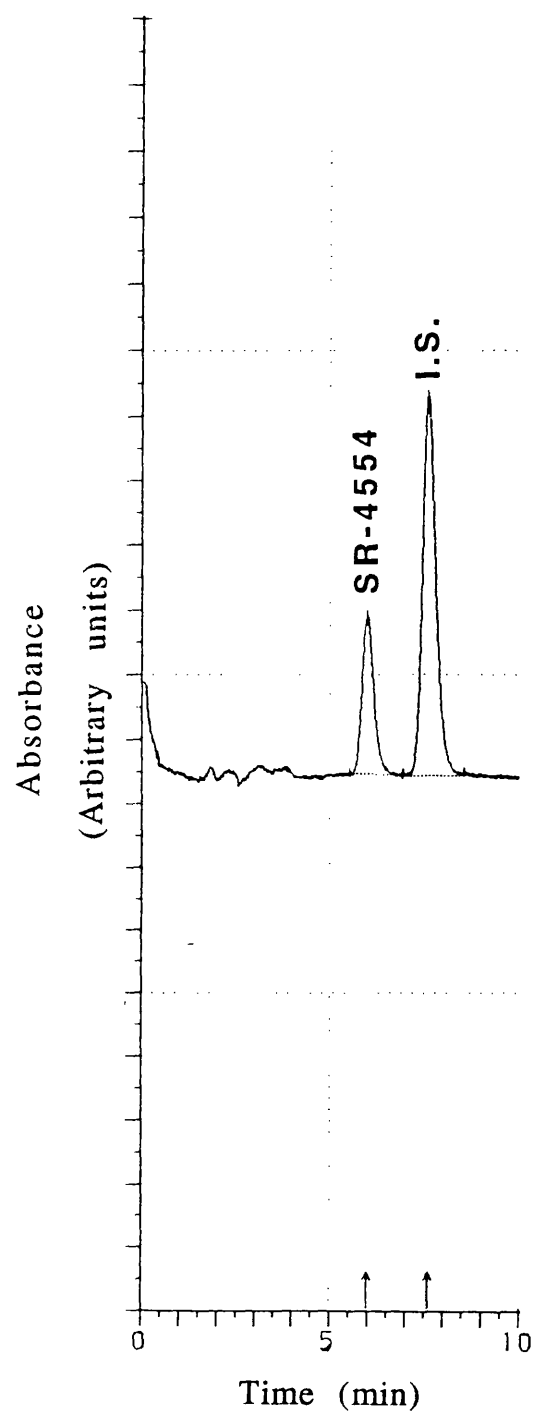


Fig. 2.2. UV-spectra of SR-4554 and internal standard (Ro 07-0269) in HPLC mobile phase using photodiode array detection. Spiked plasma samples of SR-4554 and internal standard were extracted, as described in section 2.2.6, and the UV-spectra of the compounds obtained using a Waters photodiode array detection. The λ_{max} for both compounds was 324 nm.

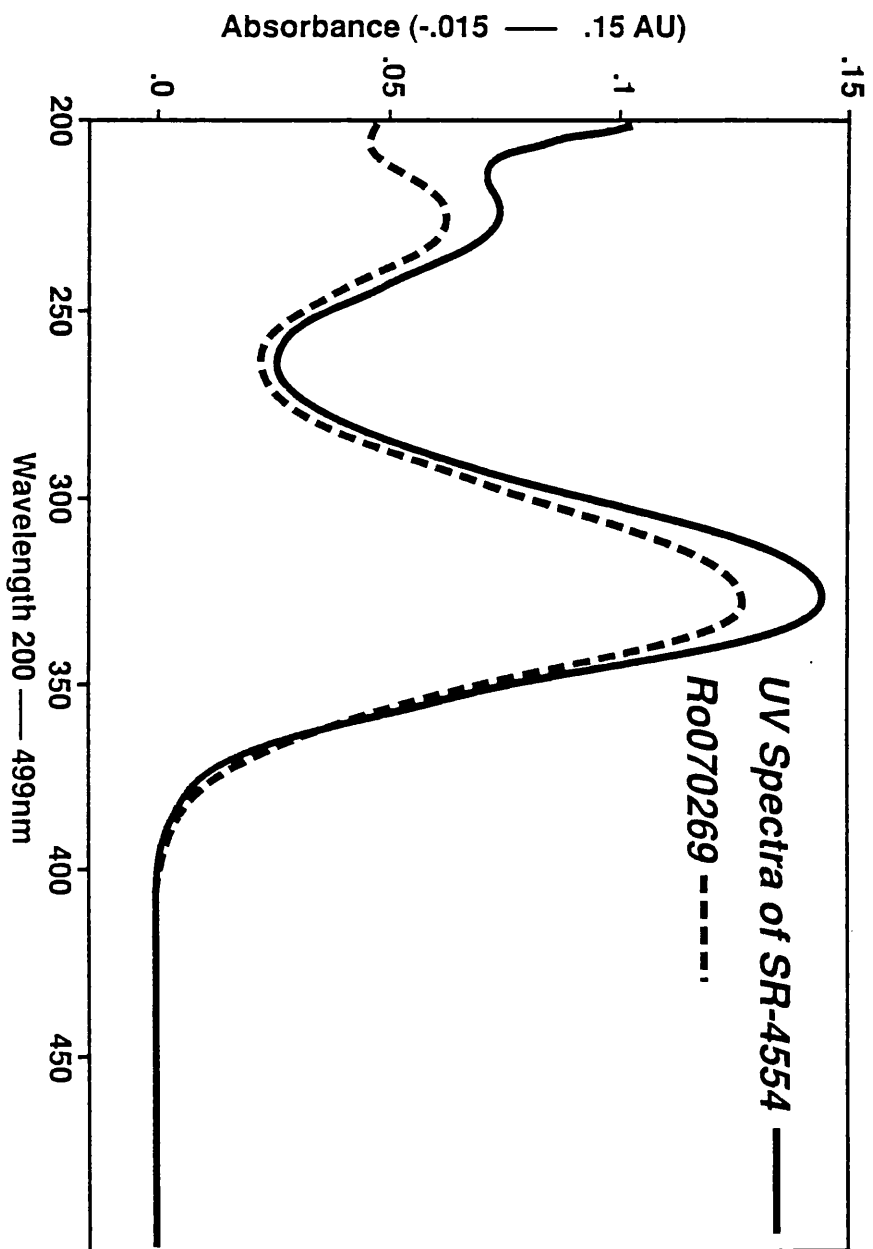


Fig. 2.3. Typical chromatograms of SR-4554 (4 $\mu\text{g/ml}$) and internal standard (I.S.) obtained from 0.1 M Tris-HCl buffer (pH 7.4) and 10% tumours homogenates using different protein precipitation techniques as described in section 2.2.6. The chromatograms represent (a) unextracted, (b) 30% w/v silver nitrate (1:10) extract, (c) methanol (1:1) extract, and (d) acetonitrile (1:1) extract.

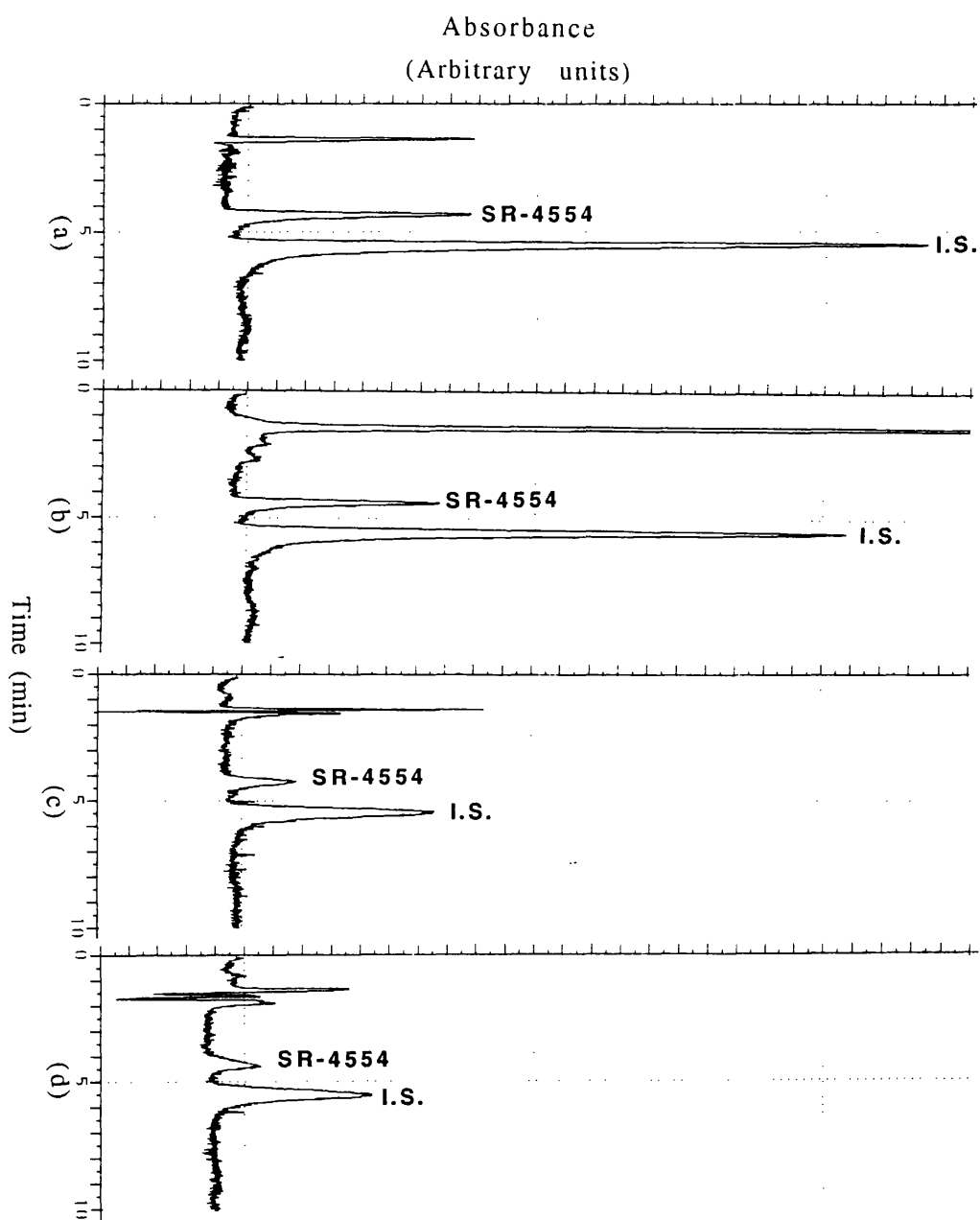


Table 2.1. Recovery of SR-4554 from tissue homogenates using different clean-up techniques.

Tissue	Precipitant	Mean Recovery (%)	s.d.
Tumour	Methanol	90.6	0.2
Tumour	Acetonitrile	91.9	0.3
Tumour	Silver nitrate	97.4	0.2
Liver	Silver nitrate	94.8	0.2
Brain	Silver nitrate	96.0	0.1

The concentration of SR-4554 present in each tissue homogenate was 4 µg/ml. Four determinations were made for each tissue.

Fig. 2.4. Chromatograms of SR-4554 (4 $\mu\text{g/ml}$) and internal standard (I.S.) obtained by silver nitrate (30% w/v; 1:10) extraction of 10% liver (a), and brain (b) homogenates spiked with SR-4554.

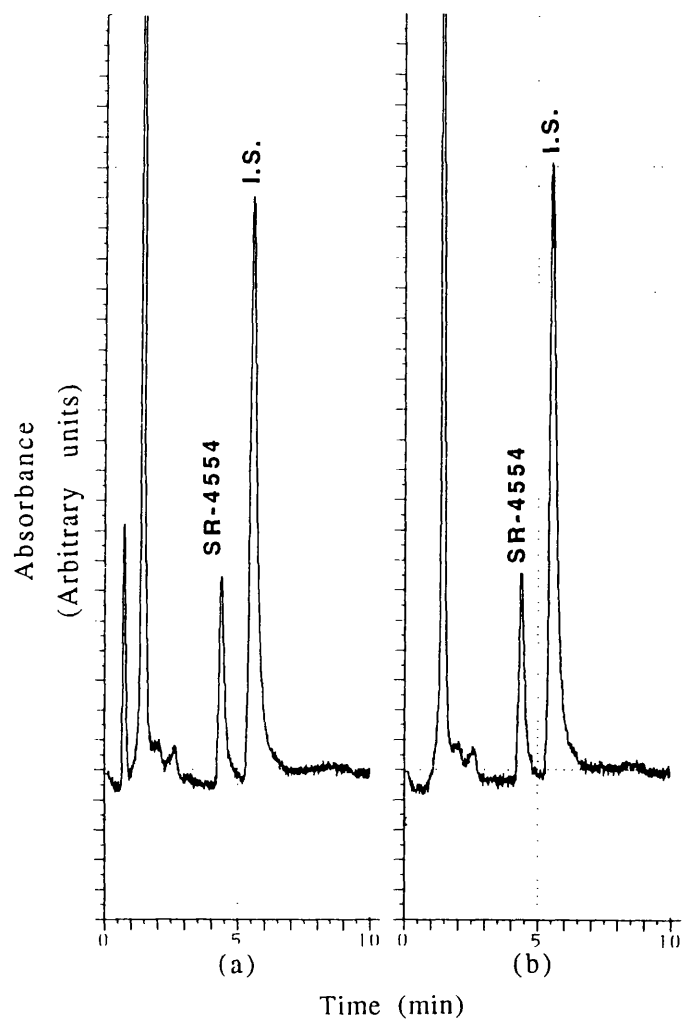


Fig. 2.5. Positive ion chemical ionisation spectrum of SR-4554. The spectrum was determined as described in section 2.2.8, and shows the protonated molecular ion peak ($M + 1$), as well as, other peaks corresponding to ($M - NO_2$), and methane adduct ($M + C_2H_5$).

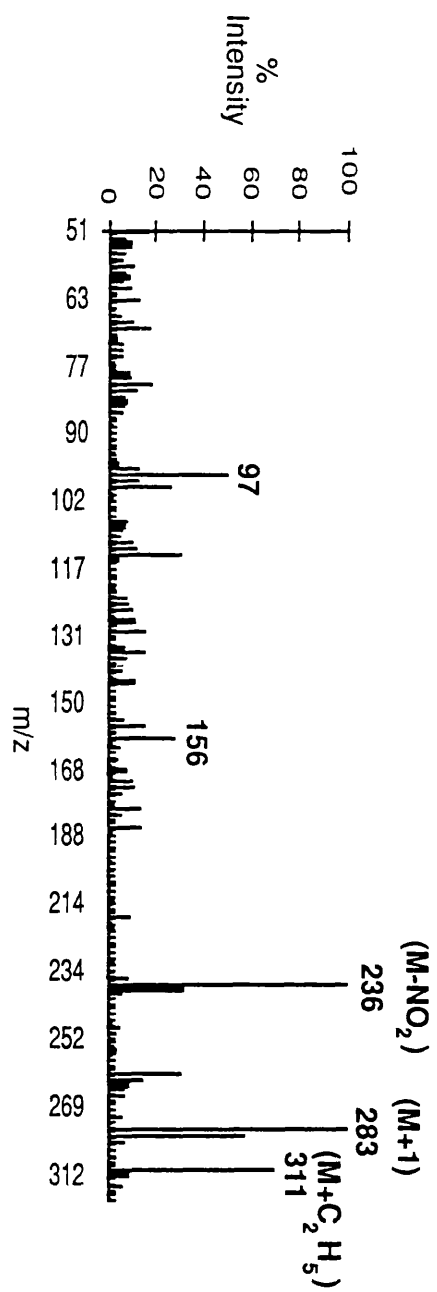


Table 2.2. Within and between day variability of the HPLC assay for SR-4554 at six different drug concentrations.

Within day variability

QC	GIVEN CONC.	CALCULATED CONC. ($\mu\text{g/ml}$)		
	($\mu\text{g/ml}$)	mean	%C.V.	%Deviation
1	Blank	-	-	-
2	0.025	0.02	6.0	1.2
3	0.1	0.1	4.0	6.7
4	10	10.2	3.3	1.9
5	100	96.4	3.3	-3.6
6	160	148.9	1.5	-6.9

Between day variability

QC	GIVEN CONC.	CALCULATED CONC. ($\mu\text{g/ml}$)		
	($\mu\text{g/ml}$)	mean	%C.V.	%Deviation
1	Blank	-	-	-
2	0.025	0.02	11.9	-3.8
3	0.1	0.1	3.9	11.2
4	10	9.8	6.5	-2.9
5	100	97.1	6.3	-2.9
6	160	147.2	3.8	-8.0

Plasma samples were determined in each case as described in section 2.2.5.

Weighted calibration curves (weight = $1/y^2$) for SR-4554 were found to be linear over the concentration 0.025-160 $\mu\text{g/ml}$ and had near zero intercepts. For instance, the calibration curve for the peak area ratio of SR-4554 to internal standard vs concentration of SR-4554 used in the determination of within assay variability had a slope of 0.6 and an intercept of 0.013 ($r = 0.99$; s.d. = 0.03).

The recovery of SR-4554 from mouse plasma was determined from the slopes of the extracted standards vs recovery standards (Fig. 2.6). The mean recovery from four determinations was found to be $81.1 \pm 6.9\%$ (C.V. = 8.6%), whilst the recovery of the internal standard at a single concentration of 1 $\mu\text{g/ml}$ was 80.6 ± 3.8 (C.V. = 4.7%).

Table 2.3 summarizes the freeze thaw and long term stability of SR-4554 in mouse plasma. SR-4554 was stable up to three cycles of freezing and thawing as well as to storage at -70°C for 32 days.

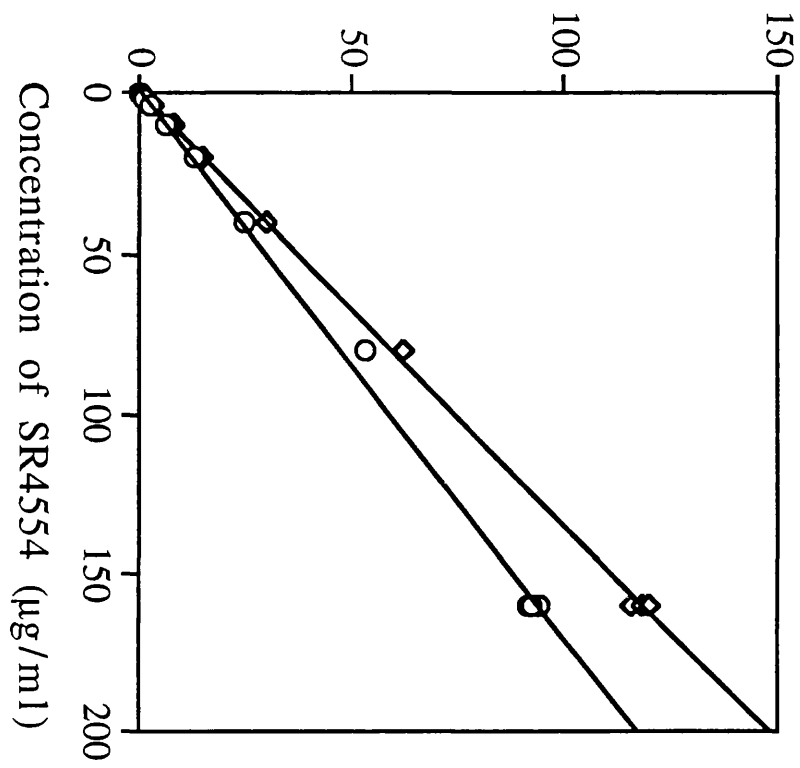
2.4 DISCUSSION

A rapid and sensitive HPLC method has been developed for the determination of SR-4554 in small volumes (250 μl) of mouse plasma and tissues. The method for extraction of plasma employs a semi-automated solid-phase extraction procedure followed by a fully automated HPLC assay. Extraction of tissues involved a simple protein precipitation using silver nitrate which was found to be superior to ice cold methanol and acetonitrile in terms of sensitivity. A run time of 10 min for both plasma and tissues allow several samples to be routinely analysed over a relatively short period of time. Both SR-4554 and the internal standard (Ro 07-0269) had similar UV-spectra, which made it possible to monitor the elution of analytes at a single wavelength of 324 nm, representing the λ_{max} of both compounds. The sensitivity of the assay described here (25 ng/ml for plasma and 100 ng/ml for tissues) is much better than that for most 2-nitroimidazoles reported to date (De Silva *et al.*, 1970; Flockhart *et al.*, 1978a; Workman *et al.*, 1978). The assay is also highly specific and sufficiently reproducible for routine use. The specificity of the assay was confirmed by UV-spectra and mass spectral analysis.

Although the parent drug was readily detected, it should be noted that no metabolites of SR-4554, be it degradation or bio-reduced products, were observed in plasma or tissue samples. Although this

Fig. 2.6. Recovery of SR-4554 from mouse plasma. The regression lines represent unextracted and extracted SR-4554 at different concentrations. The recovery or extraction efficiency was the ratio of the slopes of the extracted to unextracted regression lines.

SR4554/I.S.
Peak area ratio



○ Extracted standards
◇ Recovery standard

Table 2.3. Freeze-thaw and long-term stability of SR-4554 in mouse plasma.

	Mean conc. (μ g/ml)	%Deviation	%C.V.
--	-----------------------------	------------	-------

Freeze-thaw stability

Fresh	10.3	2.8	1.4
Cycle 1	10.1	1.1	2.4
Cycle 2	10.3	2.7	1.6
Cycle 3	10.2	1.9	3.9

Long-term stability

Day 1	10.6	5.9	2.5
Day 32	11.5	14.9	1.9

Plasma samples were determined as in section 2.2.5.

assay is specific for an intact nitroimidazole chromophore, the analysis of samples at other wavelengths, and also with MS, did not give any indication of the presence of any SR-4554 metabolites. There are, however, obvious limitations to this assay. In particular, this technique will be unable to detect bio-reduced metabolites in free or bound form (i.e. bound to macromolecules) due to loss of the characteristic UV-chromophore of the nitroimidazoles. The absence of degradation products, however, is an important property with respect to the use of SR-4554 as an MRS probe for tumour hypoxia, since the side chain containing the fluorine label is stable to *in vivo* metabolic processes other than nitroreduction.

SR-4554 and internal standard (Ro 07-0269), the only analytes observed by the HPLC method developed in this chapter, were completely resolved ($R > 1.0$). Due to slight peak tailing, however, peak areas instead of peak heights were used in the quantitation of the drug and internal standard peaks (Davidson, 1988). The recovery of SR-4554 from both plasma and tissues using this HPLC assay was found to be high and reproducible. In addition, the within- and between day variability of the assay, as well as the accuracy of determining SR-4554 were found to be within 15%. The results of the stability studies also showed that, plasma samples of SR-4554 were stable for up to three cycles of freezing and thawing, as well as to storage at -70°C for up to 32 days.

In an attempt to develop a suitable rapid and sensitive method for the analysis of SR-4554 in mouse plasma, other techniques were investigated. One such method, which involved a methanol extraction step and UV-HPLC analysis, offered good sample clean-up but had low sensitivity (MQL = 200 ng). In addition, an unsuccessful attempt was made to develop an HPLC technique with fluorescent detection for SR-4554, in spite of its good fluorescent properties ($\lambda_{\text{excitation}} = 272 \text{ nm}$; $\lambda_{\text{emission}} = 371, 546 \text{ nm}$). A solid phase extraction with UV detection was ultimately employed with an increase in sensitivity. Various sorbents such as C_{18} , C_8 , propylsulfonic acid (PRS) and benzenesulfonic acid (SCX) were tested for their ability to retain and release the drug at various pH values in Tris-HCl buffer. The elution capabilities of other solvents such as methanol and acetonitrile were also tested. C_{18} cartridges proved superior to other sorbents due to good sample retention, recovery and low background interference, without

resorting to solvents which could affect the stability of the drug or sorbent. The reconstitution of the extract in HPLC mobile phase, prior to analysis by HPLC, allowed a high injection volume to be used without a significant compromise in the efficiency of the chromatographic separation.

The HPLC method developed in this chapter has been designed to be suitable for studying the pharmacokinetics of SR-4554 in mice (chapter 5). This HPLC assay can also been applied to the analysis of other 2-nitroimidazole, either directly or with slight modifications in mobile phase composition (chapter 5). Finally, it would be expected that this HPLC assay developed here would form the basis for the analysis of SR-4554 during its anticipated clinical use as a non-invasive MRS probe for tumour hypoxia.

CHAPTER 3

Metabolism of 2-nitroimidazoles

3.1 INTRODUCTION

As described in section 1.5, nitroreduction is an important mechanism for the hypoxia selective tumour retention and cytotoxicity of these nitroimidazoles. A wide variety of enzymes including NADPH: cytochrome P450 reductase, NADPH: cytochrome P450, xanthine oxidase, DT-diaphorase and aldehyde dehydrogenase can potentially act as nitroreductases, although many of these appear to have quite low substrate specificities for the reduction of 2-nitroimidazoles (Workman, 1992). The major membrane-bound microsomal nitroreductases in liver are NADPH: cytochrome P450 reductase and NADPH: cytochrome P450 (Feller *et al.*, 1971). These enzymes have been implicated in the metabolism of 2-nitroimidazoles in murine tumours and cell lines (Joseph *et al.*, 1994; Walton & Workman, 1987). In their study, Walton and Workman showed that the loss of benznidazole was dependent on NADPH: cytochrome P450 reductase levels, while formation of its amine metabolite was dependent on both NADPH: cytochrome P450 reductase and NADPH: cytochrome P450 levels. Joseph *et al.* (1994) on the other hand, transfected monkey kidney cells with recombinant plasmids in order to effect intracellular overexpression of NADPH: cytochrome P450 reductase and DT-diaphorase. An increase (5-7 fold) in metabolic binding of 2-nitroimidazoles was demonstrated in the NADPH: cytochrome P450^{reductase} line (80 fold increased activity), whereas the DT-diaphorase line only showed a small (1.5 fold) increase in metabolic binding of 2-nitroimidazoles, in spite of the (1000 fold) increased activity of DT-diaphorase in this line (Joseph *et al.*, 1994). From their data Joseph *et al.* (1994) also suggested that a tissue's capacity for binding 2-nitroimidazole drug under hypoxia should be proportional to the square root of its intracellular NADPH: cytochrome P450 reductase activity. Interestingly, both Walton (1987) & Workman and Joseph *et al.* (1994) showed that, xanthine oxidase was an inefficient reductase for 2-nitroimidazole reduction. These studies have therefore demonstrated that NADPH: cytochrome P450 reductase is probably the most important reductive enzyme for 2-nitroimidazoles, and that DT-diaphorase and xanthine oxidase do not

play a major role in this reductive metabolism. Using purified butter milk xanthine oxidase, however, Prekeges *et al.* (1991) have demonstrated the capability of this cytosolic nitroreductase to reduce the 2-nitroimidazole fluoromisonidazole.

Different methods have been used to characterise the reductive metabolism of 2-nitroimidazoles. In this regard, radiochemical methods have the ability to measure levels of 2-nitroimidazole adducts in the acid insoluble fraction of incubates (Joseph *et al.*, 1994; Mcmanus *et al.*, 1982). HPLC with UV-detection, as well as direct UV-spectrometric methods can measure either the loss of parent drug (loss of the nitro chromophore) or the formation of the amine metabolites (Prekeges *et al.*, 1991; Walton & Workman, 1987). Although loss of parent drug and adduct or amine formation do not occur at similar rates, both processes occur as a function of enzyme levels and oxygen content and can be used to characterise 2-nitroimidazoles equally well.

In this chapter the metabolism of SR-4554 has been characterised using mouse liver microsomes, tumour homogenates and purified rat and human NADPH: cytochrome P450 reductase enzyme. An HPLC method has been employed and loss of parent drug monitored. In addition, and for the first time, a high resolution ^{19}F NMR technique has been implemented to study metabolite formation in a series of 2-nitroimidazoles. Finally, the activity of NADPH: cytochrome P450 reductase enzyme in a panel of human and murine tumour xenografts has been determined in order to ascertain the capability of these tumours to reduce 2-nitroimidazoles. The results of these studies are important to the interpretation of MRS studies in chapter 6, where the oxygenation status of these same tumours have been evaluated using SR-4554.

3.2 MATERIALS AND METHODS

3.2.1 Chemicals and reagents

The structures of the 2-nitroimidazoles used in this chapter including SR-4554, CCI-103F, Ro 07-2044, KU-2285 and fluoromisonidazole (Ro 07-0741), are shown in Fig. 1.3. trifluoropropanal and fluoromisonidazole were obtained from Roche products, Welwyn Garden City, Herts, UK. CCI-103F was obtained from Dr. J. Raleigh, Cross Cancer Institute, Edmonton, Canada. KU-

2285 was obtained from Dr. S.-I. Nishimoto, Department of Hydrocarbon Chemistry, Kyoto University, Kyoto, Japan. The compounds were assessed for chromatographic purity and used without further purification. Thallium chloride ($\text{TlCl}_3 \cdot 4\text{H}_2\text{O}$), cytochrome c, bovine albumin and NADPH were obtained from Sigma Chemical Co. (Dorset, UK). The Biorad protein assay kit was obtained from BIORAD Laboratories (Hertfordshire, UK). Purified rat and human NADPH: cytochrome P450 reductase protein were obtained from Prof. C.R. Wolf (ICRF Laboratory of Molecular pharmacology, Dundee, UK). Zero grade N_2 gas, as well as, various gas mixtures of oxygen in N_2 were obtained from Air Products Ltd., Glasgow, UK. All other reagents were analytical or HPLC grade.

3.2.2 Experimental animals and tumours

Mice used in this chapter were obtained either from Harlan Olac Ltd., (Oxon, UK) or from the Department of Experimental Clinical Oncology, University of Aarhus, Aarhus, Denmark. Tumours (Table 3.1) were free from mycoplasma and grown subcutaneously on the flank of the various mice. All human tumour xenografts were passaged from *in vitro* culture at a cell concentration of 10^6 cells in 0.1 ml. KHT tumours were passaged as tumour pieces of approximately 1 mm in diameter. The remaining murine tumours were passaged from *in vitro* culture at a cell concentration of approximately 2×10^5 cells in 0.1 ml. Tumours ranged between 200 and 500 mm^3 at the time of the experiment. Liver microsomes and S9 were specifically prepared from male Balb/c mice.

3.2.3 Preparation of mouse liver microsomes, S9 fraction and tumour samples

All tissues (livers and tumours) were excised rapidly and snap frozen prior to analysis. S9 fractions and microsomes were prepared according to the methods of Omura and Sato, 1964 (Omura & Sato, 1964a). Briefly, tissues were homogenised in an equivalent volume of 50 mM Tris-150 mM KCl-HCl buffer, (pH 7.4). The homogenates were initially centrifuged ($10,000 \times g$ for 30 min) at 4°C to remove nuclei, mitochondria and cell debris. The supernatant obtain from this initial centrifugation step was the S9 fraction. To obtain microsomes, the S9 fraction, was further centrifuged at $100,000 \times g$ for 1 hr (4°C). The

Table 3.1. Sources and characteristics of cell lines used in this chapter.

CELL LINE	MOUSE STRAIN	HISTOLOGY	SOURCE
<i>Murine</i>			
RIF-1 ^a	C3H	Fibrosarcoma	St. George's Hospital Medical School, London, UK
SCCVII ^a	C3H	Squamous cell carcinoma	MRC Radiobiology Unit, Didcot, UK
KHT	C3H	Fibrosarcoma	MRC Radiobiology Unit, Didcot, UK
EMT6	Balb/c	Adenocarcinoma	MRC Clinical Oncology Unit, Cambridge, UK
C3H	CDF ₁	Carcinoma	University of Aarhus, Aarhus, Denmark
<i>Human</i>			
HT-29	MF1 <i>nu-nu</i>	Colon carcinoma	Imperial Cancer Research Fund, Edinburgh, UK
BE	MF1 <i>nu-nu</i>	Colon carcinoma	University of Southern California, L.A., USA
WIL	MF1 <i>nu-nu</i>	Non-small cell lung carcinoma	Institute for Cancer Research, Sutton, UK
HN5	MF1 <i>nu-nu</i>	Squamous cell carcinoma (H&N)	Institute for Cancer Research, Sutton, UK

^a Tumours were also obtained from the University of Aarhus, Aarhus, Denmark.

pellet obtained by this process was resuspended and recentrifuged ($100,000 \times g$ for 1 hr) at 4°C . Samples were kept on ice throughout the experiment in order to avoid loss of enzyme activity. The pellet obtained from this final centrifugation step, as well as the S9 fractions were stored at -70°C prior to use. Reconstituted microsomes, and S9 fractions, could be stored at -70°C for up to 6 weeks without loss of activity. To study the *in vitro* metabolism of SR-4554 by tumour homogenates, SCCVII tumours were homogenised in an equal volume of 0.1 M Tris-HCl buffer (50% w/v) and the homogenate used directly without further treatment.

3.2.4 Protein and enzyme assay

The protein concentrations of microsomes and S9 fractions were assayed by a Biorad protein assay kit which measures the absorbance at 595 nm of an acidic solution of Coomassie Blue-protein complex (Bradford, 1976; Spector, 1978). Bovine albumin was used as standard.

Tissue NADPH: cytochrome P450 reductase activity was determined by measuring the reduction of cytochrome c at 550 nm (Masters *et al.*, 1967). In addition, the NADPH: cytochrome P450 activity in liver microsomes was determined by difference spectroscopy as described by Omura and Sato (Omura & Sato, 1964a; Omura & Sato, 1964b).

3.2.5 Characteristics of reductive metabolism of SR-4554

Incubation mixtures

SR-4554 ($50 \mu\text{M}$) was metabolised *in vitro* (at 37°C) by 2 mg/ml mouse liver microsomes in the presence of excess cofactor (5 mM NADPH) and under hypoxia (N_2 gas) in a total volume of 3 ml. Each hypoxic incubation was preceded by pre-incubation of microsomes, cofactor, and buffer (0.1 M Tris-HCl, pH 7.4) with N_2 for 8 min. Inhibitory studies were carried out using 0.2 mg/ml $\text{TiCl}_3 \cdot 4\text{H}_2\text{O}$ (an inhibitor of NADPH: cytochrome P450 reductase), carbon monoxide (an inhibitor of NADPH: cytochrome P450) and air.

The effect of microsomal protein concentration on the metabolism of SR-4554 ($50 \mu\text{M}$) was studied at 0.2 to 8 mg/ml protein. On the other hand, the effect of substrate (SR-4554)

concentration on microsomal metabolism was studied at a microsomal protein concentration of 2 mg/ml. In this study, substrate concentrations ranged between 0.05 and 4 mM. Microsomal metabolism of SR-4554 (50 μ M) was also performed with different gas mixtures of oxygen in N₂ (20.9, 5, 1, 0.7, 0.4, 0.2, 0.1, 0.01, and 0% oxygen) to evaluate the oxygen dependence of metabolism.

Purified enzyme

Reduction of 50 μ M SR-4554 under hypoxia by both purified human and rat NADPH: cytochrome P450 reductase was carried out as above. In place of microsomal protein, however, 1.3 U/ml (1U = 1 μ mol cytochrome c reduced/min/mg protein measured at 37°C) of purified rat or human cytochrome P450 reductase and 5 mg/ml bovine albumin were used. This reaction was also carried out in the presence of 0.2 mg/ml TiCl₃.4H₂O.

Tumour homogenate

The reduction of 50 μ M SR-4554 by tumour homogenates was also investigated as above. As a typical example, SCCVII tumours were used in order to show that tumours could reduce SR-4554. In this case, however, 50% w/v SCCVII tumour homogenate in 0.1 M Tris-HCl buffer (pH 7.4) was used as the enzyme source and as previously described by Walton & Workman (1987). Specifically, 800 μ l of the tumour homogenate was used per 3 ml of the incubation mixture. This reaction was also carried out in the presence of 0.2 mg/ml TiCl₃.4H₂O.

HPLC analysis

To assess the reductive metabolism (loss) of parent drug, 250 μ l of the incubation mixture was withdrawn at 0, 3, 6, 9, 12 and 15 min into Eppendorf tubes containing the internal standard Ro 07-0269 (Fig. 1.3). The incubation samples were immediately extracted with 30% w/v silver nitrate (25 μ l) and kept on ice prior to analysis. Aliquots (50 μ l) of the samples were analysed by HPLC as previously described in section 2.2.7.

3.2.6 Identification of reductive metabolites of 2-nitroimidazoles by high resolution ¹⁹F NMR

To evaluate the formation of hypoxia dependent metabolites, SR-4554 (250 μ M) was incubated under hypoxia with excess cofactor (5 mM NADPH) and 2 mg/ml mouse liver microsomes as described

above. At 5, 15, and 30 min, 0.7 ml of the incubation mixtures were withdrawn and immediately kept on ice. Samples were spiked with 125 μ M CCI-103F (Fig. 1.3; as an internal standard and chemical shift reference), freeze-dried and reconstituted in 0.7 ml D₂O for nuclear magnetic resonance (NMR) analysis. High resolution ¹⁹F NMR analysis was carried out on a Bruker AM 200 (Aspect 3000), 200 MHz NMR system using a total of 2048 scans and operating in ¹H decoupled mode at 25°C. As part of the study, samples were also extracted with 30% w/v silver nitrate (1:10 v/v) or filtered through an ultrafiltration membrane with a cut-off of approximately 30,000 (Amicon Div., W.R. Grace & Co., Danvers, MA, USA) prior to freeze drying and analysis. Due to the better clean-up and hence higher achievable concentrations of analytes with the silver nitrate precipitation, subsequent experiments were carried out using this precipitation step.

The hypoxia dependent metabolism of a series of fluorinated 2-nitroimidazoles including CCI-103F, Ro 07-2044, KU-2285 and fluoromisonidazole (Fig. 1.3), was also investigated with high resolution NMR. In each case samples were incubated with 2 mg/ml mouse liver microsomes and 5 mM NADPH for 30 min. In parallel studies, the same incubation mixtures were also extracted and analysed by HPLC. HPLC analysis of Trifluoropropanal, KU-2285 and fluoromisonidazole were similar to that described in section 2.2.7. On the other hand, CCI-103F was analysed using a modification of the method described by Walton & Workman (1987) for benznidazole. In this latter method, analytes were separated on a C₁₈ column with a mobile phase comprising of 25% acetonitrile/0.2 M glycine-HCl buffer (pH 2.5) and/5 mM octane sulphonic acid. The mobile phase was delivered at a flow rate of 3 ml/min and column effluents monitored by UV-detection at 324 nm.

3.2.7 *In vivo* reductive metabolism of SR-4554 analysed by high resolution ¹⁹F NMR

EMT6 tumour bearing female Balb/c mice were injected i.p. with 180 mg/kg (0.06 ml/g) of SR-4554 prepared in saline. Liver, brain and tumour samples were excised and snap frozen at 15 min, 4 hr and 6 hr post-injection of SR-4554. Three mice per time point were used and 10 ml of pooled tumour homogenates (10% w/v) were

extracted with 30% w/v AgNO₃ (1:10 v/v), freeze-dried and reconstituted in 0.7 ml D₂O. The samples were then analysed by ¹⁹F NMR (using 25,000 scans) to determine the presence and extent of hypoxia dependent metabolism *in vivo*.

3.2.8 Statistical analysis

The kinetic parameters, apparent K_m and apparent V_{max} were generated using an enzyme kinetic application programme (EnzymeKinetics, Version 1.11; Trinity Software, Campton, NH, USA). Modelling of rate of reduction vs oxygen tension was carried out using GraphPAD Inplot, Version 3.14 (GraphPAD Software Inc., San Diego, CA, USA). All other statistical parameters were generated using either Minitab Release 9 (Minitab, State College, PA, USA) or Microsoft Excel, Version 4.0 (Microsoft, Redmond, WA, USA).

3.3 RESULTS

3.3.1 Enzyme activity

The level of NADPH: cytochrome P450 in the liver microsomes as determined by difference spectroscopy was 1.03 ± 0.1 nmol/mg. The activity of NADPH: cytochrome P450 reductase in the microsomes and S9 fractions were measured by a UV spectrophotometric method to be 231 ± 11 and 121 ± 26 nmol cytochrome c reduced/min/mg protein respectively (mean \pm s.d.; n = 3). NADPH: cytochrome P450 reductase activity was also measured in S9 fractions of a panel of human and murine tumour xenografts which were used in MRS studies (section 6.2). Table 3.2 indicated, in general, that the activity of NADPH: cytochrome P450 reductase were low and only varied by about 3 fold between different tumour types. Interestingly, the levels also varied within tumour types as shown by the standard errors in the measurements.

3.3.2 Characteristics of reductive metabolism

SR-4554 was reduced by NADPH: cytochrome P450 and NADPH: cytochrome P450 reductase containing mouse liver microsomes under hypoxia. This was assessed by measuring parent drug loss with time by HPLC. Fig. 3.1 illustrates typical chromatograms obtained from the incubation of SR-4554 with mouse liver microsomes under hypoxic conditions. SR-4554 concentrations were calculated from peak area

Table 3.2. NADPH Cytochrome P450 reductase activities in a panel of murine and human tumour xenografts.

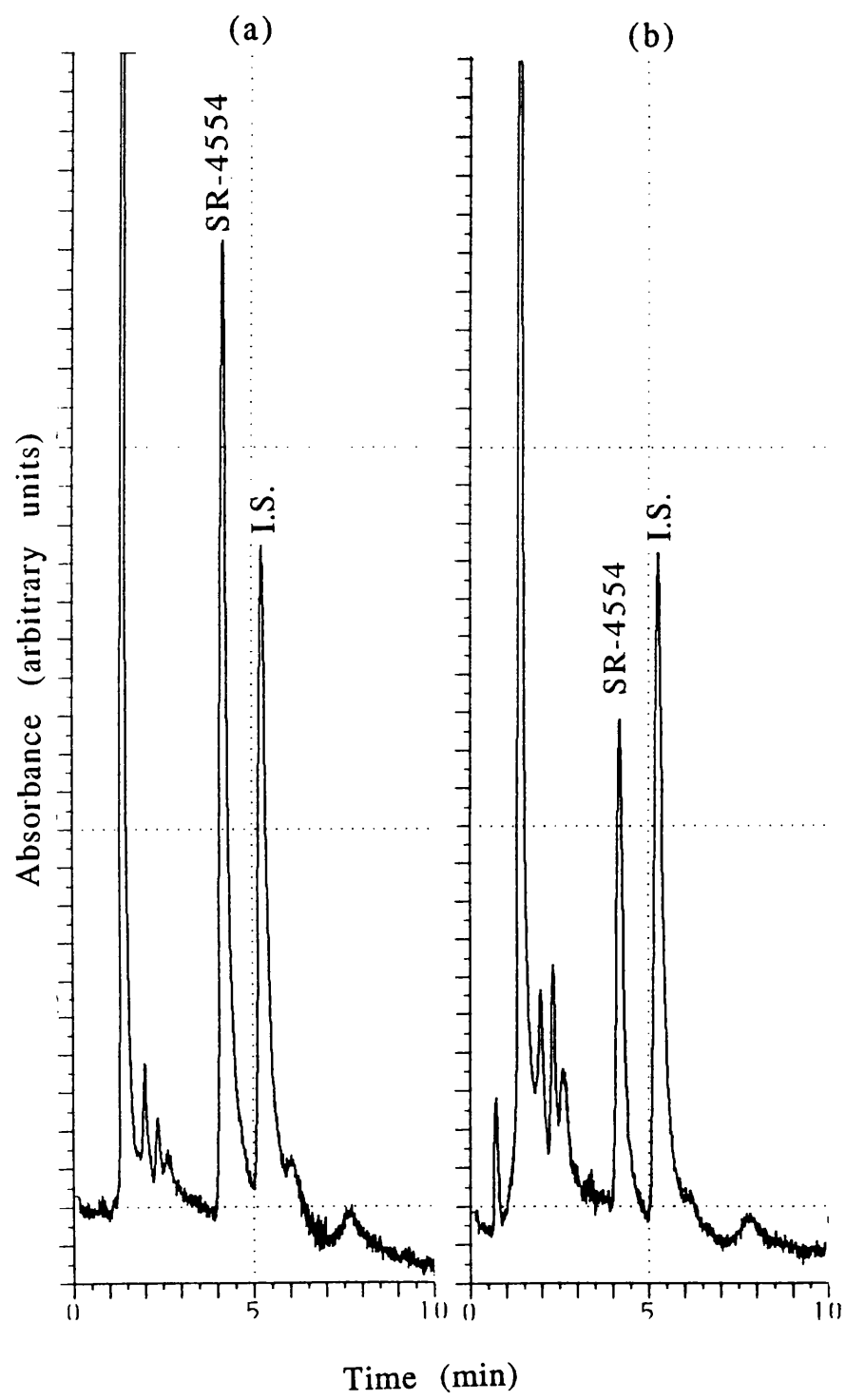
Tumour type	NADPH cytochrome P450 reductase activity (nmol/min/mg) ^a	s.e.
<i>Murine</i>		
EMT6	6.9 ^b	0.4
C3H-mammary carcinoma ^c	5.6	0.8
SCCVII	5.0	0.7
SCCVII ^c	4.9	0.8
RIF-1	4.2	0.5
RIF-1 ^c	4.4	1.0
KHT	3.4	0.4
<i>Human</i>		
HN5	11.9	1.8
WIL	10.5	1.2
BE	6.6	1.3
HT-29	5.2	0.2

a units of activity: nmol of cytochrome c reduced/min/mg protein.

b Means and standard errors were calculated from four individual tumours per tumour type.

c These tumours were obtained from the University of Aarhus, Aarhus, Denmark. All other tumours were grown at the department of Medical Oncology, Glasgow, UK.

Fig. 3.1. Typical HPLC chromatograms of extracts obtained from the hypoxic incubation of SR-4554 at zero time (a), and 15 min (b). The chromatograms illustrates the solvent front; SR-4554; the internal standard (I.S.; Ro 07-0269), and also demonstrates parent drug loss at the latter time point. The minor peak are contaminants from the microsome-NADPH mixture.



ratio of SR-4554 to internal standard Ro 07-0269. The rate of metabolism was obtained from the slope of SR-4554 concentration vs time plots which were linear within the time studied. This reductive process was almost completely inhibited in air, in the absence of cofactor (NADPH) and in the presence of $\text{TiCl}_3 \cdot 4\text{H}_2\text{O}$ (an inhibitor of NADPH: cytochrome P450 reductase). In contrast, however, carbon monoxide (an inhibitor of NADPH: cytochrome P450) only caused a 21% inhibition of microsomal metabolism (Table 3.3).

Linearity of SR-4554 reduction with time was also observed at different protein concentrations. The rate of reduction of SR-4554 as a function of microsomal protein concentration is illustrated in Fig. 3.2a. No detectable reduction was observed at protein concentrations below 0.5 mg/ml. The rate of reduction with protein concentration was linear ($r = 0.99$) up to the highest protein concentration studied (8 mg/ml). The percentage of drug loss as a function of microsomal protein concentration is shown in Fig. 3.2b. At a substrate concentration of 50 μM , complete reduction occurred between 4 and 8 mg/ml protein within 15 min. Even under these conditions, no metabolites of SR-4554 were identified on the chromatogram. Both non-linear regression and the Hanes-Woolf transformation were used to model the kinetics of microsomal reduction of SR-4554 (Fig. 3.3). The K_m and V_{max} were determined as 590 μM and 16 nmol SR-4554 reduced/min/mg respectively ($r = 0.99$).

The relationship between hypoxia dependent metabolism of SR-4554 and the oxygen content of incubation mixtures was investigated in order to assess the potential of this compound as a hypoxia probe. The results of this study is shown in Fig. 3.4. The slope of the linear portion of the curve was -1.1 ± 0.17 and the concentration of oxygen required to decrease the hypoxia dependent metabolism by 50% compared to nitrogen (half-maximum inhibition) was estimated to be $0.48 \pm 0.06\%$.

The characteristics of SR-4554 reduction by mouse liver microsome suggested that NADPH: cytochrome P450 reductase was an important reductive enzyme for this compound. In order to confirm this observation, purified NADPH: cytochrome P450 reductase was used as the enzyme source to metabolise SR-4554. SR-4554 was as expected, metabolised by both rat and human NADPH: cytochrome P450 reductase. Table 3.4 shows that the rat enzyme metabolised SR-

Table 3.3. Characteristics of the metabolism of SR-4554 by mouse liver microsomes.

Incubation Conditions	Rate of SR-4554 Reduction (nmol/min/mg) ^a	% Inhib. ^b
Complete system ^c	1.12 ± 0.14 ^d	0
Complete system in the presence of TiCl ₃ ·4H ₂ O	0.15 ± 0.04	87
Complete system in the presence of Carbon monoxide	0.88 ± 0.03	21
Complete system in the absence of NADPH	5.2e-3 ± 0.13	100
Oxic (Air) ^e	5.6e-2 ± 0.10	95

^a Units of rate: nmol of SR-4554 reduced/min/mg protein

^b % inhibition was calculated as the difference between the rate of reduction under a particular condition and that of the complete system, expressed as a percentage.

^c In the complete system, SR-4554 (50 μM) was metabolised in the presence of 2 mg/ml microsomal protein and 5 mM NADPH in Tris-HCl buffer, under hypoxia (see section 3.2.5).

^d Mean rate of reaction ± s.d. (n = 3).

^e This was similar to the complete system, except that metabolism was carried out in air.

Fig. 3.2. (a) The effect of microsomal protein concentration on the rate of reduction of SR-4554 under hypoxia. The rate of reduction (nmol SR-4554 reduced/min/mg protein) was determined as described in section 3.2.5. (b) Relationship between the percentage of SR-4554 reduced by hypoxic incubation for 15 min and microsomal protein concentration.

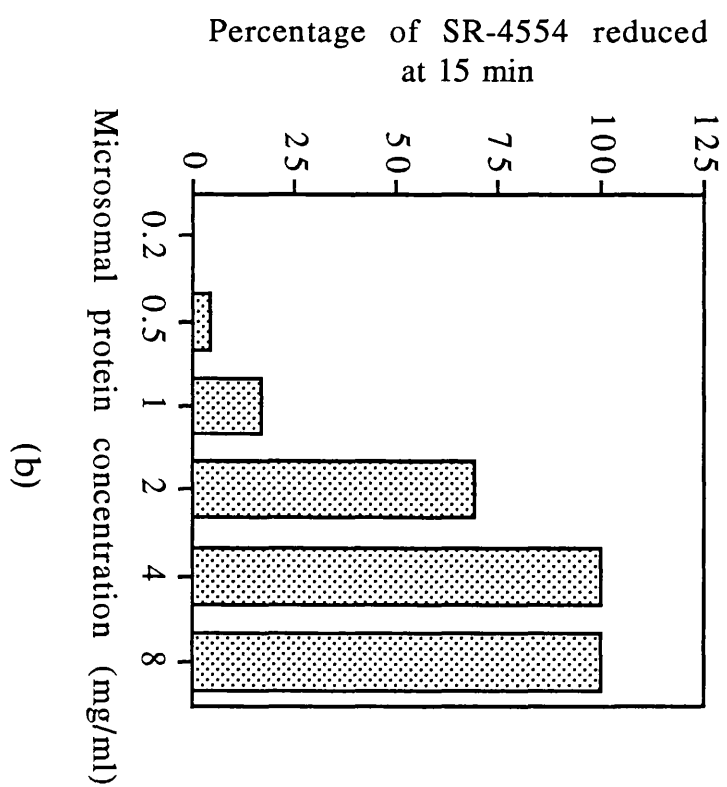
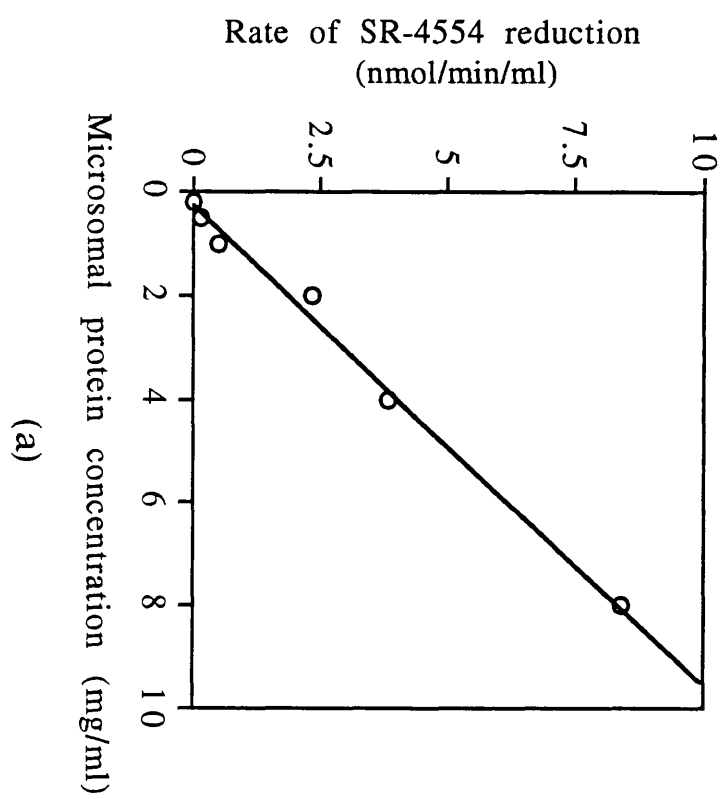
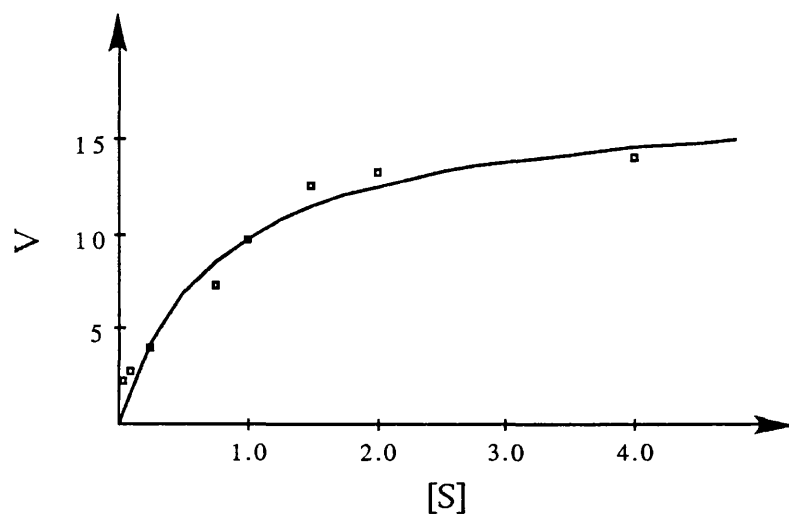


Fig. 3.3. The kinetics of reduction metabolism of SR-4554 by mouse liver microsomes, showing the classical V vs $[S]$ plot (a), and the corresponding Hanes Woolf plot (b). The units of V and $[S]$ were nmol SR-4554 reduced/min/mg protein and μM respectively. Eight concentrations of SR-4554 (each determined in duplicate) were used in the study. The apparent K_m and apparent V_{max} were estimated as described in section 3.2.7.

(a)



(b)

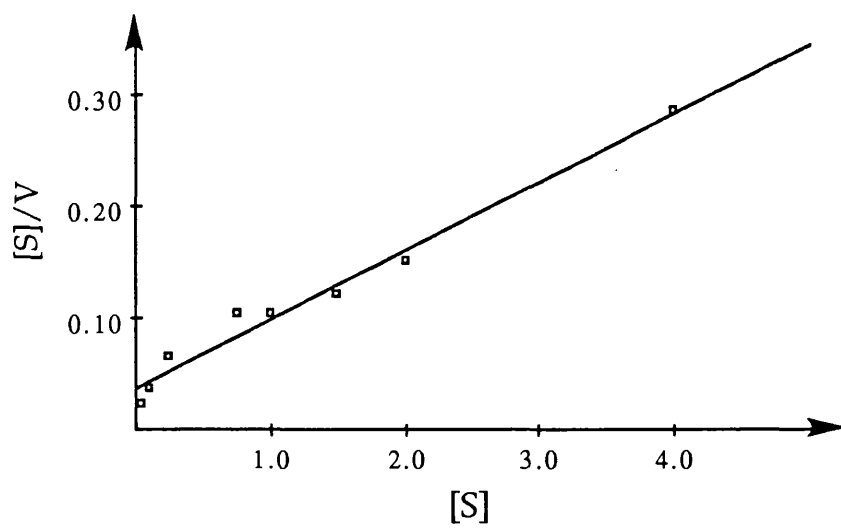


Fig. 3.4. The reduction rate of SR-4554 (nmol SR-4554 reduced/min/mg protein) by mouse liver microsomes at various oxygen concentrations. The concentration of oxygen which produces half-maximal inhibition was estimated to be 0.48%.

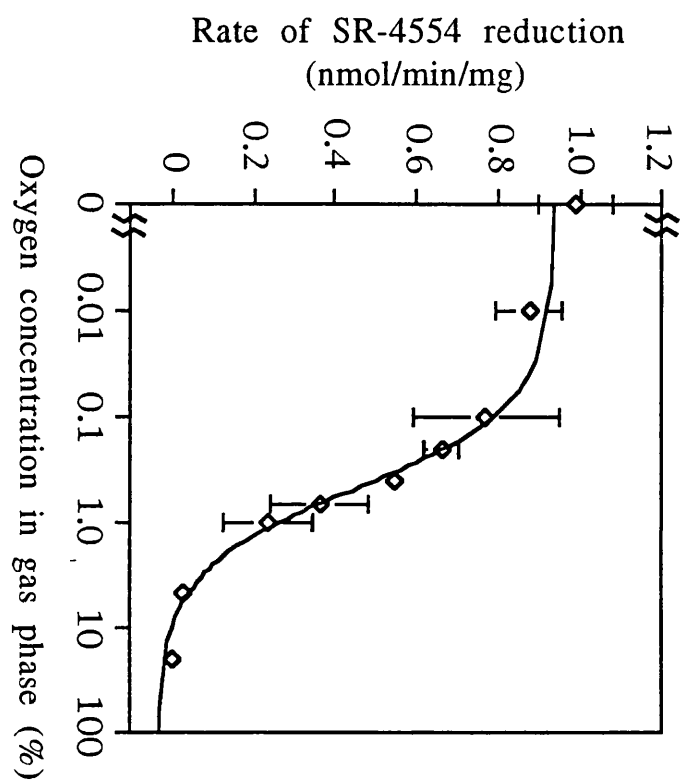


Table 3.4. Reduction of SR-4554 by purified rat and human NADPH cytochrome P450 reductase.

Enzyme	Rate of SR-4554 reduction (nmol/min/mg) ^a
Rat NADPH cytochrome P450 reductase	17.8 ± 0.9 ^b
Human NADPH cytochrome P450 reductase	5.0 ± 1.0

Incubation mixtures contained 1.3 U/ml of each enzyme.

^a Units of rate: nmol of SR-4554 reduced/min/mg protein

^b Data represent mean reduction rates ± s.d. (n = 4).

4554 at a higher rate than the human enzyme, suggesting interspecies variation. Importantly, the reduction of SR-4554 by both the rat and human enzymes was completely inhibited by $\text{TiCl}_3 \cdot 4\text{H}_2\text{O}$. In addition to metabolism by microsomes and purified NADPH:cytochrome P450 reductase, SR-4554 was also metabolised by SCCVII tumour homogenate at a rate of 1.2 ± 0.4 nmol/min/ml ($n = 3$). The reduction was, however, not completely inhibited by $\text{TiCl}_3 \cdot 4\text{H}_2\text{O}$ (rate = 0.5 ± 0.2 nmol/min/ml; $n = 3$).

3.3.3 Identification of reductive metabolites

An attempt was made to evaluate the exact nature of the MR-visible metabolites. Preliminary *in vitro* studies with microsomes using ^{19}F NMR showed the presence of three SR-4554 metabolite peaks at 10.3, 16.2 and 22.7 Hz downfield from the parent drug peak (Fig. 3.5). These peaks could also be metabolite(s) in different chemical shift environments. The same peaks were also found to be present in the supernatant of silver nitrate precipitates and in ultrafiltrates obtained by passing incubation mixtures through an ultrafiltration membrane (cut-off 30,000), but not in the resuspended pellet of silver nitrate precipitates. The formation of reductive metabolites of SR-4554 and corresponding loss of parent compound as determined by high resolution ^{19}F NMR is illustrated in Fig. 3.6. The figure also shows that the formation of these reductive metabolite(s) is inhibited in air.

The microsomal reduction of other fluorinated 2-nitroimidazoles was also characterised by ^{19}F NMR. Figures 3.7, 3.8, 3.9 and 3.10 show NMR spectra of extracts obtained from 30 min hypoxic incubation of CCI-103F, Ro 07-2044, KU-2285 and fluoromisonidazole respectively. In most cases, the peaks representing fluorinated 2-nitroimidazole metabolites were shifted to higher frequencies (downfield). HPLC analysis confirmed that the parent (fluorinated 2-nitroimidazole) compound was in all cases, reduced by more than half of the original concentration following hypoxic incubation for 30 min. The NMR spectral characteristics, however, differed markedly. For instance no differences in chemical shift was observed following hypoxic incubation of CCI-103F (octanol/water partition coefficient = 20), whereas all the other compounds showed chemical shift differences. SR-4554 and Ro 07-2044 (octanol/water partition

Fig. 3.5. Reductive metabolism of SR-4554 by mouse liver microsomes. The figure shows a high resolution NMR spectrum of a microsomal extract, obtained 30 min after the incubation of SR-4554 under hypoxia. The spectrum represents original SR-4554 (vertical arrow) and its hypoxic metabolites.

PPM

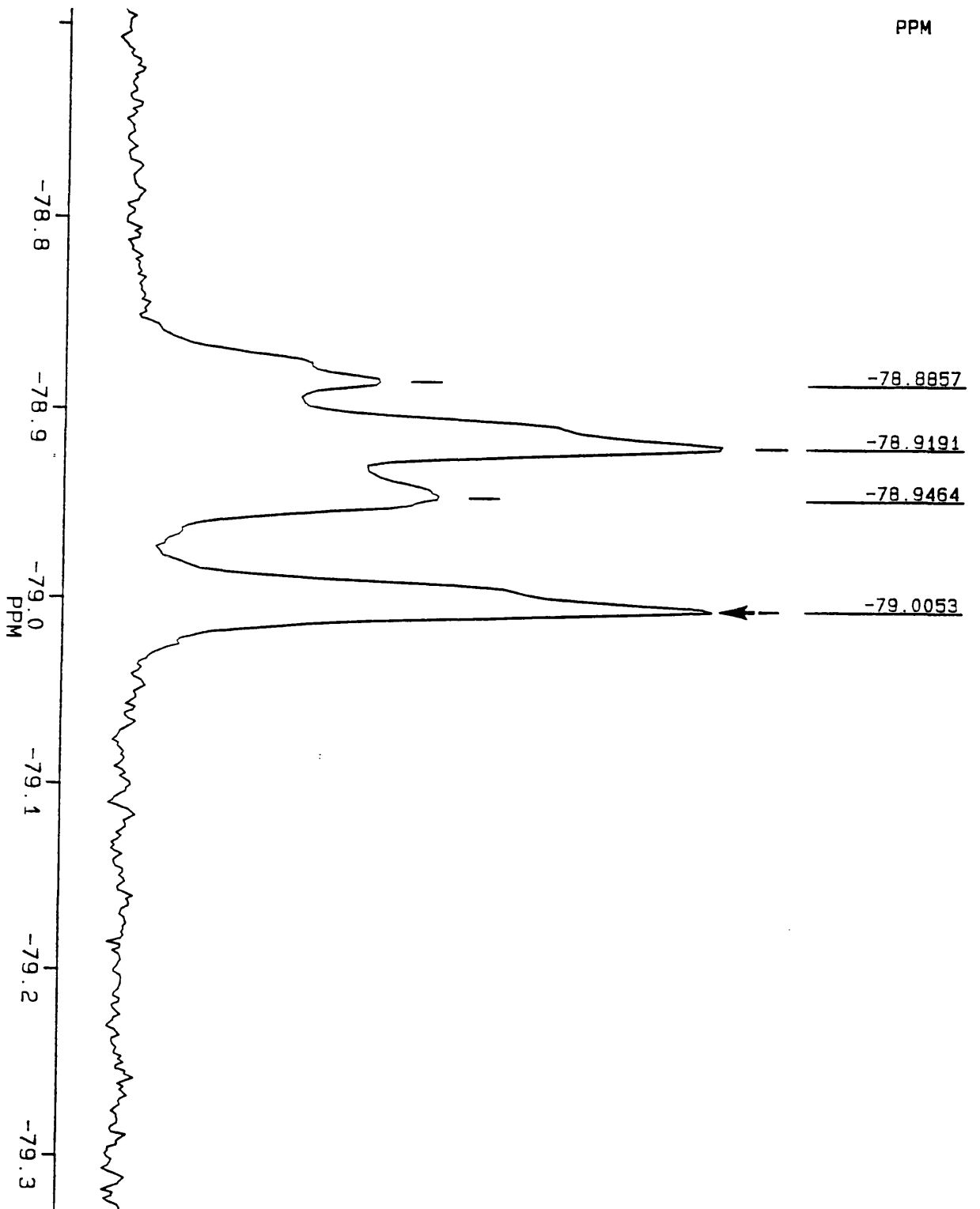


Fig. 3.6. Hypoxia-dependent metabolism of SR-4554. (a), (b) and (c) represent the time-dependent reductive metabolism of SR-4554 under hypoxia at 5, 15 and 30 min respectively. The spectra show that loss of parent drug was associated with the formation of metabolites. (d) and (e), on the other hand, represent incubation of SR-4554 in air at 5 and 30 min respectively. Reduction of SR-4554 was inhibited under these conditions. CCI-103F was used as the internal standard in these experiments.

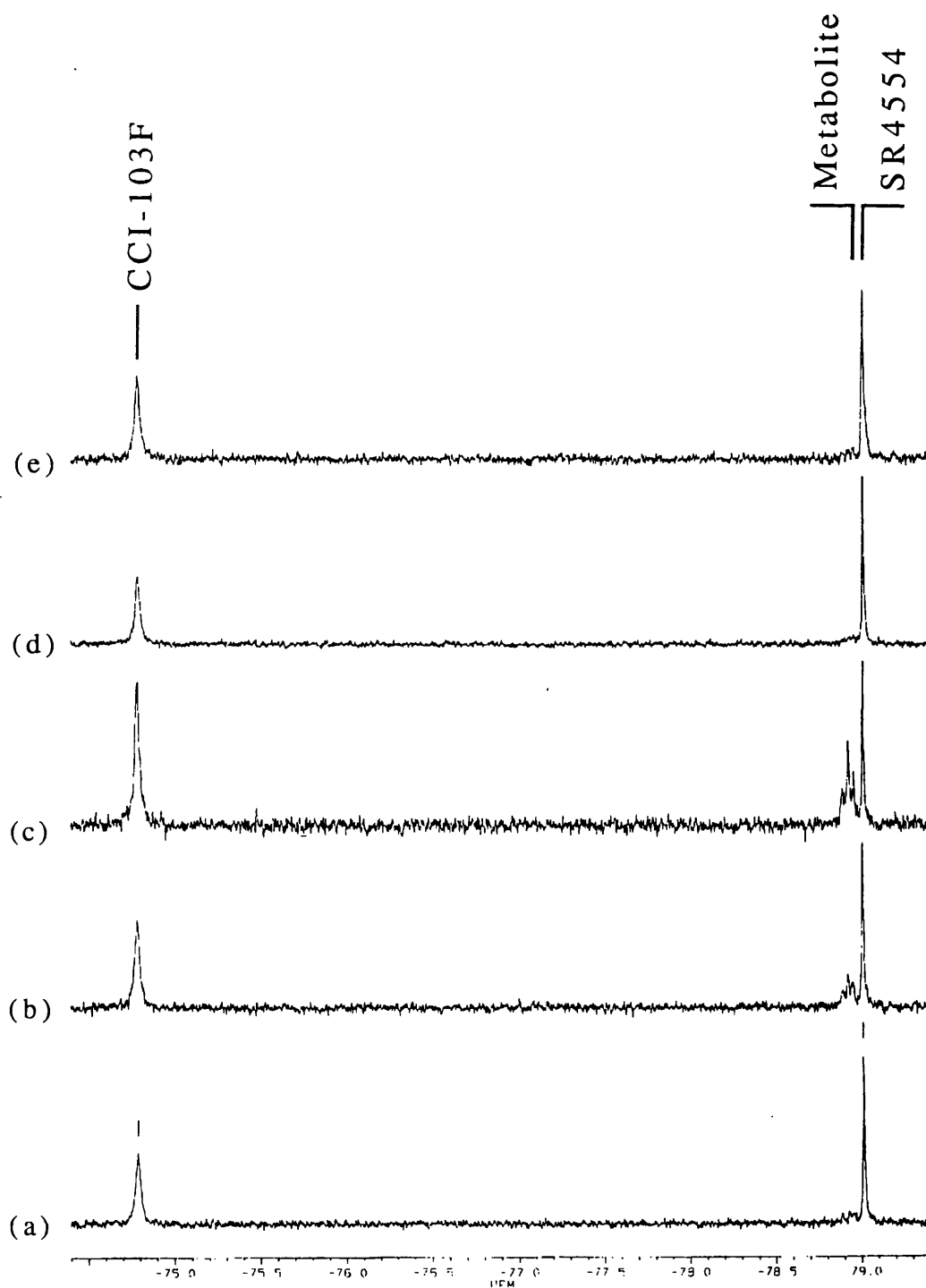


Fig. 3.7. Reductive metabolism of CCI-103F by mouse liver microsomes. The figure shows a high resolution NMR spectrum of a microsomal extract, obtained 30 min after the incubation of CCI-103F under hypoxia. The spectrum represents original CCI-103F (vertical arrow) and its hypoxic metabolites. No chemical shift was observed between CCI-103F and its metabolite(s), although HPLC analysis of the same incubation mixture indicated loss of parent drug.

PPM

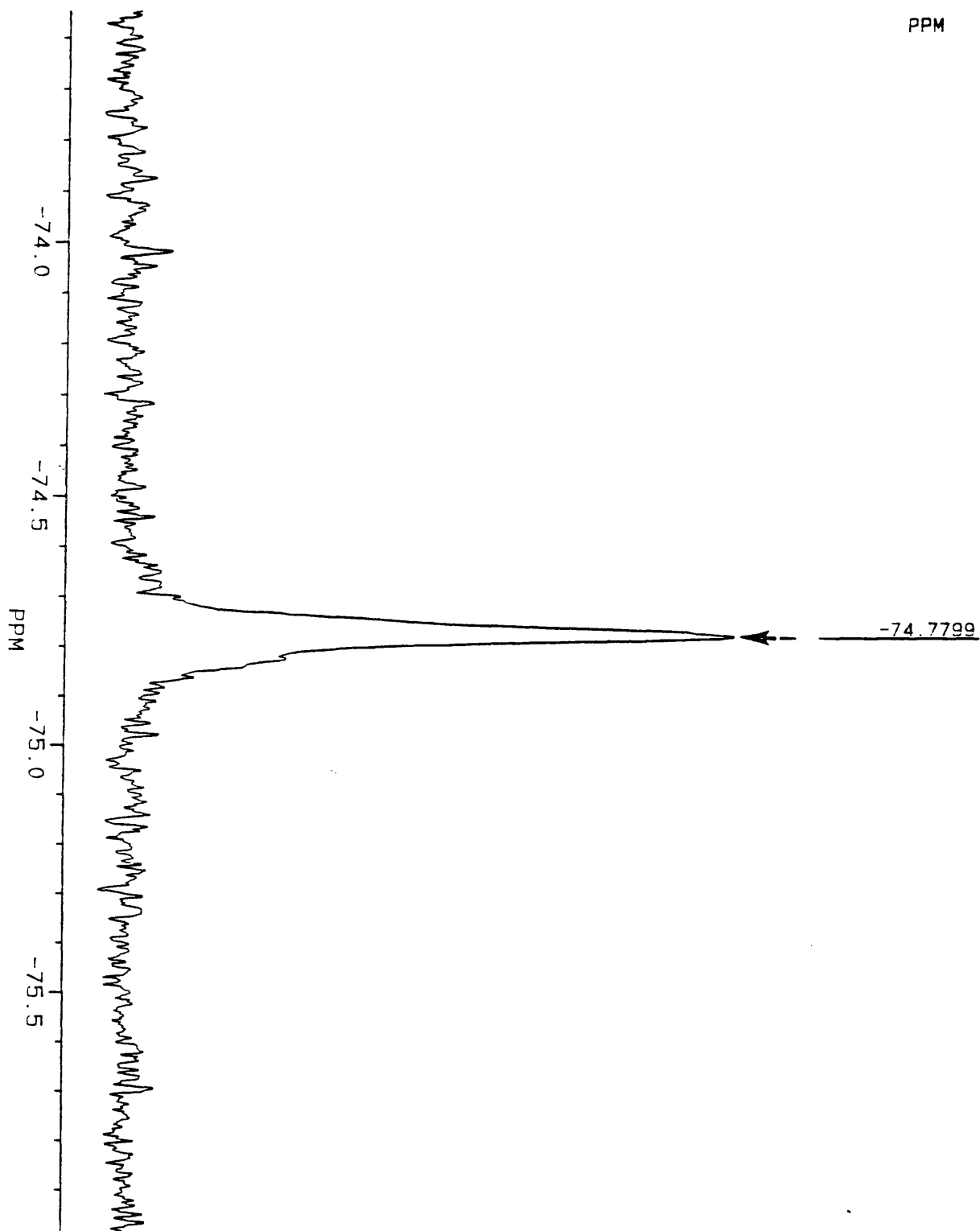


Fig. 3.8. Reductive metabolism of Ro 07-2044 by mouse liver microsomes. The figure shows a high resolution NMR spectrum of a microsomal extract, obtained 30 min after the incubation of Ro 07-2044 under hypoxia. The spectrum represents original Ro 07-2044 (vertical arrow) and its hypoxic metabolites.

PPM

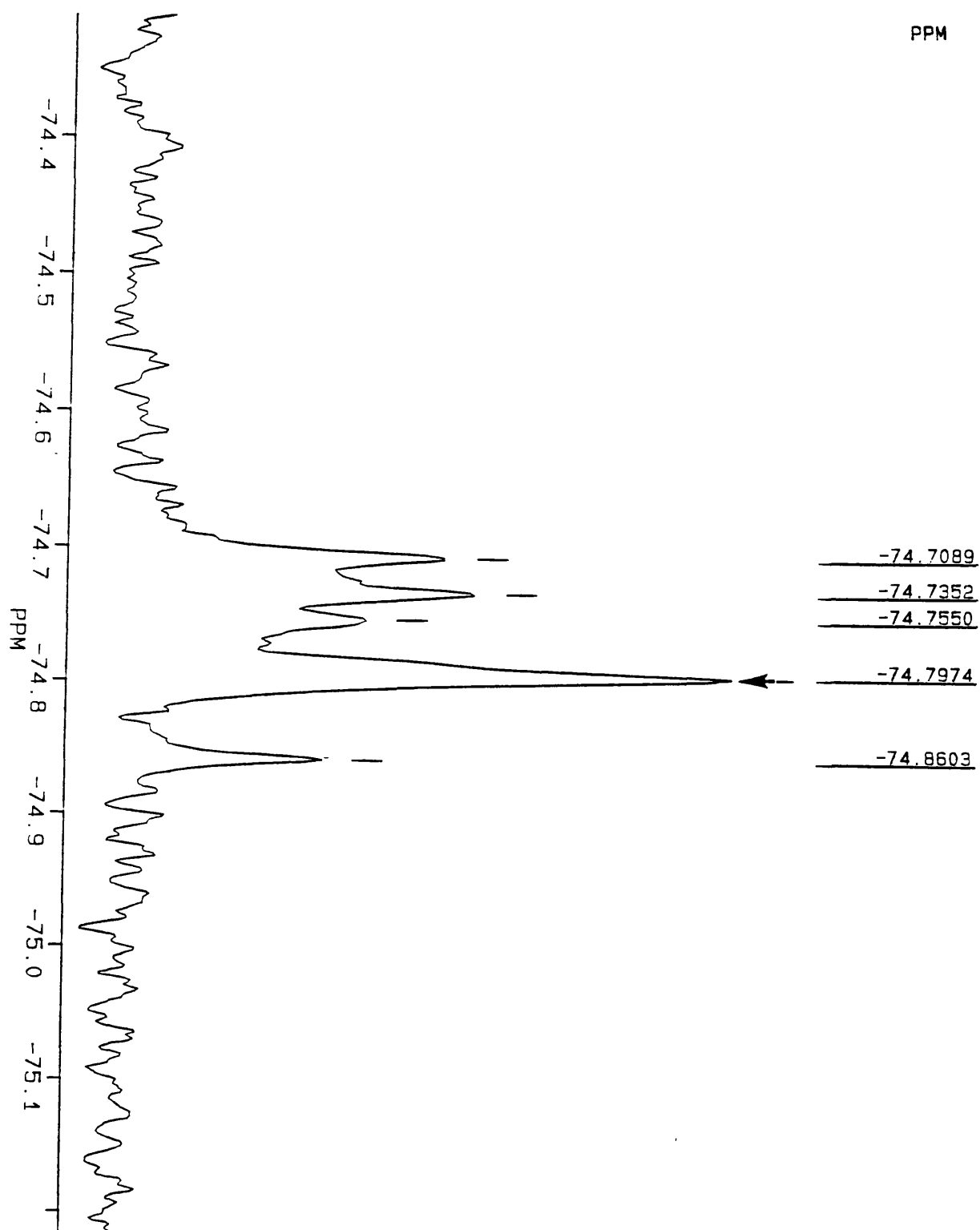


Fig. 3.9. Reductive metabolism of KU-2285 by mouse liver microsomes. The figure shows a high resolution NMR spectrum of a microsomal extract, obtained 30 min after the incubation of KU-2285 under hypoxia. The spectrum represents original KU-2285 (vertical arrow) and its hypoxic metabolites.

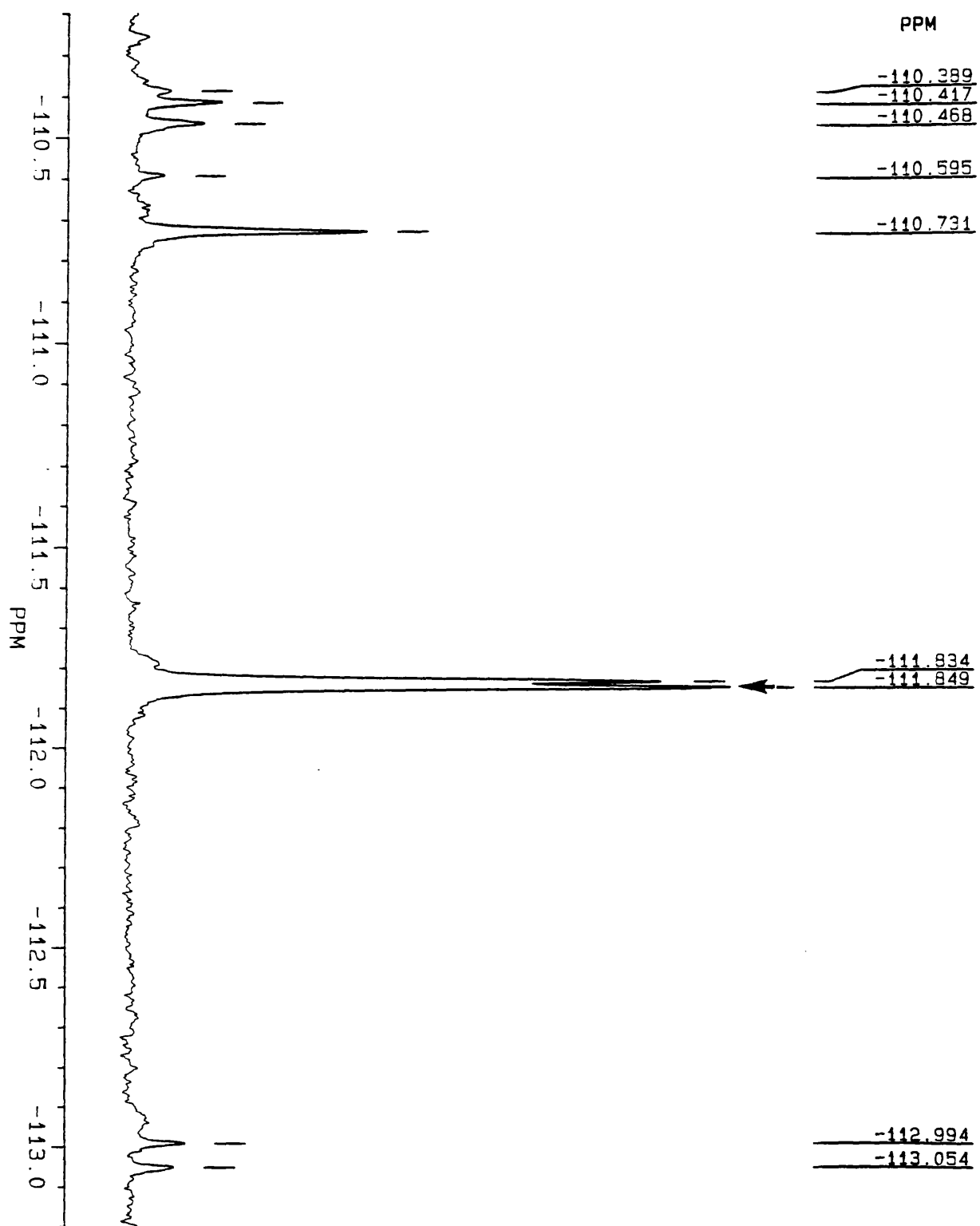
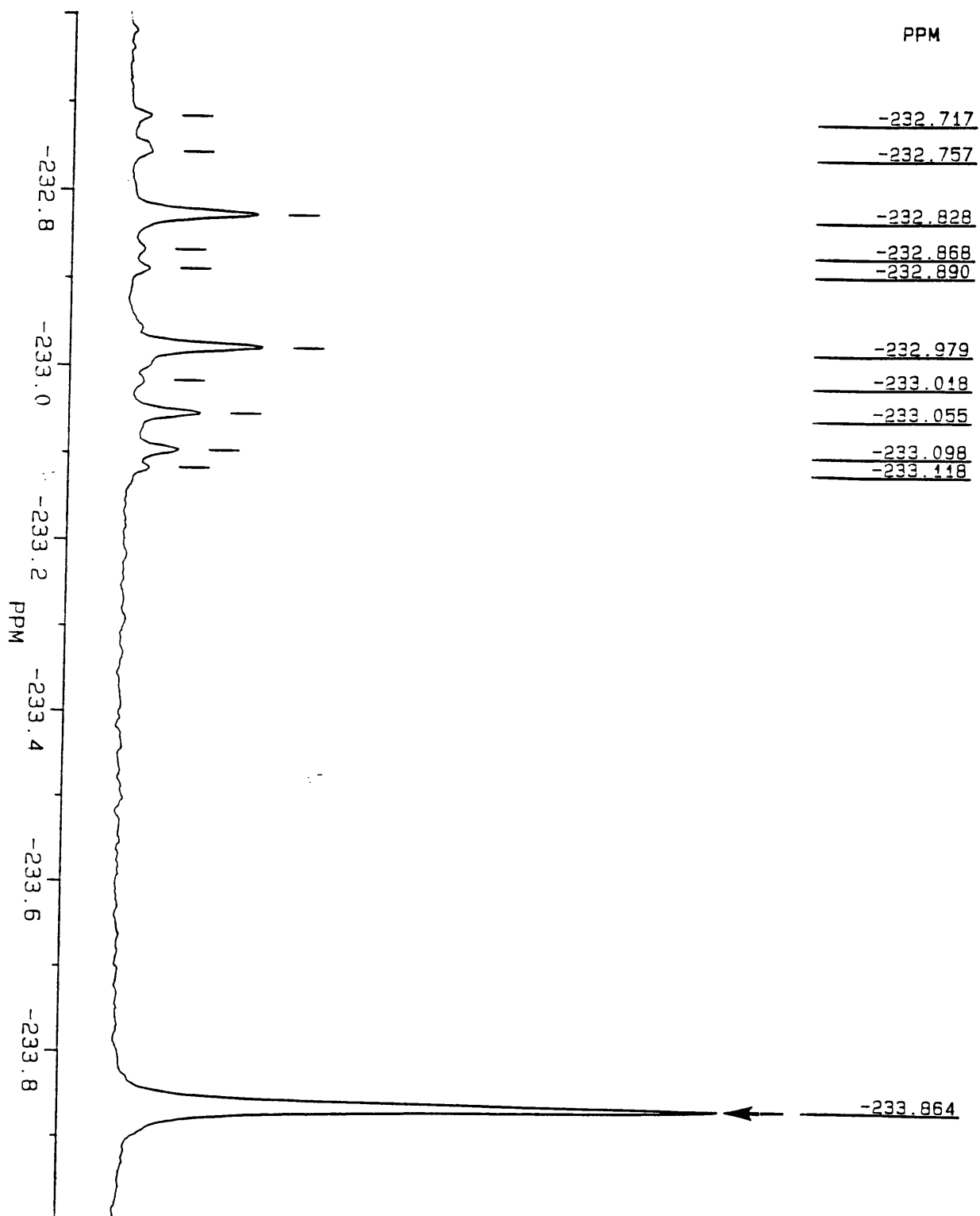


Fig. 3.10. Reductive metabolism of fluoromisonidazole (Ro 07-0741) by mouse liver microsomes. The figure shows a high resolution NMR spectra of a microsomal extract, obtained 30 min after the incubation of fluoromisonidazole under hypoxia. The spectrum represents original fluoromisonidazole (vertical arrow) and its hypoxic metabolites.



coefficients of 0.64 and 3.35 respectively) showed intermediate chemical shift differences of between 0.05 to 0.8 ppm. The two compounds with lowest partition coefficients, fluoromisonidazole and KU-2285 (0.41 and 0.25 respectively) showed higher chemical shift differences (up to 1.5 ppm) between metabolite peaks and original drug peaks. Interestingly, these same compounds have their fluorine atoms closer to the site of nitroreduction.

3.3.4 *In vivo* reductive metabolism of SR-4554

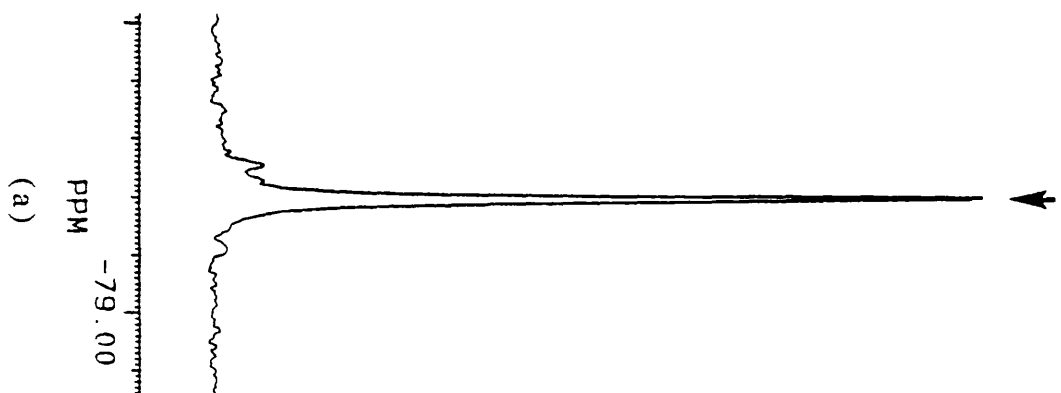
Two of the three NMR metabolites observed with microsomes were also identified *in vivo* in silver nitrate extracts of EMT6 tumours excised after SR-4554 administration to tumour bearing mice (Fig. 3.11). This figure shows that *in vivo*, parent drug levels are high at the early time point (15 min post-injection), and gradually converted into metabolites (2 and 4 hr). At 6 hr post-injection, only bio-reduced metabolites remained. The low levels of the metabolite at 6 hr suggested that the bio-reduced metabolite was also eliminated, albeit at a slower rate. These same peaks were also observed in liver but not brain (Fig. 3.12). Urine samples obtained from non-tumour bearing mice over 24 hr showed the presence of other metabolites (Fig. 3.13). The urinary fluorine spectrum was, however, dominated by unchanged SR-4554 suggesting that this is the major elimination route for the compound.

3.4 DISCUSSION

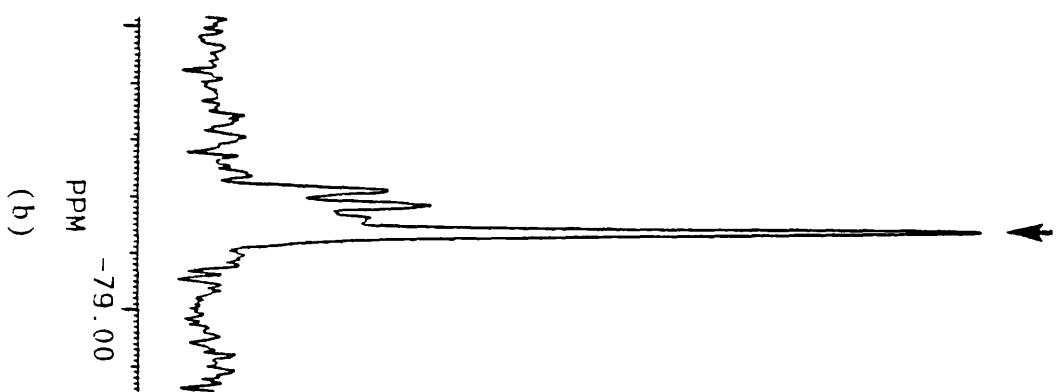
The metabolism of 2-nitroimidazoles has been shown to be mainly dependent on oxygen tension and enzyme content (Franko *et al.*, 1987; Joseph *et al.*, 1994; Koch *et al.*, 1984; Walton & Workman, 1987). In this chapter, the characteristics of this enzymatic bio-reductive metabolism of the hypoxia probe SR-4554, were investigated. Loss of parent drug, as determined by HPLC with UV detection, was used as a measure of SR-4554 nitroreduction. It should be noted that no metabolite was observed by this HPLC method even at the highest protein concentration of SR-4554. Walton and Workman, however, detected the amine metabolite of benznidazole using a similar technique (Walton & Workman, 1987). In this case, the additional chromophore introduced by the aromatic ring in the N-1 side chain of benznidazole (see Fig. 1.3) was

Fig. 3.11. SR-4554 (vertical arrow) and its metabolites in EMT6 tumours excised from drug treated mice at (a) 15 min, (b) 2 hr, (c) 4 hr, and (d) 6 hr post-injection. Drug injection, sample preparation and NMR analysis were carried out as described in section 3.2.6.

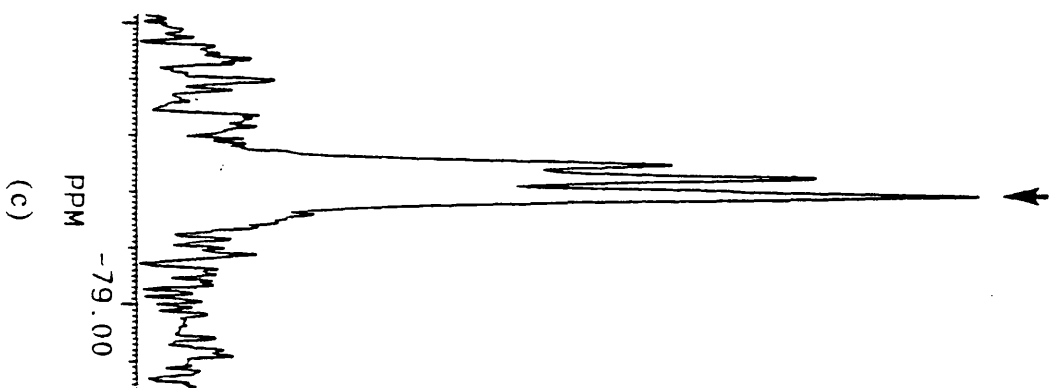
15 mins



2 hrs



4 hrs



6 hrs

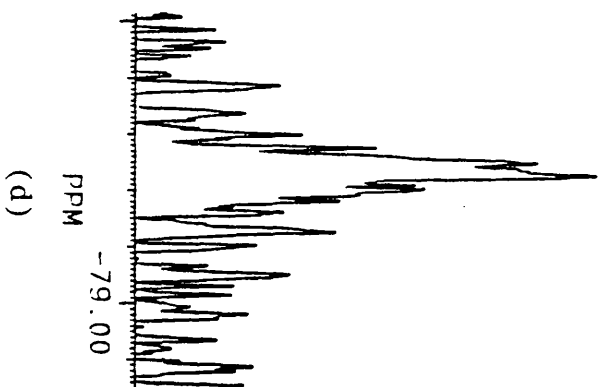
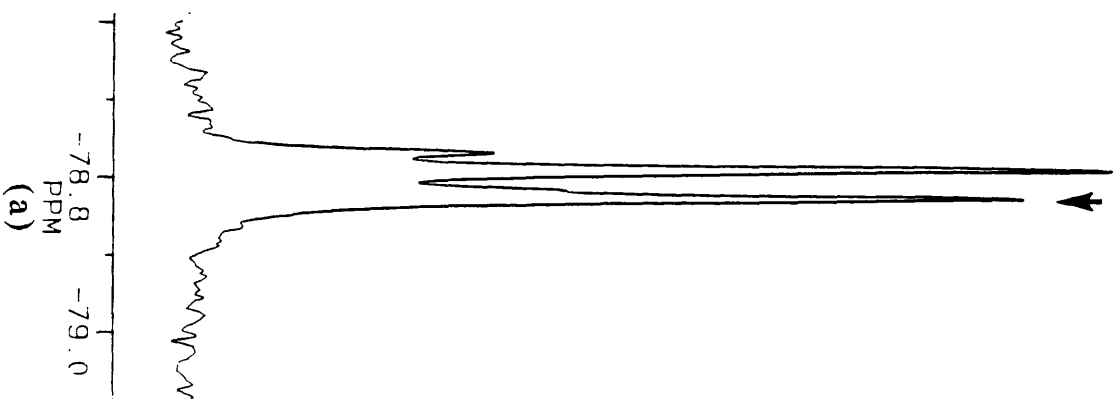
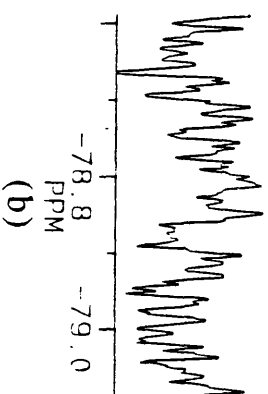


Fig. 3.12. SR-4554 (vertical arrow) and its metabolites in liver (a) and (b), and brain (c) and (d), of Balb/c mice. SR-4554 was present in both liver and brain at the early time point (15 min) and eliminated by 6 hr. Liver samples contained high levels of metabolites even at 15 min, whereas no metabolites were observed in brain sample.

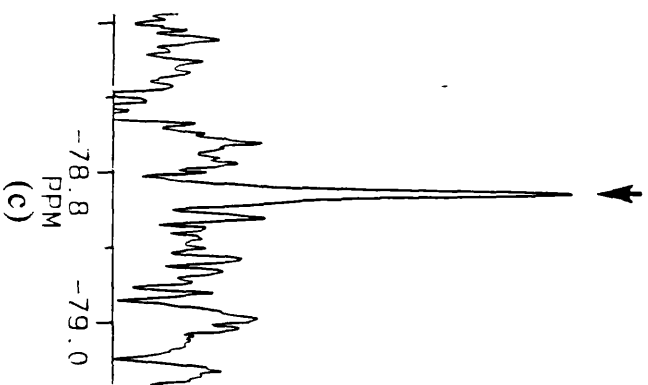
Liver (15 min)



Liver (6 hr)



Brain (15 min)



Brain (6 hr)

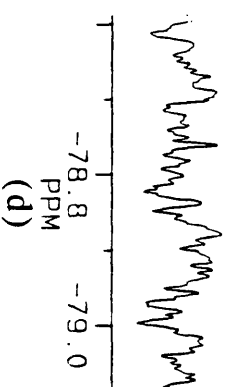
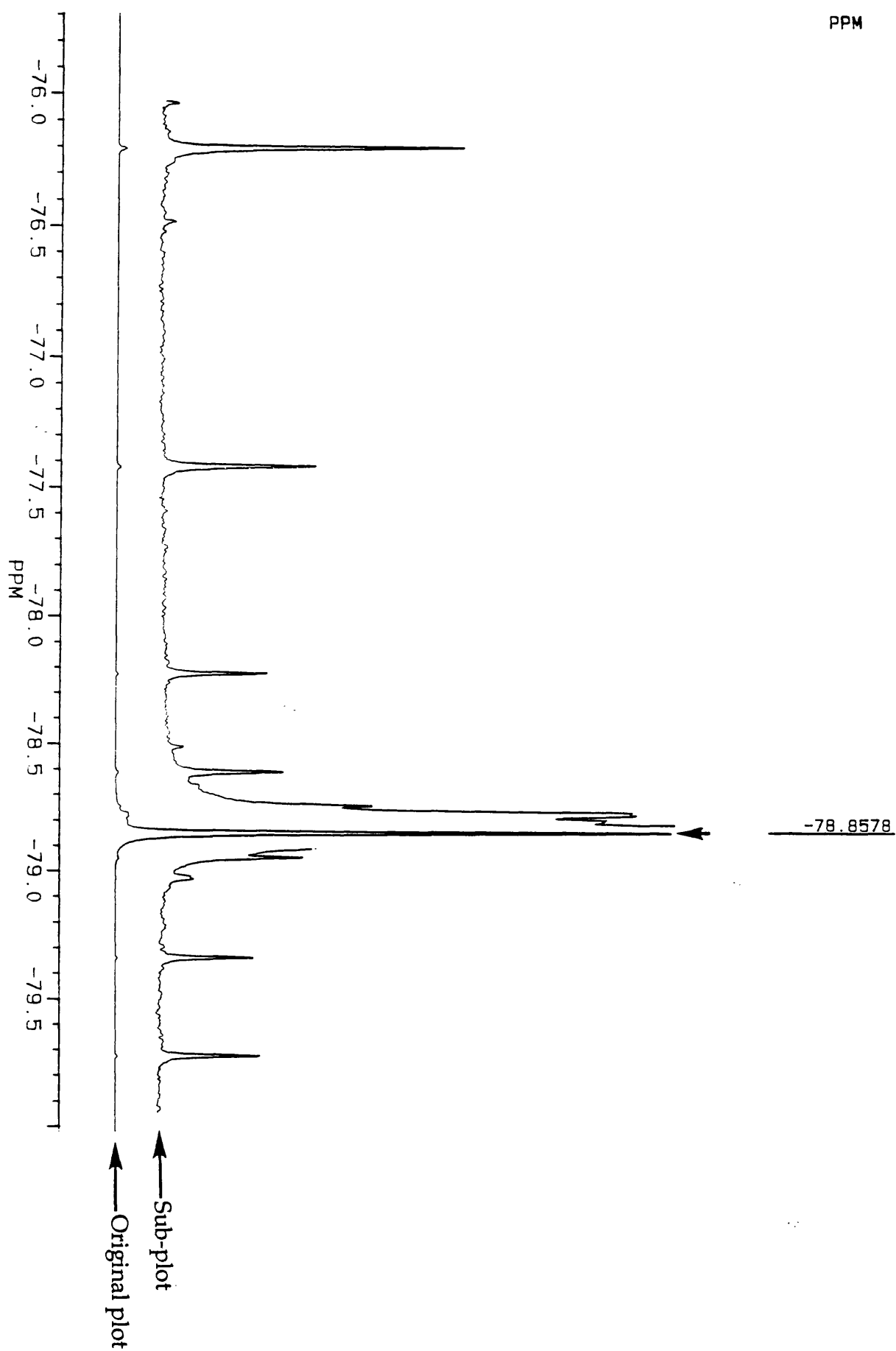


Fig. 3.13 SR-4554 (vertical arrow) and its metabolites in non-tumour bearing mouse urine collected over 24 hr. The original plot shows that parent drug was the major metabolite in urine. The sub-plot represents an expansion of the smaller peaks in the spectrum.

PPM



responsible for the UV detection ability at the lower λ_{max} of the amine metabolite (Walton & Workman, 1987).

SR-4554 metabolism was found to be dependent on two major enzymes, NADPH: cytochrome P450 reductase and NADPH: cytochrome P450. Inhibition of NADPH: cytochrome P450 reductase activity by its chemical inhibitor $\text{TiCl}_3 \cdot 4\text{H}_2\text{O}$, almost completely suppressed the reduction of SR-4554. This suggests that NADPH: cytochrome P450 reductase may be involved in the early steps of the reductive process (see Fig. 1.4). The lower efficiency of inhibition of the reduction process by carbon monoxide (an inhibitor of NADPH: cytochrome P450) suggests that NADPH: cytochrome P450, on the other hand, is not a major nitroreductase in the early steps of the reductive process. Interestingly, NADPH: cytochrome P450 was shown to be only important in the latter steps of benznidazole nitroreduction resulting in the formation of the amine metabolite (Walton & Workman, 1987). The importance of NADPH: cytochrome P450 in the reductive metabolism of SR-4554 was confirmed by metabolism with rat and human NADPH: cytochrome P450 reductases. Since the rat enzyme was more efficient in reducing SR-4554 than the human equivalent, this limited study suggests that interspecies variations are likely, and should be considered in the future clinical development of the compound. The possibility that reductases other than NADPH: cytochrome P450 reductase may be involved in the metabolism of the drug was suggested by experiments with SCCVII tumour homogenates. In this case, $\text{TiCl}_3 \cdot 4\text{H}_2\text{O}$ did not completely inhibit the reductive process.

SR-4554 reduction was also found to be dependent on both protein and substrate concentration. The linearity of SR-4554 reduction with microsomal protein concentration suggests that differences in enzyme concentrations of the order used in this experiment should produce marked differences in reduction rates. The substrate dependence of reduction was characterised by an apparent K_m (590 μM) and apparent V_{max} (16 nmol SR-4554 reduced/min/mg protein) indicating relatively high substrate specificity for the enzymes involved in the reduction process. It would be interesting to investigate whether the high substrate specificity will translate into a high rate for the hypoxia-dependent

binding kinetics of SR-4554 to macromolecules. This study will become possible when radiolabelled SR-4554 becomes available.

SR-4554 metabolism was also shown to be dependent on oxygen tension. The reductive process was completely inhibited in air (20.9% oxygen) and partially inhibited by increasing levels of oxygen in nitrogen. The oxygen concentration which produced 50% inhibition of SR-4554 reduction between nitrogen and air (0.48%) was similar to that previously reported for other 2-nitroimidazole binding such as misonidazole and desmethylmisonidazole (Franko, 1986; Franko *et al.*, 1987; Joseph *et al.*, 1994; Koch *et al.*, 1984). This observation is interesting, since the effect of oxygen tension on the *in vitro* reduction rates of 2-nitroimidazoles (i.e. loss of parent drug) *per se* has not been reported.

Due to the importance of NADPH: cytochrome P450 reductase in the reduction of SR-4554, this enzyme was profiled in a panel of murine and human tumour xenografts used in section 6.2, to investigate whether enzyme activity in these tumours would significantly affect the absolute retention of SR-4554 in its use as a hypoxia probe. The activity of NADPH: cytochrome P450 reductase in these tumours ranged between 3.4 and 11.9 nmol cytochrome c reduced/min/mg protein. Interestingly, both between and within tumour type variations were observed. The activities of NADPH: cytochrome P450 reductase observed in these tumours were found to be similar to those previously reported for untransformed cell lines (Fitzsimmons *et al.*, 1995; Joseph *et al.*, 1994) and biopsy samples of gliomas (Rampling *et al.*, 1994). As demonstrated in this chapter, these activities were not much less than that of liver S9 fractions (10-30 fold) or microsomes (20-60 fold). At similar oxygen tensions, tumour cells would be expected to metabolise SR-4554 at different rates, and at a much lower rate than that of the model system (liver microsomes) used in this chapter. According to Joseph *et al.*, the ability of tissues to bind 2-nitroimidazoles would be a function of the square root of their reductase content (Joseph *et al.*, 1994). The enzyme profiling studies in this chapter, therefore, indicate that NADPH: cytochrome P450 reductase activities in the panel of tumours used here, and in future chapters, will be unlikely to markedly affect the reduction and hence selective retention of the nitroimidazole, and

that oxygen tension *per se* would be the most important determinant of selective 2-nitroimidazole retention.

Although no metabolites of SR-4554 were detectable by HPLC, these were seen in high resolution ^{19}F NMR studies. Hypoxic reduction of SR-4554 was characterised by three peaks in microsomal incubation mixtures. These metabolites were also found to have low molecular weight (less than that of plasma proteins; 30,000). Similar metabolites were observed *in vivo* in mouse liver, EMT6 tumours and mouse urine collected over 24 hr, but not in mouse brain which also had low levels of the parent drug. Although original SR-4554 was the main compound present in urine, low concentrations of other metabolites not previously present in microsomes were also observed. It was noted that the appearance of metabolites was very rapid in mouse liver compared to tumours suggesting a higher reductive capacity due to the high levels of reductive enzymes. Although the exact nature of these metabolites were not fully elucidated, they are likely to be bound to low molecular weight molecules. Firstly, and as previously discussed, the higher proportion of 2-nitroimidazole adducts are represented by those bound to RNA and glutathione both of which are low molecular weight compounds (Chapman *et al.*, 1990; Koch, 1990). Secondly, the ability of *in vivo* MRS to give sharp peaks (Workman *et al.*, 1992), indicates that low molecular weight adducts may play a major part in 2-nitroimidazole binding. Since the parent drug was cleared faster than the metabolite, the reductive metabolism could be used to selectively measure hypoxia. This NMR method would, therefore, complement radiolabelled studies which measure adduct formation in the acid insoluble fraction.

A high resolution NMR method was also used to identify the characteristics of reductive metabolism of other fluorinated 2-nitroimidazole. The five 2-nitroimidazoles, SR-4554, CCI-103F, Ro 07-2044, KU-2285 and fluoromisonidazole were characterised according to their NMR spectra. The chemical shifts observed in this series are characteristic of the intracellular and/or transmembrane shifts previously reported in NMR literature (Keniry *et al.*, 1986; London, 1994; Xu *et al.*, 1993). Initially it was hypothesised that differences in 'through-bond' distances between the fluorine atoms and the site of nitroreduction could give differences in chemical shifts. Contrary to this notion, however, it was demonstrated that partition coefficient

rather than 'through-bond' distance *per se* was of greater importance in the limited series investigated. This lipophilicity effect could be due to the presence of different drug metabolites or metabolite(s) in different compartments or chemical shift environments. Although other analogues would be required to test this hypothesis fully, it should be noted that only chemical shifts of up to 1.5 ppm were observed. This study, therefore, suggests that side chain fluorine atoms may not produce resolved MRS spectra of parent and reduced metabolite at current clinically relevant magnetic field strengths, and that this effect may only lead to spectral broadening in *in vivo* MRS studies.

Studies in this chapter have characterised the enzymology and bioreductive activation of SR-4554. As a consequence, the data produced in this chapter will form the basis experiments in future chapters of this thesis, as well as in the clinical development of SR-4554.

CHAPTER 4

Localisation of SR-4554 in multicellular spheroids as measured by electron energy loss spectroscopic imaging

4.1 INTRODUCTION

4.1.1 Subcellular localisation of 2-nitroimidazoles

Nitroimidazoles, including misonidazole, have been under evaluation as potential diagnostic probes for hypoxic cells. This is due to the specific reductive metabolism of the drugs to reactive metabolites which bind to macromolecules within hypoxic cells (see section 1.5.2 and Fig. 1.4). The characteristic of covalent binding of 2-nitroimidazoles has been evaluated in various cell lines and tumours, and although the exact nature of the metabolites is unknown, various candidates have been implicated in this process (Chapman *et al.*, 1983; Chapman *et al.*, 1990; Miller *et al.*, 1982). These candidates include glutathione, ribonucleoproteins and lipoproteins. For instance previous subcellular fractionation studies in EMT6 cells with ^{14}C misonidazole indicated that 23 and 77% of the total activity was associated with the acid-insoluble and the acid-soluble fractions respectively (Miller *et al.*, 1982). Further, the acid-insoluble fraction was distributed amongst RNA (17%), DNA (1%), lipid (4%), and protein (1%) (Miller *et al.*, 1982). In another study, the involvement of intracellular enzymes in the activation process was implicated, since the temperature dependence for this process showed an activation energy of 33.5 kcal/mol (Chapman *et al.*, 1983). This latter investigation demonstrated that the binding rate of misonidazole within hypoxic cells was at least 50 times greater than that observed within aerobic cells. The data also suggested that the activation sites may be lipid-associated, thus favouring the bioreduction of more lipophilic compounds. Various techniques such as autoradiography, immunohistochemistry and flow cytometry have been employed to localise 2-nitroimidazoles in spheroids and tumour biopsies (Garrecht & Chapman, 1983; Hodgkiss *et al.*, 1994; Lord *et al.*, 1993; Raleigh *et al.*, 1991b). These studies have shown that 2-nitroimidazoles label hypoxic cells within tumours and are, therefore, particularly suitable as markers. In this regard, electron energy loss spectroscopy (EELS) has been investigated in this thesis as a method for localising 2-

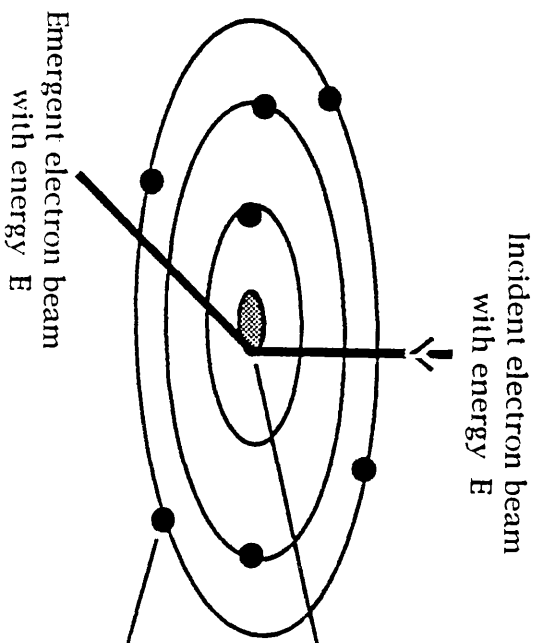
nitroimidazole in spheroids. This technique is described in section 4.1.2.

4.1.2 Electron energy loss spectroscopy (EELS) and electron spectroscopic imaging (ESI)

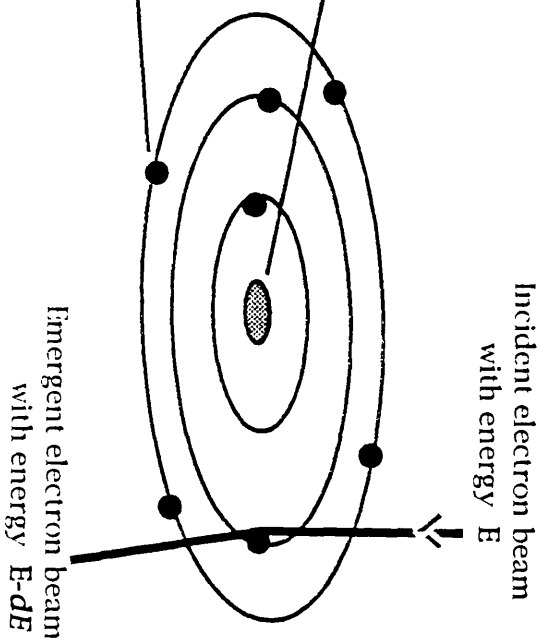
Electron energy loss spectroscopic analysis (EELS) and electron spectroscopic imaging (ESI) are emerging techniques for *in situ* examination of compounds in cells and tissues. Although the technique has been used frequently on biological samples, it has only recently been applied to anticancer drug localisation (Huxham *et al.*, 1993; Huxham *et al.*, 1992). The technique is capable of relating spatial chemical composition of biological systems to cell ultrastructure and also of providing relative concentrations of specific elements within unstained areas of the cells on a nanometer scale.

EELS relies upon the measurement of electron energy distribution of transmitted electrons that have lost energy following interaction with a specimen *in vacuo*. Specifically at high voltage (80-100 kV), the incident electron beam directed at a specimen produces both elastically and inelastically scattered electrons (Fig. 4.1). Elastically scattered electrons result from the interaction of the incident electron beam with positively charged nuclei in the specimen. This leads to a significant change in direction of the emergent electrons but with no change in energy. Such electrons can therefore be excluded by the insertion of an objective aperture in the microscope. In contrast, inelastically scattered electrons result when the incident electron beam interacts with electrons in the specimen. This leads to a slight change in energy but little or no change in direction of the resultant emergent beam. Such energy loss provides valuable information since it is characteristic of the element, electron orbital and shell with which the incident beam interacts. Using an energy filtering transmission electron microscope (EFTEM), the emergent electrons can be analysed according to the intensity of their energy loss to give an energy loss spectrum (Fig. 4.2) or alternatively can be used for the production of an electron spectroscopic image (ESI). These filtered electron spectroscopic or image sequences contain information about the element-specific energy loss population (equivalent to energy loss edge) superimposed on the non-specific energy loss population (equivalent to background). By varying

Fig. 4.1. Elastically (a) and inelastically (b) scattered electrons produced by the interaction of the incident electron beam with specimen nuclei and electrons respectively. Exclusion of the elastically scattered (zero-loss) electrons allows the energy loss spectrum or image of a particular atomic species in the specimen to be produced.

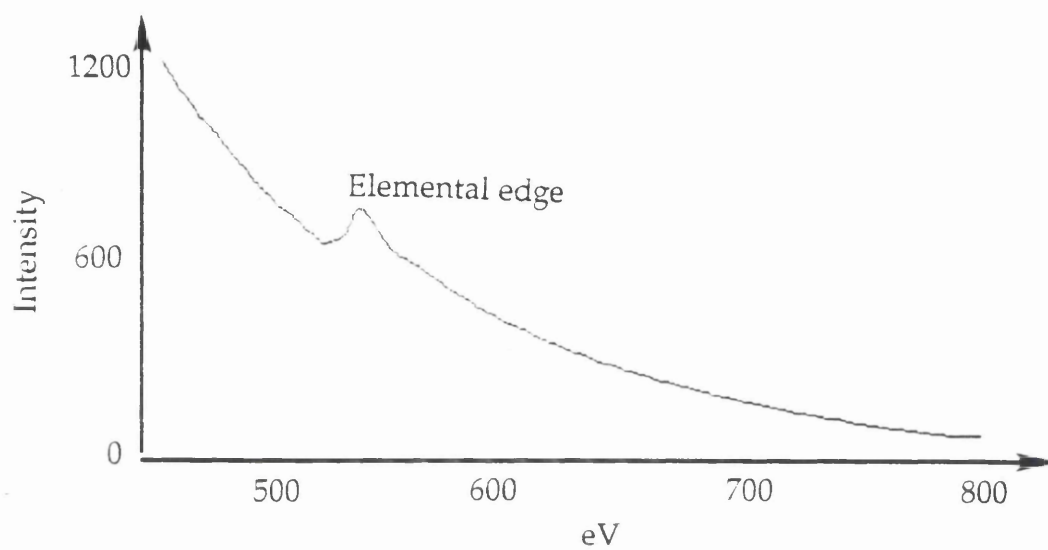


(a) Elastic collision

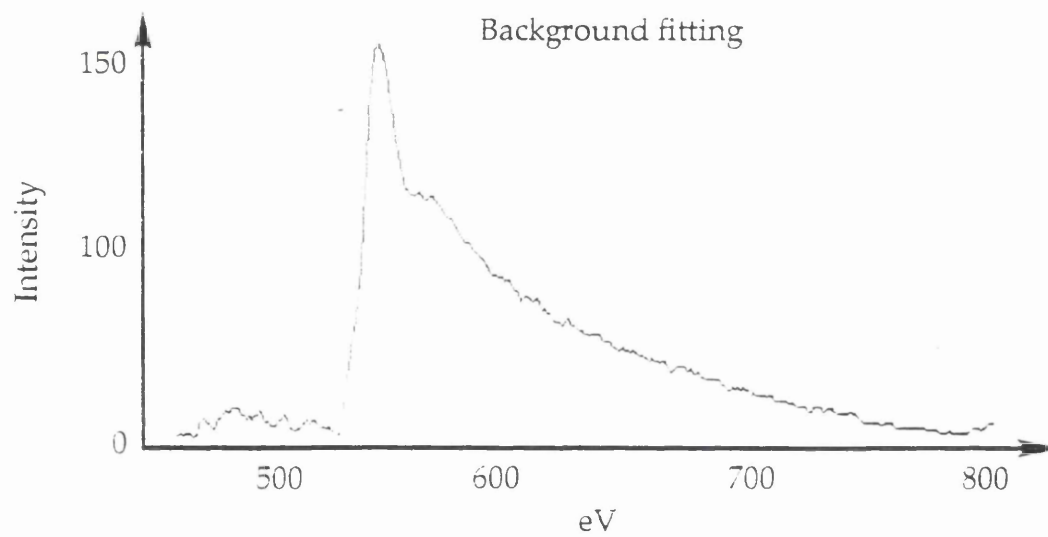


(b) Inelastic collision

Fig. 4.2. (a) Typical energy loss spectrum showing a continuously decreasing background and an elemental edge. (b) The spectra in (a) after undergoing a background removal process to reveal the true elemental contribution. (Produced by A.D. Johnson, Division of Molecular and Cellular Biology, University of Glasgow).



(a)



(b)

precisely the source of high energy voltage whilst maintaining the mirror voltage constant, the different regions of the energy loss spectrum are scanned selectively and the specimen imaged at these values. Data are processed mathematically to obtain edge intensity information which relates directly to the elemental concentration of the specimen. Comparing the intensity of two elements, as performed here, can thus disclose semi-quantitative elemental information on a local (nm) scale.

In this chapter, EELS was used to study the localisation of SR-4554 within A2780 human ovarian multicellular spheroids. The A2780 spheroid model was chosen because it provides the co-existence of both aerobic and hypoxic cells under normal aerobic cell culture conditions, allowing manipulations of both types of cells to be carried out simultaneously. Moreover, EELS has previously been applied to the localisation of fluorine-containing drugs in this spheroid model (Huxham *et al.*, 1993; Huxham *et al.*, 1992).

Together with the bioreductive metabolism studies reported here, the present localisation studies will help in our understanding of the characteristics of metabolism induced binding of SR-4554 and of 2-nitroimidazoles in general.

4.2 MATERIALS AND METHODS

4.2.1 Chemicals and reagents

Human ovarian cancer cells A2780 were obtained from Dr. R.F. Ozols (NCI, Bethesda, MD, USA). The cells were cultured in a medium consisting of RPMI (Life Technology, Paisley, Scotland) supplemented with 10% foetal calf serum (Globepharm, Esher, Sussex, England), and 0.001% (w/v) insulin (Lewes, Sussex, England). The 2-nitroimidazoles used in this chapter have been previously described (Fig. 1.3).

4.2.2 Reductive metabolism of SR-4554 by A2780 cells

A2780 cells were cultured as monolayers and grown to near confluence. The cells were then trypsinized, and plated at a concentration of 5×10^6 cells/ml in 5 ml. Cells were then allowed to adhere to the flasks and the medium replaced with one containing 10 and 20 μ M SR-4554. The flasks were then incubated for various lengths of time up to 3 hr under hypoxic (98% nitrogen, and 2% CO₂) or aerobic (2% CO₂, and 20% oxygen in nitrogen) conditions. Drug

containing media obtained at 0, 0.5, 1, 2, and 3 hr were then analysed by HPLC (see chapter 2).

Aliquots (250 μ l) of the incubation media were spiked with 20 μ l of an internal standard (8 μ g/ml Ro 07-0269) and the mixture extracted with 25 μ l of 30% w/w silver nitrate solution. Samples were vortexed, centrifuged (at $1000 \times g$) for 10 min, and the supernatants analysed by HPLC (see chapter 2). Calibration standards (0.35 to 35.46 μ M) were prepared in RPMI medium and also analysed by HPLC. The concentrations of parent drug in the incubation samples were determined and plotted against time. Rates of reduction were estimated from the initial slope of the concentration of SR-4554 versus time curve which was linear within the time period studied.

4.2.3 Preparation of A2780 multicellular spheroids

Human ovarian A2780 cells were plated (in RPMI medium) at a concentration of 2×10^6 cells/50 ml and incubated in stirrer flasks at 37°C to form spheroids. After 3.5 days in culture, spheroids of approximately 0.8 to 1.4 mm in diameter were obtained for use in the EELS experiment.

4.2.4 Incubation of A2780 spheroids with SR-4554

A2780 spheroids were incubated with culture medium containing a non-toxic concentration of 1 mM SR-4554 at 37°C for 3 hr. Incubations were carried out under normal aerobic cell culture conditions. Half of the spheroids were then transferred onto ice to stop further reaction. The other half were washed with fresh culture medium and 'chased' at 37°C for 2 hr under normal aerobic conditions. These were also transferred onto ice to stop further reaction.

4.2.5 Electron energy loss spectroscopic analysis

For analytical electron microscopy, all spheroids were briefly washed in phosphate buffered saline (PBS), and chemically fixed (on ice) with 1% glutaraldehyde in PBS for 1.5 hr. The spheroids were dehydrated in a series of alcohols for embedding at low temperature in Lowicryl K4M, a nitrogen-free hydrophilic methacrylate resin, without the use of heavy metal stains to avoid electron scattering. Ultra-thin sections were mounted onto 700 mesh copper grids for

electron spectroscopic analysis using a Zeiss TEM902 microscope (Karl Zeiss Oberkochen Ltd, Oberkochen, Germany) operating at 80 kV and 12,000 times magnification. The microscope was fitted with an electron energy filter for analysis of the local electron associated with fluorine (K-edge onset at $\Delta E = 688$ eV) and nitrogen (K-edge onset at $\Delta E = 405$ eV). This novel technique has a resolution of about 2 nm and an energy resolution of about 5 eV for sections of resin embedded cells, and a theoretical detection limit of fluorine of about 500 atoms (Huxham *et al.*, 1992; Johnson *et al.*, 1995).

Energy filtered image sequences were recorded between $\Delta E = 650$ -750 eV for fluorine and between ΔE 350-450 eV for nitrogen, changing only the (measurable) video camera (Dage SIT, Michigan, MN, USA) kV setting between each sequence pair to accommodate the change in energy loss intensity relative to the dynamic range of the video camera. Comparisons between defined regions within peripheral (outer) and cells approximately 150-160 μm from the edge of the spheroid (inner cells) were made using in-house software. Energy loss contribution of both fluorine and nitrogen were measured following background modelling for each pixel in median filtered energy loss image sequence. This was accomplished using the least mean square determination of the parameters which describe the energy loss curve (De Bruijn *et al.*, 1993; Johnson *et al.*, 1995). Cumulative background-stripped grey level values from 12 image sequences over a 30 eV portion of the post-ionization edge for fluorine and nitrogen were used to calculate elemental ratios. In this way, variations in the density of cellular material between one domain and another could be normalised as a function of the nitrogen content for each region of interest, to produce local semi-quantitative elemental maps. Data were also expressed as average grey level value representing energy loss for fluorine as a function of section area for each pixel.

4.2.6 Statistical analysis

Statistical parameters were generated using Minitab Release 9 (Minitab, State College, PA, USA) or Microsoft Excel, Version 4.0 (Microsoft, Redmond, WA, USA). The Mann-Whitney test of significance was employed to assess differential subcellular binding. A 95% confidence level was used.

4.3 RESULTS

4.3.1 Metabolism of SR-4554 by A2780 cells

SR-4554 was reduced by A2780 cells in culture under hypoxic conditions. This was assessed by chromatographic analysis of parent drug metabolised by the cells in culture. Fig. 4.3 shows a typical chromatogram of a hypoxic compared to an aerobic incubation sample also containing the internal standard (Ro 07-0269). No UV absorbing metabolites were observed. The rates of reduction of SR-4554 by A2780 cells under aerobic and hypoxic culture conditions are shown in Table 4.1. These data, obtained at 37°C, demonstrate the selective reduction of SR-4554 under hypoxia in contrast to normal aerobic conditions. As expected, the reduction rates increased at a higher substrate concentration.

4.3.2 Growth characteristics of A2780 spheroids

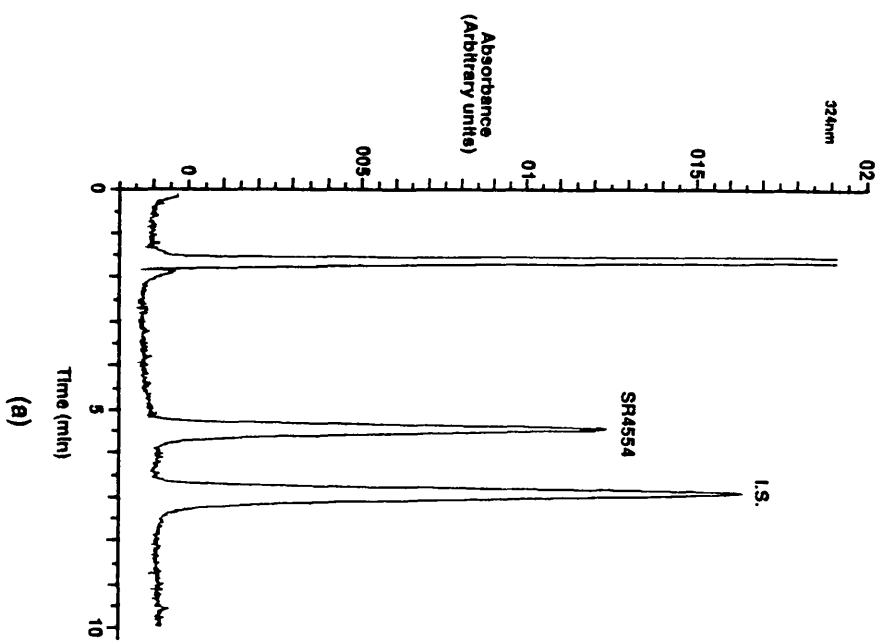
Initially, the cells aggregate but after 3.5 days in culture, they form tight proliferating spheroids as demonstrated by the presence of mitotic bodies indicating dividing cells. Under these conditions the large spheroids develop a region of hypoxia between the outer and the inner necrotic core. For this study, the most outer cell layer of the spheroid were taken as being aerobic, whereas cells in the inner region of the spheroid at approximately 150-160 μm from the surface, but separate from any necrotic core, were selected as hypoxic as shown by Miller *et al.* (1989) using EMT6 spheroids. A2780 spheroids are similar to EMT6 spheroids in that both form tight spheroid structures. In this regard, spheroid models showing differences in oxygen levels and binding of 2-nitroimidazoles has previously been established (Franko *et al.*, 1987; Franko *et al.*, 1992).

4.3.3 Sub-cellular localisation of SR-4554 in A2780 spheroids

EELS analysis of spheroids incubated with SR-4554 enabled the localisation of fluorine atoms in subcellular components within the spheroid. Fig. 4.4 shows an unstained, energy filtered image (reversed contrast) of A2780 cells from a spheroid after culture in SR-4554 containing medium, recorded at $\Delta E = 150 \text{ eV}$. By means of spectroscopic imaging, most intracellular structures of unstained

Fig. 4.3. Typical HPLC plot of SR-4554 after incubation with A2780 cells for 30 min under (a) Aerobic and (b) Hypoxic conditions. From left to right the three peaks illustrated indicate the solvent front, SR-4554 and internal standard (I.S.; Ro 07-0269) respectively.

Aerobic



Hypoxic

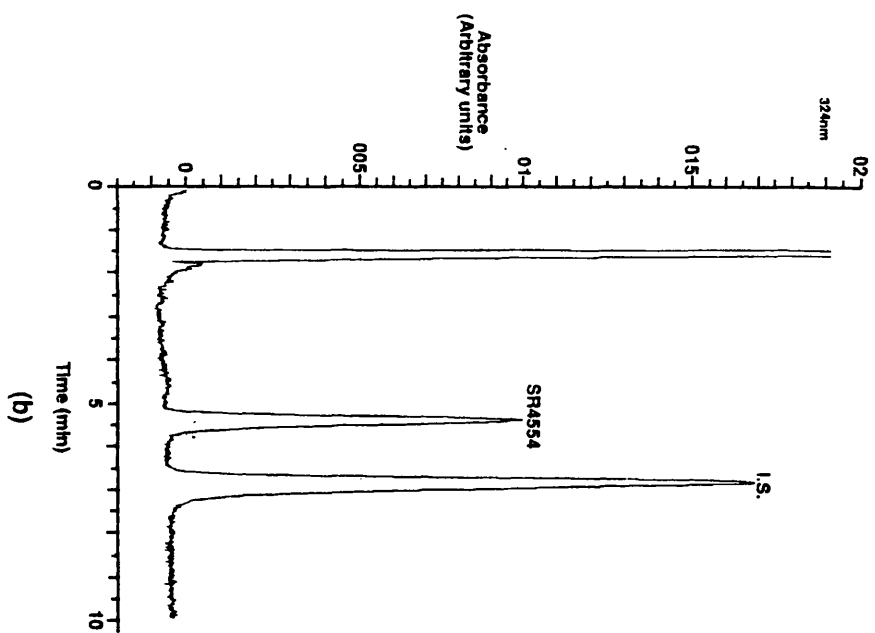
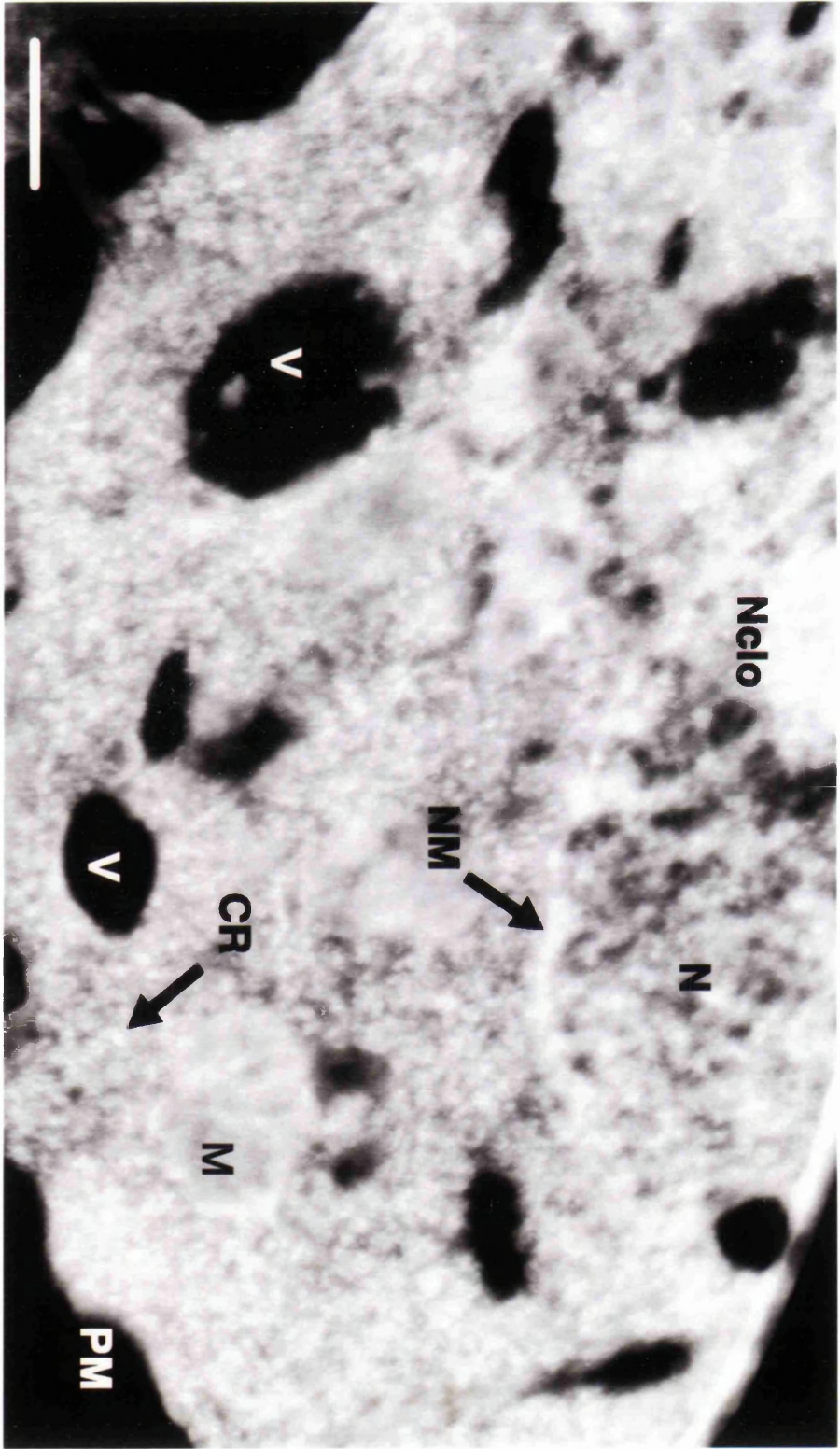


Table 4.1. Rate of loss of SR-4554 incubated with A2780 cells

Conditions	Drug concentration (μ M)	Rate of loss (nmoles/hr/ 10^6 cells)
Aerobic	20	No loss detected
	10	No loss detected
Hypoxic	20	7.5 ± 0.1
	10	4.3 ± 0.2

SR-4554 was incubated with A2780 cells under aerobic and hypoxic conditions. The levels of parent drug remaining at various time periods were determined as described in section 4.2.2. The values for rate of loss of compound are means \pm standard deviation from at least three separate determination.

Fig. 4.4. Energy filtered image of a portion of a heavy metal free A2780 cell within SR-4554 treated multicellular spheroids after a 'chase' culture, recorded at $\Delta E = 150$ eV, showing enhanced contrast in phosphorus-rich regions. The image shows a well defined nuclear region (N), nucleolus (Nclo), nuclear membrane (NM), vessicle (V), plasma membrane (PM), mitochondria (M) and cytoplasmic polyribosomes (CR). Bar = 700 nm.



material, otherwise difficult to see without filtering, could be identified for analysis. Using our in-house image analysis software, regions of interest (ROI) for each electron spectroscopic image sequence (ESIS) were defined simply by drawing on the reference image on the display screen. The same ROI was used for analysis of both nitrogen and fluorine ESIS sequences. The energy loss for nitrogen and fluorine were then determined by plotting the cumulative grey level value for the ROI for each ESIS. A representative projected distribution of fluorine (green) within a section of the inner region of the spheroid after the 'chase' process is shown in Fig. 4.5. This represents residual bound drug in the cell.

4.3.4 Semi-quantitative localisation of SR-454 in A2780 spheroids

An analysis of cytoplasmic domains (which includes cytoplasm, mitochondria, vesicle perinuclear regions) of cells (Fig. 4.6) suggests that the drug was

located in the plasma membrane regions) of the spheroid after a 3 hr culture. In the spheroids, only marginally less drug was found in the inner regions compared to the equivalent components of the outer spheroids. Interestingly, an eight fold higher level of drug was found in the cytoplasmic domains of these inner cells compared to the outer cells, as most of the drug which was used away following the 'chase' process. The drug by the inner cells is located within the inner cells of the

ZAVEDOS[®]
DAFABUCH

Do you know or are there any reports of intrinsic nitrogen content

Table 4.2 demonstrates that the drug distribution present within the cells from both the inner and outer regions of 'chased' spheroids was not uniform. Relative to the intrinsic nitrogen content of specific intracellular regions, which takes into account local variations of biological material, the amount of drug within the inner cells was found to be comparatively high at the periphery of intracellular vesicles, within the cytoplasm, in the nucleus and at its periphery. In contrast, the amount of drug was comparatively low within mitochondria and at the plasma membrane. Mann-Whitney

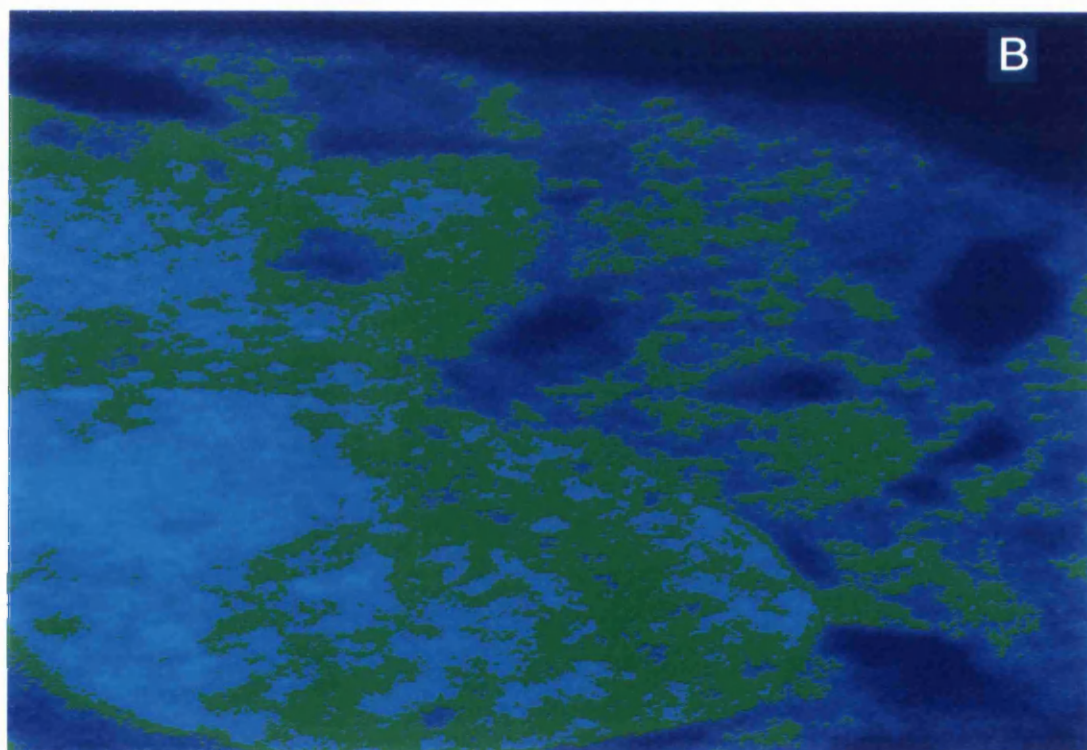
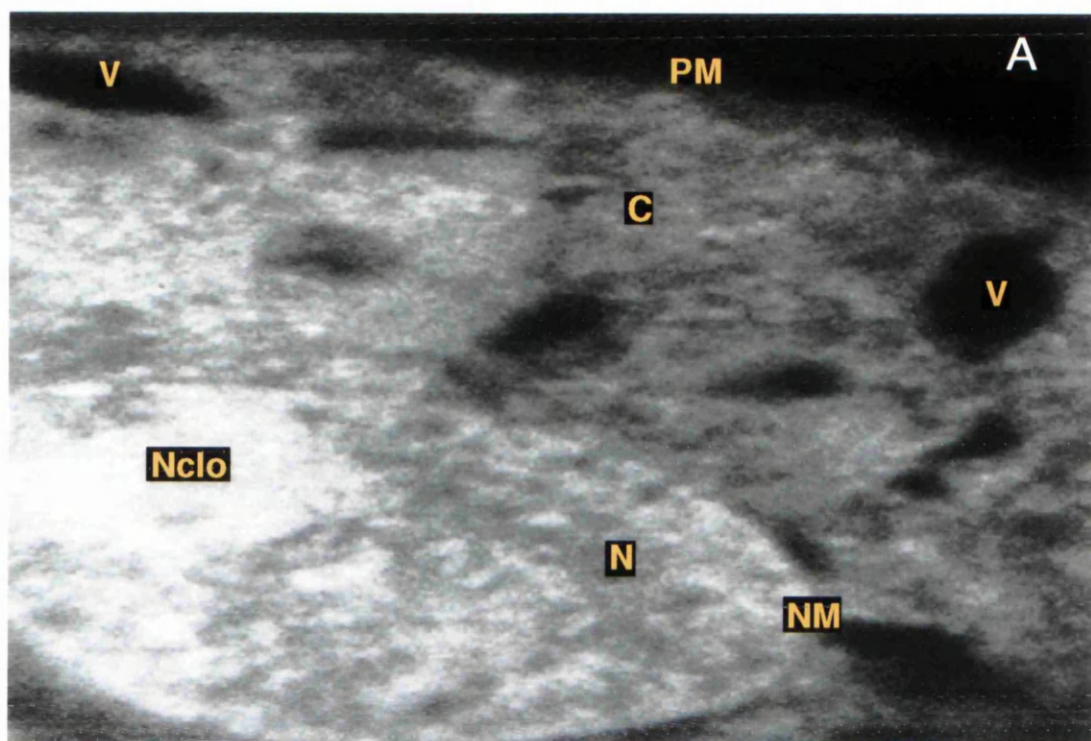
material, otherwise difficult to see without filtering, could be identified for analysis. Using our in-house image analysis software, regions of interest (ROI) for each electron spectroscopic image sequence (ESIS) were defined simply by drawing on the reference image on the display screen. The same ROI was used for analysis of both nitrogen and fluorine ESIS sequences. The energy loss for nitrogen and fluorine were then determined by plotting the cumulative grey level value for the ROI for each ESIS. A representative projected distribution of fluorine (green) within a section of the inner region of the spheroid after the 'chase' process is shown in Fig. 4.5. This represents residual bound drug in the cell.

4.3.4 Semi-quantitative localisation of SR-454 in A2780 spheroids

An analysis of cytoplasmic domains (which includes cytoplasm, mitochondria, vesicle periphery and plasma membrane regions) of cells within A2780 spheroids (Fig. 4.6) suggests that the drug was distributed into cells across the whole spheroid after a 3 hr culture. Following chemical fixation of these spheroids, only marginally less drug was bound to intracellular components within cells of the inner region of the spheroid as compared to the equivalent components of cells in the outer region. More importantly, an eight fold higher level of drug was present within the cytoplasmic domains of these inner cells after 'chasing' with drug-free media, as most of the drug which was present in the outer cells had diffused away following the 'chase' process. This selective retention of drug by the inner cells is indicative of increased bioactivation within the inner cells of the spheroids.

Table 4.2 demonstrates that the drug distribution present within the cells from both the inner and outer regions of 'chased' spheroids was not uniform. Relative to the intrinsic nitrogen content of specific intracellular regions, which takes into account local variations of biological material, the amount of drug within the inner cells was found to be comparatively high at the periphery of intracellular vesicles, within the cytoplasm, in the nucleus and at its periphery. In contrast, the amount of drug was comparatively low within mitochondria and at the plasma membrane. Mann-Whitney

Fig. 4.5. (a) Reference image of a section from an inner A2780 cell within SR-4554 treated multicellular spheroids after a 'chase' culture, recorded $\Delta E = 150$ eV. The image shows the plasma membrane (PM), vesicles (V), cytoplasm (C), nuclear membrane (NM), nucleus and nucleolus (Nclo). (b) The same image upon which the projected fluorine distribution is superimposed (green). The green binary fluorine map simply shows regions in which fluorine was found to be present (i.e. a stripped grey level value above background). TIFF images were reproduced on a Kodak ColoureseTM printer (field width = 5 μ M).



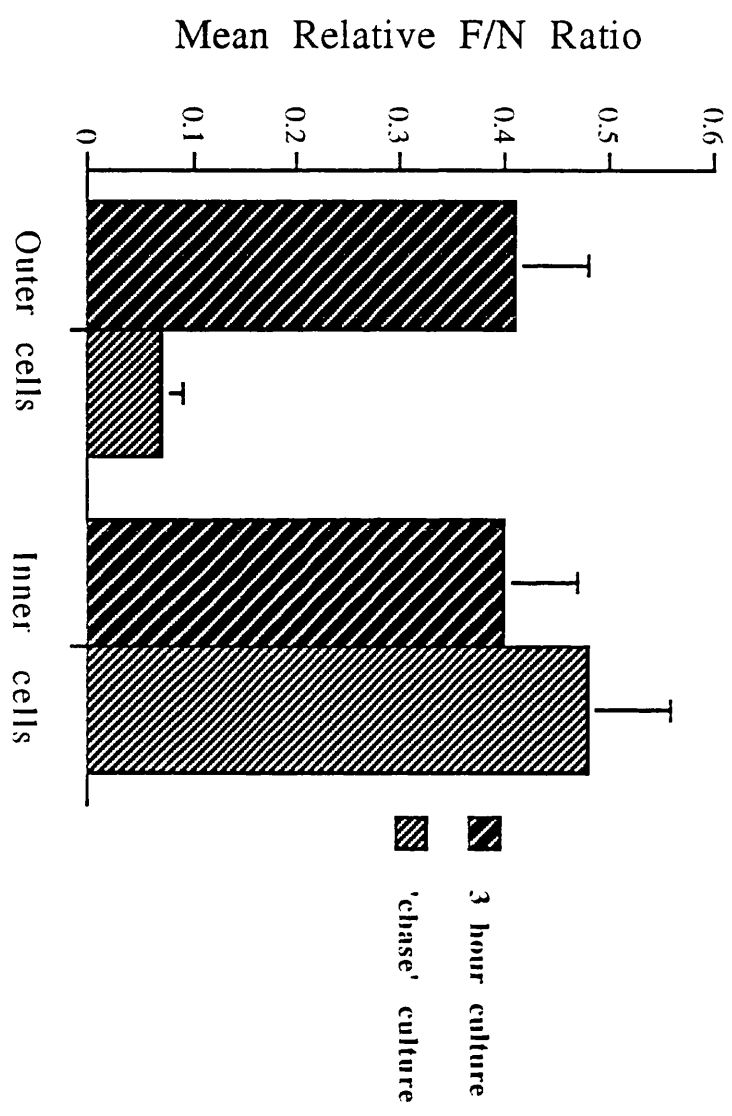


Fig. 4.6. Histograms showing the mean \pm standard deviation of fluorine/nitrogen (F/N) elemental ratios for cytoplasmic domains (which includes cytoplasm, mitochondria, vesicle periphery and plasma membrane regions) from the outer and inner cells of A2780 multicellular spheroids cultured for 3 hr (dark hatch) in SR-4554 and after a 2 hr 'chase' (light hatch) in drug-free media.

Table 4.2. The relative average fluorine and fluorine/nitrogen elemental ratios for six intracellular domains of both outer and inner cells from A2780 multicellular spheroids following a 'chase' culture with SR-4554.

Domain	Nucleus	Nuclear Periphery	Cytoplasm	Mitochondria	Vesicle Periphery	Plasma Membrane	
F/pixel	Outer	0.6 ± 0.3 ¹	0.4 ± 0.2	0.7 ± 0.2	ND ²	0.6 ± 0.2	ND
	Inner	2.1 ± 0.5	4.2 ± 0.7	2.0 ± 0.4	0.8 ± 0.2	0.2 ± 0.06	0.5 ± 0.1
	F/N ratio						
Outer	0.03 ± 0.02	0.03 ± 0.01	0.1 ± 0.04	ND	0.07 ± 0.03	ND	
Inner	0.2 ± 0.02	0.2 ± 0.08	0.3 ± 0.08	0.06 ± 0.02	0.3 ± 0.06	ND	

¹Average value from 12 areas ± standard deviation for each domain expressed as the relative amount of fluorine per pixel [8 nm²] (F/pixel) or as a fluorine to nitrogen (F/N ratio).

²ND is not detected.

test revealed that there were statistically significant differences ($p < 0.05$) when the following comparisons were made:

Outer cells F/N ratio:

- a. cytoplasm vs nuclear periphery and nucleus.

Inner cells F/pixel:

- a. mitochondria vs nucleus and nuclear periphery.
- b. nuclear periphery vs cytoplasm, vesicle periphery and plasma membrane.

Inner cells F/N:

- a. vesicle periphery vs mitochondria and plasma membrane
- b. mitochondria vs nucleus, nuclear periphery and cytoplasm.

Although the nitrogen atoms in the drug will contribute to the total nitrogen intensity signal of the EELS technique, by far the greater contribution will come from the biological macromolecules of the cell to which the drug is localised. When simply expressed in terms of the average amount of fluorine per unit area of cell section, the data suggested that there was a relative accumulation of fluorine at the nuclear periphery and in the nucleus compared to other regions, more representative of the projected fluorine distribution shown in Fig. 4.5. In addition, it was observed that across all domains, there was less drug (3-10 fold) localised within the outer (aerobic) cells compared to the inner (hypoxic) cells.

4.4 DISCUSSION

The localisation of 2-nitroimidazoles following reduction by tumour cells is important in our understanding of the use of these compounds as hypoxic probes. The aim of this study was to study the uptake, subcellular localisation, and hypoxia selective retention of SR-4554 within A2780 spheroids. The human ovarian A2780 cell line was used in this study since this cell line has been previously well characterised (Tsuruo *et al.*, 1986), and has also been shown to express NADPH: cytochrome P450 reductase, an important enzyme involved in the reductive metabolism of 2-nitroimidazoles (see chapter 3), by enzyme assay and PCR analysis (data not shown). This cell line was also considered likely to develop a hypoxic region in spheroids over the size range used and was, therefore, used in the reductive drug localisation studies.

SR-4554 was metabolised by A2780 cells in culture under hypoxia, albeit at a slower rate than in mouse liver microsomes. This may be due to the higher enzyme levels in microsomes compared A2780 cells. This hypoxia mediated metabolism was selectively inhibited in the presence of air. This is due to the reversal of 2-nitroimidazole reduction by oxygen, as previously demonstrated with SR-4554 in chapter 3, as well as with other analogues such as misonidazole, desmethylmisonidazole and benznidazole (Chapman *et al.*, 1983; Joseph *et al.*, 1994; Walton & Workman, 1987).

The use of the novel EELS technique permitted the localisation of the SR-4554 within human ovarian carcinoma spheroids. It should be noted that the EELS technique measures fluorine atoms within SR-4554 and will therefore not differentiate between original parent drug and (bound or unbound) metabolites. In cultures not subjected to 'chasing', no significant differential was observed between cells of the inner and outer regions of the spheroid. This presumably is due to the presence of both original parent drug and bound drug. The method of 'chasing' in drug-free media to differentiate between bound and unbound drug was, therefore, employed to allow the assessment and localisation of bound metabolites.

Interestingly, the results obtained in our study using spheroids and EELS were in accordance with the metabolism-induced binding of 2-nitroimidazoles to macromolecules as previously demonstrated by other methods with limited spatial resolution such as autoradiography and immunohistochemistry (Lord *et al.*, 1993; Miller *et al.*, 1982). In contrast to these other methods, the EELS technique also allows the ability to measure drug binding in relation to the density of other local macromolecular components. Although some non-specific binding occurred in the cells of the outer (aerobic) region of the spheroids, levels of fluorine in the cytoplasm of cells from the inner (hypoxic) regions were at least eight fold higher. This differential is the more likely to occur in an *in vivo* situation where elimination processes will result in the removal of unbound drug compared to the bound metabolite. Importantly, the localisation characteristics shown in this study are very relevant to the use of this novel fluorinated compound as a non-invasive marker of tumour hypoxia in the clinic. The presence of three magnetically equivalent fluorine atoms in the structure of the compound, which remains intact on enzyme

reduction, is important in terms of its detection by magnetic resonance techniques, as well as EELS.

Further studies using EELS enabled the more detailed analysis of the subcellular localisation of SR-4554 within cells in the outer and inner regions of the spheroid. In this study, the mitochondria and plasma membrane did not appear to bind significant amounts of drug. Of interest, however, were the high levels of SR-4554 localised to the nuclear periphery, nucleus and cytoplasm within the inner hypoxic cells. These data are in agreement with previously published studies using subcellular fractionation of cells labelled with ^{14}C misonidazole, considering that the molecular components in these regions consist mainly of RNA, DNA, lipids and proteins (Chapman *et al.*, 1990; Miller *et al.*, 1982). In addition, the distribution of 2-nitroimidazoles to cytoplasm, nuclear and perinuclear regions were also mentioned by Cline *et al.* (1994) who used antibodies, which were raised against the hexafluorinated 2-nitroimidazole CCI-103F/CCI-103F adducts, in order to follow the distribution of hypoxia and/or reductive enzymes within cells of canine tumours. In contrast, and as expected, there was less drug localised by EELS within all the domains in the outer cells.

The initial steps in the reductive metabolism of 2-nitroimidazoles are mainly catalysed by NADPH: cytochrome P450 reductase and to a lesser extent by NADPH: cytochrome P450, both of which are found in the endoplasmic reticulum (Mcmanus *et al.*, 1982; Walton & Workman, 1987). The subcellular distribution of SR-4554 demonstrated in these studies, was consistent with the view that the reactive intermediate is short lived and binds to macromolecules within the vicinity of the metabolism site or to nucleophiles such as RNA close to these sites. Importantly, the evidence would suggest that the reactive metabolites do not diffuse far from their sites of activation, a fact which has previously been suggested by Franko & Koch (1984) from their experiments with misonidazole. This characteristic is also relevant to the design of bioreductive drugs, based on 2-nitroimidazoles, which will target the nucleus of the cell to deliver radioisotopes or alkylating moieties.

Currently, SR-4554 is undergoing pre-clinical development prior to scheduled clinical trials as a probe for investigating tumour hypoxia by non-invasive MRS. Important to the direction of these

studies, the observations made in this chapter are useful in the interpretation of data from non-invasive MRS studies. In addition, the EELS technique itself can also be used to study the distribution of hypoxic regions within tumours labelled *in vivo* with SR-4554 even though this will involve invasive (biopsy) procedures. As a semi-quantitative technique, however, it offers the potential of measuring hypoxia on a cell to cell basis at a molecular level with good resolution compared to antibody techniques and also the investigation of drug-cellular macromolecule interactions without the use of radioisotopes.

CHAPTER 5

Toxicity and pharmacokinetics of SR-4554 in mice

5.1 INTRODUCTION

Pharmacokinetics is defined as the study and characterisation of the time course of drug absorption, distribution metabolism and excretion. The two processes of metabolism and excretion are referred to as elimination. Both pre-clinical pharmacokinetic studies and toxicity profiles provide useful data to enable the establishment of a safe human dose, as well as the intensity and time course of therapeutic effect.

The literature on the pharmacokinetics of nitroimidazoles, particularly those in use as radiosensitizers, is very large (see review by Workman, 1983b). This is due to the major influence of pharmacokinetics on the activity and toxicity of these agents. In general there are two major properties which are considered important in the design of 2-nitroimidazoles. These are their reduction potential and lipophilicity (octanol/water partition coefficient; P_{oct}) (Adams *et al.*, 1979; Brown & Workman, 1980; Workman & Brown, 1981). The reduction potential of N-1 substituted 2-nitroimidazoles, which relates to the rate of metabolic reduction and adduct formation, varies only slightly from one 2-nitroimidazole to another (Adams *et al.*, 1979; Workman & Brown, 1981). In contrast, however, the lipophilicity and hence tissue penetration particularly into the nervous system of 2-nitroimidazoles vary very widely. This property of the compounds is very important with regard not only to their toxicity, but also to their pharmacokinetics and distribution to reductive sites (White *et al.*, 1982; White & Workman, 1980; White *et al.*, 1980; Workman, 1979; Workman, 1982).

The dose limiting toxicity of the prototype 2-nitroimidazole, misonidazole, is neurotoxicity presented mainly as peripheral neuropathy and also central effects such as ototoxicity (Urtasun *et al.*, 1978). It has been demonstrated in mice that for a series of 2-nitroimidazoles with varying N-1 substituents, the more lipophilic 2-nitroimidazoles are more toxic than misonidazole, whereas the more hydrophilic 2-nitroimidazoles, such as etanidazole and desmethylmisonidazole, are less toxic (Workman & Brown, 1981). This is also exemplified by the fact that etanidazole can be

administered at the equivalent of three times the dose of misonidazole in man to give the same degree of peripheral neuropathy as misonidazole (Coleman *et al.*, 1986). Experiments conducted in mice and dogs have shown that exclusion of the more hydrophilic 2-nitroimidazoles from the brain and nervous system but not from tumours, as well as their increased plasma clearance is responsible for the direct correlation between lipophilicity and neurotoxicity (White *et al.*, 1982; White & Workman, 1980; White *et al.*, 1980; Workman & Brown, 1981).

The mechanism of nitroimidazole neurotoxicity is still a subject of continuing research. Results obtained using rat phaeochromocytoma and mouse neuroblastoma cell lines suggest that nitroimidazoles cause the disruption and degeneration of dendritic projections (Stevenson *et al.*, 1989). The identity of the proximal toxic species is, however, still a matter of controversy. The presence of reactive metabolites of misonidazole in the urine of patients treated with misonidazole, led Varghese & Whitmore (1984a) to suggest that nitroreduction products such as the hydroxylamine species and glyoxal (see Fig. 1.4 and 1.5), may be involved in neurotoxicity.

Generally, metabolism is the major elimination mechanism for lipophilic nitroimidazoles whereas renal clearance predominates for more hydrophilic analogues and metabolites (Workman, 1983b; Workman & Brown, 1981). It is therefore not unexpected to find that misonidazole exhibits non-linear elimination kinetics, whereas more hydrophilic analogues such as desmethylmisonidazole exhibits linear kinetics (Workman, 1980). In spite of these differences, tumour concentrations of 2-nitroimidazoles appear not to vary markedly. For instance, the tumour concentrations of neutral (un-ionised) N-1 substituted 2-nitroimidazoles consistently averages around 70-100% of circulating concentration (Brown & Workman, 1980; Workman, 1983b; Workman & Brown, 1981).

The structural features of SR-4554 as a potential MRS hypoxia probe are unique, in that apart from the presence of three magnetically equivalent fluorine atoms, the compound has also been designed to include an amide side chain similar to etanidazole. This feature was incorporated with the expectation that it would reduce nervous tissue penetration and exposure in a similar way to that seen with etanidazole, thereby reducing toxicity. This chapter therefore

looks at the toxicity (or tolerability) and the pharmacokinetics of SR-4554 in mice to assess the effect of the trifluoromethyl (lipophilic) and amide (hydrophilic) functions. These studies would also aid in modelling MRS/MRI protocols for SR-4554 in animals and in man.

5.2 MATERIALS AND METHODS

5.2.1 Chemicals and reagents

SR-4554 and etanidazole (SR-2508) were synthesized and supplied by SRI international, Menlo Park, CA, USA. Misonidazole (Ro 07-0582), desmethylmisonidazole (Ro 05-9963), fluoromisonidazole (Ro 07-0741), Ro 07-2044, ethylmisonidazole (Ro 07-0913), and chloromisonidazole (Ro 07-0269) were obtained from Roche products, Welwyn Garden City, Herts, UK. CCI-103F was obtained from Dr J. Raleigh, Cross Cancer Institute, Edmonton, Canada. The structures of these compounds are shown in Fig. 1.3. The compounds were assessed for chromatographic purity and used without further purification. All other reagents and chemicals used were of analytical or HPLC grade.

For the preparation of dose solutions used in this chapter, SR-4554 was weighed and dissolved in warm (50°C) saline to a final concentration of between 2.7 and 6.5 mg/ml. In all studies, dose solutions were prepared just before use. Quality control of dose solutions was carried out by taking samples from dose solutions before and after the experiments and freezing them at -70°C. The exact concentrations of the dose solutions were then verified by direct HPLC analysis.

5.2.2 Experimental animals and tumour implantation

Female Balb/c mice (6-9 weeks old) were obtained from Harlan Olac Ltd., UK and were allowed laboratory chow and water *ad libitum*. The mouse mammary tumour line EMT6 was obtained from Dr P.R. Twentyman (MRC Clinical Oncology and Radiotherapeutics unit, Cambridge, UK) and cultured as a monolayer according to the methods of Twentyman *et al.* (1986). The cells were trypsinized, washed with culture medium, and resuspended in phosphate buffered saline (PBS) just before use. Female Balb/c mice were inoculated intradermally in the right flank with 10^5 cells in 0.1 ml PBS. Tumours were used when they reached between 100 and 200 mm³.

5.2.3 Partition coefficient of SR-4554

The partition coefficient of SR-4554, together with misonidazole and etanidazole, were determined spectrophotometrically as previously described by Yang *et al.* (1995) in order to establish the relative affinity for lipid vs aqueous environments prior to toxicity and pharmacokinetic studies. Partition coefficients were determined at room temperature by shaking solutions of the various compounds (0.1, 0.2, and 0.5 mM) in 50 ml 1-octanol with 150 ml distilled water for 3 min. The phases were separated by centrifugation ($2000 \times g$ for 30 min) and the partition coefficients were determined from the amount of compound remaining in the aqueous phase (concentration in non-aqueous phase by difference). Sample blanks were prepared by using the same volumes of 1-octanol and distilled water as test samples. The spectrophotometric assay was carried out at 324 nm in a Lambda 2 spectrophotometer (Perkin-Elmer, Ueberlingen, Germany). Partition coefficient of each compound was determined in triplicate and the mean and standard deviations calculated.

As an alternative means of comparing the lipophilic vs hydrophilic character of 2-nitroimidazoles, the retardation of a series of 2-nitroimidazoles (SR-4554, misonidazole, chloromisonidazole, etanidazole, desmethylmisonidazole, ethylmisonidazole, Ro 07-2044, fluoromisonidazole and CCI-103F) on a C_{18} column were evaluated. All samples (10 $\mu\text{g/ml}$) except CCI-103F were analysed individually and then together using the same conditions as described in section 2.2.7. To allow comparison with the other 2-nitroimidazoles, CCI-103F (10 $\mu\text{g/ml}$) was analysed together with chloromisonidazole (Ro 07-0269) using a mobile phase consisting of 25% acetonitrile, 5 mM octane sulphonic acid and 0.2 M glycine/HCl buffer (pH 2.5). The mobile phase was delivered isocratically at a flow rate of 3 ml/min and analytes monitored by UV photodiode detection at 324 nm. The ratio of the time the analyte spends in the stationary phase to the time in the mobile phase, expressed as the capacity factor (k) for the various 2-nitroimidazoles was calculated using the equation below (Davidson, 1988):

$$k = (t_R - t_0)/t_0$$

where t_R and t_0 are the retention and void times respectively.

5.2.4 Toxicity studies

Initially this study was designed to establish the lethal dose which would kill 50% (LD_{50}) or 10% (LD_{10}) of mice. Due to the limited solubility of SR-4554 in saline (maximum solubility in saline = 6.5 mg/ml), however, only a limited study could be carried out to determine the tolerability of SR-4554 at selected doses. SR-4554 was administered in four different schedules to non-tumour bearing Balb/c mice. In the first schedule, SR-4554 (3.82 mg/ml) was administered as a short (30 sec) i.v. infusion through the tail vein at a dose of 191 mg/kg (0.05 ml/g). In the second schedule, SR-4554 (3.82 mg/ml) was administered i.p. at a dose of 382 mg/kg (0.1 ml/g). In the third and fourth schedules, SR-4554 (6.5 mg/ml; maximum solubility) was administered i.p. at a dose of 650 mg/kg (0.1 ml/g) and 1300 mg/kg (two dose of 0.1 ml/g separated by 30 min) respectively.

With each dose schedule two mice were treated with drug and two mice received an equivalent volume of 0.9% saline. Mice were weighed and observed immediately after treatment and then daily for 23 days.

5.2.5 Plasma and tissue pharmacokinetic studies

To study the plasma and tissue pharmacokinetics of SR-4554 in mice, the drug solution (2.7 mg/ml) was administered as a single i.p. injection of 162 mg/kg body weight (0.06 ml/g) to mice bearing the EMT6 tumour. Control mice received 0.9% saline alone. Mice were sacrificed at 5, 10, 15, 30, 45, 60, 90, 120, 240, and 360 min following i.p. injection of the drug. Three mice per time point were used and whole blood was removed under ether anaesthesia by cardiac puncture into heparinised tubes. Plasma was obtained by centrifugation ($3000 \times g$ for 5 min). Tumour, liver, and brain tissue were excised from each mouse into pre-weighed plastic vials. All samples were immediately frozen using solid CO_2 and stored at $-70^\circ C$ prior to analysis.

To allow comparison of pharmacokinetic studies with MR-experiments, the plasma and tumour pharmacokinetics of SR-4554 were repeated at 180 mg/kg (3 mg/ml; 0.06 ml/g). In these studies,

livers and brains were also excised and frozen at 5, 45, 120 and 360 min. In addition to this, a limited sampling (3 mice per time point at 5, 120 and 360 min) plasma pharmacokinetic study was carried out at a dose of 337 mg/kg (5.62 mg/ml; 0.06 ml/g) in EMT6 tumour bearing female Balb/c mice to enable a dose response model for SR-4554 to be established.

Prior to the determination of SR-4554 concentration in plasma samples, the samples were thawed and aliquots (250 µl) extracted together with a fresh calibration standard. Samples were then analysed by HPLC as previously described (section 2.2.6 and 2.2.7). Tissue samples were also thawed and homogenized (10%) in 0.1 M Tris-HCl buffer. Aliquots (250 µl) of the samples and fresh calibration standards prepared in untreated tissue homogenates were extracted and analysed by HPLC as previously described (section 2.2.6 and 2.2.7). All samples from mice were analysed individually to enable the assessment of variability.

5.2.6 Bioavailability studies

In order to assess the bioavailability of SR-4554 and to allow comparison with other 2-nitroimidazoles such as misonidazole and etanidazole, the drug was administered to non-tumour bearing female Balb/c mice at a dose of 90 mg/kg body weight via the i.v. (tail vein), i.p. and p.o. (oral) routes. This lower dose was chosen due to solubility and volume constraints with the formulation and route of administration of the compound. Again three mice per time point were used and the drug was administered as 0.02 ml/g body weight (4.5 mg/ml) for i.p. and i.v. routes and 0.0138 ml/g body weight (6.5 mg/ml) for the oral route. Plasma samples were collected and prepared as above prior to analysis.

5.2.7 Elimination of SR-4554

To assess the route and extent of drug elimination, SR-4554 was injected as a single i.p. dose of 180 mg/kg (3 mg/ml; 0.06 ml/g) to non-tumour bearing female Balb/c mice. Following the administration of SR-4554, mice were housed in metabolic cages (Metabowl Mark III; Jencons Scientific Ltd, Leighton Buzzard, UK) for 24 hr. They were allowed laboratory chow and water *ad libitum* during this period. The total urinary volume over 24 hr was

measured and aliquots stored at -70°C prior to analysis. Faecal pellets obtained from the same mice were weighed and stored at the same temperature.

For the analysis of SR-4554 concentration, urine samples were thawed and diluted (125 fold) in 0.1 M Tris-HCl buffer (pH 7.4). The samples were then clarified by centrifugation ($3000 \times g$) for 10 min and aliquots (50 μ l) of the supernatant analysed directly by HPLC. Faecal pellets from individual mice were thawed and prepared as 10% homogenates in 0.1 M Tris-HCl buffer (pH 7.4) followed by agitation on a shaker for 2 hr. The samples were then extracted with an equal volume of methanol and centrifuged ($3000 \times g$) for 10 min. Aliquots (50 μ l) of the extracts were subsequently analysed by HPLC.

5.2.8 Pharmacokinetic analyses

Pharmacokinetic parameters were determined by fitting the data using a computer generated iterative least square regression programme with appropriate weighting functions (ADAPT II) (D'Argenio & Schumitzky, 1979). Following i.v. administration, drug concentrations fitted a two compartment (bi-exponential) open model (D'Argenio & Schumitzky, 1979):

$$C_t = [D(\alpha - K_{pc})/V_{d1}(\alpha - \beta)]e^{-\alpha t} + [D(K_{pc} - \beta)/V_{d1}(\alpha - \beta)]e^{-\beta t}$$

All other data fitted a one compartment (mono-exponential) open model:

$$C_t = [FDK_a/V_d(K_a - K_e)](e^{-K_e t} - e^{-K_a t})$$

where C_t is the plasma or tissue concentration at time t , D is the dose administered, F is the fraction of dose absorbed, V_d and V_{d1} are the volume of distribution and volume of the central compartment respectively, the constants K_a , K_e , K_{pc} , α and β are absorption rate constant, elimination rate constant, peripheral to central compartment microconstant, distribution rate constant and the terminal rate constant respectively. The half life ($t_{1/2}$), clearance (CL) and central to peripheral microconstant K_{cp} were also estimated using these models.

The area under the concentration time curve (AUC) was derived using the trapezoidal rule (Curvfit: L. Hart Institute of Cancer Research, Sutton, Surrey, UK) and extrapolated to infinity using the elimination rate constant:

$$AUC(t_{last} - \infty) = C_{last}/\beta$$

where C_{last} is the final concentration of SR-4554 measured at time t_{last} . The bioavailability F , from an extravascular (ex) dose was determined as follows:

$$F = AUC_{(ex)} \times Dose_{(i.v.)} / AUC_{(i.v.)} \times Dose_{(ex)}$$

The optimal sampling times used for the plasma pharmacokinetic study were generated using ADAPT. Bayesian parameter estimates of V_d , K_e , and K_a were also derived using ADAPT. The coefficient of variation in the model parameter estimates was fixed at 50%. The model dependent AUC in this case was derived as follows:

$$AUC_{(0-\infty)} = Dose/CL$$

The amount of SR-4554 excreted unchanged in the urine was calculated as a percentage of the dose administered to each mouse.

5.2.9 Plasma protein binding studies

The *in vitro* mouse and human plasma protein binding of SR-4554 was studied by centrifugal ultrafiltration, using two different protocols. In the first protocol, fresh female Balb/c mouse plasma and human plasma (from healthy volunteers) were spiked with stock solutions of SR-4554 (2 mg/ml) in 0.1 M Tris-HCl buffer (pH 7.4) to give 1, 50 and 150 μ g/ml at room temperature (25°C). To assess non-specific binding, SR-4554 standards were prepared at the same concentrations in buffer.

Plasma protein binding was measured using an Amicon micropartition system, MPS1 (Amicon Div., W.R. Grace and Co, Danvers, MA, USA) with a cut-off of 30,000. For the separation of free and protein bound microsoluble, all samples were centrifuged

using fixed angle rotor ($3000 \times g$ for 15 min) at 20°C . The samples were then directly analysed by HPLC (section 2.2.7). The percentage of protein bound SR-4554 was assessed by comparing the peak area of the plasma peak to that of unfiltered standard. Correction for non-specific binding was made by comparing filtered and un-filtered standards. Four samples were determined at each concentration.

To allow comparison with other 2-nitroimidazoles, in the second protocol, the procedure was repeated for SR-4554 and misonidazole at $30 \mu\text{g/ml}$. The method was, however, modified to include the incubation of samples in a water bath at 37°C for 1 hr prior to ultrafiltration (Workman & Brown, 1981).

5.3 RESULTS

5.3.1 Partition coefficient studies

The partition coefficients (P_{oct}) of SR-4554, misonidazole (Ro 07-0528) and etanidazole (SR-2508) as determined by spectrophotometric assay (mean \pm s.d.) were 0.65 ± 0.10 , 0.41 ± 0.10 , 0.048 ± 0.01 respectively.

The chromatographic retardation of a series of 2-nitroimidazoles on a C_{18} column is illustrated in Fig. 5.1. Fig. 5.2 shows that a plot of $\log k$ vs $\log P$ (the latter derived from both this study and from literature values (Brown & Workman, 1980; Raleigh *et al.*, 1991a; Rauth *et al.*, 1978)) was linear, i.e. the higher the partition coefficient (P_{oct}), the higher the capacity factor (k) or retardation. Importantly, however, even though P_{oct} of SR-4554 was higher than that of misonidazole, the k (or $\log k$) of SR-4554 was actually lower than that of misonidazole (Ro 07-0582).

5.3.2 Toxicity studies

The pilot dose ranging studies of SR-4554 in non-tumour bearing mice showed that SR-4554 was non-toxic up to a dose of 1300 mg/kg (Fig. 5.3). No deaths or significant change in body weight (as a percentage of day 1) were observed in both drug treated mice and saline controls at the four selected doses (Mann Whitney test; 95 confidence level). In addition, no visual changes (neurological, gastrointestinal, performance status, hair characteristics, feeding status, lacrymation, urine colouration) or abnormal anatomical status at day 23 were observed.

Fig. 5.1. HPLC retardation of a series of 2-nitroimidazoles (10 $\mu\text{g/ml}$) on a C_{18} column. Analytes were eluted with either 15% methanol-water (top chromatogram) or 25% acetonitrile-5 mM octane sulphonic acid-0.2 M glycine/HCl buffer (pH 2.5) (bottom chromatogram), and monitored by UV detection at 324 nm.

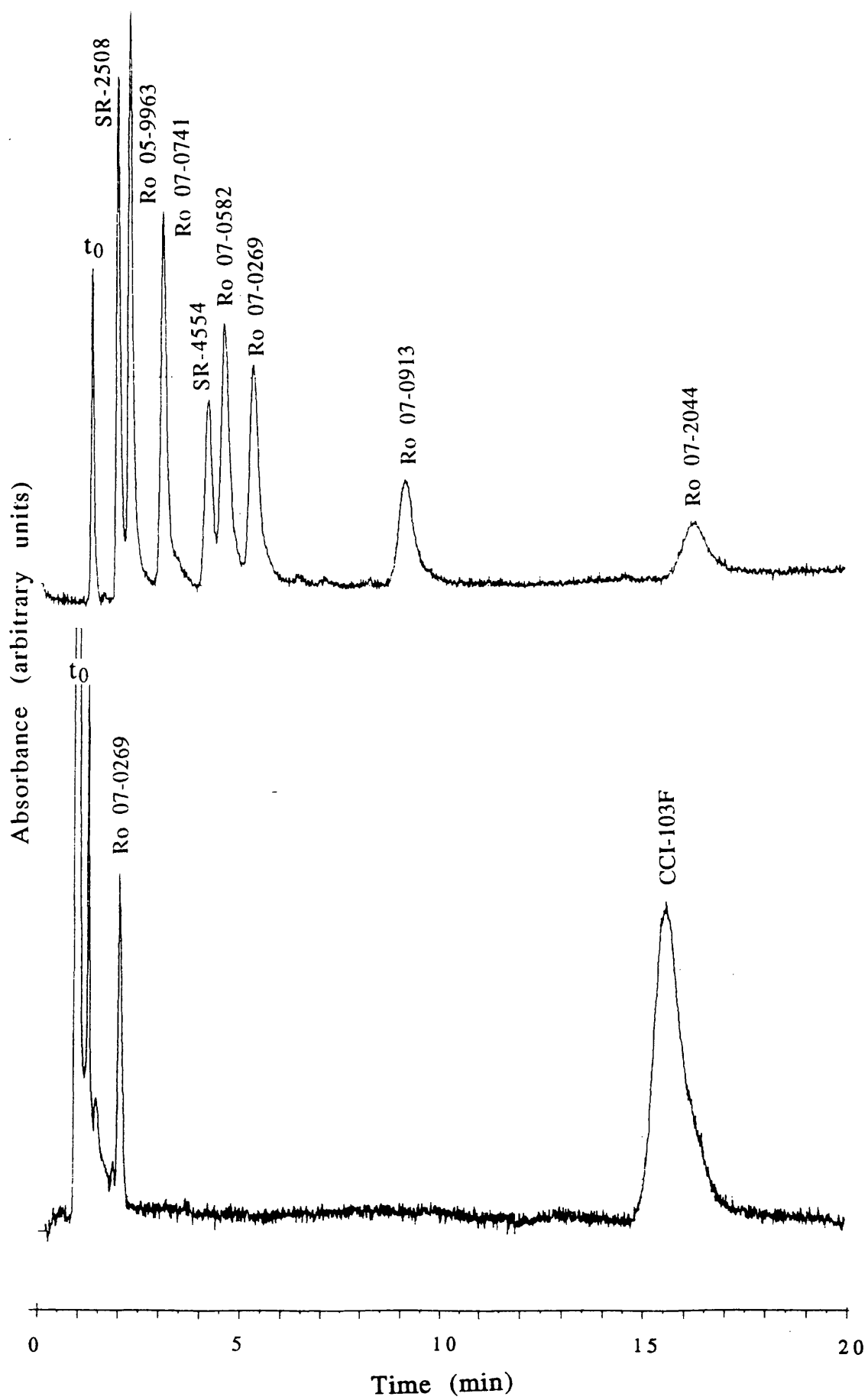


Fig. 5.2. HPLC retardation of a series of 2-nitroimidazoles on C_{18} column (15% methanol-water mobile phase) vs partition coefficient. The figure shows a plot of $\log k$ vs $\log P_{oct}$ of the various 2-nitroimidazoles (see text).

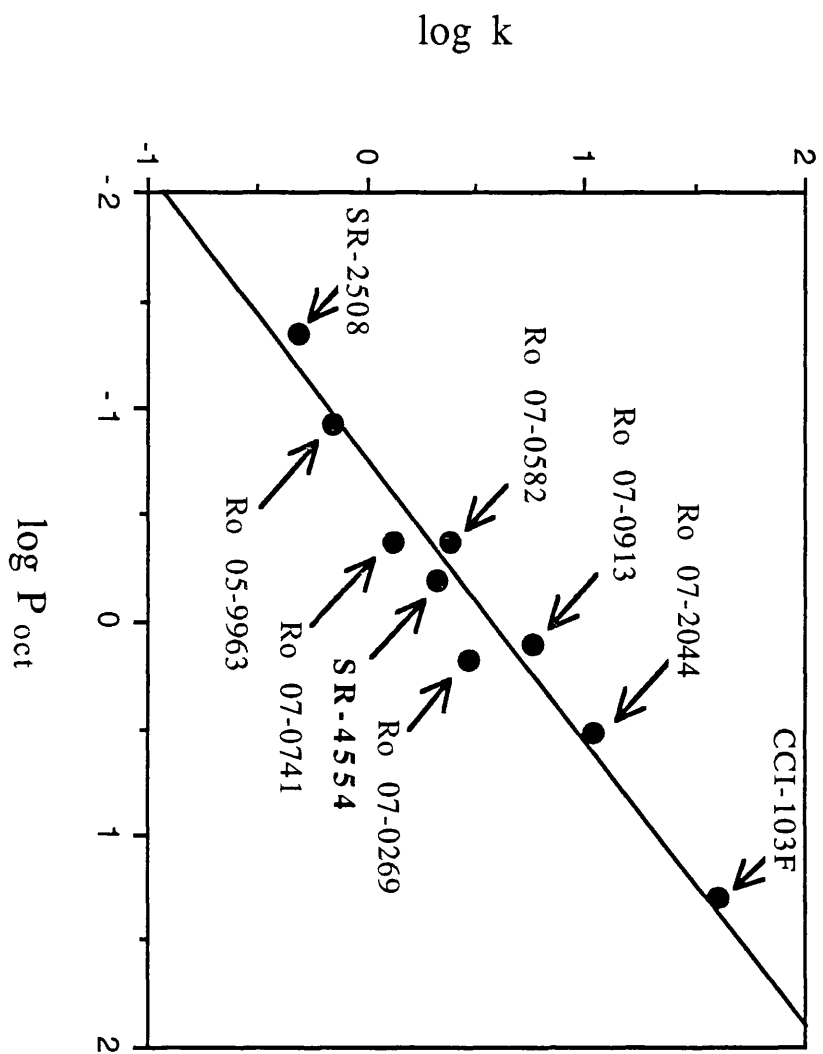
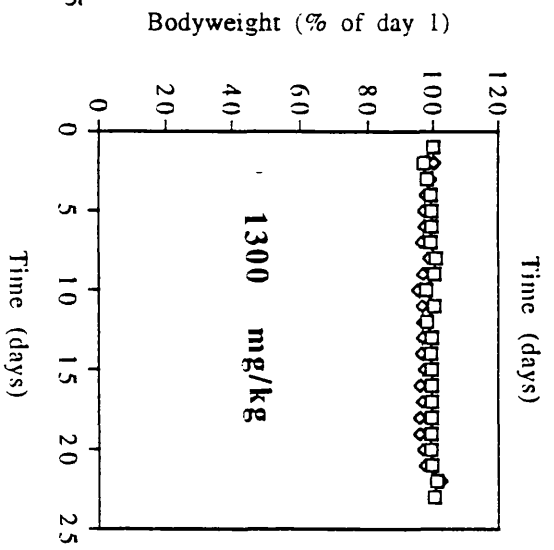
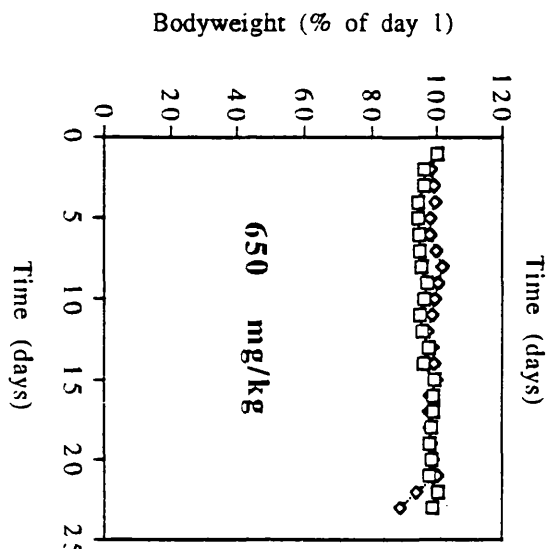
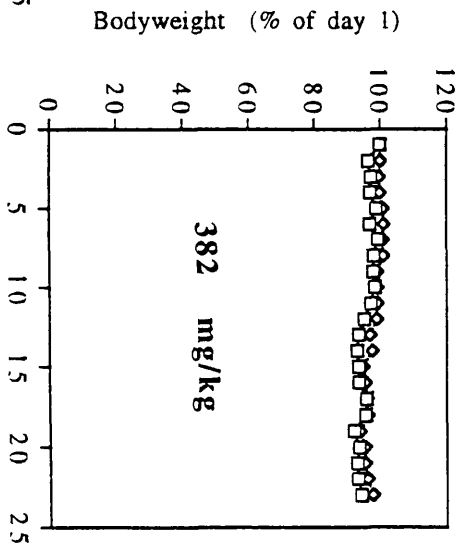
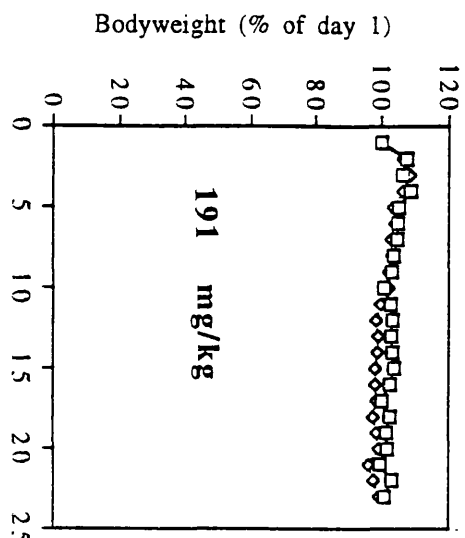


Fig. 5.3. Pilot toxicity studies with SR-4554. Non-tumour bearing female Balb/c mice were injected with saline or SR-4554 and their body weight monitored daily. The mean body weight as a percentage of day 1 from two mice per dose level (191 mg/kg i.v.; 382, 650, 1300 mg/kg i.p.) are presented.



—□— Saline control
—◇— SR-4554 treated

5.3.3 Pharmacokinetic studies

The pharmacokinetics and tissue distribution properties of SR-4554 were examined in the mouse. Plasma, tumour, liver, brain, urine and faecal samples were extracted and analysed by HPLC. Fig 5.4 shows typical chromatograms of extracts obtained from the plasma of control and drug treated mice. No UV-visible metabolites were observed on the analysis of all samples analysed by HPLC.

The plasma pharmacokinetics of SR-4554 in tumour bearing female Balb/c mice at a dose of 162 mg/kg fitted a one compartment open model (Fig. 5.5; Table 5.1). The drug was rapidly absorbed with a t_{\max} and C_{\max} of 15 min and 93 $\mu\text{g/ml}$ respectively. SR-4554 was eliminated thereafter with plasma drug levels near the MQL at 6 hr post-injection. The biodistribution of SR-4554 at the same dose in tumour, liver and brain is illustrated in Fig. 5.6. The drug-concentration vs time profile also fitted a one compartment open model. SR-4554 was eliminated from these tissues by 4 hr post-injection. The pharmacokinetic parameters obtained from this study are presented in Table 5.1. The table shows that SR-4554 was rapidly absorbed into the liver ($t_{\max} = 10$ min; $C_{\max} = 46$ $\mu\text{g/ml}$), but less rapidly into tumour ($t_{\max} = 30$ min; $C_{\max} = 64$ $\mu\text{g/ml}$) and brain ($t_{\max} = 45$ min; $C_{\max} = 6$ $\mu\text{g/ml}$). Relevant to the potential toxicity of SR-4554, the level of drug in the brain remained generally low. Tissue to plasma ratios are illustrated in Fig. 5.7. Expectedly, the exposure of the drug to brain tissue (AUC) was also low compared to that of plasma, tumour and liver. Tissue to plasma exposure ratios over the entire time course were calculated from the AUCs, and were found to be 0.84, 0.35, and 0.07 for tumour, liver and brain tissues respectively. The ratio $\text{AUC}_{\text{brain}}/\text{AUC}_{\text{tumour}}$ which serves as a measure of the relationship between toxicity and MR detection sensitivity of the drug was determined to be very low (0.08), indicating a low CNS level relative to tumour.

The plasma and tissue pharmacokinetics of SR-4554 at 180 and 337 mg/kg showed similar profiles as above. The pharmacokinetic parameters generated using ADAPT are presented in Table 5.2. The AUCs at the above doses together with that at 90 mg/kg (see section 5.3.4) were used to derive the relationship between SR-4554 dose

Fig. 5.4. Typical chromatograms of plasma extracts obtained from (a) control, and (b) SR-4554 treated mice. Plasma samples were extracted using a C₁₈ solid-phase cartridge and analysed by HPLC as described in chapter 2.

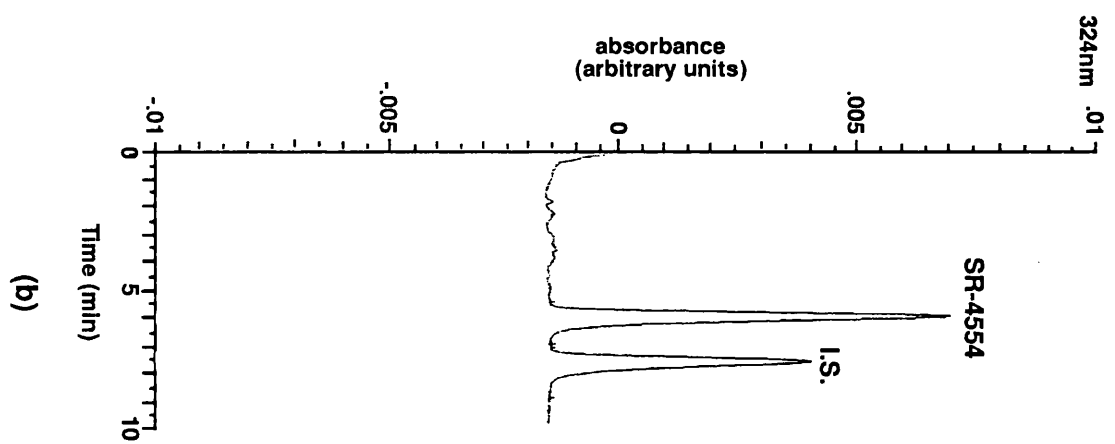
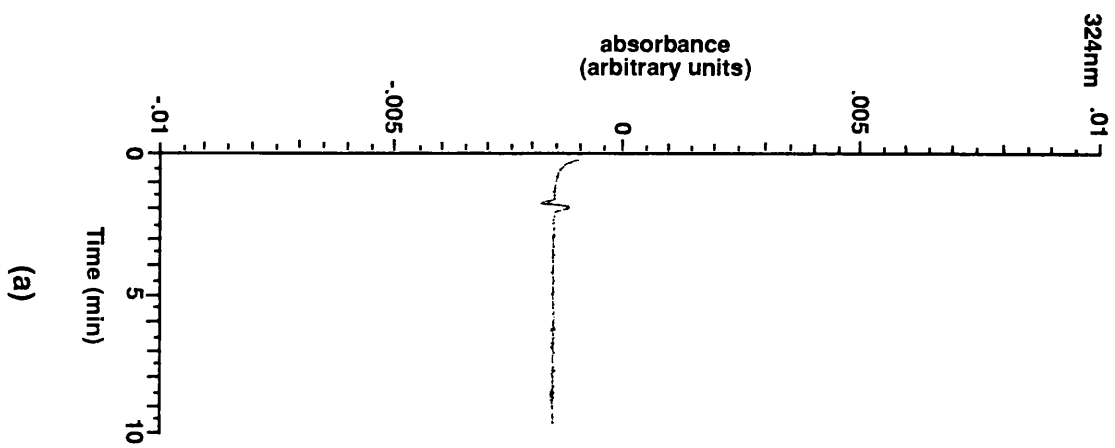


Fig. 5.5. Plasma pharmacokinetics of SR-4554 at 162 mg/kg body weight in EMT6 tumour bearing female Balb/c mice. Three mice were used at each time point and the data was modelled using ADAPT as described in section 5.2.8.

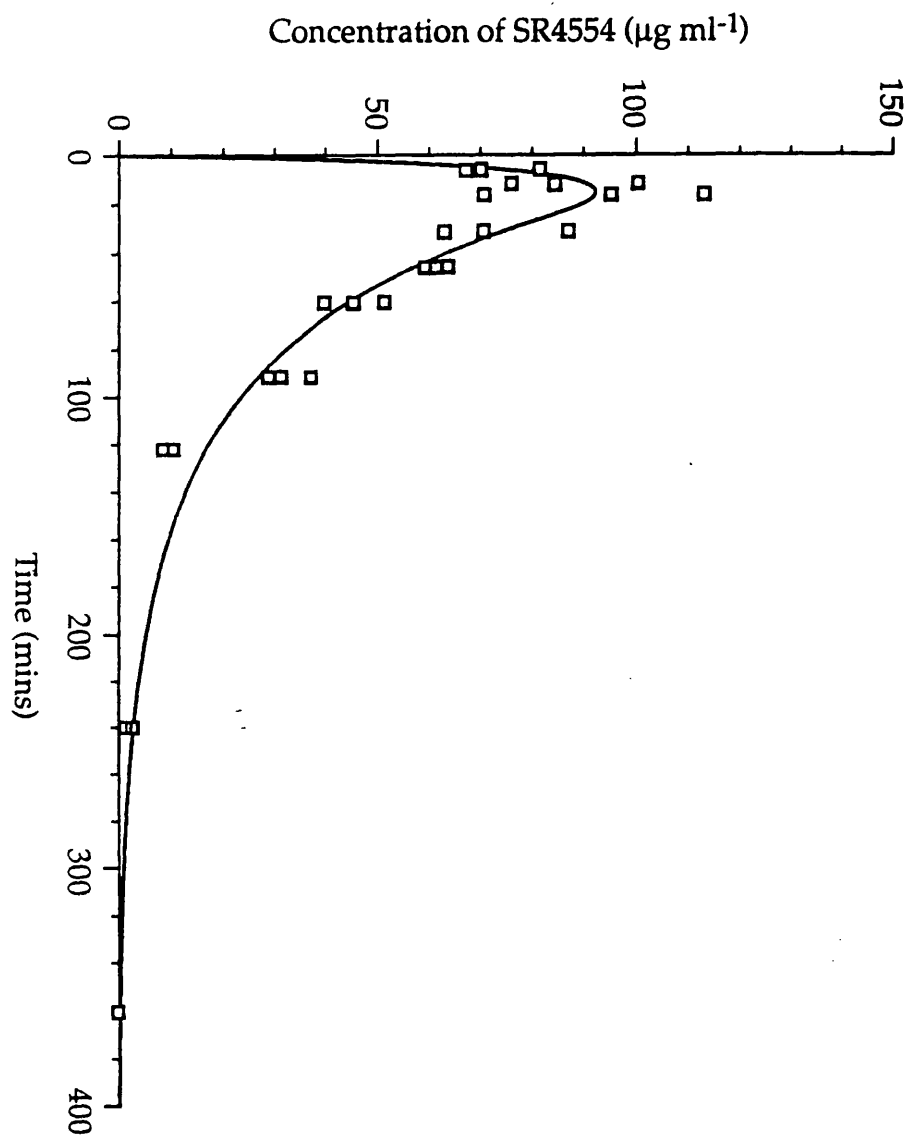


Table 5.1. Pharmacokinetic parameters for SR-4554 following i.p. administration of 162 mg/kg to mice bearing the EMT6 tumour.

	K _a (min ⁻¹)	K _e (min ⁻¹)	T _{1/2} (min)	CL (ml.min ⁻¹ .kg ⁻¹)	AUC _(0-∞) (mg.ml ⁻¹ .min)
Plasma	0.21	0.02	42	24	6.8
EMT-6 Tumour	0.05	0.02	29	-	5.7
Liver	1.04	0.02	37	-	2.4
Brain	0.01	0.08	9	-	0.5

Pharmacokinetic parameters: absorption rate constant (K_a), elimination rate constant (K_e), half-life (T_{1/2}), clearance (CL) and area under the concentration vs time curve (AUC_(0-∞)).

Fig. 5.6. Biodistribution of SR-4554 (162 mg/kg) in tumour (□), liver (O) and brain (Δ) of tumour bearing mice. The tissues were prepared as 10% homogenates in buffer prior to analysis by HPLC. Mean values from three mice per time point are presented.

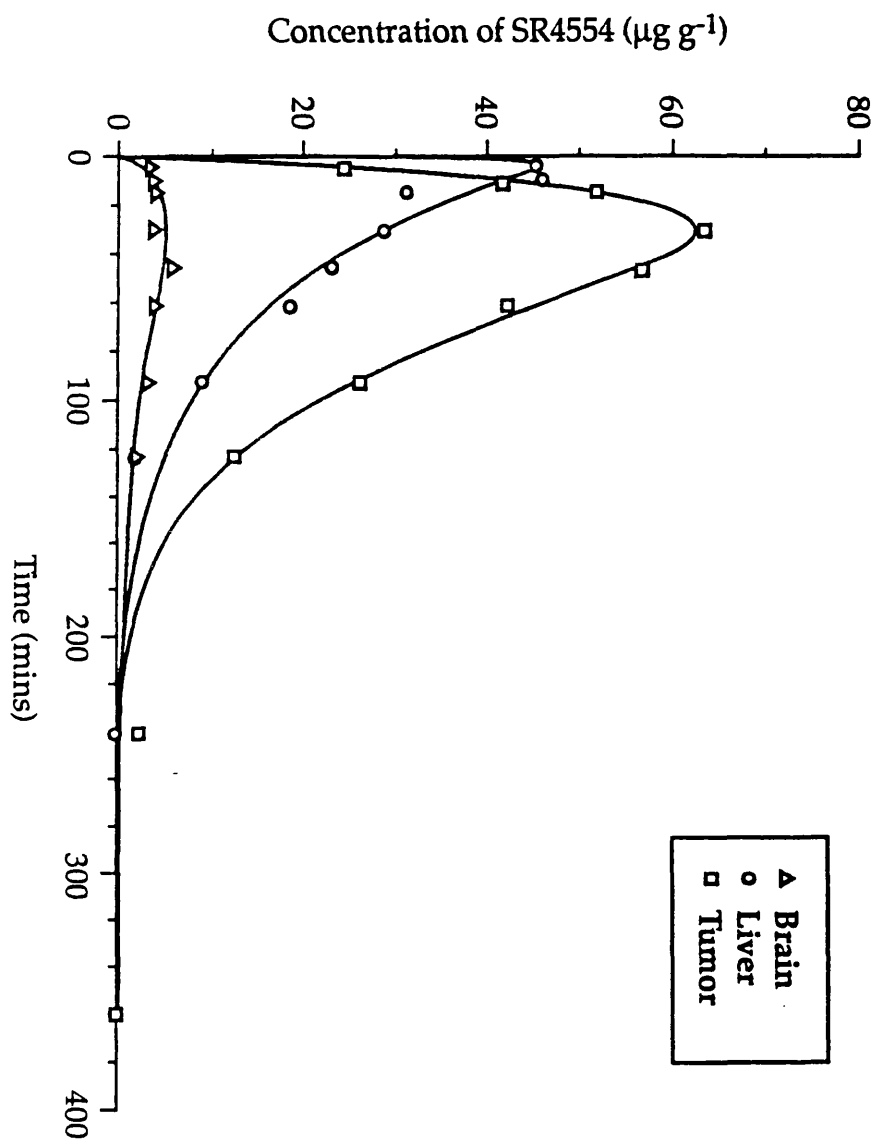


Fig. 5.7. Tissue to plasma ratio of SR-4554 as a function of time following a 162 mg/kg i.p. injection.

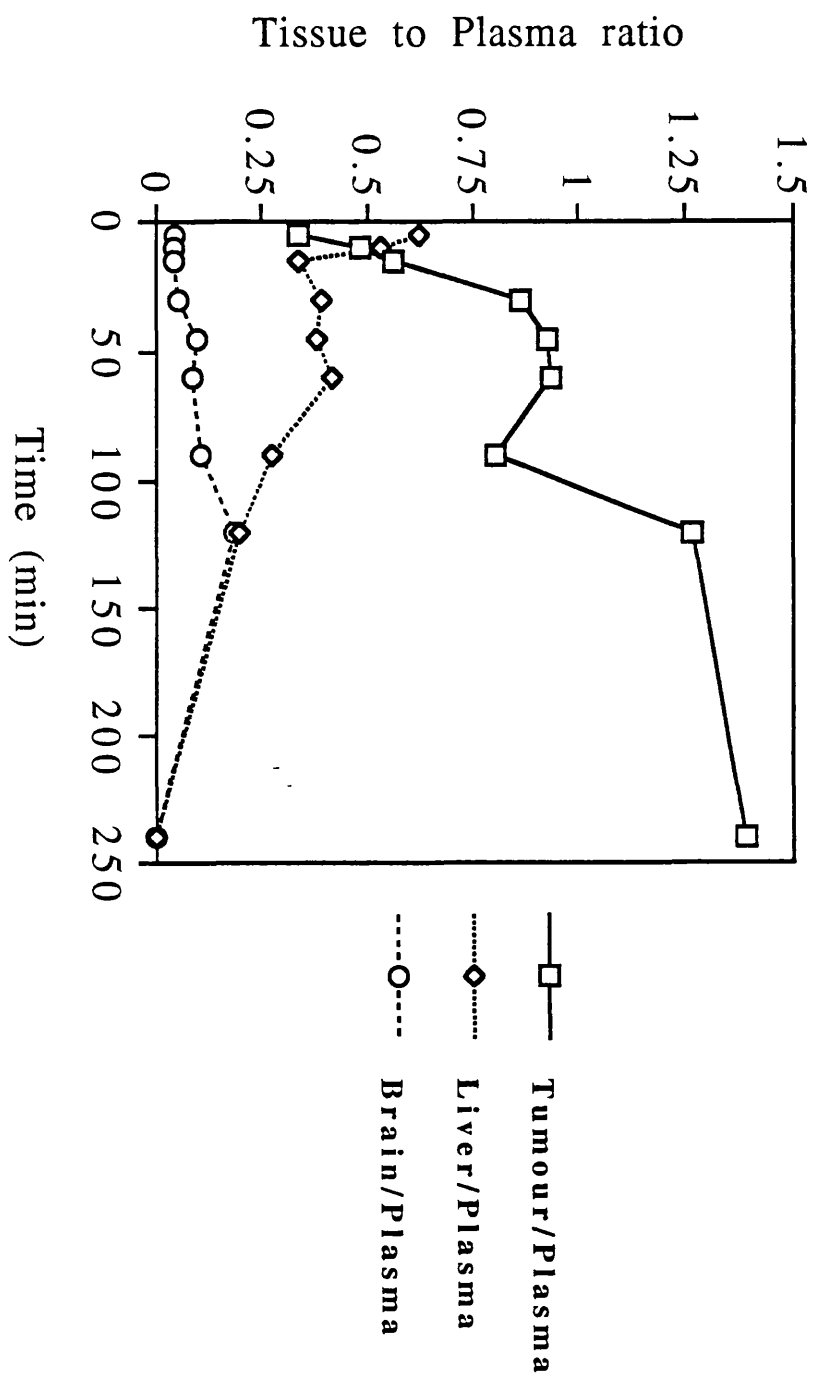


Table 5.2. Pharmacokinetic parameters for SR-4554 following i.p. administration of 180 and 337 mg/kg to mice bearing the EMT6 tumour.

Dose of SR-4554 (mg/kg)	K _a (min ⁻¹)	K _e (min ⁻¹)	T _{1/2} (min)	CL (ml.min ⁻¹ .kg ⁻¹)	AUC _(0 - ∞) (mg.ml ⁻¹ .min)
180	0.23	0.14	51	13	14§ (12 †)
337	0.10	0.14	49	13	26 †

Pharmacokinetic parameters: absorption rate constant (K_a), elimination rate constant (K_e), half-life (T_{1/2}), clearance (CL) and area under the concentration vs time curve (AUC_(0 - ∞)).

† Model dependent AUC derived from the ratio of dose to clearance.

§ Trapezoidal AUC.

and AUC (Fig.5.8). SR-4554 showed linear pharmacokinetics from 90 mg/kg up to 337 mg/kg body weight.

5.3.4 Bioavailability studies

The bioavailability of SR-4554 by different routes of administration was studied in non-tumour bearing female Balb/c mice at a dose of 90 mg/kg. The plasma drug-concentration vs time profiles for i.v., i.p., and p.o. routes are shown in Fig. 5.9. Pharmacokinetic parameters generated from these models are presented in Table 5.3. Administration of SR-4554 by the i.v. route gave very high peak plasma levels (Fig. 5.9) comparable to the i.p. administration at 162 mg/kg and fitted a two compartment open model. The i.p. and p.o. routes, however, fitted a one compartment open model and gave lower peak plasma concentrations compared to the i.v. route. The bioavailability of SR-4554 from the i.p. and p.o. routes was calculated to be 100% and 96% respectively.

5.3.5 Elimination of SR-4554

Analysis of faecal pellets from non-tumour bearing mice treated with 180 mg/kg of SR-4554 showed no drug or UV-visible metabolites. SR-4554 was, however, excreted in the urine. Table 5.4 shows that between 53 and 76% (mean \pm s.d. of $68 \pm 8\%$; $n = 7$) of SR-4554 was excreted unchanged in urine collected over 24 hr. Absence of radiolabelled SR-4554 precluded a definitive mass balance study being performed.

5.3.6 Plasma protein binding studies

The binding of SR-4554 to plasma proteins was found to be low (Table 5.5). Plasma protein binding of SR-4554 and misonidazole were found to be higher in mouse compared to human plasma. In particular, human plasma protein binding was less than 5% in all cases. The results also indicate that at 30 μ g/ml, SR-4554 was bound to a lesser extent compared to misonidazole. Plasma binding of SR-4554 was also higher at 1 μ g/ml compared to 50 and 150 μ g/ml.

5.4 DISCUSSION

SR-4554 was rationally designed to have both low toxicity and high sensitivity for detection by MRS. Of particular note, the

Fig. 5.8. Linear relationship between i.p. dose of SR-4554 injected and the corresponding area under the concentration vs time curve AUC in female Balb/c mice ($r = 0.99$). All AUC's were obtained using the Trapezoidal rule except for the highest dose which was calculated from the ratio of dose to clearance.

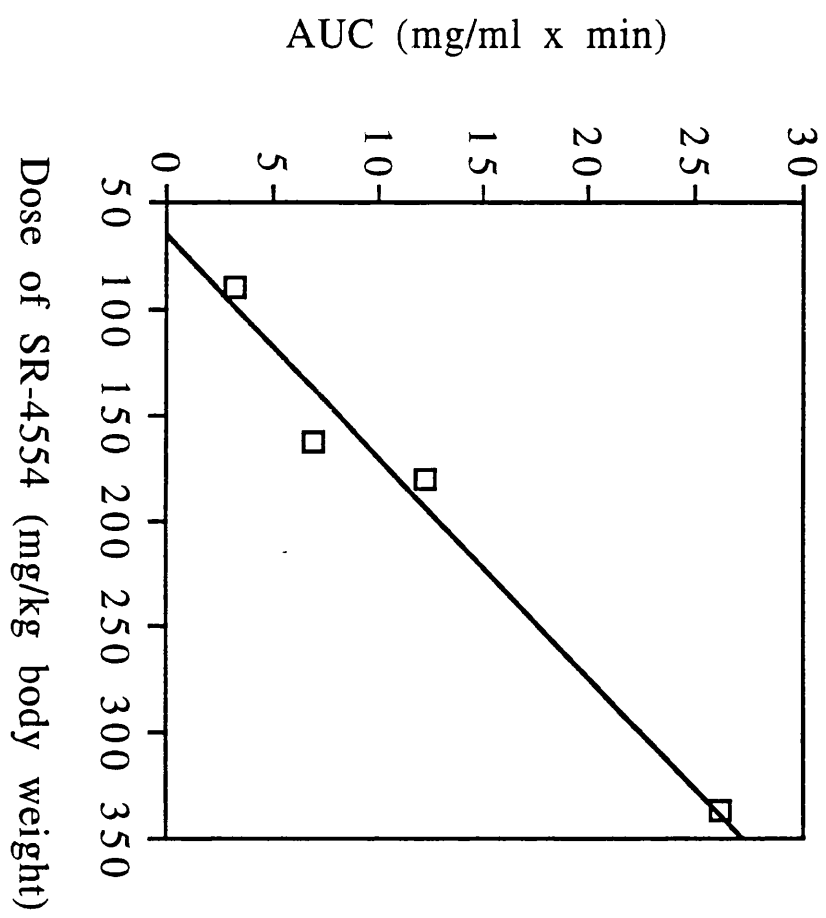


Table 5.3. Pharmacokinetic parameters for SR-4554 following i.v., i.p. and p.o. administration at a dose of 90 mg/kg in non-tumour bearing female Balb/c mice.

Ka (min ⁻¹)	Ke (min ⁻¹)	Kcp (min ⁻¹)	Kpc (min ⁻¹)	T _{1/2} (min)	CL (ml.min ⁻¹ .kg ⁻¹)	AUC _(0-∞) (mg.ml ⁻¹ .min)	F*
I.V. -	0.04	0.02	0.04	α: 8 β: 33	28	3.4	100
I.P. 0.15	0.03	-	-	24	28	3.4	100
P.O. 0.08	0.03	-	-	26	34	3.2	96

* The exact dose of SR-4554 injected was used in the calculation of bioavailability (F).
Pharmacokinetic parameters: absorption rate constant (Ka), elimination rate constant (Ke), half-life (T_{1/2}), clearance (CL) and area under the concentration vs time curve (AUC_(0-∞)).

Fig. 5.9. Intravenous (i.v.; \square), intraperitoneal (i.p.; O) and oral (p.o.; Δ) plasma pharmacokinetics of SR-4554 (at 90 mg/kg) in female Balb/c mice. Mean values from three mice per time point are presented. The bioavailabilities following i.p. and p.o. routes were calculated from the AUC of these curves.

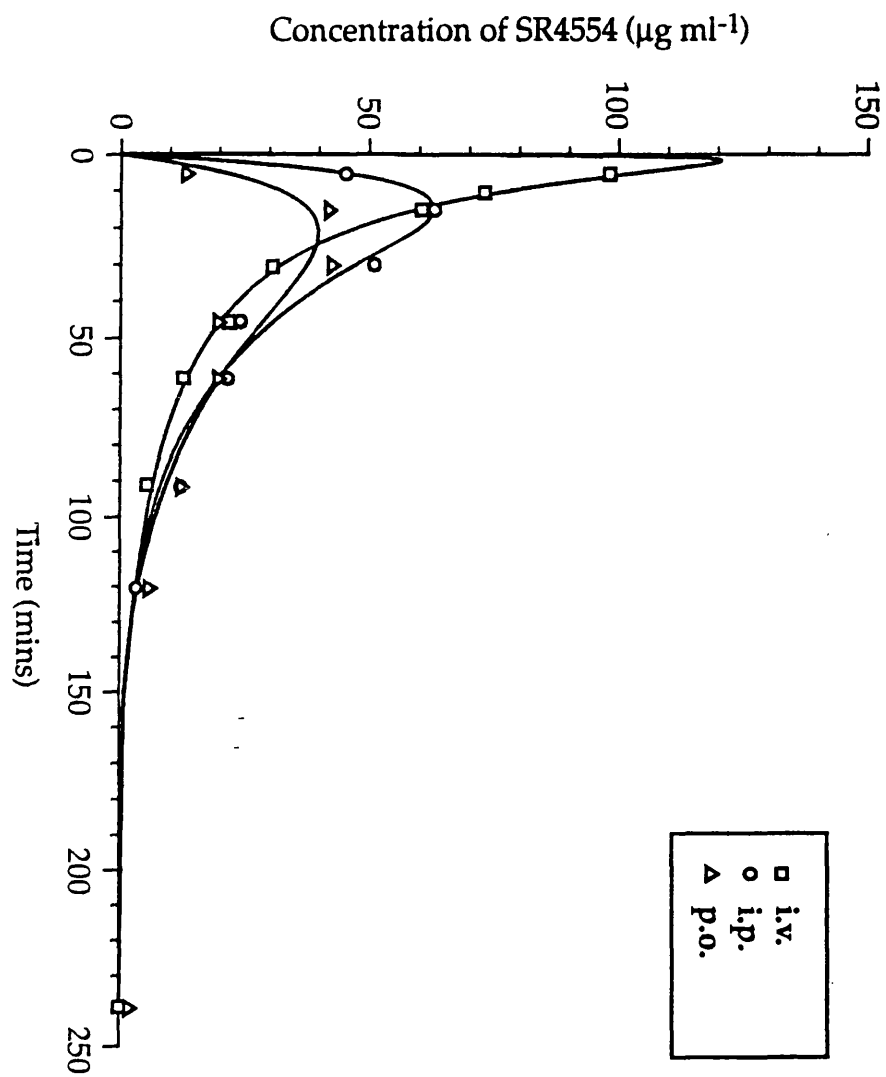


Table 5.4 Urinary excretion of SR-4554 in non-tumour bearing female Balb/c mice.

Mouse	Total SR-4554 Dose (mg)	Total SR4554 excreted (mg)	F _(unc) (%)
1	3.6	2.6	73.8
2	3.3	2.4	71.6
3	3.5	1.8	52.6
4	4.3	2.6	61.6
5	4.0	3.0	76.1
6	4.0	2.9	73.4
7	4.1	2.6	64.2

Results from 2 independent studies. The average amount of SR-4554 excreted unchanged in the urine \pm s.d. was $68 \pm 8 \%$.

F_(unc) is the fraction of SR-4554 excreted unchanged in the urine as a percentage of the amount injected.

Table 5.5 *In vitro* plasma protein binding studies with SR-4554 and compared to misonidazole.

	Temperature (°C)	Concentration of drug (µg/ml)	% Plasma protein binding	
			Mouse	Human
SR-4554	25	150	8.4 ± 1.4 [†]	4.2 ± 1.9
	25	50	7.4 ± 0.3	4.7 ± 0.7
	25	1	18.3 ± 0.01	14.8 ± 0.03
	37	30	5.3 ± 0.6	1.5 ± 0.5
Misonidazole	37	30	19.9 ± 3.2	2.3 ± 0.4

[†]The mean of four determinations ± standard deviation.
 Samples were analysed by direct injection of ultrafiltrate into the HPLC as described in section 2.2.7.

compound was designed to contain an amide side chain similar to etanidazole. It was anticipated that the hydrophilic character and hydrogen bonding capability introduced by the amide and hydroxyl functions should discourage penetration into the nervous system and reduce the risk of neurotoxicity. However, the P_{oct} value of SR-4554 determined in this chapter (0.65), as well as that reported by SRI International who supplied the compound (0.63), were found to be higher than that of both etanidazole (0.048) and misonidazole (0.41) (reported in this study and elsewhere (Brown & Workman, 1980; Rauth *et al.*, 1978)). Thus in apparent contrast to the design specifications, these predictions of overall lipophilic character would suggest that SR-4554 can penetrate the nervous system, if anything, to a greater extent than either misonidazole or etanidazole. In contrast to the prediction from the P_{oct} measurements, however, the retardation (k) of SR-4554 was lower than that of misonidazole on a C_{18} /methanol-water system. The interpretation of this latter finding is that SR-4554 may actually exhibit less lipophilic character than misonidazole, contradicting the P_{oct} data.

Dose ranging studies with SR-4554 showed that SR-4554 was non-toxic up to a dose of 1300 mg/kg. Further studies to determine the true LD_{50} or LD_{10} of this compound in saline may be limited by its low solubility (maximum solubility in saline = 6.5 mg/ml), and future experiments would need to explore ways of increasing the solubility of the drug to enable the administration of higher doses. Despite the absence of toxicity, the doses used in these studies are relatively high and readily facilitates the detection of SR-4554 in both plasma and tissue by HPLC and ^{19}F MRS (see chapter 6).

Using an HPLC assay developed in this thesis (section 2.2.6 and 2.2.7), plasma and tissue samples obtained from both tumour and non-tumour bearing mice treated with SR-4554 were analysed. No metabolites were observed when both plasma and tissue samples were analysed by this method. The detection of metabolites by NMR (see chapter 3) but not HPLC therefore illustrates the limitation of the UV detection technique, a situation which may be addressed when radio-labelled SR-4554 becomes available. It is unlikely that this HPLC assay will detect bio-reduced metabolites, since such metabolites would have lost the nitro moiety responsible for the characteristic UV absorption properties of 2-nitroimidazoles. Compared to

misonidazole, however, the data indicate the relative stability of the amide group of SR-4554 (Flockhart *et al.*, 1978b; Workman *et al.*, 1978). This is important to the development of SR-4554 as a probe for tumour hypoxia by MRS since it is important that fluorine atoms are retained.

The plasma and tumour pharmacokinetics of SR-4554 were found to deviate from the trend shown by most 2-nitroimidazoles in comparison to their lipophilicities as measured by P_{oct} (Brown & Workman, 1980; Workman, 1982; Workman & Brown, 1981). For instance, compared with misonidazole (Table 5.6), SR-4554 has a shorter plasma half-life and lower AUC at similar doses in spite of its higher P_{oct} . Tumour SR-4554 concentrations generally followed that of plasma giving tumour to plasma ratios which increased with time until approximately 30 min post injection and varied less markedly afterwards. The tumour to plasma ratios of SR-4554 (between 30 and 120 min post injection) were found to vary between 0.86 and 1.27. In general, most 2-nitroimidazoles have a tumour to plasma ratio at these time points of between 0.7 and 100 (Brown & Workman, 1980; Workman, 1982; Workman & Brown, 1981). The data obtained with SR-4554 (Fig. 5.7) is therefore consistent with previous studies. Following i.p. injection, the drug was also absorbed quickly into the liver but cleared rapidly suggesting a high metabolic activity in the liver. This may be explained at least in part by the high levels of reductive enzymes and consequent bioreductive metabolism of SR-4554 by liver as described in chapter 3.

The most unexpected and interesting property of this compound, however, was the low brain levels and the consequent low brain to plasma and brain to tumour ratios observed. Brown & Workman (1980) have previously showed that 2-nitroimidazoles with a P_{oct} of greater than 0.41 have a brain to plasma ratio of approximately 0.9 to 1.0. The very low brain to plasma ratio of SR-4554 observed in this study is therefore characteristic of the more hydrophilic 2-nitroimidazoles such as etanidazole ($P_{oct} = 0.048$). This unique property may be due to the additional hydrophilic character and hydrogen bonding capability of the amide group in SR-4554. The fact that hydrogen bonding may play a role is supported by the HPLC retardation (k) studies which indicated that SR-4554 is more hydrophilic than misonidazole. Additional supportive evidence is

Table 5.6. Pharmacokinetic parameters for selected 2-nitroimidazoles in Balb/c mice (Workman & Brown, 1981): Comparison with SR-4554 (this thesis).

Drug	Dose (mmole/kg)	Half-life (h)	AUC (mM.h)	Clearance (l.kg ⁻¹ .h ⁻¹)
Misonidazole (Ro 07-0582)	0.5	0.66	0.6	0.83
Etanidazole (SR-2508)	0.25	α : 0.11 β : 0.98	0.21	0.99
Fluoromisonidazole (Ro 07-0741)	0.5	1.02	0.72	0.69
SR-4554	0.64	0.85	0.83	0.78
	0.57	0.69	0.40	0.80

provided by molecular models of SR-4554, misonidazole and etanidazole (Appendix B). The similarity of SR-4554 to etanidazole, but not lipid-soluble structures such as in misonidazole, implies that stabilisation of the acetamide side chain in SR-4554 by hydrogen bonding, may result in its slower uptake across lipophilic blood brain barrier compared to misonidazole (Dabrow *et al.*, 1993; Workman, 1982). For instance, Dabrow *et al.* (1993) reported the presence of intermolecular hydrogen bonding between the amide nitrogen and the terminal hydroxyl group, as well as between the carboxy group and the terminal hydroxyl group in etanidazole. In contrast, no hydrogen bonding was seen with misonidazole (Dabrow *et al.*, 1993).

Although a correlation between brain to plasma ratio and toxicity of some fluorinated 2-nitroimidazoles have been previously reported (Kagiya *et al.*, 1992), the authors in this study attributed this trend to the introduction of the fluorine group. This is an unlikely explanation, however, since the fluorinated 2-nitroimidazoles which showed low brain to plasma ratios in that particular study also had amide side chains. In addition to these studies, physiological models (based on permeability rate-limited distribution of drug into brain) correctly predict misonidazole brain concentrations and gives a reasonable fit to etanidazole brain data, but not to that of SR-4554 (unpublished report, Zeneca Pharmaceuticals, Macclesfield, UK). These discrepancies suggest that P_{oct} is not a good model for predicting brain penetration of SR-4554. The inability of P_{oct} to predict compound entry into brain has also been observed in a series of centrally acting H_2 receptor histamine antagonists (Young *et al.*, 1988). To shed further light on this, it would be interesting to use other model solvent systems such as propylene glycol dipelargonate (PGDP) due to the differing balance of proton donor/acceptor properties which these alternative solvents show (Leahy *et al.*, 1989).

Bioavailability studies indicated that SR-4554 is almost completely absorbed following i.p. and oral administration. In addition, the absence of any significant variation in absorption rate constant (K_a) at high doses of SR-4554, suggests that the high bioavailability may still be the case for SR-4554 at higher doses. Previous studies with a series of 2-nitroimidazoles ($P_{oct} = 0.01-1.0$) in dogs showed that whereas lipophilic 2-nitroimidazoles tend to be rapidly and completely absorbed following oral administration, the

hydrophilic analogues including etanidazole in general display lower bioavailability (White *et al.*, 1980). The data obtained with SR-4554 in this chapter, therefore compares well with that of other 2-nitroimidazoles with similar lipophilicities confirming the observation that absorption of 2-nitroimidazoles from an extravascular dose is largely a function of lipophilicity, i.e. P_{oct} is a good indicator for nitroimidazole bioavailability. The reason why P_{oct} appears to predict well for the oral bioavailability of SR-4554 but poorly for the uptake into brain is not clear. This unusual balance of properties is, however, favourable with respect to the potential clinical use of the compound as an MRS hypoxia probe.

Another property of SR-4554 which could not be predicted by P_{oct} is urinary excretion. A high percentage of the administered dose of SR-4554 was excreted unchanged in the urine ($68 \pm 8\%$). This together with the absence of metabolites such as glucuronides is a property characteristic of more hydrophilic 2-nitroimidazoles such as etanidazole (Workman & Brown, 1981). Thus in this respect, the urinary excretion is more in keeping with the low brain levels than the high oral bioavailability.

SR-4554 does not bind extensively to plasma proteins. The studies showed that the binding of SR-4554 and misonidazole to mouse plasma were low at biologically relevant concentrations and temperatures (5.3 and 19.9% respectively). As expected, binding to human plasma was significantly less than to mouse plasma (Mann Whitney 95% confidence level), e.g. 1.5 and 2.3% at 37°C for SR-4554 and misonidazole respectively. The lower binding of 2-nitroimidazoles of varying lipophilicities to human, compared to mouse, plasma has previously been reported (Workman & Brown, 1981). Importantly, this may be relevant in helping to predict human doses of SR-4554 from mouse data. Based on the results in this chapter, however, it can be inferred that although, protein binding is of minor significance in determining the biological properties of SR-4554, it could not be predicted from P_{oct} .

SR-4554 was designed to have low toxicity by increasing its hydrophilic character. It has been shown in this chapter that the reduction in brain drug levels is greater than could be predicted by pre-existing trends. In this particular respect and in terms of its high oral bioavailability, linear kinetics, relatively short plasma half-life,

high urinary excretion and lower protein binding, SR-4554 is ideal for MRS/MRI studies in animal and human tumours.

CHAPTER 6

In vivo magnetic resonance spectroscopy and imaging of SR-4554

6.1 INTRODUCTION

As described in sections 1.4 and 1.5, by means of a variety of detection techniques, 2-nitroimidazole probes can be employed to measure hypoxia within tumours on a cell to cell basis and when labelled appropriately can allow non-invasive detection to be carried out. For instance, the labelling of 2-nitroimidazoles with the naturally occurring, stable isotope of fluorine (^{19}F) enables the detection of the compounds by magnetic resonance spectroscopy (MRS) and imaging (MRI) techniques. This detection technique for tumour hypoxia has been encouraged by the availability and use of MR facilities in many hospitals throughout Europe and America. ^{19}F is suitable for MRS and MRI studies because it has a spin of $\frac{1}{2}$, low background signal *in vivo*, high natural abundance (100%), and a relatively high sensitivity for detection (0.83 relative to protons).

As mentioned in sections 1.4 and 1.5, 2-nitroimidazoles are reduced by cellular reductases under hypoxia to reactive intermediates which form adducts with cellular components (Chapman *et al.*, 1983; Urtasun *et al.*, 1986b; Walton & Workman, 1987). Since the adducts are cleared at a slower rate compared to the original 2-nitroimidazole, it was envisaged that the degree of hypoxia in tumours could be assessed by the injection of 2-nitroimidazole probes followed by measurement of residual (metabolised) probe after the 'washout' of the original compound (Chapman, 1984). The low concentration of bound adducts generated in tumours, however, means that generally only probes with multiple fluorine substitution or which can be given in relatively high doses (in the order of 0.1 mmol/kg/magnetically equivalent fluorine atom) are suitable for MRS/MRI studies (Workman *et al.*, 1992). Other important design criteria for these probes include their chemical/biological stability (other than bioreduction), pharmacokinetic/toxicity considerations (see chapter 5), and oxygen dependence of binding. In addition to these considerations, the signal attenuation due to macromolecular binding and its influence on the stoichiometry of the retention of

these compounds is relevant to the quantitation of hypoxia in tumours.

Pioneering research in the use of ^{19}F MRS as a detection technique, has employed the 2-nitroimidazole probes Ro 07-0741 and CCI-103F (Fig. 1.3). For instance, using ^{19}F MRS as a detection technique, the selective retention of the fluorinated 2-nitroimidazole probes, Ro 07-0741 and CCI-103F in mouse tumours with high radiobiological hypoxic fraction (EMT6 and KHT) has been reported (Maxwell *et al.*, 1988). In the same study, less dramatic residual ^{19}F signals were observed from RIF-1 tumours, a tumour model with low hypoxic fraction. By means of a $^1\text{H}/^{19}\text{F}$ technique, Jin *et al.* (1990) confirmed the selective retention of CCI-103F in mouse tumours compared to normal tissues. This study also showed that the both the half-life of CCI-103F, as well as the amount retained after 4 hr in tumours were higher in hypoxic SCCVII tumours than in RIF-1 tumours. Other workers have reported the selective retention of CCI-103F in rat Dunning R3327 prostate adenocarcinomas and Walker-256 carcinosarcomas (Kwock *et al.*, 1992; Raleigh *et al.*, 1991a). Parallel studies using CCI-103F immunostaining in Dunning prostate adenocarcinomas showed that the distribution of residual CCI-103F adducts correlated with the expected oxygen concentration gradients within the tumour (Kwock *et al.*, 1992).

Although Ro 07-0741 and CCI-103F have provided useful data in this field, the two compounds are not ideal as MRS markers for tumour hypoxia. Due to the presence of one ^{19}F atom per drug molecule, high *in vivo* concentrations of Ro 07-0741 are required to enable its detection by MRS. CCI-103F, on the other hand, shows high sensitivity for detection by MRS due to the presence of six magnetically equivalent ^{19}F atoms. Initial comparative studies with ^3H compound in EMT6 tumour bearing mice, however, revealed extensive loss of the fluorine label (Raleigh *et al.*, 1986). The compound has also been reported to have a high octanol/water partition coefficient of 20 (Raleigh *et al.*, 1986), thus making it a potentially toxic compound.

With regard to the technical aspects of MRS detection, it is worth noting that, most of the methods reported so far for the study of selective retention of fluorinated 2-nitroimidazoles are based on relative ^{19}F probe levels rather than absolute concentrations of the

^{19}F probes (Kwock *et al.*, 1992; Maxwell *et al.*, 1988). This is due to the intrinsic difficulty in defining parameters such as the observation volume, magnetic field inhomogeneities and coil loading. Initial studies by Thulborn and Ackerman (1983), however, showed that by means of multi-tuned circuits, it was possible to obtain absolute metabolite concentration by using ^1H signal from water as an internal intensity reference standard. This method relies on the mapping of the sample volumes of two (or more) nuclides when saturation effects are set equal, so as to define, in effect, the observation volume of *in vivo* MRS experiments. Under these conditions, if the concentration of one of the nuclides is constant (e.g., ^1H in water is $\sim 111\text{ M}$), the ratio of the signal intensities observed for the two nuclides (e.g., X-nuclide in drug to ^1H signal in water) provides a measure of the concentration of X-nuclide which is independent of the sample volume for a given coil. The dynamic range and spectral resolution limitations associated with ^1H MRS at high static magnetic fields, however, led to the use of ^2H as an internal intensity reference standard (Evelhoch *et al.*, 1989; Shungu *et al.*, 1992; Song *et al.*, 1992). On the other hand, the ^2H nucleus has a relatively low sensitivity and a potential for line broadening due to quadrupolar relaxation. The relatively short T_1 relaxation times, however, allow for some recovery in the effective sensitivity achievable per unit time since more rapid data averaging can be performed. This concept has been implemented in the non-invasive measurement of both the trideuteromethyl analogue of misonidazole (Evelhoch *et al.*, 1989) and phosphorus metabolites (Shungu *et al.*, 1992; Song *et al.*, 1992) *in vivo*. In the study by Evelhoch *et al.* (1989) this non-invasive technique was validated by comparison with scintillation counting of ^3H misonidazole.

These factors have prompted the design of superior fluorinated 2-nitroimidazole probes, as well as the application of the absolute quantitation technique, for detecting and quantifying tumour hypoxia. Thus SR-4554 was rationally designed to have low toxicity (chapter 5) and enhanced sensitivity for non-invasive detection by MRS/MRI. It was also envisaged that this compound would have lower non-specific binding compared to misonidazole-based analogues (Koch, 1990; Koch *et al.*, 1993). In this chapter a model based on the pharmacokinetics of unchanged drug (section 5.3.3), as well as the formation of hypoxia-dependent adducts, is employed to quantify hypoxia present

within tumours by MRS (Fig. 6.1). With regard to the technical aspects of the work, the concept of multi-tuned circuits has, for the first time, been extended to allow for the quantitation of ^{19}F signals levels from SR-4554 in phantom studies, and *in vivo* in mouse tumours. Due to the absence of an *in vivo* internal reference standard for fluorine, suitable external reference standards have been used to enable signal quantitation. The development of MRI techniques to visualise drug distribution and sites of bio-reduction has also been investigated with SR-4554.

6.2 MATERIALS AND METHODS

6.2.1 Chemicals and reagents

The fluorinated 2-nitroimidazoles used in this chapter have already been described (Fig. 1.3; section 5.2.1). Hypnorm (10 mg/ml fluanisone; 0.315 mg/ml fentanyl citrate) was obtained from Janssen Pharmaceutical Ltd., Oxford, UK. Hypnovel (5 mg/ml medazolam) was obtained from Roche Products Ltd., Welwyn, UK. Hydralazine hydrochloride was obtained from Sigma, St. Louis, MO, USA. All other reagents were analytical or HPLC grade.

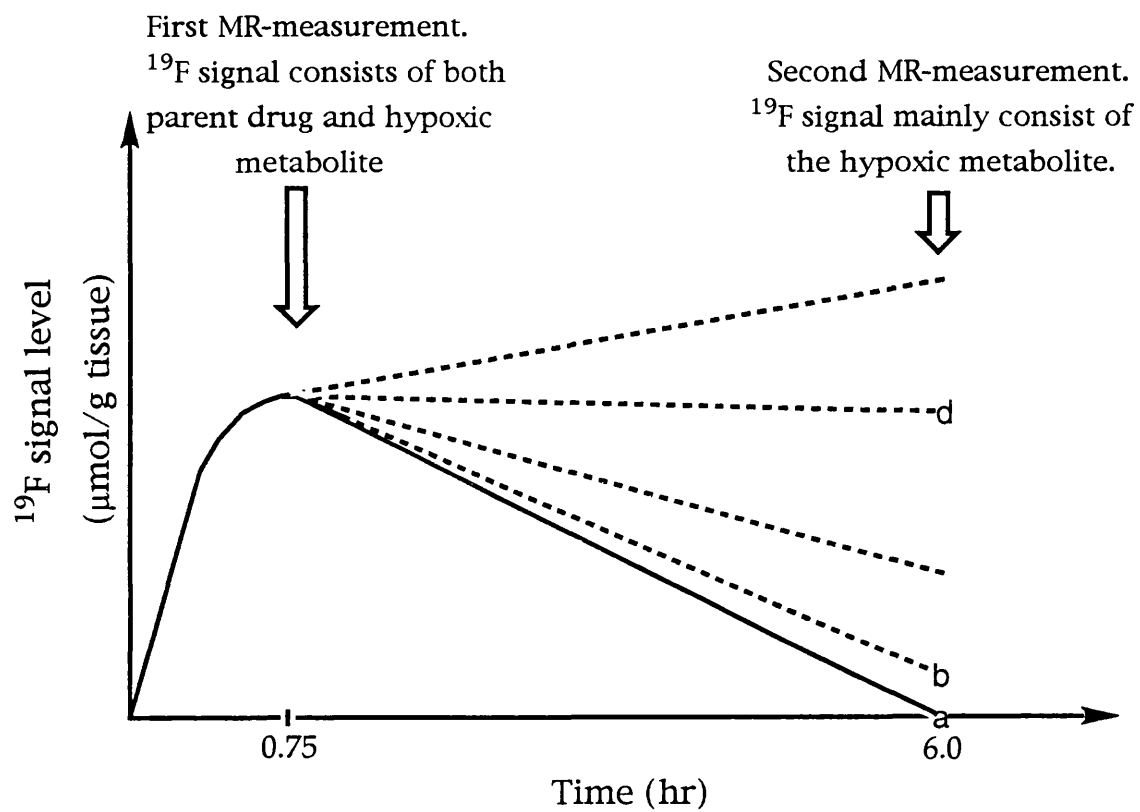
6.2.2 Experimental animals and tumour models

The mice used in this chapter were obtained from Harlan Olac Ltd., Oxon, UK, and the Department of Experimental Clinical Oncology, University of Aarhus, Denmark. All mice weighed between 18 and 26 g at the time of the experiments. Nude mice were specifically kept under pathogen-free conditions. Tumours used in this study were grown subcutaneously as described in section 3.2.2 (Table 3.1), on the flank of the various mice, except for the C3H mammary tumour, which was either grown on the flank or foot. Tumours ranged between 200 and 600 mm³ at the time of experiment, except in studies to investigate the effect of tumour mass on ^{19}F retention (up to 1500 mm³).

6.2.3 Development of an MRS method for the absolute quantitation of ^{19}F levels

In order to obtain the absolute concentration of ^{19}F signal levels following SR-4554 treatment in mice, a multi-tuned circuit technique was developed and evaluated *in vitro* in 1.6 cm diameter

Fig. 6.1. A model for studying hypoxia in tumours using ^{19}F MRS. The continuous line represent the absorption and disposition of original drug, whilst the broken line represent total drug. a, b, c, d, and e represent increasing retention of reductive metabolite within the tumour.



spherical glass phantoms. SR-4554 was accurately weighed and dissolved in 0.1 M NaCl to give a concentration of 4 mM. Other concentrations (2, 1, 0.5, 0.25, 0.152, and 0.0625) were prepared by serial dilution in 0.1 M NaCl. The concentrations of these standard solutions were determined by MRS in triplicate using a double tuned ($^{19}\text{F}/^2\text{H}$) circuit. Sample solutions were secured on a surface coil (1.7 cm diameter) in a 4.7 T MR-spectrometer (SISCO; Freemont, USA). A (~30 μl) reference bulb containing the external standards 5-Fluorotryptophan (5-FTP; Sigma, Dorset, UK) and Acetic acid- d ($\text{AcOH-}d$; Sigma) in DMSO was attached to the coil on the opposite side of the sample. 'Shimming' was performed on the proton resonance of water using the same transmitter/receiver coil. Typical linewidths of between 10 and 25 Hz were obtained. The spectrometer was tuned to fluorine and ^{19}F signals from SR-4554 (in glass phantom) and 5-FTP (in the reference bulb) measured using 64 transients (scans) acquired at a pulse repetition time of 7.5 sec. Without changing the position of the phantom, the spectrometer was tuned to deuterium and ^2H spectra from water (HOD; internal standard in phantom) and acetic acid- d ($\text{AcOH-}d$; in a reference bulb) obtained using 128 transients acquired at a pulse repetition time of 3 sec. To ensure equal flip angles for ^{19}F and ^2H , a calibrated 90° pulse width (with respect to the phantom) was used in each case for spectroscopic measurements. The internal standard (HOD), and the external standards - 5FTP and $\text{AcOH-}d$ - were used for the absolute quantitation of SR-4554 concentrations according to the equation 6.1 below:

$$[\text{SR} - 4554] (\text{mM}) = \frac{SI_{\text{SR-4554}}}{SI_{5\text{-FTP}}} \times \frac{SI_{\text{AcOH-}d}}{SI_{\text{HOD}}} \times F \quad \text{equation 6.1.}$$

where $SI_{\text{SR-4554}}$, $SI_{5\text{FTP}}$, $SI_{\text{AcOH-}d}$, and SI_{HOD} are the integrated signal intensities of SR-4554, 5FTP, $\text{AcOH-}d$ and HOD respectively and F is a factor that depends on the concentration of internal and external standards as well as the number of fluorine atoms per drug molecule ($F = 0.15$ mM for SR-4554 in phantoms). The longitudinal relaxation constant (T_1) was determined by means of an auto-programme using an inversion recovery sequence. For the determination of T_1 , 2 mM SR-4554 solutions were used and the spectral acquisitions were 'interleaved'.

6.2.4 Drug administration

Unless otherwise stated, SR-4554 (3 mg/ml in 0.9% saline) was administered as a single i.p. injection of 180 mg/kg body weight. In some experiments, hydralazine (5 mg/ml in 0.9% saline) was administered as a single i.v. injection of 5 mg/kg via the tail vein 1 hr prior to the administration of SR-4554.

Mice were anaesthetised in all cases with a combination of Hypnorm, Hypnovel and water in the ratios of 1:1:2 (0.01 ml/g i.p.), except in direct pO₂ measurements to investigate the effect of SR-4554 and anaesthesia on ¹⁹F retention, which were carried out on conscious mice. In imaging experiments where mice were studied continuously for long periods of time, an i.p. line was set up and anaesthesia maintained at a dose of 0.0025 ml/g/hr beginning 2 hr after induction.

6.2.5 *In vivo* MRS protocol

SR-4554 was injected into mice and anaesthesia induced between 8 and 20 min post-injection. Anaesthetised mice were secured horizontally with the tissue of interest (tumour, brain or thigh) resting on a surface coil (1.0 or 1.7 cm diameter, ¹⁹F/²H double-tuned coil) in a 4.7 or 7.0 T *in vivo* MR spectrometer. 'Shimming' and pulse acquisition were carried out as previously described (see section 6.2.3). Typical proton linewidths of between 50 to 80 Hz were obtained. ¹⁹F signals from SR-4554 (in the tumour) and 5-FTP (in the reference bulb) were measured at 45 min and 6 hr post-injection of SR-4554. The absolute quantitation of ¹⁹F signal levels (due to drug and hypoxic metabolites) was achieved by integrating ²H spectra from HOD (in tumour) and AcOH-*d* (in reference bulb) and comparing ¹⁹F and ²H signal intensities. In this case in tissues, however, a correction to the equation 6.1 for the water weight per gram of tissue (0.82) and the assumption that tissue water has a density of 1 g/ml were made (Evelhoch *et al.*, 1989). Based on these criteria, *F* was calculated to be 0.12 μmol/g tissue wet weight. Mice were kept warm throughout the studies. T₁ values were determined *in vivo* in a RIF-1 tumour model using an inversion recovery sequence with the spectral acquisitions 'interleaved'.

6.2.6 Retention of ^{19}F in tumours

To compare the *in vivo* retention of three fluorinated 2-nitroimidazoles, SR-4554, fluoromisonidazole (Ro 07-0741), and CCI-103F, the compounds were administered concurrently in a 'cocktail', as a single i.p. injection to SCCVII tumour bearing mice. The doses (based on fluorine sensitivity) of the individual compounds administered in the 'cocktail' were respectively 0.32, 1.0, and 0.125 mmol/kg. ^{19}F and ^2H MR spectra were determined repeatedly in tumours up to 24 hr post-injection of the compounds.

In all other MRS studies, SR-4554 was administered at a dose of 180 mg/kg to tumour bearing mice and MR-spectra were obtained at both 45 min and 6 hr post-injection. ^{19}F signal levels were calculated for each tumour at 45 min and 6 hr using equation 6.1 above (section 6.2.3 and 6.2.5). The ^{19}F retention index was defined as the ratio of ^{19}F signal levels determined by MRS at 6 hr relative to 45 min. In addition to ^{19}F retention index determination, RIF-1 tumours were also excised immediately after MRS studies and original (unmetabolised) SR-4554 concentrations determined by HPLC (see section 2.2) in order to evaluate the contribution of original SR-4554 to the MR signal at 6 hr post-injection. The ^{19}F retention index was determined for murine (RIF-1, KHT, SCCVII, EMT6) and human (BE, HT-29, WIL, HN5) tumour xenografts with varying degrees of hypoxia to evaluate the ability of ^{19}F MRS to measure tumour hypoxia. Subsequently the relationship between ^{19}F retention index and tumour mass was studied in RIF-1 tumours to assess whether increased tumour mass correlates with increased hypoxia. In this study mouse tumours were excised whole and weighed immediately after each MRS measurement.

To evaluate whether tumour bioenergetics could account for the differences in the observed ^{19}F retention, ^{31}P spectra of KHT tumours were obtained in-between the two ^{19}F MRS measurements by means of an image selected *in vivo* spectroscopy (ISIS) sequence (Ordidge *et al.*, 1986). Localised spectra were obtained from a 1 cm^3 voxel, using a 500 μsec adiabatic sincos pulse. Three arrays of 160 transients each were obtained at a pulse repetition time of 3 sec. Summed spectra were used to investigate the correlation between tumour bioenergetics and ^{19}F retention. The tumour pH was

determined from the α -nucleotide triphosphate (α -NTP) and inorganic phosphate (P_i) resonances as previously described (Howe *et al.*, 1993).

6.2.7 Correlation between ^{19}F retention index and the oxygenation status of mouse tumours

The oxygen tension ($p\text{O}_2$) of mouse tumours was determined using a fine needle oxygen electrode (Eppendorf, Hamburg, Germany). Between 4 and 7 parallel tracks were made in each tumour. For each track, the electrode was inserted up to a depth of 1 mm into the tumour and moved automatically through the tissue in forward (0.7 mm increments) and backward (0.3 mm) steps prior to each measurement. A total of 50 to 100 measurements were made within each tumour. Initially, this technique was employed to assess whether SR-4554 and anaesthesia individually or combined, had any effect on tumour oxygenation. In this study, $p\text{O}_2$ measurements were performed in C3H mammary tumours 1 hr after SR-4554 injection and 40 min after anaesthesia. For comparisons between $p\text{O}_2$ and ^{19}F retention index, however, MRS signals were determined as previously described in section 6.2.5. Electrode measurements within the same tumours were carried out at 3 hr after SR-4554 injection, i.e. between the two MRS measurements.

6.2.8 Effect of agents that modulate tumour blood flow and/or oxygenation on the ^{19}F retention index

Three modulators including hydralazine, carbogen and carbon monoxide were used in this study. RIF-1 tumour bearing mice were treated with 5 mg/kg of hydralazine 1 hr before the administration of SR-4554 and the tumour ^{19}F retention index determined and compared to that in untreated RIF-1 tumour bearing mice. In another experiment, C3H mammary (flank) tumour bearing CDF1 mice were made to breath either air, carbogen (95% O_2 + 5% CO_2) or carbon monoxide gas mixture (660 ppm CO + 20.99% O_2 in N_2). Carbogen and carbon monoxide gas mixtures were delivered through a nozzle at a rate of 2.5 L/min (Nordsmark *et al.*, 1995). Mice were allowed to breath carbogen for a total of 82 min starting at 8 min after SR-4554 injection. Alternatively, mice were allowed to breath carbon monoxide for a total of 60 min starting at 25 min after SR-4554

treatment. To enable a comparison between the change in oxygenation and corresponding ^{19}F retention index to be assessed, the pO_2 of C3H mammary tumours in mice from the same batch (as used for the MRS studies) were also assessed in parallel studies using an oxygen needle electrode (Eppendorf) as described in section 6.2.8. The mean pO_2 was determined for untreated controls and gas breathing mice.

6.2.9 *In vivo* MRI protocol

Both 1- and 2-dimensional chemical shift imaging (1-D and 2-D CSI) techniques were used to visualise the distribution of ^{19}F across the tumour region in a RIF-1 tumour bearing mouse. A $^1\text{H}/^{19}\text{F}$ surface coil (1 cm diameter) was used and data were acquired using a pe1D and SISCO csi3D pulse sequences for 1-D and 2-D imaging respectively. A sincos pulse with a pulse width of 2000 μsec was employed in these studies. In 1-D experiments, 8 transients for each phase encoding increment were acquired with a spectral width of 18 kHz and an acquisition time of 0.128 sec. Mouse tumours hung into the surface coil and a 'zxy' orientation was used. In 2-D experiments, 32×32 increments were used and the data interpolated to a 256×256 matrix size.

The application of whole body ^{19}F MRI to study drug distribution and localisation of bioreductively activated 2-nitroimidazoles was investigated using a 4 cm diameter $^1\text{H}/^{19}\text{F}$ Hemholtz transmitter/receiver coil. RIF-1 and SCCVII tumour bearing C3H mice were treated with SR-4554 at doses of 180 mg/kg and 360 mg/kg (0.06 ml/g) respectively. In each case the mice were anaesthetised, and placed horizontally in the coil. An i.p. line was surgically placed in the peritoneum of the mice to enable anaesthesia to be maintained (see section 6.2.4). A 'shorter' pulse sequence (i.e. a spin echo pulse sequence optimised for short echo times) was used for both ^1H and ^{19}F imaging. The proton sequence consisted of a multislice 1000 μsec gauss pulse, a relaxation delay of 1.0 sec, 64 repetitions, 32 phase encoding increments, and an echo time of 3.2 msec. The pulses were calibrated and data acquired with the frequency set on-resonance according to the nucleus of interest. Proton images consisted of 3.6 mm slices while ^{19}F images were acquired from a slice thickness of approximately 4 times that of

protons. The fields of view in both cases were set equal to 8 and 5 cm in the readout and phase encoding directions respectively. In order to assess the relationship between ^{19}F sensitivity and echo time, a whole body T_2 relaxation of ^{19}F was determined using the Hemholtz coil.

6.3 RESULTS

6.3.1 MRS studies

Fluorine and deuterium signals were obtained *in vitro* and *in vivo*. Fig. 6.2 show typical fluorine and deuterium spectra obtained from a RIF-1 tumour. Even with the low number of transients used, resolution of tissue and reference signals was possible in both cases. Such spectra were used in the quantitation of ^{19}F signal levels from drug and bio-reduced metabolites in tissues. Validation of this method in a glass 'phantom' was carried out by comparing SR-4554 concentrations obtained from the MRS study and corresponding nominal concentrations (Fig. 6.3). Regression analysis of data showed that the calibration curve was linear over the range 0.125 to 4 mM ($r = 0.99$; slope = 1.02). The limit of detection was 0.125 mM (> 3 noise) with a standard deviation of 0.03 ($n = 3$). The *in vitro* (2 mM SR-4554 in 100 mM NaCl) and *in vivo* (180 mg/kg SR-4554 in RIF-1 tumour) T_1 values of the ^{19}F and ^2H compounds as determined by an inversion recovery sequence are presented in Table 6.1. The results show lower T_1 values for SR-4554 and HOD *in vivo*. As expected, the T_1 of external reference standards were similar in both *in vitro* and *in vivo* protocols.

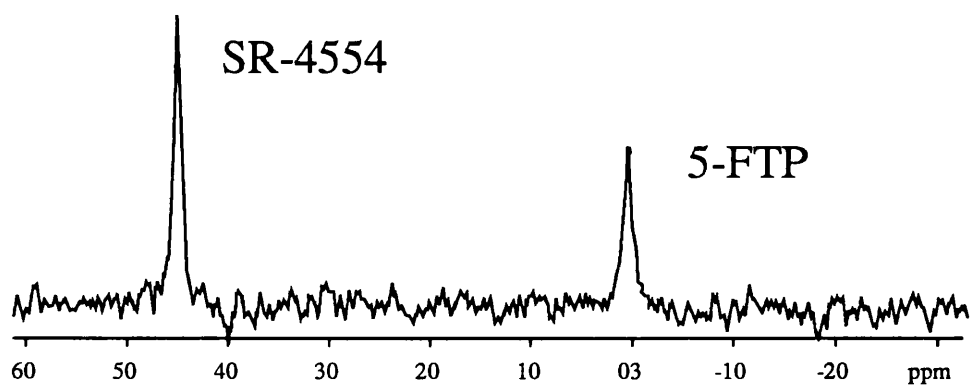
6.3.2 Retention of ^{19}F signals in mouse tumours

Initial experiments to compare the retention of the fluorinated 2-nitroimidazoles SR-4554, fluoromisonidazole (Ro 07-0741) and CCI-103F in SCCVII tumours, indicated that the three compounds exhibited similar retention profiles *in vivo* (Fig. 6.4). The ^{19}F signal levels of the three compounds within the same tumour were higher at 4.7 hr compared to those at 35 min. Subsequently, the signal levels decreased until the last time point at 24.0 hr post-injection.

In Table 6.2, ^{19}F signal levels have been computed for tumour (RIF-1) and brain (head region) of C3H mice from MRS and HPLC measurements. The MRS data in this case indicated biodistribution of

Fig. 6.2. Typical fluorine (a) and deuterium (b) spectra obtained from a RIF-1 tumour (and reference bulb) after the injection of 180 mg/kg of SR-4554. The spectra were acquired by means of a double-tuned ($^{19}\text{F}/^2\text{H}$) circuit using 64 and 128 transient (7.5 and 3 sec pulse repetition times) for fluorine and deuterium respectively.

(a) ^{19}F Spectra



(b) ^2H Spectra

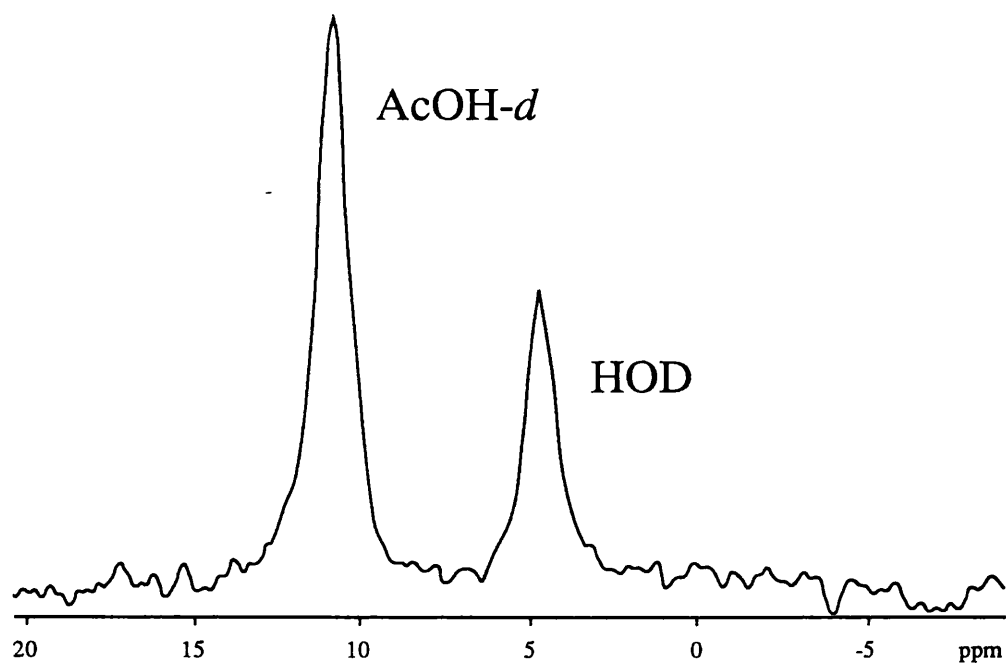


Fig. 6.3. Quantitation of SR-4554 in 100 mM saline solution using a double tuned ($^{19}\text{F}/^2\text{H}$) MRS circuit at 4.7 Tesla. The graph shows the mean and corresponding standard deviations (error bars) of replicates ($n = 3$). The error bars were too small to be observed. MRS concentrations were calculated by comparison of ^{19}F and ^2H spectral intensities obtained from SR-4554, and natural abundance deuterium (in glass phantom), and 5-fluorotryptophan and acetic acid-*d* (in reference bulb). The correlation coefficient and gradient of the calibration curve was 0.99 and 1.02 respectively.

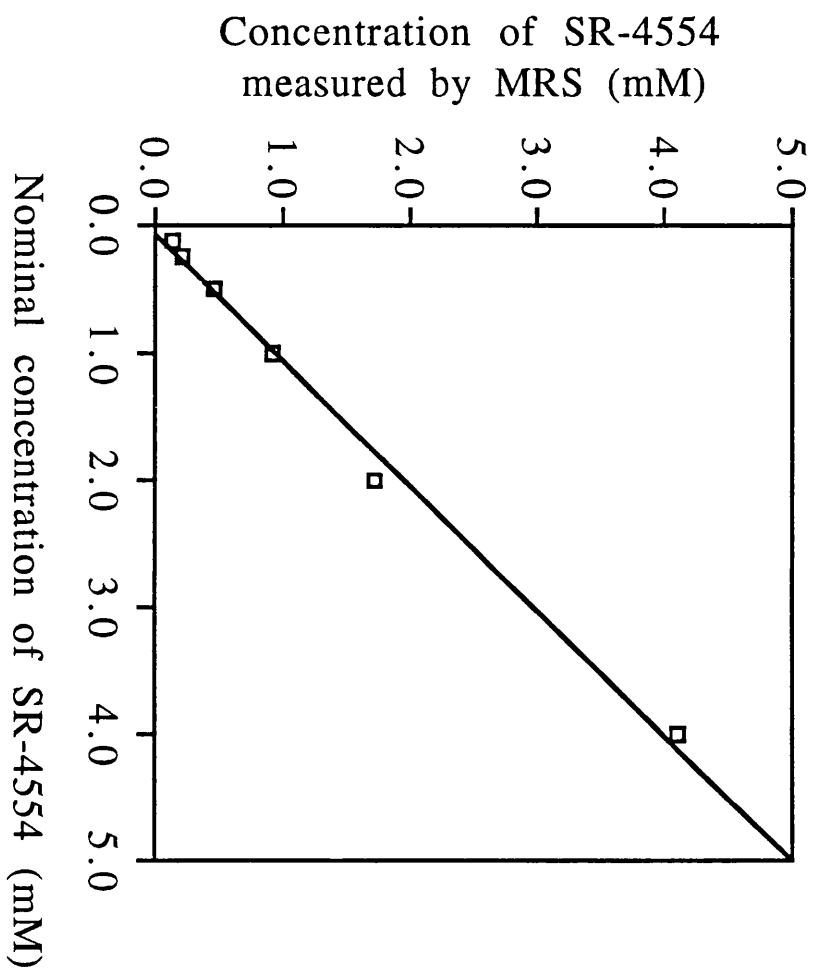


Table 6.1. T_1 values of fluorinated and deuterated compounds measured in both *in vitro* and *in vivo* experiments by means of an inversion recovery sequence.

Compound	T_1 (sec)	
	<i>In vitro</i>	<i>In vivo</i>
SR-4554	1.52 ± 0.12	0.66 ± 0.19
HOD	0.45 ± 0.08	0.24 ± 0.03
5-FTP	0.73 ± 0.17	0.59 ± 0.13
AcOH- <i>d</i>	0.06 ± 0.002	0.04 ± 0.002

Values represent mean $T_1 \pm$ s.e. determined using an auto-programme.

HOD, 5FTP, and AcOH-*d* are natural abundance deuterium in water, 5-fluorotryptohan and Acetic acid-*d* respectively.

Fig. 6.4. Typical ^{19}F spectra obtained from a tumour (SCCVII) bearing mouse after the co-injection of fluoromisonidazole (Ro 07-0741) (1 mmol/kg), SR-4554 (0.32 mmol/kg) and CCI-103F (0.125 mmol/kg). The spectra were acquired at 35 min (a), 4.68 hr (b) and 24 hr (c) post-injection. In (a) and (b), 64 transients (at 7.5 sec pulse repetition time) were used, whilst 128 transients were used for spectral acquisition in (c).

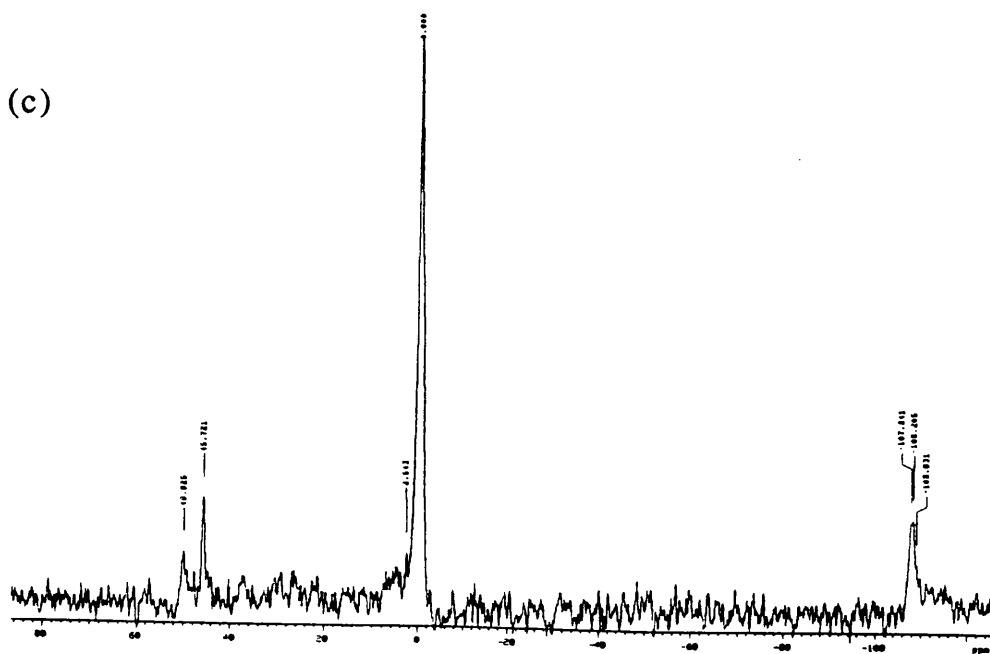
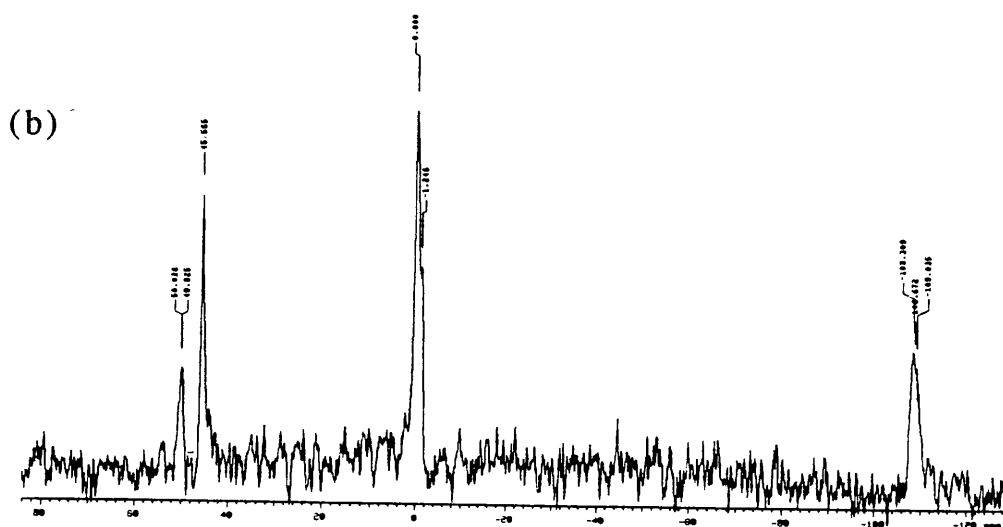
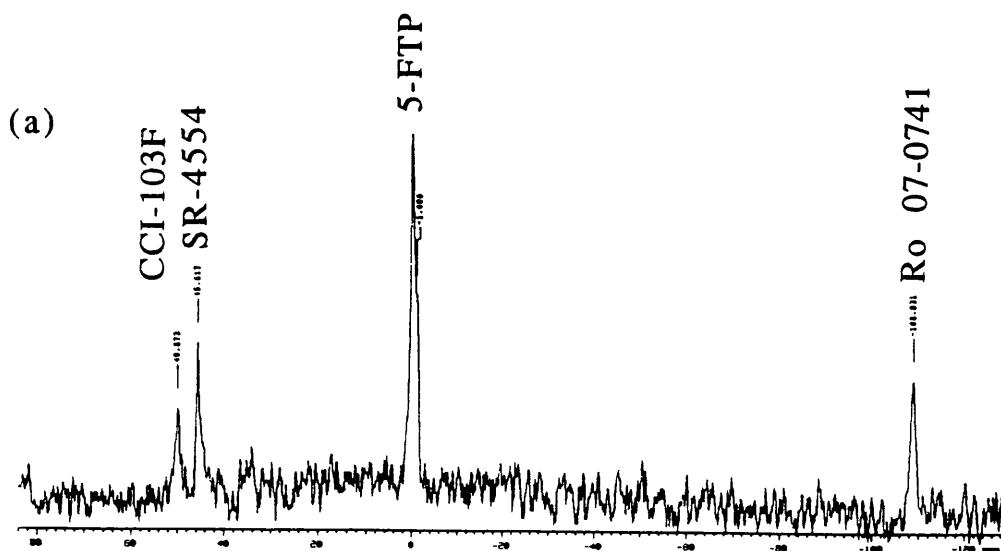


Table 6.2. Retention of ¹⁹F signals from SR-4554 in RIF-1 tumours.

<i>TUMOUR</i>			
Mouse No.	Total drug levels (MRS) at 45 min. (μmol/g tissue)	Total drug levels (MRS) at 6 hr (μmol/g tissue)	SR-4554 levels (HPLC) at 7 hr (μmol/g tissue)
1	0.432 ^a	0.129	0.009
2	0.800	0.298	0.008
3	0.349	0.192	0.007
4	0.531	0.225	ND
<i>BRAIN</i>			
Mouse No.	Total drug levels (MRS) at 1.08 hr (μmol/g tissue)	Total drug levels (MRS) at 6.3 hr (μmol/g tissue)	
1	0.284	ND	
2	0.232	ND	
3	0.191	ND	
4	0.405	ND	

^a Data represent absolute ¹⁹F levels calculated using equation 6.1
ND Not detected

SR-4554 to tumour and brain region (45 min), although in all cases, the concentrations of total drug in tumours were higher than in the brain. The parent compound (SR-4554) was cleared from tumours by 6 hr post-injection as indicated by the HPLC measurements.

The ^{19}F retention indices of a variety of human and murine tumour xenografts with different reported hypoxic fractions were measured following the injection of SR-4554 (180 mg/kg) in order to assess the ability of ^{19}F MRS to detect tumour hypoxia. The results of this study in eight tumour types are presented in Fig. 6.5 and represents the mean and corresponding 95% confidence levels (analysis of variance of transformed data) of ^{19}F retention indices obtained from 4 to 13 mice per tumour type. The data showed that within each tumour type, there was a marked individual variation in ^{19}F retention index. When pooled together, however, the mean ^{19}F retention index for each murine tumour type, in general, correlated well with the reported radiobiological hypoxic fraction (Table 6.3). For instance, a more hypoxic tumour such as EMT6 gave a higher (not statistically significant) mean ^{19}F retention index compared to RIF-1, a less hypoxic tumour. Apart from the WIL tumours, the other human xenografts showed less retention of ^{19}F compared to the murine tumours with HT-29 giving the lowest mean ^{19}F retention index. In WIL tumours, however, a high variation in ^{19}F retention index was observed with maximum and minimum ^{19}F retention indices of 2.1 and 0.0 respectively.

In RIF-1 tumours, the ^{19}F retention index correlated with tumour mass as illustrated in Fig. 6.6. A correlation coefficient of 0.83 was obtained from regression analysis of the data. The absence of any correlation between ^{19}F retention index and tumour mass or volume in KHT tumours, for example, prompted studies to investigate whether this effect was due to differences in bioenergetic status using ^{31}P MRS. Fig. 6.7 illustrates a typical ^{31}P spectrum obtained from a KHT tumour. No correlations were, however, observed between ^{31}P parameters such as Pi/PCr , Pi/Total NTPs , PME/Total NTPs or pH_i and ^{19}F retention index ($n = 6$). The pH_i of the KHT tumours varied between 6.98 and 7.41.

Fig. 6.5. The retention of ^{19}F signals from SR-4554 in murine and human xenografts. The graph shows mean ^{19}F retention indices and associated 95% confidence intervals calculated on the basis of transformed data (i.e. square root of individual ^{19}F retention indices) and then transformed back to original scale. Tukey HSD multiple comparison test showed that the data were significant ($p < 0.05$) for EMT6 vs HT-29 and SCCVII vs HT-29. The p-values for KHT vs HT-29 and RIF-1 vs HT-29 were both = 0.08.

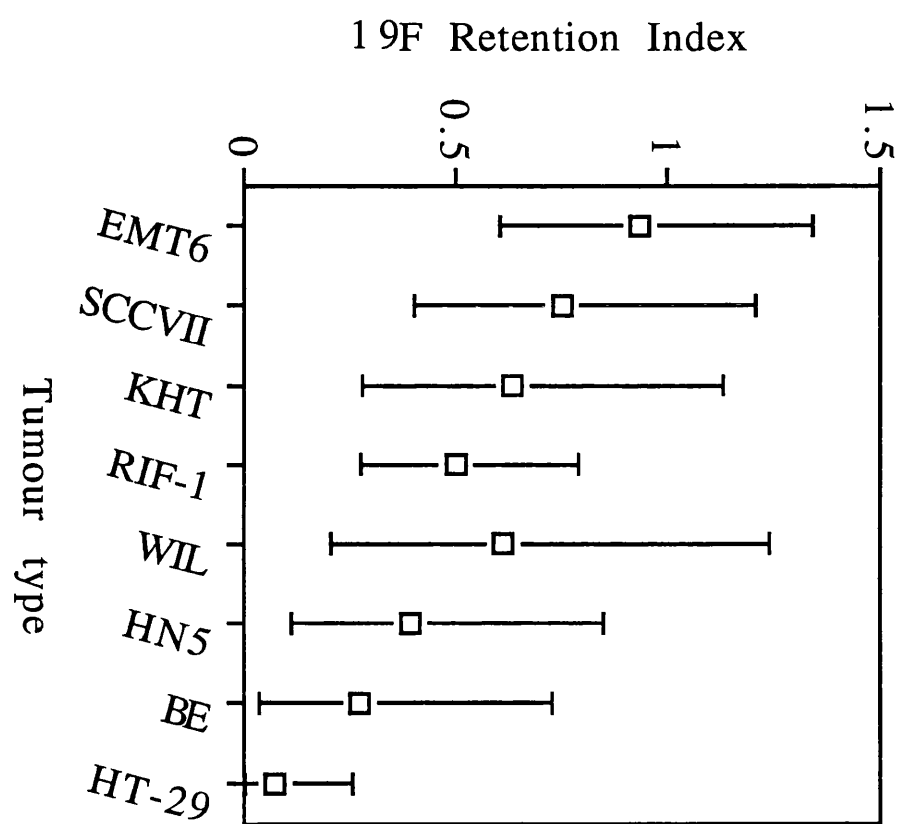


Table 6.3. Hypoxic fraction of solid tumours as measured by radiobiological assays.

TUMOUR	HYPOXIC FRACTION (%)	REFERENCES
RIF-1	1.6 (1.1 - 2.1)	(Brown <i>et al.</i> , 1980)
	4.7 (3.3 - 6.6)	(Shibamoto <i>et al.</i> , 1986)
	1.0	(MRCRU, Lab data, 1994)
EMT6	50 (31 - 80)	(Guichard <i>et al.</i> , 1977)
	21 (8.8 - 49)	(Guichard <i>et al.</i> , 1977)
	20 (13 - 31)	(Rockwell, 1981)
	56 (38 - 82)	(Rockwell, 1981)
	14 (9.9 - 19)	(Shibamoto <i>et al.</i> , 1986)
SCCVII	8.5 (6.9 - 11)	(Shibamoto <i>et al.</i> , 1986)
	8.4 (6.6 - 12)	(Shibamoto <i>et al.</i> , 1986)
	2.5	(MRCRU, Lab. data, 1994)
KHT	15 (8.2 - 28)	(Van Putten & Kallman, 1968)
	12 (8.6 - 18)	(Hill, 1980)
	39 (30 - 52)	(Hill, 1980)
	1.0	(MRCRU, Lab. data, 1994)
HT-29	17 (9.2 - 31)	(Leith <i>et al.</i> , 1991)
	1.2	(Guichard <i>et al.</i> , 1983)

MRCRU: MRC Radiobiology Unit, Didcot, UK.

Tumour sizes ranged between 5 and 20 mm diameter or 0.5 and 2 g.

Fig. 6.6. Relationship between ^{19}F retention index and tumour mass in RIF-1 tumours. Each point represents a single tumour. The correlation coefficient of the regression line was 0.83.

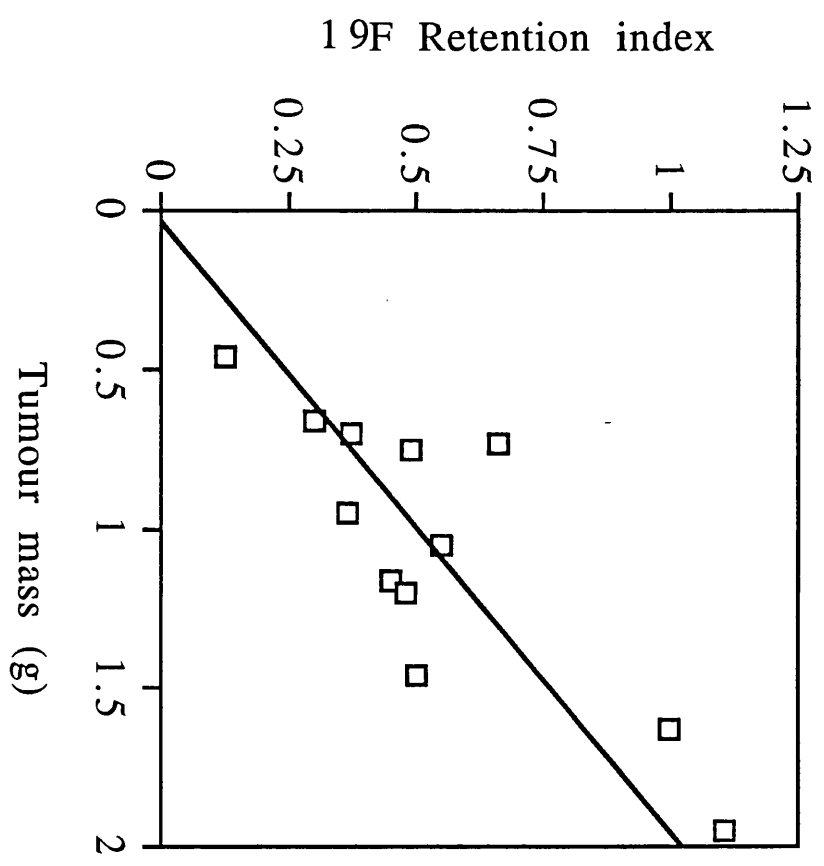
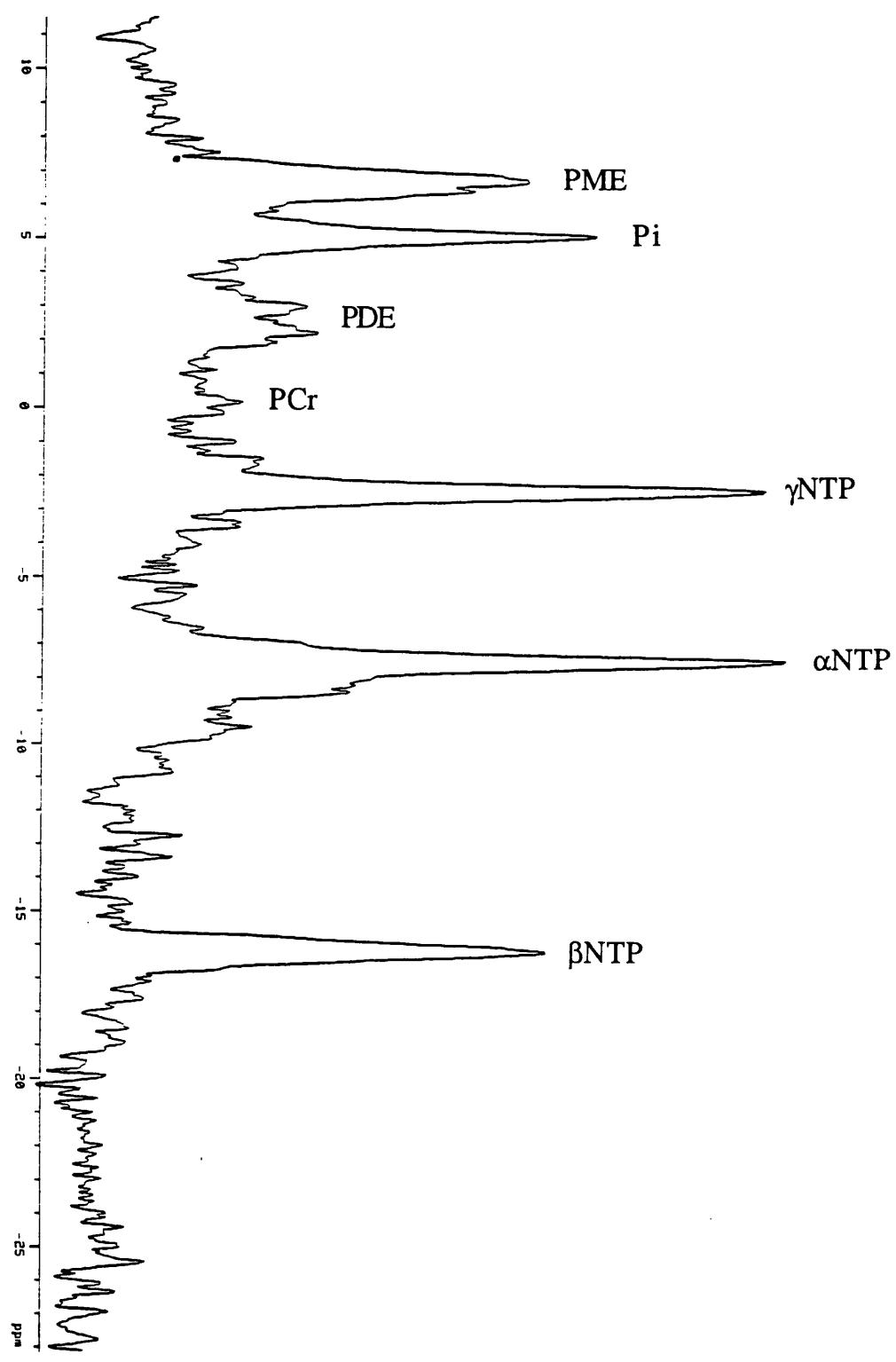


Fig. 6.7. A localised ^{31}P spectra obtained from a KHT tumour by means of an ISIS sequence. The spectra shows the various phosphorus metabolites including phosphomonoester (PME), inorganic phosphate (Pi), phosphodiester (PDE), phosphocreatine (PCr), and α -, β -, and γ -nucleotide triphosphates (α -, β , and γ -NTP's). The intracellular pH (pH_i) was calculated from the difference between the Pi and α -NTP peaks.



6.3.3 Correlation between ^{19}F retention index and the oxygenation status of mouse tumours

To investigate whether the MR protocol used in this thesis could affect the phenomenon of interest (i.e. influence tumour oxygenation), tumour pO_2 measurements in SR-4554 treated vs untreated and anaesthetised vs unanaesthetised mice were obtained (Table 6.4). Statistical analysis of the data (Kruskal-Wallis test; 95% confidence level) showed no significant differences between means and % of pO_2 values ≤ 5 and 10 mmHg. Significant differences were, however, observed upon comparison of medians and % of pO_2 values ≤ 2.5 mmHg (Kruskal-Wallis test; 95% confidence level). Further analysis of the data (medians and % pO_2 values ≤ 2.5 mmHg) showed that a small but significant increase was produced by SR-4554 and the combination of SR-4554 and anaesthetic (median pO_2 of 3 and 1 mmHg respectively).

Three tumour models (two sites) were characterised according to their ^{19}F retention index and pO_2 . The relationship between ^{19}F retention index and pO_2 parameters including median pO_2 , and % of pO_2 values ≤ 2.5 , 5, or 10 mmHg are illustrated in Fig. 6.8. No strong correlation was found between the pO_2 parameters and ^{19}F retention index for each tumour type alone or for all tumour types combined. The variability between these two techniques was particularly evident at high oxygenation or low ^{19}F retention indices. Although the different tumour types showed relatively different trends, in general, high ^{19}F retention indices were associated with low median pO_2 and high % of pO_2 values ≤ 2.5 , 5 or 10 mmHg. In particular ^{19}F retention index of greater than 0.5 corresponded to median pO_2 of less than 2.5 mmHg (9 out of 10 tumours) and % of pO_2 values ≤ 5 mmHg of greater than 60% (10 out of 10 tumours).

6.3.4 Effect of agents that modulate tumour blood flow and/or oxygenation on the ^{19}F retention index

The computed ^{19}F retention indices following alterations in tumour microenvironment are presented in Table 6.5. Administration of hydralazine at a dose of 5 mg/kg caused greater than two fold increase in ^{19}F retention index of RIF-1 tumours compared to untreated controls. Analysis of three hydralazine treated tumours by

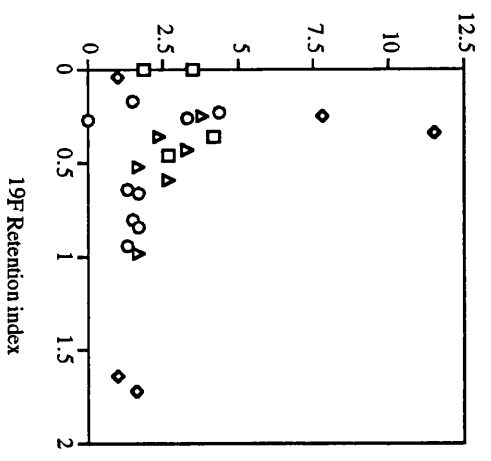
Table 6.4. The effect of SR-4554 and anaesthesia on the oxygenation of C3H mammary foot tumours implanted in female CDF1 mice.

SR-4554 treatment	Anaesthesia	Tumour size (mm ³)	Mean pO ₂ (mmHg)	Median pO ₂ (mmHg)	pO ₂ values ≤ 2.5 mmHg (%)	pO ₂ values ≤ 5 mmHg (%)
-	-	215 ± 12	5.7 ± 0.9	1.7 ± 0.3	61.7 ± 4.8	68.6 ± 4.4
+	-	214 ± 12	8.8 ± 1.3	4.6 ± 1.1	28.5 ± 4.6	62.5 ± 5.1
-	+	212 ± 12	6.9 ± 1.3	2.5 ± 1.4	59.7 ± 6.3	67.9 ± 5.7
+	+	222 ± 13	8.0 ± 1.0	4.5 ± 0.7	25.3 ± 11.0	53.3 ± 10.6

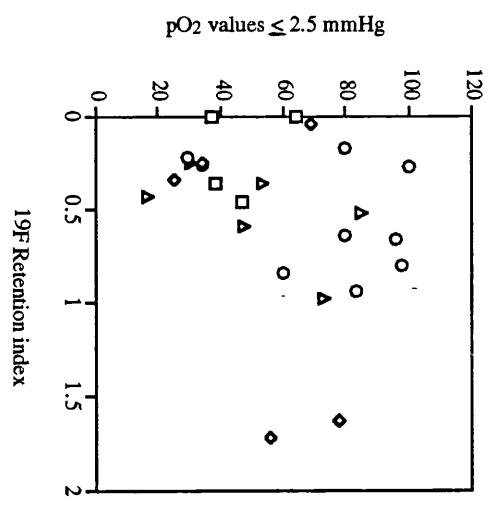
Data represent means ± s.d. At least 5 mice were used in each experiment.
+ and - represent treatment and no treatment respectively.

Fig. 6.8. Relationship between ^{19}F retention index and pO_2 parameters: (a) median pO_2 , (b) % pO_2 values ≤ 2.5 mmHg, (c) % of pO_2 values ≤ 5 mmHg, and (d) % of pO_2 values ≤ 10 mmHg.

RIF-1 } were
 SCCVII } they
 of }
 Same derivation as
 i.e. Howell as used in
 a (not put in file)

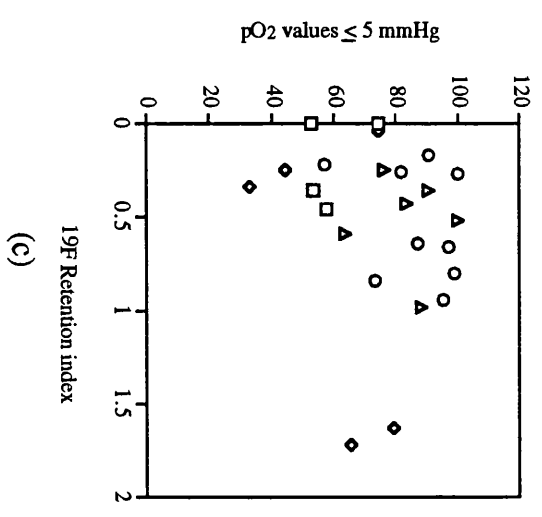


(a)

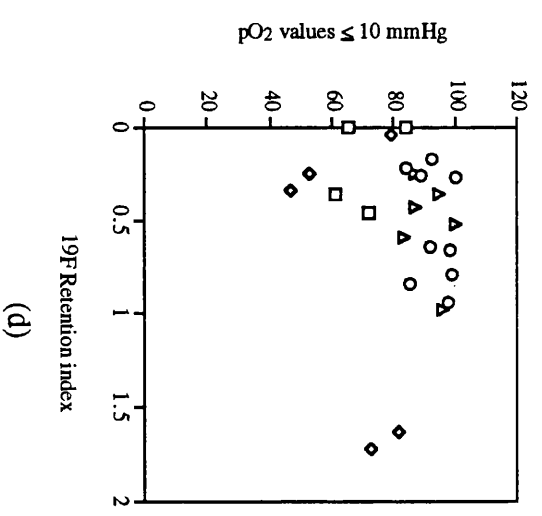


(b)

- C3H-mammary;foot
- ◇ C3H-mammary;flank
- SCCVII;flank
- △ RIF-1;flank

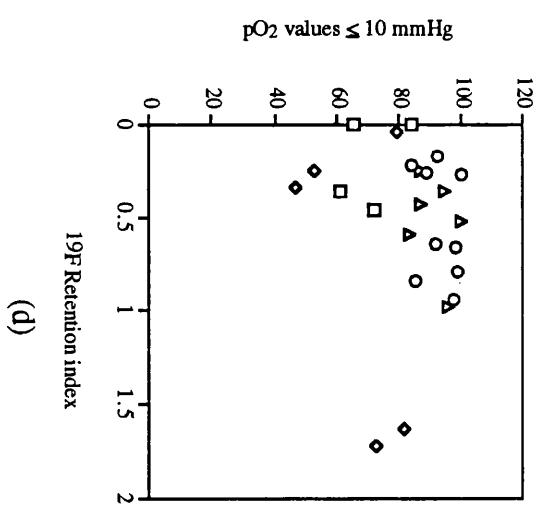
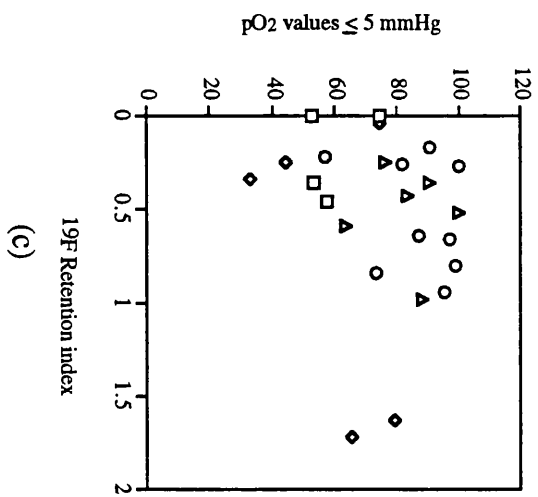
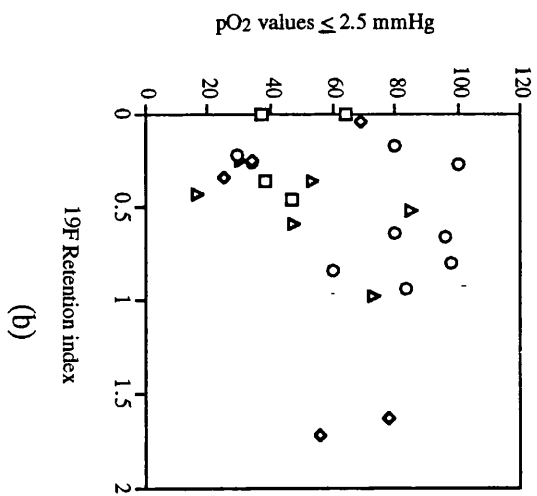
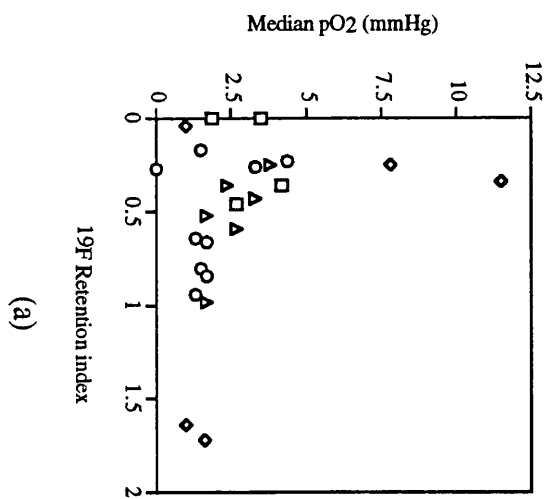


(c)



(d)

Fig. 6.8. Relationship between ^{19}F retention index and pO_2 parameters: (a) median pO_2 , (b) % pO_2 values ≤ 2.5 mmHg, (c) % of pO_2 values ≤ 5 mmHg, and (d) % of pO_2 values ≤ 10 mmHg.



□ C3H-mammary;foot
 ◆ C3H-mammary;flank
 ○ SCCVII;flank
 ▲ RIF-1;flank

Table 6.5. Detection of changes in tumour microenvironment using ¹⁹F MRS. Studies with hydralazine, carbogen and carbon monoxide.

TUMOUR MODEL	TREATMENT	¹⁹ F RETENTION INDEX	MEAN pO ₂ (mmHg)
RIF-1	Untreated controls	0.53 ± 0.3 (n=13)	ND
	Hydralazine pre-treated	1.27 ± 0.5 (n=6)	ND
C3H mammary carcinoma	Untreated controls (air)	0.64 ± 0.3 (n=4)	15.8 ± 4.9 (n=5)
C3H mammary carcinoma	Carbogen gas	0.11 ± 0.1 (n=4)	24.9 ± 8.2 (n=7)
C3H mammary carcinoma	Carbon monoxide gas	0.34 ± 0.2 (n=4)	2.4 ± 0.8 (n=6)

Data represent means ± s.d. (number of animals used).

ND Not done.

Using the Kruskal-Wallis test, significant differences (p < 0.05) between untreated RIF-1 vs hydralazine pre-treated RIF-1 and untreated C3H mammary carcinoma vs carbogen breathing C3H mammary carcinoma tumours were observed. The same test for untreated C3H mammary carcinoma vs carbon monoxide breathing C3H mammary carcinoma tumours gave p = 0.08.

HPLC showed that significant amounts of original drug were present ($0.07 \pm 0.02 \mu\text{mol/g}$ tissue). Fig. 6.9 shows typical ^{19}F tumour spectra obtained from control and carbogen breathing mice at 45 min and 6 hr post-injection. Carbogen breathing decreased the ^{19}F retention index in C3H mammary tumours by six fold compared to untreated controls (Table 6.5). Oxygen tension (pO_2) measurements in another set of mice from the same batch showed that this decrease in ^{19}F retention index was associated with an increase in mean pO_2 of about 9 mmHg (Table 6.5). Surprisingly, however, even though carbon monoxide breathing caused a decrease in mean pO_2 of about 13 mmHg, the corresponding ^{19}F retention index compared to controls, was lower rather than higher.

6.3.5 MRI studies

In Fig. 6.10a, the 1-D chemical shift image of SR-4554 in a RIF-1 tumour, as well as that of the reference tube containing 5-FTP is shown. The use of an adiabatic pulse enabled two regions of SR-4554 dependent ^{19}F signal to be obtained. These regions corresponded to the tumour and bladder regions. The image also shows a signal from the reference tube at the relative resonance frequency of 5-FTP. Fig. 6.10b illustrates a 2-D chemical shift image carried out in the same manner as the 1-D experiment but without the reference bulb. The image in the two phase encoding axes confirms the observation in Fig. 6.10a.

The application of whole body ^{19}F MRI to the imaging of drug biodistribution was also investigated in C3H mice bearing either the RIF-1 and SCCVII tumours. In each case a ^1H image of the mouse was obtained prior to the ^{19}F image to enable the visualisation of mouse anatomy and also to aid in the subsequent slice selection used for the ^{19}F imaging. Examples of ^1H spin echo images from the SCCVII tumour bearing mouse are illustrated in Fig. 6.11. The three images represent the top, middle and bottom 3.6 mm slices along the length of the mouse. The bladder is easily seen in the bottom slice while the tumour is seen in all slices. Fig. 6.12a shows a ^{19}F image (9 hr after SR-4554 injection) superimposed on the corresponding ^1H image of a SCCVII tumour bearing C3H mouse. The figure shows that residual ^{19}F signal was present in the bladder and tumour and to a lesser extent in the liver region. A similar image in a RIF-1 tumour bearing

Fig. 6.9. Typical tumour ^{19}F spectra obtained from control [(a) and (b)] and carbogen breathing [(c) and (d)] CDF₁ mice at 45 min [(a) and (c)] and 6 hr [(b) and (d)] after the injection of SR-4554. Whereas the ^{19}F signal is retained in control tumours, it is almost completely lost in carbogen breathing mice. The spectra also shows the reference standard 5-fluorotryptophan.

CONTROL

(a)
45 min

5-FTP

(b)
6 hr

SR-4554

CARBOGEN

(c)
45 min

(d)
6 hr

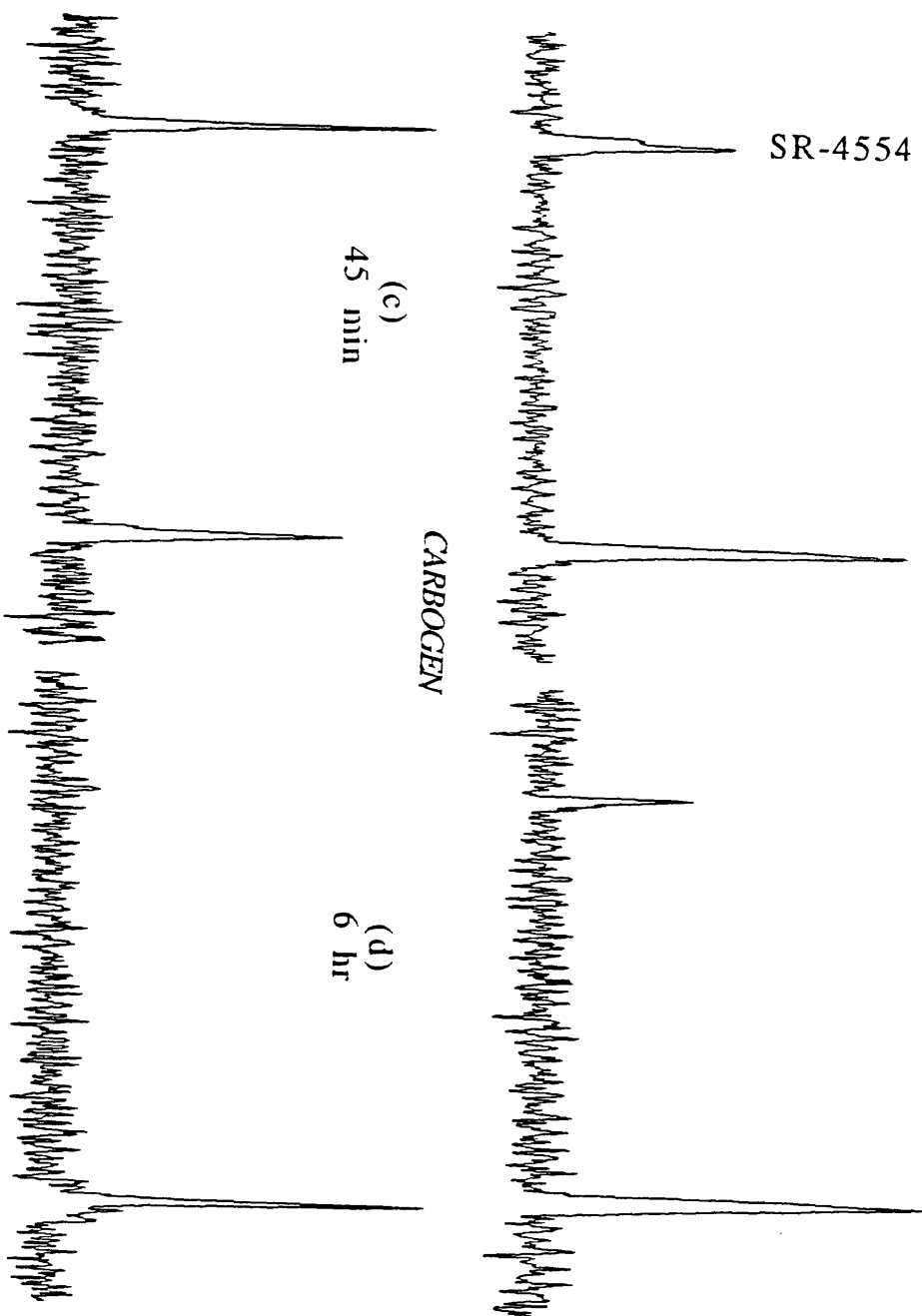
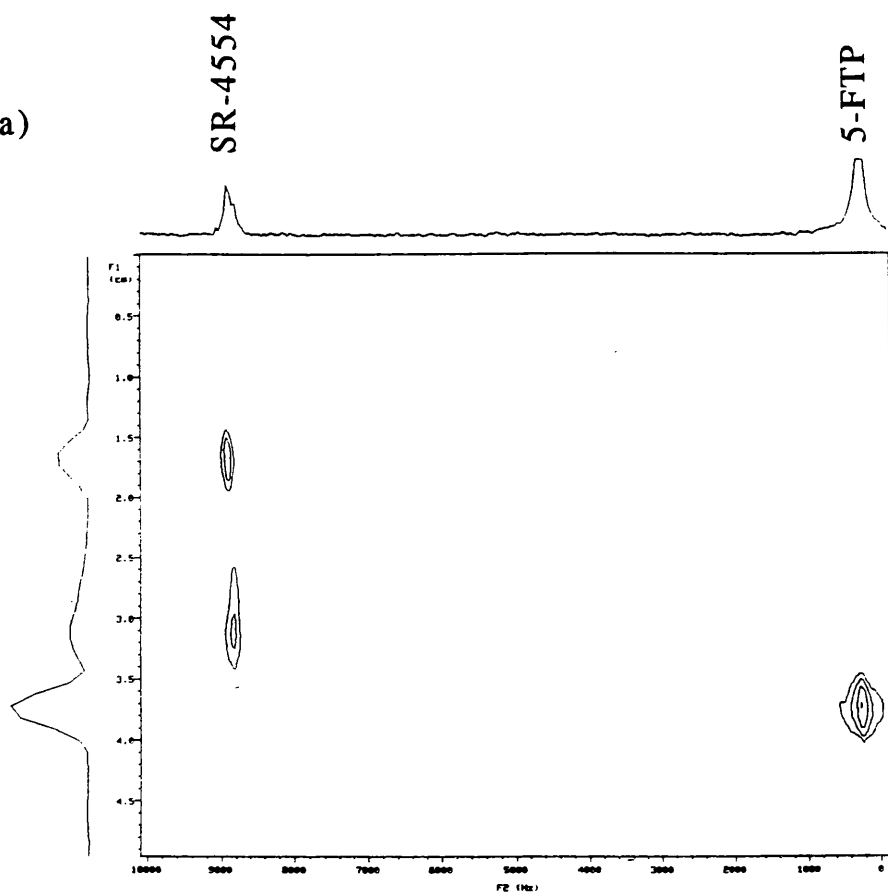


Fig. 6.10. (a) A typical 1-D CSI of SR-4554 (3 hr post-injection) in RIF-1 tumour showing drug signals from tumour and bladder regions. The image also shows signals from the reference standard 5-fluorotryptophan. (b) A 2-D CSI of the same tumour (4 hr post injection) without the reference standard showing a similar drug localisation profile as in (a). The image in the two phase encoding axes is presented in (b).

(a)



(b)

SR-4554

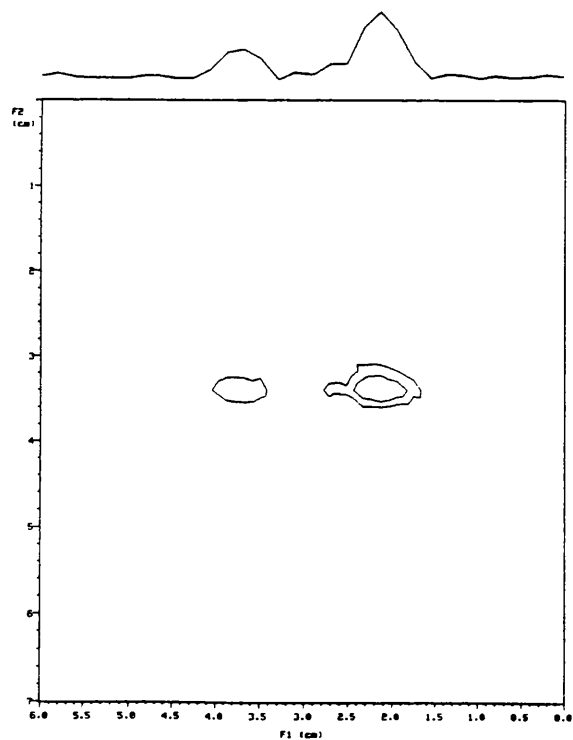
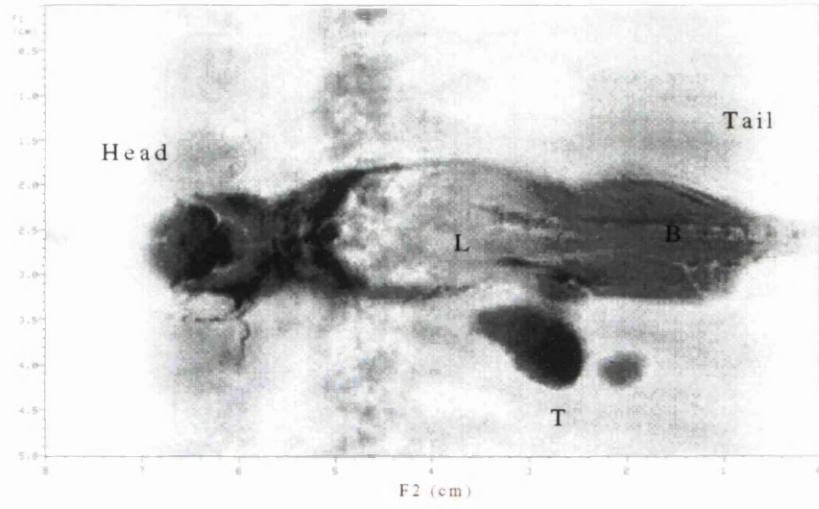
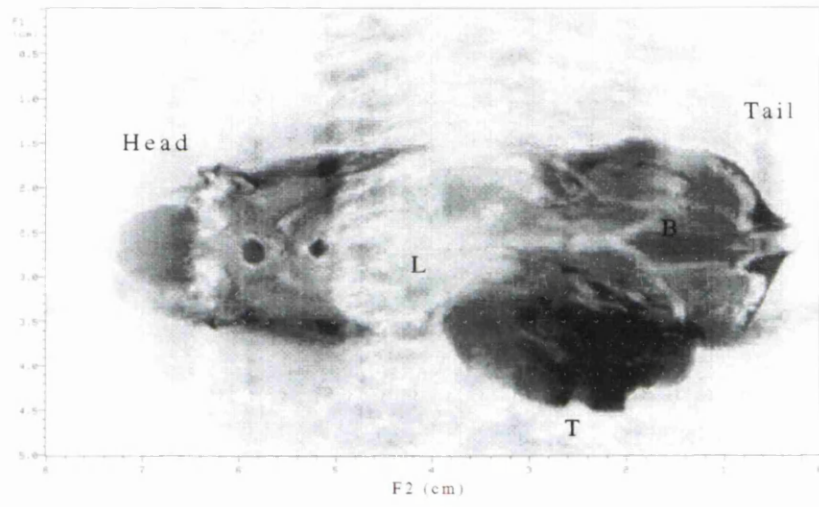


Fig. 6.11. The ^1H spin echo images obtained from a tumour (SCCVII) bearing mouse. The 3 images represent the top (a), middle (b), and bottom (c) 3.6 mm slices along the length of the mouse.

(a)



(b)



(c)

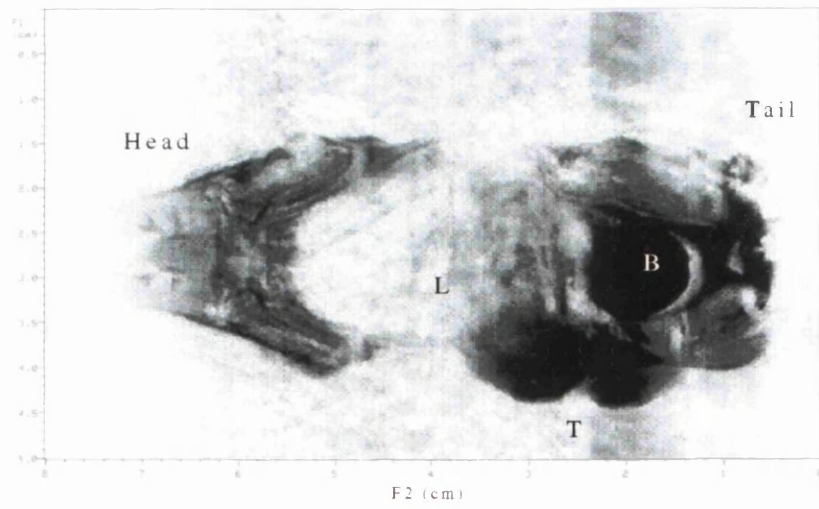
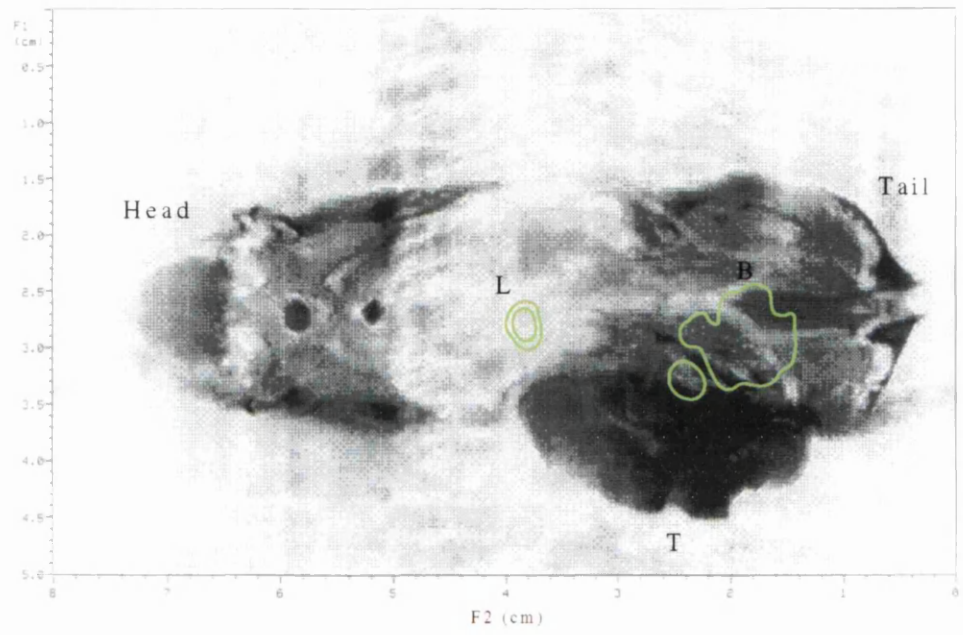
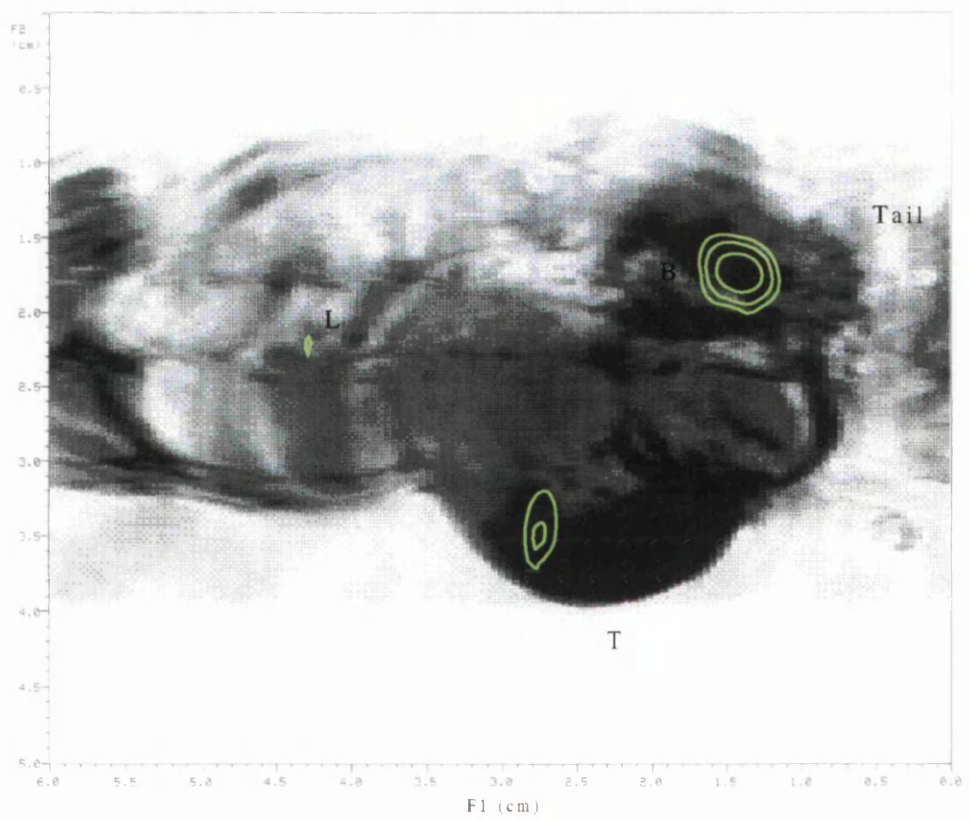


Fig. 6.12. (a) A ^{19}F spin echo image (green contours) superimposed on the corresponding ^1H image of a tumour (SCCVII) bearing C3H mouse. The image was obtained with a 4 cm Hemholtz coil at 9 hr after the administration of 360 mg/kg SR-4554. (b) A similar image in a tumour (RIF-1) bearing C3H mouse obtained at 5 hr after the administration of 180 mg/kg SR-4554. The image in both cases show localisation of ^{19}F in the tumour (T), bladder (B), and liver (L) regions. Motion artefacts in the phase encoding direction may account for the 'smearing' observed.

(a)



(b)



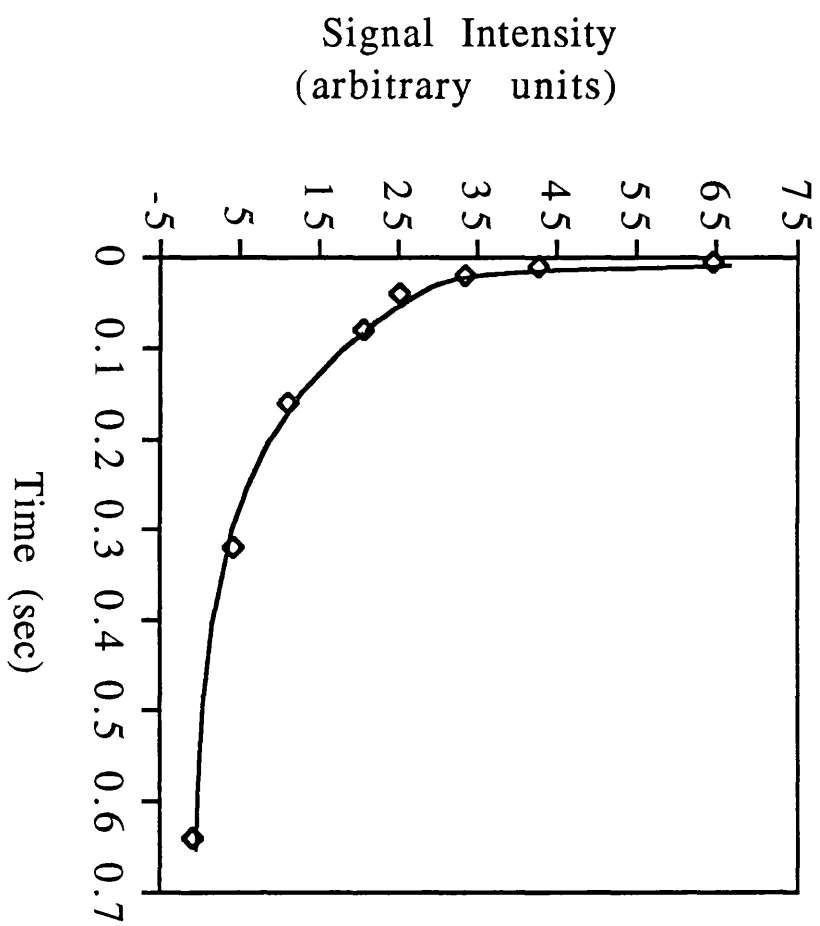
mouse (5 hr after SR-4554 injection) is presented in Fig. 6.12b. Similar studies in other tumour bearing mice showed that the distribution was not always the same as in Fig. 6.12. In some cases ^{19}F signal was not present in the tumour region 4 hr post-injection of SR-4554 whereas in one case retention was found in the kidneys. It should be noted that these are T_2 -weighted images, and that the actual distribution in a particular organ may not be apparent. In addition, the sensitivity of ^{19}F was not high enough to allow tissue heterogeneity to be studied by this technique. A typical T_2 curve obtained from a RIF-1 tumour bearing mouse (3 hr post-injection) using the Hemholtz coil fitted a bi-exponential model with a short T_2 component of 4.6 ms and a long component of 141 msec is shown in Fig. 6.13.

6.4 DISCUSSION

The development of improved and clinically relevant techniques for the detection and quantitation of hypoxia in tumours is important to the design of appropriate therapeutic modalities for hypoxic tumours. This led to the design and synthesis of SR-4554 which was envisaged to be less toxic, more stable, and more sensitive for detection by MRS and MRI techniques. The pre-clinical development of SR-4554 as an MRS/MRI probe for tumour hypoxia has been presented in this chapter.

As part of the study and for the first time, a simple $^{19}\text{F}/^2\text{H}$ method for the absolute *in vivo* quantitation of ^{19}F was implemented. This was based on a modification of the multi-tuned MRS technique first described by Thulborn & Ackerman (1983). Naturally abundant deuterium in tissue water was used as internal standard, whilst a combination of 5-fluorotryptophan and acetic acid-*d* served as external standards for the quantitation of drug levels. The external standards also served as chemical shift references, as well as eliminating errors due to coil loading and tuning. As previously suggested by Thulborn and Ackerman (Thulborn & Ackerman, 1983), this technique allows metabolite concentrations to be determined and is valid for inhomogeneous B_1 as produced by surface coils at higher frequencies. Using the $^{19}\text{F}/^2\text{H}$ technique, nominal concentrations of SR-4554 correlated with MRS concentrations over the range 0.125 to 4 mM ($r = 0.99$). A reasonable limit of detection was obtained (0.125

Fig. 6.13. A T_2 curve obtained from a RIF-1 tumour bearing mouse at 3 hr after the injection of 180 mg/kg SR-4554. Spectra were acquired using a 4 cm Hemholtz coil and the data fitted a bi-exponential model with a short T_2 component of 4.6 msec and a long T_2 component of 141 msec.



mM) due to the presence of three equivalent fluorine atoms per drug molecule. This method is therefore more sensitive than the method described by Evelhoch *et al.* (1989) using trideuteromethyl misonidazole (which had a limit of detection of 0.5 mM). It is worth noting that water weight per gram tumour may vary slightly from one tumour to the other, even with tumours of similar histologies. It is envisaged therefore that the exact tumour concentrations may vary slightly. However, a comparison of tumour concentrations at different times (45 min and 6 hr) corrects for these probable differences, as well as possible variations in SR-4554 delivery.

Due to the more effective relaxation of spins by tissue components, T_1 values for drug and HOD were found to be lower *in vivo*. The *in vitro* vs *in vivo* T_1 data reported here are also similar to those obtained by Evelhoch *et al.* (1989). For each nuclide, therefore, spectra were acquired at > 5 times the T_1 value of the species with the higher T_1 to avoid any saturation effects.

The fluorinated hypoxia probes SR-4554, fluoromisonidazole (Ro 07-0741) and CCI-103F showed similar tumour retention profiles. Although any possible interactions between the three compounds are unknown, the data suggested that at the doses used, the compounds will probably be similar in assessing tumour oxygenation. Initial studies in C3H mice bearing the RIF-1 tumour suggested that the ^{19}F signal from SR-4554 was selectively retained in tumours compared to brain. It could be assumed that the retention of high concentrations of fluorinated probe at 6 hr, despite the much lower (20 fold) concentration of original drug detected by HPLC at 7 hr, represents one or more nitroreduced metabolites. This is in agreement with previous high resolution NMR studies with excised tumours (chapter 3). By comparing brain concentrations of SR-4554 by MRS to similar concentrations determined in pharmacokinetic experiments (see section 5.3.3) it was observed that the MRS measurements were slightly higher than expected. In view of the fact that bioreduced drug is absent from the brain (see section 3.3.2), this observation could only be explained by a possible signal contamination from skin (Cobb *et al.*, 1990) and other structures within the head region, using the surface coil, rather than from the brain *per se*.

The ^{19}F signal levels from SR-4554 were normalised for delivery and expressed as the ratio of integrated signal at 6 hr to that

at 45 min post injection to give the ^{19}F retention index. The selection of these time points was based on studies in this chapter, as well as previous pharmacokinetic studies (section 5.3.3) which showed that at a dose of 180 mg/kg, original drug (SR-4554) peaks at 45 min post injection within tumours and is completely eliminated at 6 hr post-injection. The ^{19}F retention index was subsequently determined for a number of murine and human tumour xenografts. When taken individually, the ^{19}F retention index within tumours of the same origin and histological classification varied markedly. For instance, the WIL tumour showed a marked variation in ^{19}F retention index. *In vitro* this cell line exists as a mixed population of anaplastic and differentiated cells. The marked variation in ^{19}F retention index could therefore be explained by the heterogeneous growth characteristics of this tumour. The mean ^{19}F retention indices for murine tumours correlated with the reported radiobiological hypoxic fraction. A comparison could not be made in the case of the human xenografts, due to lack of radiobiological hypoxic fraction data in most of the tumours. Radiobiological hypoxic fraction data, however, are usually based on the best statistical fit and may not necessarily reflect the variability in the data. For instance, based on the scattering of their data, Guichard *et. al.* (1983) reported in their studies with HT-29 that a 0% hypoxic fraction was just as statistically acceptable for this tumour model as the best fit of 12%. In addition, RIF-1 tumours which have a reported radiobiological hypoxic fraction of 1% showed a mean ^{19}F retention index of 0.5. Additional supporting evidence for the high retention index obtained for RIF-1 tumours can be obtained from studies in this chapter. For instance, ^{19}F retention index vs pO_2 measurements, demonstrated that this high retention was associated with an equally high % pO_2 values ≤ 5 mmHg of 83.7 ± 5.1 , thus justifying the ^{19}F retention index obtained. A major assumption of the MRS studies discussed here, is that the activities of reductases in these tumours are non-limiting. As discussed in chapter 3, this assumption may be justified, since differences in NADPH cytochrome P450 reductase activities between the tumour types used in this study are small (up to 3 fold), and may not significantly affect the absolute reduction rate and selective retention of SR-4554 within these tumours.

In RIF-1 tumours, the ^{19}F retention index increased with increasing tumour mass suggesting increased hypoxia in bigger tumours. Similar results have been reported by Kwock *et al.* (1992) using ^{19}F MRS and immunostaining. In their study, only the less well vascularised and more hypoxic Dunning rat prostate adenocarcinoma with diameters > 3 cm had detectable ^{19}F signals (from CCI-103F) after 24 hr, and also stained immunohistochemically in locations without obvious necrosis. Correlations between tumour size and hypoxia have also been reported in RIF-1, KHT, human ovarian carcinoma MLS, SCCVII, FSaII, and the radiosensitive Meth-A mouse tumour using bioenergetic status parameters determined by ^{31}P MRS (Fu *et al.*, 1990; Koutcher *et al.*, 1990; Okunieff *et al.*, 1986; Rofstad *et al.*, 1989). No correlation between ^{31}P parameters and ^{19}F retention index (of SR-4554 in this chapter) was, however, observed in KHT tumours ($n = 6$) suggesting that bioenergetic status of the tumour may not necessarily correlate to the labelling of hypoxic cells by fluorinated 2-nitroimidazoles. This is not unexpected, since 2-nitroimidazoles label only hypoxic cells, whilst a component of the signals from ^{31}P experiments (especially P_i) may also be due to necrosis (Tozer & Griffiths, 1992).

Oxygen tension (pO_2) measurements indicated that the anaesthetic used (Hypnorm-Hypnovel-water) did not significantly alter tumour oxygenation. In contrast, SR-4554 and the combination of SR-4554 and anaesthetic produced a significant increase in tumour oxygenation when medians or % pO_2 values ≤ 2.5 mmHg were compared (Kruskal-Wallis test; 95% confidence level). This observation is contrary to the decrease in tumour blood flow (and hence oxygenation) produced by another 2-nitroimidazole pimonidazole at pharmacological doses (Chaplin, 1991). It is unknown whether this effect of SR-4554 at low (≤ 2.5 mmHg) pO_2 readings is due to a direct interference of the compound with the oxygen electrode e.g. by an electrochemical mechanism. Provided the same protocol is used in all cases, however, this increase in oxygenation produced by the combination will not be expected to affect measurement of tumour oxygenation by SR-4554. In addition, no significant differences (Kruskal-Wallis; 95% confidence level) in ^{19}F retention were observed between tumours which had their pO_2 measured and those which did not, indicating that the pO_2

measurements did not significantly affect the retention of SR-4554 (data not shown). To determine the relationship between ^{19}F retention indices and pO_2 in mouse tumours, three different tumour models (two sites) were used in the study to allow for variability in oxygenation status. No precise correlations were observed when the two techniques were compared. The inability to observe a strong correlation, from the relatively small group of animals used in the study, is not altogether surprising. It can be imagined that pO_2 measurements using oxygen electrodes can give low pO_2 values resulting from regions within the tumour not containing viable hypoxic cells, such as necrotic regions. The data, however, indicated that substantial retention of ^{19}F signal was associated with a high level of tumour hypoxia (low tumour oxygenation). Previous studies in C3H mammary foot tumours suggested that when median pO_2 was less than 2.5 mmHg and the % of $\text{pO}_2 \leq 5$ mmHg was 60%, the equivalent clonogenic hypoxic fraction was 10% (Nordsmark *et al.*, 1995). It can therefore be predicted that substantial retention of ^{19}F will be evident in tumours with a radiobiological hypoxic fraction of $> 10\%$. In general, the studies in this chapter have also demonstrated the ability of ^{19}F MRS to detect tumour oxygenation at critical levels that have been reported to limit radiocurability of human tumours (i.e. 26% of tumour cells with $\text{pO}_2 \leq 8$ mmHg) (Gatenby *et al.*, 1988).

It is conceivable from the above discussions that determination of changes in oxygenation as measured by ^{19}F MRS may be more sensitive than absolute hypoxic fraction. Changes in tumour oxygenation resulting from the administration of hydralazine, carbogen and carbon monoxide were investigated in RIF-1 and C3H mammary tumours using ^{19}F MRS. It was demonstrated that the mean ^{19}F retention index increased two-fold in response to the administration of 5 mg/kg hydralazine compared to untreated controls. Hydralazine decreases tumour blood flow and subsequently decreases tumour oxygenation (Honess & Bleehen, 1992). Direct measurement of this reduction in tumour perfusion has also been reported in RIF-1 (Bhujwaller *et al.*, 1990), C3H mammary carcinoma (Horsman *et al.*, 1989), KHT (Honess & Bleehen, 1991), SCCVII (Trotter *et al.*, 1989), FSaII (Kalmus *et al.*, 1990), and Lewis lung tumours (Chaplin, 1988; Chaplin & Acker, 1987). Honess & Bleehen (1992) reported that at 5 mg/kg hydralazine decreased the perfusion of KHT

tumours to 35% (Honess & Bleehen, 1992). This same dose was also shown to reduce liver and kidney perfusion to 64 and 73% respectively. Based on their data, Honess & Bleehen (1992) suggested that there may be an impairment in the metabolism and/or elimination of drugs which are metabolised or eliminated by these organs following the administration of hydralazine. This may explain the presence of original drug in hydralazine treated RIF-1 tumours at 7 hr post-injection of SR-4554 (this chapter). The levels of original drug present in the tumours, however, could not account for the enhanced signal obtained, suggesting that the effect is mainly due to hypoxia. In addition, ^{19}F levels within hydralazine treated tumours were high even at 45 min indicating that the reduced perfusion does not impede delivery of SR-4554 to the tumour.

On the other hand, carbogen breathing drastically increased the oxygenation of C3H mammary tumours as indicated by both ^{19}F retention index and pO_2 (Eppendorf measurements). This effect of carbogen on tumours has also been previously investigated with oxygen electrodes and ^{31}P MRS (Nordsmark *et al.*, 1995), as well as ^1H functional imaging (Robinson *et al.*, 1994). Surprisingly, however, the relationship between ^{19}F retention index and pO_2 in mice breathing carbon monoxide was contrary to the expected result. Carbon monoxide decreases tumour oxygenation by two mechanisms, (a) a decrease in the oxygen carrying capacity of blood and, (b) a reduction in tumour blood flow (Grau *et al.*, 1994). Data from this chapter, and as reported by others (Nordsmark *et al.*, 1995), indicated that pO_2 values in C3H mammary tumours decreased dramatically when mice breathed carbon monoxide gas. The ^{19}F retention index in these tumours, however, were low (instead of high) compared to control mice, in spite of high ^{19}F signals at 45 min suggesting unimpeded delivery. Hirst *et al.* (1985) showed that acute hypoxia induced by reduced haematocrit was associated with an increase in ^{14}C labelled misonidazole binding. This response was subsequently shown to be accompanied by compensatory mechanisms which act to increase cardiac output and maintain the supply of oxygen to tissues (Sensky *et al.*, 1994). Such an effect is unlikely to be observed in the ^{14}C misonidazole model used by Hirst *et al.* since the oxygen carrying capacity of blood will remain low throughout the measurement period (Hirst *et al.*, 1985). In the carbon monoxide model, however, such

compensatory effects could occur due to reoxygenation and may account for the unexpectedly low ^{19}F retention index observed. In addition, the decreased ^{19}F retention index may be attributed in part to the partial inhibition of SR-4554 bio-reduction produced by the inhibitory effect of carbon monoxide on the NADPH: cytochrome P450 enzyme (section 3.3.1) and possibly other haem containing reductases. Using ^{31}P MRS, tumour bioenergetics were also shown (Nordsmark *et al.*, 1995) to be unaffected by carbon monoxide breathing (660 ppm) in spite of the high degree of radiobiological hypoxia induced by this protocol. It was suggested that this unusual ^{31}P MRS behaviour produced by carbon monoxide may be due to the continued supply of glucose and other nutrients to the tumour making such tumours resistant to a decrease in oxygen content (Nordsmark *et al.*, 1995).

By means of ^{19}F MRI, SR-4554 was demonstrated to localise in bladder, tumour and liver of mice after 5 hr post-injection. This is in accordance with the route of excretion (bladder; see section 5.3.5), as well as sites of bio-reduction (liver and tumour; see section 3.3.2) of SR-4554. It is worth noting that the signal from the liver region could be predominantly from the gall bladder, rather than liver *per se*. In addition, unabsorbed drug in the peritoneum could not be definitely ruled out. Although the sensitivity of ^{19}F MRI is insufficient to achieve the high resolution shown by techniques employing 2-nitroimidazole probes such as electron energy loss spectroscopy (see chapter 4), immunohistochemistry (Lord *et al.*, 1993), positron emission tomography (Koh *et al.*, 1991), and autoradiography (Urtasun *et al.*, 1986b), it allows the whole body biodistribution of the probe to be studied in mice thus complementing these techniques. Further modification of the protocol (including the NMR coil) is, however, required to allow for the imaging of SR-4554 at early time points and also for enhancing sensitivity.

The distribution of ^{19}F between tissue and body fluid could account for the bi-exponential nature of the T_2 curve. The implication of this is apparent. For instance at the short T_2 of 4.6 msec, fluorine sensitivity decreases in the order 65, 52, 42, 18, and 3% at echo times (TE) of 2, 3, 4, 8, and 16 msec respectively. In contrast, at a TE of 16 msec, the sensitivity is only decreased to 89% when the T_2 component is 141 msec. Due to the short T_2 component, very low TE's are required in the detection of fluorine signal from

tissues and thus care should be taken in interpreting the resultant T₂ weighted images as the exact tissue distribution may not be apparent. At present, this is highly undesirable and may, in fact, hamper the development of fluorinated 2-nitroimidazoles as MRI (but not MRS) agents, unless newer pulse sequences which can overcome this effect are developed.

In general, however, MR detection of fluorinated 2-nitroimidazole probes and in particular spectroscopy, offer great potential for the detection and quantitation of tumour hypoxia within individual tumours. The data presented in this chapter indicate that ¹⁹F MRS can be employed to detect clinically relevant hypoxia as demonstrated by murine and human tumour xenografts. These studies are therefore important to the future clinical development of SR-4554 as a non-invasive probe for quantifying hypoxia in tumours.

CHAPTER 7

Summary and conclusions

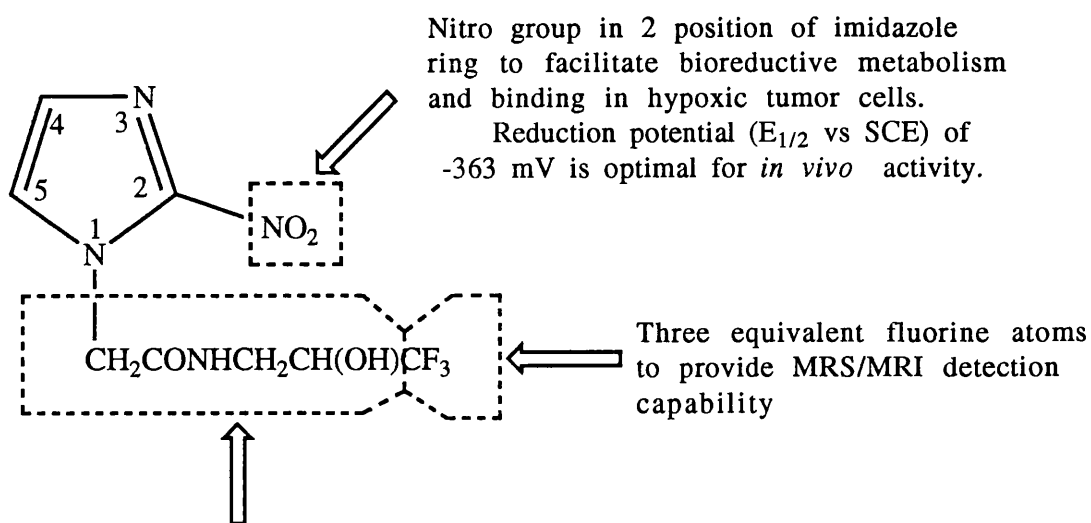
The principal aims of this thesis were two fold. Firstly, to study the pharmacological properties and toxicity of the novel 2-nitroimidazole SR-4554 and secondly, to assess the ability of ^{19}F MRS (of SR-4554) to detect and quantify hypoxia within tumours. Both of these aims have been achieved in chapters 2 to 6 and summarised in this chapter.

Since the suggestion in 1955 by Thomlinson and Gray, that tumours may contain viable hypoxic cells which can limit therapeutic outcome (Thomlinson & Gray, 1955), several attempts have been made to detect, characterise, and quantify these cells within tumours as a prelude to rational therapies designed to kill all cancer cells. In this regard, the 2-nitroimidazoles which were previously of very limited success as radiosensitizers (Overgaard, 1989), were developed as markers for hypoxic cells (Workman, 1992). Early methods focused on the development of radiolabelled probes of misonidazole as hypoxia markers (Chapman, 1984). Although this formed the basis of current invasive and non-invasive techniques (Table 1.1), radiolabelled probes were not suitable for clinical use. ^{19}F MRS offers an easy, comparatively cheap, non-invasive and relatively non-toxic potential for measuring hypoxia within tumours. In this thesis, the characterisation of a rationally designed superior hypoxia probe, SR-4554, has been described and the relationship between its retention and the oxygenation within tumours reported.

Design features of SR-4554

Some of the design features of SR-4554, which makes it suitable for quantifying hypoxia within tumours, are summarised in Fig 7.1. The nitro group facilitates bioreductive metabolism of the compound and binding to hypoxic cells. The reduction potential of the compound was found to be similar to that of misonidazole (Greenstock *et al.*, 1978) and will be expected to have similar reduction properties. Importantly, the amide side chain was introduced to increase the hydrophilic character of SR-4554, and thus decrease its potential toxicity as in the case of etanidazole (Brown & Workman, 1980), thereby making it more suitable for clinical use. The MRS detection

Fig. 7.1. Design features of the fluorinated 2-nitroimidazole SR-4554: non-invasive MRS probe for quantifying tumour hypoxia.



Hydrophilic character and hydrogen bonding capability introduced by amide and hydroxyl functions. This should discourage penetration into the nervous system and reduce the risk of neurotoxicity.

capability of this compound is due to the presence of three equivalent fluorine atoms. Hence MRS/MRI techniques can be used to detect SR-4554 non-invasively and thus enable hypoxia-dependent labelling of tumour cells to be measured.

Outline of methods developed or used in this thesis

In chapter 2, a rapid, sensitive and selective HPLC assay was developed for the analysis of SR-4554 in mouse plasma and tissues. The UV method of detection employed by this technique relies on the presence of a nitro chromophore attached to the imidazole ring and would therefore not measure bio-reduced product in which the nitro group has been converted to other species. This HPLC technique was, however, used to evaluate the metabolic reduction and pharmacokinetics of SR-4554 in subsequent chapters of this thesis. In order to elucidate the possible bio-reduced products, however, a high resolution NMR method was developed (chapter 3). Although this technique involves a longer sample preparation step, it enabled both original and bio-reduced fluorinated 2-nitroimidazoles to be characterised with respect to the formation of reductive metabolites. In addition to HPLC and NMR techniques, UV spectrophotometric methods were employed to determine both the protein and enzyme content of various tumours and liver microsomes. In the absence of radiolabelled SR-4554, the subcellular localisation of SR-4554 was carried out with the aid of EELS (chapter 4), a technique which is only now emerging as a useful tool in oncology. This technique measures the energy loss of the fluorine atoms in SR-4554 within cells (at the molecular level), and offers the potential for measuring tumour hypoxia on biopsy samples. This could be useful as an additional methodology during the early development of SR-4554.

In order to non-invasively detect and quantify hypoxia within tumours, both MRS and MRI techniques were employed to study the selective retention of SR-4554 in mouse tumours (chapter 6). These methods measure the concentration and spatial spin distribution of the equivalent fluorine atoms in SR-4554. In addition, fine needle oxygen electrodes (Eppendorf) were also used to directly measure tissue oxygenation in mouse tumours and hence to validate the use of SR-4554.

Metabolic properties of SR-4554

SR-4554 was reduced by mouse liver microsomes, SCCVII tumour homogenates and purified rat and human NADPH: cytochrome P450 reductase (chapter 3). Reduction of SR-4554 by mouse liver microsomes (loss of parent drug) was linear with time and protein concentration, and was characterised by an apparent K_m and apparent V_{max} of 590 μM and 16 nmol SR-4554 reduced/min/mg protein respectively. Inhibitory studies indicated that NADPH: cytochrome P450 reductase was the most important enzyme involved in the reductive activation of SR-4554. A panel of murine and human tumour xenografts were profiled to investigate whether the activity of NADPH: cytochrome P450 reductase varied markedly and would influence the *in vivo* retention of SR-4554 within tumours. The activity of this enzyme in tumours only varied between 3.4 and 11.9 nmol cytochrome c reduced/min/mg protein. Its unlikely that these differences will markedly influence the *in vivo* retention profile of SR-4554 within the tumours studied in chapter 6. Importantly, the reduction rate of SR-4554 was dependent on oxygen tension. The concentration of oxygen which produced 50% inhibition of SR-4554 reduction between nitrogen and air (half-maximal inhibition) was found to be 0.48%.

Hypoxia-dependent metabolites of SR-4554 were detected by high resolution NMR spectroscopy. In this regard, loss of parent drug was found to be associated with the formation of metabolites. Both processes were inhibited under aerobic conditions. These metabolites were found to be low molecular weight species. Similar metabolites were detected in liver and urine from SR-4554 treated mice, but were not found in brain which also had low levels of SR-4554 itself. Other metabolites unrelated to these hypoxia dependent metabolites were also observed in the urine samples, but by far the major contribution in urine was the original parent compound, SR-4554. Other fluorinated 2-nitroimidazoles (CCI-103F, Ro 07-2044, KU-2285 and fluoromisonidazole) were also characterised with regard to the formation of reductive metabolites. The chemical shifts of the metabolites were found to be similar to intracellular/extracellular shifts previously reported in NMR literature (London, 1994; Xu *et al.*, 1993), and were related to the partition coefficient of the compounds. Only small chemical shifts (up to 1.5 ppm in general; 0.05 to 0.1 ppm

for SR-4554) between the original 2-nitroimidazole and its metabolites were observed. It is unlikely that such shifts would be resolved in *in vivo* MRS studies (at currently available clinically relevant field strengths), to allow metabolite mapping to be carried out. This also implies that *in vivo* MRS spectra of SR-4554, for instance, will comprise of both the original compound and metabolites.

Localisation of SR-4554

Following the uptake of SR-4554 into cells of the human ovarian carcinoma multicellular spheroid, A2780, the compound localised to a greater extent (at least 8 fold) in the inner hypoxic regions of the spheroid compared to the outer more aerobic regions. Detailed subcellular localisation studies with EELS revealed that SR-4554 does not significantly bind to mitochondria and plasma membrane. The compound was mainly localised to the nuclear periphery, nucleus and cytoplasm. This is in agreement with previous subcellular fractionation studies with radiolabelled misonidazole by Miller *et al.* (1992) which indicated that reduced misonidazole was predominantly bound to RNA, DNA lipids and proteins (Miller *et al.*, 1982). In addition, reactive metabolites of SR-4554 do not appear to migrate out of the cells within which they are activated. This is a useful property of good marker compound.

Toxicity and pharmacokinetics of SR-4554

SR-4554 was designed to have low toxicity by including an amide side chain similar to that of etanidazole (Brown & Workman, 1980). Although the actual LD₅₀ or LD₁₀ of SR-4554 could not be determined, due to the limited solubility of the compound in saline (maximum solubility in saline = 6.5 mg/ml), dose ranging studies indicated that SR-4554 was non-toxic in mice up to a dose of 1300 mg/kg. This dose was well in excess of the dose required for MRS studies (180 mg/kg). SR-4554 plasma pharmacokinetics fitted a one compartment open model following i.p. or p.o. administration. On the other hand, plasma pharmacokinetics following an i.v. dose, fitted a two compartment open model. In addition, a linear relationship between dose of SR-4554 and plasma AUC was observed. The tumour to plasma ratios of SR-4554 (between 30 and 120 min post-injection)

were found to be between 0.86 and 1.27 and consistent with trends shown by other 2-nitroimidazoles of similar partition coefficients (Brown & Workman, 1980; Workman & Brown, 1981). Interestingly, brain to plasma ratios of SR-4554 were found to be lower (0.05 to 0.19) than is consistent with the trends reported in the literature (Brown & Workman, 1980; Workman & Brown, 1981). This unexpected and unique property of SR-4554 may be due to the additional hydrophilic character and hydrogen bonding capability of the amide group in SR-4554. Bioavailability studies indicated that SR-4554 was almost completely absorbed from i.p. (100%) and oral (96%) administration. Both data from chapter 3 and 5 showed that SR-4554 was metabolised in mouse liver. The compound was, however, excreted mainly as unchanged drug in the urine (68%), and showed minimal binding to mouse and human plasma proteins (< 20%).

Non-invasive detection of hypoxia by MRS/MRI

The selective retention of SR-4554 in mouse tumours was demonstrated using a modification of the multi-tuned MRS technique previously described by Thulborn & Ackerman, 1983). SR-4554 was administered at a dose of 180 mg/kg in these studies. It was assumed that the retention of high levels of fluorinated probe at 6 hr, despite the much lower (20 fold) concentration of original drug detected by HPLC at 7 hr, represent one or more bioreduced metabolites. The ^{19}F retention index (the MRS index for hypoxia) was found to vary within tumours of the same and of different histological classifications. The mean ^{19}F retention for each tumour type, however, correlated in general, with the reported radiobiological hypoxic fraction of the tumours. Provided reductive enzyme activities within tumours are not markedly different than those described here, this MRS technique should provide a quantitative measure of hypoxia within tumours. The ^{19}F retention index was found to increase with increasing tumour mass, but, interestingly, did not correlate with bioenergetic status of (KHT) tumours as determined by ^{31}P MRS.

Using various mouse tumour models, both ^{19}F retention index and pO_2 (oxygen needle electrodes) were measured from the same tumour. Although a precise correlation between ^{19}F retention index

and pO₂ parameters was not observed, substantial trapping of SR-4554 was always associated with tumours with a hypoxic fraction of > 10%. The ¹⁹F retention index was found to increase (2 fold) with decreased tumour blood flow, following pre-treatment of mice with hydralazine. In contrast, the retention index decreased (6 fold) when mice were made to breath carbogen gas. Surprisingly, however, carbon monoxide breathing which has previously been shown to decrease tumour oxygenation (Grau *et al.*, 1994), did not increase the ¹⁹F retention, but caused a decrease.

Using MRI techniques, SR-4554 was demonstrated to localise in bladder, tumour and liver of mice. The sensitivity of the technique is, however, low. This is due to a short T₂ component of SR-4554 in tissues (4.6 msec) and implies that extremely short echo times are required to image SR-4554.

Concluding remarks

It has been shown, in this thesis, that SR-4554 has suitable metabolic, pharmacological and MRS properties for use in the non-invasive quantification of critical levels of clinically relevant hypoxia that have been reported to limit radiocurability of human tumours (Gatenby *et al.*, 1988). On the basis of these promising results, the compound has been approved by the CRC phase I/II committee for clinical development.

Interesting aspects of the work which needs further experimentation include the following:

1. To fully characterise the reductive metabolites of SR-4554 and other related fluorinated 2-nitroimidazoles.
2. To evaluate the binding kinetics of SR-4554 with radiolabelled compound.
3. To characterise the relationship between partition coefficient and brain to plasma ratios of newer and more hydrophilic 2-nitroimidazole analogues.
4. To fully characterise the exact relationship between ¹⁹F retention index and tumour oxygenation status.

It is my ultimate goal that the work reported in this thesis will provide further impetus to the continued development of SR-4554, as well as other more superior fluorinated 2-nitroimidazoles as probes for the measurement of hypoxia within human tumours.

REFERENCES

- Adams, G.E. (1992). Redox, radiation, and reductive bioactivation. *Radiat. Res.*, **132**, 129-139.
- Adams, G.E., Clarke, E.D., Gray, P., Jacobs, R.S., Stratford, I.J., Wardman, P. & Watts, M.E. (1979). Structure-activity relationships in the development of hypoxic cell radiosensitizers. II. Cytotoxicity and therapeutic ratio. *Int. J. Radiat. Biol.*, **35**, 151-160.
- Adams, G.E., Stratford, I.J., Wallace, R.G., Wardman, P. & Watts, M.E. (1980). Toxicity of nitro compounds towards hypoxic mammalian cells *in vitro*: dependence upon reduction potential. *J. Natl. Cancer Inst.*, **64**, 555-560.
- Amellem, O., Loffler, M. & Pettersen, E.O. (1994). Regulation of cell proliferation under extreme and moderate hypoxia: the role of pyrimidine (deoxy)nucleotides. *Br. J. Cancer*, **70**, 857-866.
- Amellem, O. & Pettersen, E.O. (1991). Cell inactivation and cell cycle inhibition as induced by extreme hypoxia: the possible role of cell cycle arrest as a protection against hypoxia-induced lethal damage. *Cell Prolif.*, **24**, 127-141.
- Amellem, O. & Pettersen, E.O. (1993). Cell cycle progression in human cells following re-oxygenation after extreme hypoxia: consequences concerning initiation of DNA synthesis. *Cell Prolif.*, **26**, 25-35.
- Andrew, E.R. (1994). Introduction to nuclear magnetic resonance. In *NMR in physiology and biomedicine*, Gillies, R.J. (ed) pp. 1-23. Academic Press: San Diego.
- Bedford, J.S. & Mitchell, J.B. (1974). The effect of hypoxia in the growth and radiation response of mammalian cells in culture. *Br. J. Radiol.*, **47**, 687-696.

Bhujwaller, Z.M., Tozer, G.M., Field, S.B., Maxwell, R.J. & Griffiths, J.R. (1990). The energy metabolism of RIF-1 tumours following hydralazine. *Radiother. Oncol*, **19**, 281-291.

Biaglow, J., Varnes, M., Roizen-Towle, L., Clarke, E., Epp, E., Astor, M. & Hall, E. (1986). Biochemistry of reduction of nitroheterocycles. *Biochem. Pharmacol.*, **35**, 77-90.

Bloch, F., Hansen, W.W. & Packard, M.E. (1946). Nuclear induction. *Phys. Rev.*, **69**, 127.

Bradford, M.M. (1976). A rapid and sensitive method for the quantitation of microgram quantities of protein utilizing the principle of protein-dye binding. *Anal. Biochem.*, **72**, 248-254.

Brown, J.M. (1979). Evidence for acutely hypoxic cells in mouse tumours, and a possible mechanism of reoxygenation. *Br. J. Radiol.*, **52**, 650-656.

Brown, J.M., Twentyman, P.R. & Zamvil, S.S. (1980). Response of the RIF-1 tumour *in vitro* and in C3H/Km mice to X-radiation (cell survival, regrowth delay, and tumour control), chemotherapeutic agents, and activated macrophages. *J. Natl. Cancer Inst.*, **64**, 605-611.

Brown, J.M. & Workman, P. (1980). Partition coefficient as a guide to the development of radiosensitizers which are less toxic than misonidazole. *Radiat. Res.*, **82**, 171-190.

Bush, R.S., Jenkin, R.D.T., Ollt, W.E.C., Beale, F.A., Bean, H., Dembo, A.J. & Pringle, J.F. (1978). Definitive evidence for hypoxic cells influencing cure in cancer therapy. *Br. J. Cancer*, **37**, 302-306.

Chacon, E., Morrow, C.J., Leon, A.A., Born, J.L. & Smith, B.R. (1988). Regioselective formation of a misonidazole-glutathione conjugate as a function of pH during chemical reduction. *Biochem. Pharmacol.*, **37**, 361-363.

Chaplin, D.J. (1988). Postirradiation modification of tumour blood flow: a method to increase the effectiveness of chemical radiosensitizers. *Radiat. Res.*, **115**, 292-302.

Chaplin, D.J. (1991). The effect of therapy on tumour vascular function. *Int. J. Radiat. Biol.*, **60**, 311-325.

Chaplin, D.J. & Acker, B. (1987). The effect of hydralazine on the tumour cytotoxicity of the hypoxic cell cytotoxin RSU-1069; evidence for therapeutic gain. *Int. J. Radiat. Oncol. Biol. Phys.*, **13**, 579-585.

Chaplin, D.J., Olive, P.L. & Durand, R.E. (1987). Intermittent blood flow in a murine tumour: Radiobiological effects. *Cancer Res.*, **47**, 546-550.

Chapman, J.D. (1984). The detection and measurement of hypoxic cells in solid tumours. *Cancer*, **54**, 2441-2449.

Chapman, J.D. (1991). Measurement of tumour hypoxia by invasive and non-invasive procedures: a review of recent clinical studies. *Radiother. Oncol.*, **20**, 13-19.

Chapman, J.D., Baer, K. & Lee, J. (1983). Characteristics of the metabolism-induced binding of misonidazole to hypoxic mammalian cells. *Cancer Res.*, **43**, 1523-1528.

Chapman, J.D., Franko, A.J. & Sharplin, J. (1981). A marker for hypoxic cells in tumors with potential clinical applicability. *Br. J. Cancer*, **43**, 546-550.

Chapman, J.D., Lee, J. & Meeker, B.E. (1990). Adduct formation by 2-nitroimidazole drugs in mammalian cells: optimization of markers for tissue oxygenation. In *Selective activation of drugs by redox processes*, Adams, G.E., Breccia, A., Fielden, E.M. & Wardman, P. (eds), Vol. 198. pp. 313-323. NATO ASI. Plenum Press: New York.

Cline, J.M., Thrall, D.E., Rosner, G.L. & Raleigh, J.A. (1994). Distribution of the hypoxia marker CCI-103F in canine tumours. *Int. J. Radiat. Oncol. Biol. Phys.*, **28**, 921-933.

Cobb, M., Nolan, J. & Butler, S.A. (1990). Distribution of pimonidazole and RSU 1069 in tumour and normal tissues. *Br. J. Cancer*, **62**, 915-918.

Coleman, C.N. (1988). Hypoxia in tumours: a paradigm for the approach to biochemical and physiologic heterogeneity. *J. Natl. Cancer Inst.*, **80**, 310-317.

Coleman, C.N., Wasserman, T.H., Urtasun, R.C., Halsey, J., Hirst, V.K., Hancock, S. & Philips, T.L. (1986). Phase 1 trial of the hypoxic cell radiosensitizer SR 2508: the results of the five to six weeks schedule. *Int. J. Radiat. Oncol. Biol. Phys.*, **12**, 1105-1108.

D'Argenio, D.Z. & Schumitzky, A. (1979). A program package for simulation and parameter estimation in pharmacokinetic systems. *Comput. Prog. Biomed.*, **9**, 115-134.

Dabrow, M.B., Katz, H., O'Dwyer, P.J., Afshar, C. & Glusker, J.P. (1993). Molecular dimensions and properties of N-[1-(2-Hydroxyethyl)-2-nitro-1H-imidazol-1-yl] acetamide. *Arch. Biochem. Biophys.*, **302**, 259-264.

Damadian, R. (1971). Tumour detection by nuclear magnetic resonance. *Science*, **171**, 1151-1153.

Davidson, A.G. (1988). Chromatography. In *Practical Pharmaceutical Chemistry*, Beckett, A.H. & Stenlake, J.B. (eds), Vol. 2. pp. 120-150. Athlone Press: London.

De Bruijn, W., Sorbers, C., Gelsema, E., Beckers, A. & Jonkind, J. (1993). Energy filtering transmission electron microscopy of biological specimens. *Scanning Microscopy*, **7**, 693-709.

De Silva, J.A.F., Munno, N. & Strojny, N. (1970). Absorptiometric, polarographic, and gas chromatographic assays for the determination of N-1 substituted nitroimidazoles in blood and urine. *J. Pharm. Sci.*, **59**, 201-210.

Denekamp, J., Hill, S.A. & Hobson, B. (1983). Vascular occlusion and tumour cell death. *Eur. J. Cancer Clin. Oncol.*, **19**, 271-275.

Evelhoch, J.L., McCoy, C.L. & Giri, B.P. (1989). A method for direct *in vivo* measurement of drug concentrations from a single ^2H NMR spectrum. *Magn. Reson. Med.*, **9**, 402-410.

Feller, D.R., Morita, M. & Gillette, J.R. (1971). Reduction of heterocyclic nitro compounds in rat liver (35594). *Proc. Soc. Exp. Biol. Med.*, **137**, 433-437.

Firth, J.D., Ebert, B.L., Pugh, C.W. & Ratcliffe, P.J. (1994). Oxygen-regulated control elements in the phosphoglycerate kinase 1 and lactate dehydrogenase A genes: similarities with the erythropoietin 3' enhancer. *Proc. Natn. Acad. Sci. USA*, **91**, 6496-6500.

Fitzsimmons, S.A., Workman, P., Michael, G., Paull, K., Camalier, R. & Lewis, A.D. (1995). The differential expression of reductase enzymes in the NCI human tumour cell line panel; correlation with sensitivity to mitomycin C and the investigational indoquinone EO9. *J. Natl. Cancer Inst.*, In press.

Flockhart, I.R., Large, P., Troup, D., Malcolm, S.L. & Marten, T.R. (1978a). Pharmacokinetic and metabolic studies of the hypoxic cell radiosensitizer misonidazole. *Xenobiotica*, **8**, 97-105.

Flockhart, I.R., Malcolm, S.L., Marten, T.R., Parkins, C.S., Ruane, R.J. & Troup, D. (1978b). Some aspects of the metabolism of misonidazole. *Br. J. Cancer*, **37**, 264-267.

Franceschi, S., Levi, F., Lucchini, F., Negri, E., Boyle, P. & La Vecchia, C. (1994). Trends in cancer mortality in young adults in Europe, 1955-1989. *Eur. J. Cancer*, **30A**, 2096-2118.

Franko, A.J. (1986). Misonidazole and other hypoxia markers: metabolism and applications. *Int. J. Radiat. Oncol. Biol. Phys.*, **12**, 1195-1202.

Franko, A.J. & Koch, C.J. (1984). Binding of misonidazole to V79 spheroids and fragments of Dunning rat prostatic and human colon carcinomas *in vitro* : Diffusion of oxygen and reactive metabolites. *Int. J. Radiat. Oncol. Biol. Phys.*, **10**, 1333-1336.

Franko, A.J., Koch, C.J., Garrecht, B.M., Sharplin, J. & Hughes, D. (1987). Oxygen dependence of binding of misonidazole to rodent and human tumours *in vitro*. *Cancer Res.*, **47**, 5367-5376.

Franko, A.J., Kock, C.J. & Boisvert, D.P.J. (1992). Distribution of misonidazole adducts in 9L gliosarcoma tumours and spheroids: implications for oxygen distribution. *Cancer Res.*, **52**, 3831-3837.

Fu, K.K., Wendland, M.F., Iyer, S.B., Lam, K.N., Engeseth, H. & James, T.L. (1990). Correlations between *in vivo* ^{31}P NMR spectroscopy measurements, tumour size, hypoxic fraction and cell survival after radiotherapy. *Int. J. Radiat. Oncol. Biol. Phys.*, **18**, 1341-1350.

Garrecht, B.M. & Chapman, J.D. (1983). The labelling of EMT-6 tumours in Balb/c mice with ^{14}C -misonidazole. *Br. J. Radiol.*, **56**, 745-753.

Gatenby, R.A., Kessler, H.B., Rosenblum, J.S., Coia, L.R., Moldofsky, P.J., Hartz, W.H. & Broder, G.J. (1988). Oxygen distribution in squamous cell carcinoma metastases and its relationship to outcome of radiation therapy. *Int. J. Radiat. Oncol. Biol. Phys.*, **14**, 831-838.

Giaccia, A.J., Auger, E.A., Koong, A., D.J., T., Minchinton, A.I., Hahn, G.M. & Brown, J.M. (1992). Activation of the heat shock protein transcription factor by hypoxia in normal and tumour cell lines *in vivo* and *in vitro*. *Int. J. Radiat. Oncol. Biol. Phys.*, **23**, 891-897.

Glockner, J.F. & Swartz, H.M. (1992). *In vivo* EPR oximetry using two novel probes: fusinite and lithium phthalocyanine. *Adv. Exp. Med. Biol.*, **317**, 299-234.

Graeber, T.G., Peterson, J.F., Tsai, M., Monica, K., Fornace, A.J.J. & Giaccia, A.J. (1994). Hypoxia induces accumulation of p53 protein, but

activation of a G1-phase checkpoint by low-oxygen conditions is independent of p53 status. *Mol. Cell Biol.*, **14**, 6264-6277.

Grau, C., Nordsmark, M., Khalil, A.A. & Horsman, M.R. (1994). The effect of carbon monoxide breathing on hypoxia and radiation response in the SCCVII tumour in vivo. *Int. J. Radiat. Oncol. Biol. Phys.*, **29**, 449-454.

Grau, C. & Overgaard, J. (1990). The influence of radiation dose on the magnitude and kinetics of reoxygenation in a C3H mammary carcinoma. *Radiat. Res.*, **122**, 309-315.

Greenstock, C.L., Biaglow, J.E. & Durand, R.E. (1978). Effects of sensitizers on cell respiration:II. The effects of hypoxic cell sensitizers on oxygen utilization in cellular and chemical models. *Br. J. Cancer*, **37**, 11-15.

Grimmett, M.R. (1980). Advances in imidazole chemistry. In *Advances in heterocyclic chemistry*, Katritzky, A.R. & Boulton, A.J. (eds), Vol. 27. pp. 241-326. Academic Press: New York.

Groshar, D., McEwan, A.J.B., Parliament, M.B., Urtasun, R.C., Golberg, L.E., Hoskinson, M., Mercer, J.R., Mannan, R.H., Wiebe, L.I. & Chapman, J.D. (1993). Imaging tumour hypoxia and tumour perfusion. *J. Nucl. Med.*, **34**, 885-888.

Guichard, M., Dertinger, H. & Malaise, E.P. (1983). Radiosensitivity of four human tumour xenografts. Influence of hypoxia and cell-cell contact. *Radiat. Res.*, **95**, 602-609.

Guichard, M., Lachet, B. & Malaise, E.P. (1977). Measurement of RBE, OER, and recovery of potentially lethal damage of a 645 MeV helium ion beam using EMT6 cells. *Radiat. Res.*, **71**, 413-429.

Hahn, E.L. (1950). Spin echoes. *Phys. Rev.*, **80**, 580-594.

Hall, E.J. (1988). The oxygen effect and reoxygenation. In *Radiobiology for radiologist*, Hall, E.J. (ed) pp. 137-160. Lippencott Co.: Philadelphia.

Heacock, C.S. & Sutherland, R.M. (1986). Induction characteristics of oxygen regulated proteins. *Int. J. Radiat. Oncol. Biol. Phys.*, **12**, 1287-1290.

Heacock, C.S. & Sutherland, R.M. (1990). Enhanced synthesis of stress proteins caused by hypoxia and relation to altered growth and metabolism. *Br. J. Cancer*, **62**, 217-225.

Hill, R.P. (1980). An appraisal of *in vivo* assays of excised tumours. *Br. J. Cancer*, **41 Suppl 1V**, 230-239.

Hirst, D.G., Hazlehurst, J.L. & Brown, J.M. (1985). Changes in misonidazole binding with hypoxic fraction in mouse tumours. *Int. J. Radiat. Oncol. Biol. Phys.*, **11**, 1349-1355.

Hodgkiss, R.J., Parrick, J., Porssa, M. & Stratford, M.R.L. (1994). Bio-reductive markers for hypoxic cells: 2-nitroimidazoles with biotinylated 1-substituents. *J. Med. Chem.*, **37**, 4352-4356.

Honess, D.J. & Bleehen, N.M. (1991). Effects of two blood flow modifiers, hydralazine and flavone acetic acid, on KHT tumours and normal tissues in mice. *Int. J. Radiat. Biol.*, **60**, 249-253.

Honess, D.J. & Bleehen, N.M. (1992). Comparative effects of hydralazine on perfusion of KHT tumour, kidney and liver and on the renal function in mice. *Int. J. Radiat. Oncol. Biol. Phys.*, **22**, 953-961.

Horsman, M.R., Christensen, K.L. & Overgaard, J. (1989). Hydralazine-induced enhancement of hyperthermic damage in a C3H mammary carcinoma *in vivo*. *Int. J. Hyperther.*, **5**, 123-136.

Horsman, M.R., Khalil, A.A., Nordsmark, M., Grau, C. & Overgaard, J. (1993). Relationship between radiobiological hypoxia and direct estimates of tumour oxygenation in a mouse tumour model. *Radiother. Oncol.*, **28**, 69-71.

Horsman, M.R., Nordsmark, M., Khalil, A.A., Hill, S.A., Chaplin, D.J., Siemann, D.W. & Overgaard, J. (1994). Reducing acute and chronic hypoxia in tumours by combining nicotinamide with carbogen breathing. *Acta Oncol.*, **33**, 371-376.

Howe, F.A., Stubbs, M., Rodrigues, L.M. & Griffiths, J.R. (1993). An assessment of artefacts in localized and non-localized ^{31}P MRS studies of phosphate metabolites and pH in rat tumours. *NMR Biomed.*, **6**, 43-52.

Huxham, I.M., Barlow, A., Mairs, R., Gaze, M. & Workman, P. (1993). Elemental mapping of fluorine using ESI for the localization of an anthracycline drug ME2303 in human ovarian carcinoma cells. *Cell Biol. Int.*, **17**, 685-691.

Huxham, I.M., Gaze, M.N., Workman, P. & Mairs, R.J. (1992). The use of parallel EEL spectral imaging and elemental mapping in the rapid assessment of anti-cancer drug localization. *J. Microsc.*, **166**, 367-380.

Javed Afzal, S.M., Tenforde, T.S., Kavanau, K.S. & Curtis, S.B. (1991). Reoxygenation in a rat rhabdomyosarcoma tumour following X-irradiation. *Int. J. Radiat. Oncol. Biol. Phys.*, **20**, 473-477.

Jin, G.-Y., Li, S.-J., Moulder, J.E. & Raleigh, J.A. (1990). Dynamic measurements of hexafluoromisonidazole (CCI-103F) retention in mouse tumours by $^1\text{H}/^{19}\text{F}$ magnetic resonance spectroscopy. *Int. J. Radiat. Biol.*, **58**, 1025-1034.

Johnson, A.D., Mairs, R.J., Gaze, M.N., Sass, G. & Huxham, I.M. (1995). Electron spectroscopic imaging of organic compounds using PC-based energy sequence imaging software. *Microscopy Microanal. Microstruct.*, **6**, 65-77.

Joseph, P., Jaiswal, A.K., Stobbe, C.C. & Chapman, J.D. (1994). The role of specific reductases in the intracellular activation and binding of 2-nitroimidazoles. *Int. J. Radiat. Oncol. Biol. Phys.*, **29**, 351-355.

Kagiya, V.T., Nishimoto, S.,-I., Wang, J., Abe, M. & Sasai, K. (1992). Fluorine modification of nitroazole radiosensitizers for the enhancement of sensitizing activity with lowering toxicity: a pharmacokinetic characterization. *Int. J. Radiat. Oncol. Biol. Phys.*, **22**, 601-605.

Kallman, R.F. (1972). The phenomenon of reoxygenation and its implication for fractionated radiotherapy. *Radiology*, **105**, 135-142.

Kalmus, J., Okunieff, P. & Vaupel, P. (1990). Dose-dependent effects of hydralazine on microcirculatory function and hyperthermic response of murine FSaII tumours. *Cancer Res.*, **50**, 15-19.

Keniry, M., Benz, C., Shafer, R.H. & James, T.L. (1986). Noninvasive spectroscopic analysis of fluoropyrimidine metabolism in cultured tumour cells. *Cancer Res.*, **46**, 1754-1758.

Koch, C.J. (1990). The reduction activation of nitroimidazoles; modification by oxygen and other redox-active molecules in cellular systems. In *Selective activation of drugs by redox processes*, Adams, G.E., Breccia, A., Fielden, E.M. & Wardman, P. (eds), Vol. 198. pp. 237-247. NATO ASI. Plenum Press: New York.

Koch, C.J., Giandomenico, A.R. & Iyengar, C.W.L. (1993). Bioreductive metabolism of AF-2 [2(2-furyl)-3-(5-nitro-2-furyl)acrylamide] combined with 2-nitroimidazoles: implication for use as hypoxic cell markers. *Biochem. Pharmacol.*, **46**, 1029-1036.

Koch, C.J., Kruuv, J., Frey, H.E. & Snyder, R.A. (1973). Plateau phase in growth induced by hypoxia. *Int. J. Radiat. Biol.*, **23**, 67-74.

Koch, C.J., Stobbe, C.C. & Bump, E.A. (1984). The effect on the K_m for radiosensitization at 0°C of thiol depletion by diethylmaleate pretreatment: quantitative differences found using the radiation sensitizing agent misonidazole or oxygen. *Radiat. Res.*, **98**, 141-153.

Koh, W.J., Rasey, J.S., Evans, M.L., Grierson, J.R., Lewellen, T.L., Graham, M.M., Krohn, K.A. & Griffin, T.W. (1991). Imaging of hypoxia in human

tumours with [F-18]fluoromisonidazole. *Int. J. Radiat. Oncol. Biol. Phys.*, **22**, 199-212.

Koong, A.C., Auger, E.A., Chen, E.Y. & Giaccia, A.J. (1994a). The regulation of GRP78 and messenger RNA levels by hypoxia is modulated by protein kinase C activators and inhibitors. *Radiat. Res.*, **138**, S60-S63.

Koong, A.C., Chen, E.Y. & Giaccia, A.J. (1994b). Hypoxia causes the activation of nuclear factor kappa B through the phosphorylation of I Kappa B alpha on tyrosine residues. *Cancer Res.*, **54**, 1425-1430.

Koutcher, J.A., Alfieri, A.A., Barnett, D.C., Cowburn, D.C., Kornblith, A.B. & Kim, J.H. (1990). Changes in ^{31}P nuclear magnetic resonance with tumour growth in radioresistant and radiosensitive tumours. *Radiat. Res.*, **121**, 312-319.

Kwock, L., Gill, M., McMurphy, H.L., Beckman, W., Raleigh, J.A. & Joseph, A.P. (1992). Evaluation of a Fluorinated 2-nitroimidazole binding to hypoxic cells in tumour-bearing rats by ^{19}F magnetic resonance spectroscopy and immunohistochemistry. *Radiat. Res.*, **129**, 71-78.

La Vecchia, C., Lucchini, F., Negri, E., Boyle, P. & Levi, F. (1993a). Trends in cancer mortality in the Americas, 1955-1989. *Eur. J. Cancer*, **29A**, 431-470.

La Vecchia, C., Lucchini, F., Negri, E., Boyle, P. & Levi, F. (1993b). Trends in cancer mortality, 1955-1989: Asia, Africa and Oceania. *Eur. J. Cancer*, **29A**, 2168-2211.

La Vecchia, C., Lucchini, F., Negri, E., Boyle, P., Maisonneuve, P. & Levi, F. (1992). Trends in cancer mortality in Europe, 1955-1989. III Breast and genital sites. *Eur. J. Cancer*, **28**, 927-998.

Larmor, J. (1900). *Aether and Matter*. University Press: Cambridge.

Leahy, D.E., Taylor, P.J. & Wait, A.R. (1989). Model solvent system for QSAR Part I. Propylene glycol dipelargonate (PGDP). A new standard

solvent for use in partition coefficient determination. *Quant. Struct. -Act. Relat.*, **8**, 17-31.

Leith, J.T., Padfield, G., Faulkner, L. & Michelson, S. (1991). Hypoxic fractions in xenografted human colon tumours. *Cancer Res.*, **51**, 5139-5143.

London, R.E. (1994). *In vivo* NMR studies utilising fluorinated probes. In *NMR in physiology and Biomedicine*, Gillies, R.J. (ed) pp. 263-277. Academic Press: San Diego.

Lord, E.M., Harwell, L. & Koch, C.J. (1993). Detection of hypoxic cells by monoclonal antibody recognizing 2-nitroimidazole adducts. *Cancer Res.*, **53**, 5721-5726.

Madan, A. & Curtin, P.T. (1993). A 24-base-pair sequence 3' to the human erythropoietin gene contains a hypoxia-responsive transcriptional enhancer. *Proc. Natn. Acad. Sci. USA*, **90**, 3928-3932.

Mason, R.P. & Holtzman, J.L. (1975). The role of catalytic superoxide formation in the O₂ inhibition of nitroreductase. *Biochem. Biophys. Res. Commun.*, **67**, 1267-1275.

Masters, B.S.S., Williams, C.H. & Kamin, H. (1967). The preparation and properties of microsomal TPNH-cytochrome c reductase from pig liver. *Meth. Enzymol.*, **10**, 565-573.

Maxwell, R.J., Workman, P. & Griffiths, J.R. (1988). Demonstration of tumour-selective retention of fluorinated probed by ¹⁹F magnetic resonance spectroscopy *in vivo*. *Int. J. Radiat. Oncol. Biol. Phys.*, **16**, 925-929.

Mcmanus, M.E., Lang, M.A., Stuart, K. & Strong, J. (1982). Activation of misonidazole by rat liver microsomes and purified NADPH-Cytochrome c reductase. *Biochem. Pharmacol.*, **31**, 547-552.

- Middlestadt, M.V. & Rauth, A.M. (1982). The effects of reduction products of misonidazole on Chinese Hamster Ovary cells. *Int. J. Radiat. Oncol. Biol. Phys.*, **8**, 709-712.
- Miller, G.G., Best, M.W., Franko, A.J., Koch, C.J. & Raleigh, J.A. (1989). Quantitation of hypoxia in multicellular spheroids by video image analysis. *Int. J. Radiat. Oncol. Biol. Phys.*, **16**, 949-952.
- Miller, G.G., Ngan-Lee, J. & Chapman, J.D. (1982). Intracellular localization of radioactively labelled misonidazole in EMT-6 tumour cells in vitro. *Int. J. Radiat. Oncol. Biol. Phys.*, **8**, 741-744.
- Minchinton, A.I., Cobb, L. & Brown, J.M. (1993). Intermittent hypoxia: Its presence in experimental tumours of different histological grade. In *8th International conference on chemical modifiers of cancer treatment* pp 192: Kyoto, Japan.
- Moulder, J.E. & Rockwell, S. (1984). Hypoxic fractions of solid tumours: Experimental techniques, methods of analysis, and a survey of existing data. *Int. J. Radiat. Oncol. Biol. Phys.*, **10**, 695-712.
- Negendank, W. (1992). Studies of human tumours by MRS: a review. *NMR Biomed.*, **5**, 303-324.
- Nordmark, M., Grau, C., Horsman, M.R., Jorgensen, H.S. & Overgaard, J. (1995). Relationship between tumour oxygenation, bioenergetic status and radiobiological hypoxia in an experimental model. *Acta Oncol.*, **34**, 329-334.
- Okunieff, P.G., Koutcher, J.A., Gerweck, L., McFarland, E., Hitzig, B., Urano, M., Brady, T., Neuringer, L. & Suit, H.D. (1986). Tumour size dependent changes in a murine fibrosarcoma: use of *in vivo* ^{31}P for non-invasive evaluation of tumour metabolic status. *Int. J. Radiat. Oncol. Biol. Phys.*, **12**, 793-799.
- Olive, P. (1995). Detection of hypoxia by measurement of DNA damage in individual cells from spheroids and murine tumours exposed to bioreductive drugs. I. Tirapazamine. *Br. J. Cancer*, **71**, 529-536.

Olive, P.L., Banath, J.P. & Durand, R.E. (1990). Heterogeneity in radiation-induced DNA damage and repair in tumour and normal cells measured using the 'comet' assay. *Radiat. Res.*, **122**, 86-94.

Olive, P.L. & Durand, R.E. (1983). Fluorescent nitroheterocycles for identifying hypoxic cells. *Cancer Res.*, **43**, 3276-3280.

Olive, P.L. & Durand, R.E. (1989). Misonidazole binding in SCCVII tumours in relation to the tumour blood supply. *Int. J. Radiat. Oncol. Biol. Phys.*, **16**, 755-761.

Olive, P.L., Durand, R.E., Riche, J.L., Olivotto, I.A. & Jackson, S.M. (1993). Gel electrophoresis of individual cells to quantify hypoxic fraction in human breast cancers. *Cancer Res.*, **53**, 733-736.

Omura, T. & Sato, R. (1964a). The carbon monoxide-binding pigment of liver microsomes I. *J. Biol. Chem.*, **239**, 2370-2378.

Omura, T. & Sato, R. (1964b). The carbon monoxide-binding pigment of liver microsomes II. *J. Biol. Chem.*, **239**, 2379-2385.

Ordidge, R.J., Connelly, A. & Lohman, J.A.B. (1986). Image-Selected *in Vivo* Spectroscopy (ISIS). A new technique for spatially selective NMR spectroscopy. *J. Magn. Reson.*, **66**, 283-294.

Overgaard, J. (1989). Sensitization of hypoxic cells - clinical experience. *Int. J. Radiat. Biol.*, **56**, 801-811.

Parkin, D.M., Pisani, P. & Ferlay, J. (1993). Estimates of the worldwide incidence of eighteen major cancers in 1985. *Int. J. Cancer*, **54**, 594-606.

Pera, M.F. (1995). Differentiation and cancer. In *Oxford textbook of oncology*, Peckham, M., Pinedo, H.M. & Veronesi, U. (eds), Vol. 1. pp. 21-31. Oxford University Press: Oxford.

Prekeges, J.L., Rasey, J.S., Grunbaum, Z. & Krohn, K.H. (1991). Reduction of fluoromisonidazole, a new imaging agent for hypoxia. *Biochem. Pharmacol.*, **42**, 2387-2395.

Purcell, E.M., Torrey, H.C. & Pound, R.V. (1946). Resonance absorption by nuclear magnetic moments in a solid. *Phys. Rev.*, **69**, 37-38.

Raleigh, J.A., Franco, A.J., Kelly, D.A., Trimble, L.A. & Allen, P.S. (1991a). Development of an *in vivo* ^{19}F magnetic resonance method for measuring oxygen deficiency in tumours. *Magn. Reson. Med.*, **22**, 451-466.

Raleigh, J.A., Franko, A.J., Treiber, E.O., Lunt, J.A. & Allen, P.S. (1986). Covalent binding of a fluorinated 2-nitroimidazole to EMT-6 tumours in Balb/c mice: Detection by ^{19}F nuclear magnetic resonance at 2.35 T. *Int. J. Radiat. Oncol. Biol. Phys.*, **12**, 1243-1245.

Raleigh, J.A., La Dine, J.K., Cline, J.M. & Thrall, D.E. (1994). An enzyme-linked immunosorbent assay for hypoxia marker binding in tumours. *Br. J. Cancer*, **69**, 66-71.

Raleigh, J.A. & Liu, S.F. (1984). Reductive fragmentation of 2-nitroimidazoles: amines and aldehydes. *Int. J. Radiat. Oncol. Biol. Phys.*, **10**, 1337-1340.

Raleigh, J.A., Zeman, E.M., Rathman, M., LaDine, J.K., Cline, J.M. & Thrall, D.E. (1991b). Development of an ELISA for the detection of 2-nitroimidazole hypoxia markers bound to tumour tissue. *Int. J. Radiat. Oncol. Biol. Phys.*, **22**, 403-405.

Rampling, R., Cruickshank, G., Lewis, A.D., Fitzsimmons, S. & Workman, P. (1994). Direct measurement of pO_2 distribution and bioreductive enzymes in human malignant brain tumours. *Int. J. Radiat. Oncol. Biol. Phys.*, **29**, 427-431.

Rauth, A.M. (1984). Pharmacology and toxicology of sensitizers: Mechanism studies. *Int. J. Radiat. Oncol. Biol. Phys.*, **10**, 1293-1300.

Rauth, A.M., Chin, J., Marchow, L. & Paciga, J. (1978). Testing of hypoxic cell radiosensitizers *in vivo*. *Br. J. Cancer*, **37**, 202-205.

Rice, G.C., Hou, C.A. & Schimke, R.T. (1986). Transient hypoxia enhances the frequency of dihydrofolate reductase gene amplification in Chinese Hamster ovary cells. *Proc Natl Acad Sci USA*, **83**, 5978-5982.

Robertson, N., Haigh, A., Adams, G.E. & Stratford, I.J. (1994). Factors affecting sensitivity to EO9 in rodent and human tumour cells *in vitro*: DT-diaphorase activity and hypoxia. *Eur. J. Cancer*, **30A**, 1013-1019.

Robinson, S.P., Howe, F.A. & Griffiths, J.R. (1994). Carbogen-induced changes in tumour perfusion and oxygenation monitored by functional MRI. In *Society for magnetic resonance in medicine*, **3**. pp. 1324: San Francisco, U.S.A.

Rockwell, S. (1981). Effect of host age on the transplantation, growth and radiation response of EMT6 tumours. *Cancer Res.*, **41**, 527-531.

Rofstad, E.K. (1989). Hypoxia and reoxygenation in human melanoma xenografts. *Int. J. Radiat. Oncol. Biol. Phys.*, **17**, 81-89.

Rofstad, E.K., DeMuth, P., Fenton, B.M., Ceckler, T.L. & Sutherland, R.M. (1989). ^{31}P NMR spectroscopy and HbO_2 cryospectrophotometry in prediction of tumour resistance caused by hypoxia. *Int. J. Radiat. Oncol. Biol. Phys.*, **16**, 919-923.

Rumsey, W.L., Vanderkooi, J.M. & Wilson, D.F. (1988). Imaging of phosphorescence: a novel method for measuring oxygen distribution in perfused tissue. *Science*, **241**, 1649-1651.

Sasai, K. & Brown, M. (1994). Discrepancies between measured changes of radiobiological hypoxic fraction and oxygen tension monitoring using two assay systems. *Int. J. Radiat. Oncol. Biol. Phys.*, **30**, 355-361.

Sensky, P.L., Prise, V.E. & Hirst, D.G. (1994). Relative perfusion of tumours in two sites for up to 6 hr after the induction of anaemia. *Adv. Exp. Med. Biol.*, **345**, 375-380.

Shibamoto, Y., Yukawa, Y., Tsutsui, K., Takahashi, M. & Abe, M. (1986). Variation in the hypoxic fraction among mouse tumours of different types, sizes, and sites. *Jpn. J. Cancer Res.*, **77**, 908-915.

Shrieve, D.C. & Begg, A.C. (1985). Cell kinetics of aerated, hypoxic and re-aerated cells *in vitro* using flow cytometric determination of cellular DNA and incorporated bromodeoxyuridine. *Cell Tissue Kinet.*, **18**, 641-651.

Shrieve, D.C., Deen, D.F. & Harris, J.W. (1983). Effects of extreme hypoxia on the growth and viability of EMT6/SF mouse tumour cells *in vitro*. *Cancer Res.*, **43**, 3521-3527.

Shungu, D.C., Bhujwala, Z.M., Li, S.J., Rose, L.M., Wehrle, J.P. & Glickson, J.D. (1992). Determination of absolute phosphate metabolite concentration in RIF-1 tumours *in vivo* by ^{31}P - ^1H - ^2H NMR spectroscopy using water as an internal intensity reference. *Magn. Res. Med.*, **28**, 105-121.

Shweiki, D., Itin, A., Soffer, D. & Keshet, E. (1992). Vascular endothelial growth factor induced by hypoxia may mediate hypoxia-initiated angiogenesis. *Nature*, **359**, 843-845.

Smith, B.R. & Born, J.L. (1984). Metabolism and excretion of [^3H] misonidazole by hypoxic rat liver. *Int. J. Radiat. Oncol. Biol. Phys.*, **10**, 1365-1370.

Song, S.K., Hotchkiss, R.S. & Ackerman, J.J. (1992). Concurrent quantification of tissue metabolism and blood flow via $^2\text{H}/^{31}\text{P}$ NMR *in vivo*. I. Assessment of absolute metabolite quantification. *Magn. Res. Med.*, **25**, 45-55.

Sotak, C.H., Hees, P.S., Huang, H.N., Huang, M.H., Krespan, C.G. & Suart, R. (1993). A new perfluorocarbon for use in fluorine-19 magnetic resonance spectroscopy. *Magn. Reson. Med.*, **29**, 188-195.

Spector, T. (1978). Refinement of the coomassie blue method of protein quantitation. A simple and linear spectrophotometric assay for less than or equal to 0.5 to 50 microgram of protein. *Anal. Biochem.*, **86**, 142-146.

Spiro, I.J., Rice, G.C., Durand, R.E., Stickler, R. & Ling, C.C. (1984). Cell killing, radiosensitization and cell cycle redistribution induced by chronic hypoxia. *Int. J. Radiat. Oncol. Biol. Phys.*, **10**, 1275-1280.

Stevenson, M.A., Calderwood, S.K. & Coleman, C.N. (1989). Effects of nitroimidazoles on neuronal cells *in vitro*. *Int. J. Radiat. Oncol. Biol. Phys.*, **16**, 1225-1230.

Stone, H.B., Brown, J.M., Phillips, T.L. & Sutherland, R.M. (1993). Oxygen in human tumours: correlations between methods of measurement and response to therapy. *Radiat. Res.*, **136**, 422-434.

Tarin, D. (1995). Cancer metastasis. In *Oxford textbook of oncology*, Peckham, M., Pinedo, H.M. & Veronesi, U. (eds), Vol. 1. pp. 118-132. Oxford University Press: Oxford.

Thomlinson, R.H. & Gray, L.H. (1955). The histological structure of some human lung cancers and the possible implications for radiotherapy. *Br. J. Cancer*, **9**, 539-549.

Thulborn, K.R. & Ackerman, J.J.H. (1983). Absolute molar concentrations by NMR in inhomogeneous B₁. A scheme for analysis of *in vivo* metabolites. *J. Magn. Reson.*, **55**, 357-371.

Tozer, G.M. & Griffiths, J.R. (1992). The contribution made by cell death and oxygenation to ³¹P MRS observations of tumour energy metabolism. *NMR Biomed.*, **5**, 279-289.

Trotter, M.J., Acker, B.D. & Chaplin, D.J. (1989). Histological evidence for non-perfused vasculature in a murine tumour following hydralazine administration. *Int. J. Radiat. Oncol. Biol. Phys.*, **17**, 785-789.

Trotter, M.J., Chaplin, D.J., Durand, R.E. & Olive, P.L. (1989). The use of fluorescent probes to identify regions of transient perfusion in murine tumours. *Int. J. Radiat. Oncol. Biol. Phys.*, **16**, 931-934.

Tsuruo, T., Hamilton, T.C., Louie, K.G., Behrens, B.C., Young, R.C. & Ozols, R.F. (1986). Collateral susceptibility of adriamycin-, melphalan-, and cisplatin-resistant human ovarian tumour cells to bleomycin. *Jpn. J. Cancer Res.*, **77**, 941-945.

Twentyman, P.R., Fox, N.E., Wright, K.A., Workman, P., Broadhurst, M.J., Martin, J.A. & Bleehen, N.M. (1986). The *in vitro* effects and cross-resistance patterns of some novel anthracyclines. *Br. J. Cancer*, **53**, 585-594.

Urtasun, R.C., Chapman, J.D., Feldstein, M.L., Band, R.P., Rabin, H.R., Wilson, A.F., Marynowski, B., Starreveld, E. & Shnitka, T. (1978). Peripheral neuropathy related to misonidazole: incidence and pathology. *Br. J. Cancer*, **37**, Suppl. III, 271-275.

Urtasun, R.C., Chapman, J.D., Raleigh, J.A., Franko, A.J. & Koch, C.J. (1986a). Binding of ³H-misonidazole to solid human tumours as a measure of tumour hypoxia. *Int. J. Radiat. Oncol. Biol. Phys.*, **12**, 1263-1267.

Urtasun, R.C., Koch, C.J., Franko, A.J., Raleigh, J.A. & Chapman, J.D. (1986b). A novel technique for measuring human pO₂ at the cellular level. *Br. J. Cancer*, **54**, 453-457.

Van Putten, L.M. & Kallman, R.F. (1968). Oxygenation status of a transplantable tumour during fractionated radiation therapy. *J. Natl. Cancer Inst.*, **40**, 441-451.

Varghese, A.J. (1983). Glutathione conjugates of misonidazole. *Biochem. Biophys. Res. Commun.*, **112**, 1013-1020.

Varghese, A.J. & Whitmore, G.F. (1984a). Detection of a reactive metabolite of misonidazole in human urine. *Int. J. Radiat. Oncol. Biol. Phys.*, **10**, 1361-1363.

Varghese, A.J. & Whitmore, G.F. (1984b). Detection of a reactive metabolite of misonidazole in hypoxic mammalian cells. *Radiation Res.*, **97**, 262-271.

Varghese, A.J. & Whitmore, G.F. (1984c). Misonidazole-glutathione conjugates in CHO cells. *Int. J. Radiat. Oncol. Biol. Phys.*, **10**, 1341-1345.

Vaupel, P. (1992). Physiological properties of malignant tumours. *NMR Biomed.*, **5**, 220-225.

Vaupel, P., Kallinowski, F. & Okunieff, P. (1989). Blood flow, oxygen and nutrient supply, and metabolic microenvironment of human tumours: a review. *Cancer Res.*, **49**, 6449-6465.

Vaupel, P., Schlenger, K., Knoop, C. & Hockel, M. (1991). Oxygenation of human tumours: Evaluation of tissue oxygen distribution in breast cancers by computerized O₂ tension measurements. *Cancer Res.*, **51**, 3316-3322.

Walton, M.I. & Workman, P. (1987). Nitroimidazole bioreductive metabolism: quantitation and characterisation of mouse tissue benznidazole nitroreductases *in vivo* and *in vitro*. *Biochem. Pharmacol.*, **36**, 887-896.

Wang, G.L., Jiang, B.H., Rue, E.A. & Semenza, G.L. (1995). Hypoxia-inducible factor 1 is a basic-helix-loop-helix-PAS heterodimer regulated by cellular O₂ tension. *Proc. Natn. Acad. Sci. USA*, **92**, 5510-5514.

Wardman, P. (1985). Some reactions and properties of nitro radical-anions important in biology and medicine. *Environ. Health Perspect.*, **64**, 309-320.

Wardman, P. & Clarke, E.D. (1976). Oxygen inhibition of nitroreductase: electron transfer from nitro radical-anions to oxygen. *Biochem. Biophys. Res. Commun.*, **69**, 942-949.

White, R., Workman, P. & Owen, L. (1982). The pharmacokinetics in mice and dogs of nitroimidazole radiosensitizers and chemosensitizers more lipophilic than misonidazole. *Int. J. Radiat. Oncol. Biol. Phys.*, **8**, 473-476.

White, R.A.S. & Workman, P. (1980). Pharmacokinetics and tumour-penetration properties of the hypoxic cell radiosensitizer desmethylmisonidazole (Ro 05-9963) in dogs. *Br. J. Cancer*, **41**, 268-276.

White, R.A.S., Workman, P. & Brown, J.M. (1980). The pharmacokinetics and tumour and neural tissue penetrating properties of SR-2555 in dog-hydrophilic radiosensitizers potentially less toxic than misonidazole. *Radiat. Res.*, **84**, 542-561.

Wilson, W.R. (1992). Tumour hypoxia: challenges for cancer chemotherapy. In *The search for new anticancer drugs*, Waring, M.J. & Ponder, B.A.J. (eds) pp. 87-131. Cancer Biology and Medicine. Kluwer Academic Publishers: Dordrecht.

Workman, P. (1979). Effects of pretreatment with phenobarbitone and phenytoin on the pharmacokinetics and toxicity of misonidazole in mice. *Br. J. Cancer*, **40**, 335-353.

Workman, P. (1980). Dose-dependence and related studies on the pharmacokinetics of misonidazole and desmethylmisonidazole in mice. *Cancer Chemother. Pharmacol.*, **5**, 27-35.

Workman, P. (1982). Lipophilicity and the pharmacokinetics of nitroimidazoles. In *Advanced topics on radiosensitizers of hypoxic*

cells, Breccia, A., Rimondi, C. & Adams, G.E. (eds) pp. 143-163. Pienum Press: Amsterdam.

Workman, P. (1983a). New drugs against hypoxic cells. *Cancer Topics*, 4, 54-55.

Workman, P. (1983b). Pharmacokinetics of radiosensitizing agents. In *Pharmacokinetics of anticancer agents in humans*, Ames, M.M., Powis, G. & Kovach, J.S. (eds) pp. 291-361. Elsevier Publishers B.V.: Netherlands.

Workman, P. (1989). Optimized treatment modalities for hypoxic tumour cells. In *Drug delivery in cancer treatment II: Symptom control, cytokines, chemotherapy*, Domellof, L. (ed) pp. 79-102. Springer-Verlag: Berlin.

Workman, P. (1992). Bioreductive mechanisms. *Int. J. Radiat. Oncol. Biol. Phys.*, 22, 631-637.

Workman, P. & Brown, J.M. (1981). Structure-pharmacokinetic relationships for misonidazole analogues in mice. *Cancer Chemother. pharmacol.*, 6, 39-49.

Workman, P., Little, C.J., Marten, T.R., Dale, A.D., Ruane, R.J., Flockhart, I.R. & Bleehen, N.M. (1978). Estimation of the hypoxic cell-sensitizer misonidazole and its O-demethylated metabolite in biological materials by reversed-phase high-performance liquid chromatography. *J. Chromatogr.: Biomed. Appl.*, 145, 507-512.

Workman, P., Maxwell, R.J. & Griffiths, J.R. (1992). Non-invasive MRS in new anticancer drug development. *NMR Biomed.*, 5, 270-272.

Workman, P. & Stratford, I.J. (1993). The experimental development of bioreductive drugs and their role in cancer therapy. *Cancer Metastasis Rev.*, 12, 73-82.

Workman, P. & Walton, M.I. (1990). Enzyme-directed bioreductive drug development. In *Selective activation of drugs by redox*

processes, Adams, G.E., Breccia, A., Fielden, E.M. & Wardman, P. (eds), Vol. 198. pp. 173-191. NATO ASI. Plenum Press: New York.

Xu, A.S.L., Waldeck, A.R. & Kuchel, P.W. (1993). Transmembrane ^{19}F NMR chemical shift differences of fluorinated solutes in liposomes, erythrocytes and erythrocyte ghosts. *NMR Biomed*, **6**, 136-143.

Yang, D.J., Wallace, S., Cherif, A., Li, C., Gretzer, M.B., Kim, E.E. & Podoloff, D.A. (1995). Development of F-18-labeled fluoroerythronitroimidazole as a PET agent for imaging tumour hypoxia. *Radiology*, **194**, 795-800.

Yao, K.-S., Clayton, M. & O'Dwyer, P.J. (1995). Apoptosis in human adenocarcinoma HT29 cells induced by exposure to hypoxia. *J. Natl. Cancer Inst.*, **87**, 117-122.

Yao, K.-S., Xanthoudakis, S. & Curan, T. (1994). Activation of AP-1 and of a nuclear protein redox factor, Ref-1, in the response of HT-29 colon cancer cells to hypoxia. *Mol. Cell Biol.*, **14**, 5997-6003.

Young, R.C., Mitchell, R.C., Brown, T.H., Ganellin, C.R., Griffiths, R., Jones, M., Rana, K.K., Saunders, D., Smith, I.R., Sore, N.E. & Wilks, T.J. (1988). Development of a new physicochemical model for brain penetration and its application to the design of centrally acting H_2 receptor histamine antagonists. *J. Med. Chem.*, **31**, 656-671.

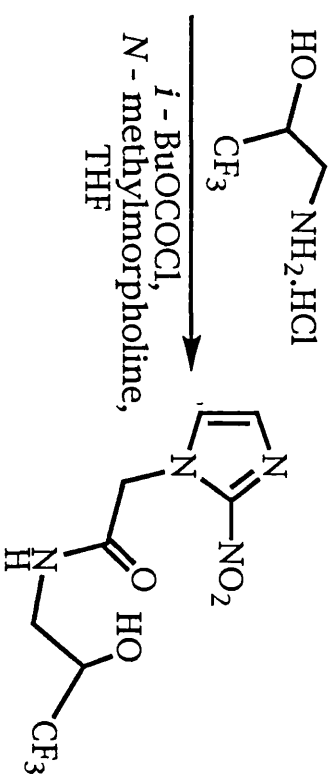
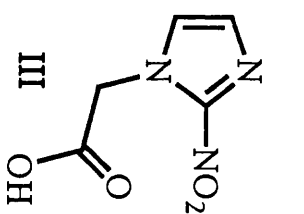
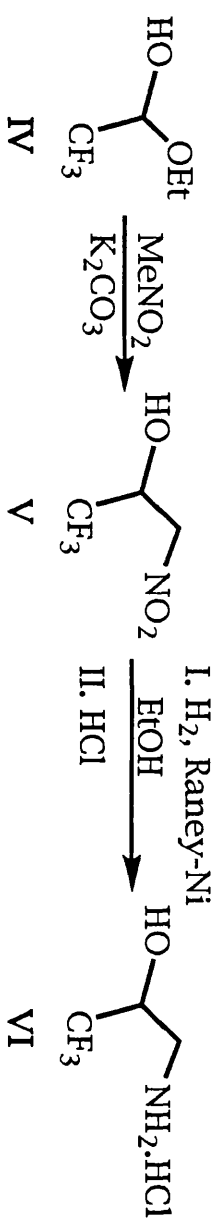
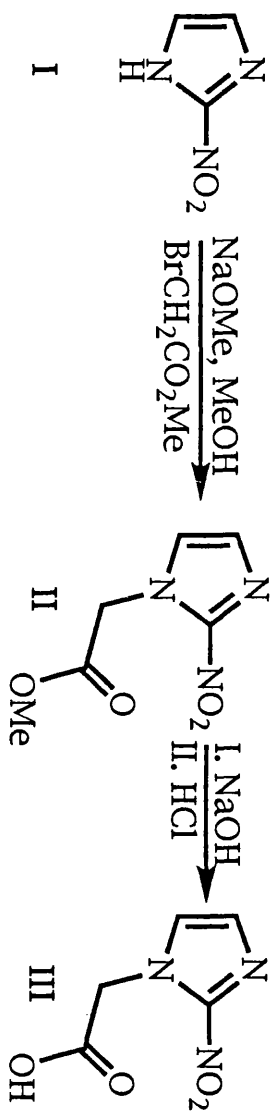
APPENDICES

APPENDIX A

Synthesis of SR-4554

The synthesis of N-(2-hydroxy-3,3,3-trifluoropropyl)-2-(2-nitro-1-imidazolyl) acetamide (SR-4554) is illustrated. 2-nitroimidazole (I) was converted to its sodium salt by treatment with sodium methoxide in methanol-DMF at 150°C for 10 min. Subsequent reaction with methyl bromoacetate in DMF at 85°C for 20 min gave the methyl ester (II). The methyl ester was then converted to the carboxylic acid (III) by treatment with 0.1 N NaOH at 100°C for 15 min followed by acidification with 1 M HCl. The fluorine labelled side chain was prepared by reaction of trifluoroacetaldehyde hemiacetal (IV) and nitromethane in the presence of potassium carbonate at 60°C for 3 h. Pure nitro compound (V) was obtained from the reaction mixture by distillation at 115°C at 60 mmHg. V was reduced by halogenation at 40 psi with Raney-nickel catalysis, followed by treatment of the filtered reaction mixture with ethereal HCl at -20°C to give the amino-compound (VI) as its HCl salt. Coupling of III with VI was carried out by first converting the acid group of III to the mixed anhydride using *iso*-butylchloroformate and N-methylmorpholine in tetrahydrofuran (THF) at 0°C. Addition of VI and a further equivalent of N-methylmorpholine resulted in the formation of SR-4554, which was purified by column chromatography and recrystallization from ethyl acetate-hexanes.

A1. Synthesis of SR-4554.



SR-4554

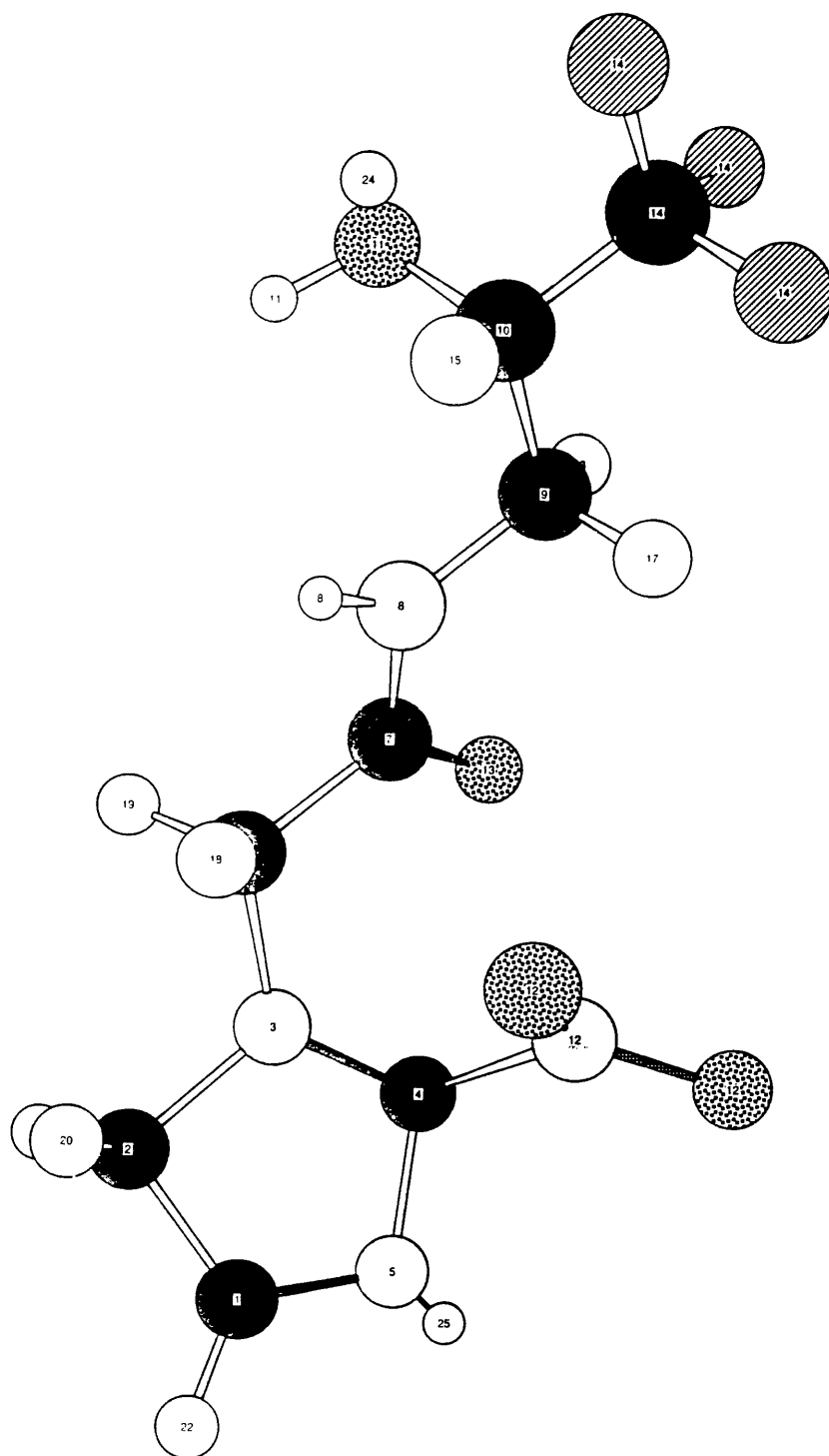
APPENDIX B

Molecular models of 2-nitroimidazoles

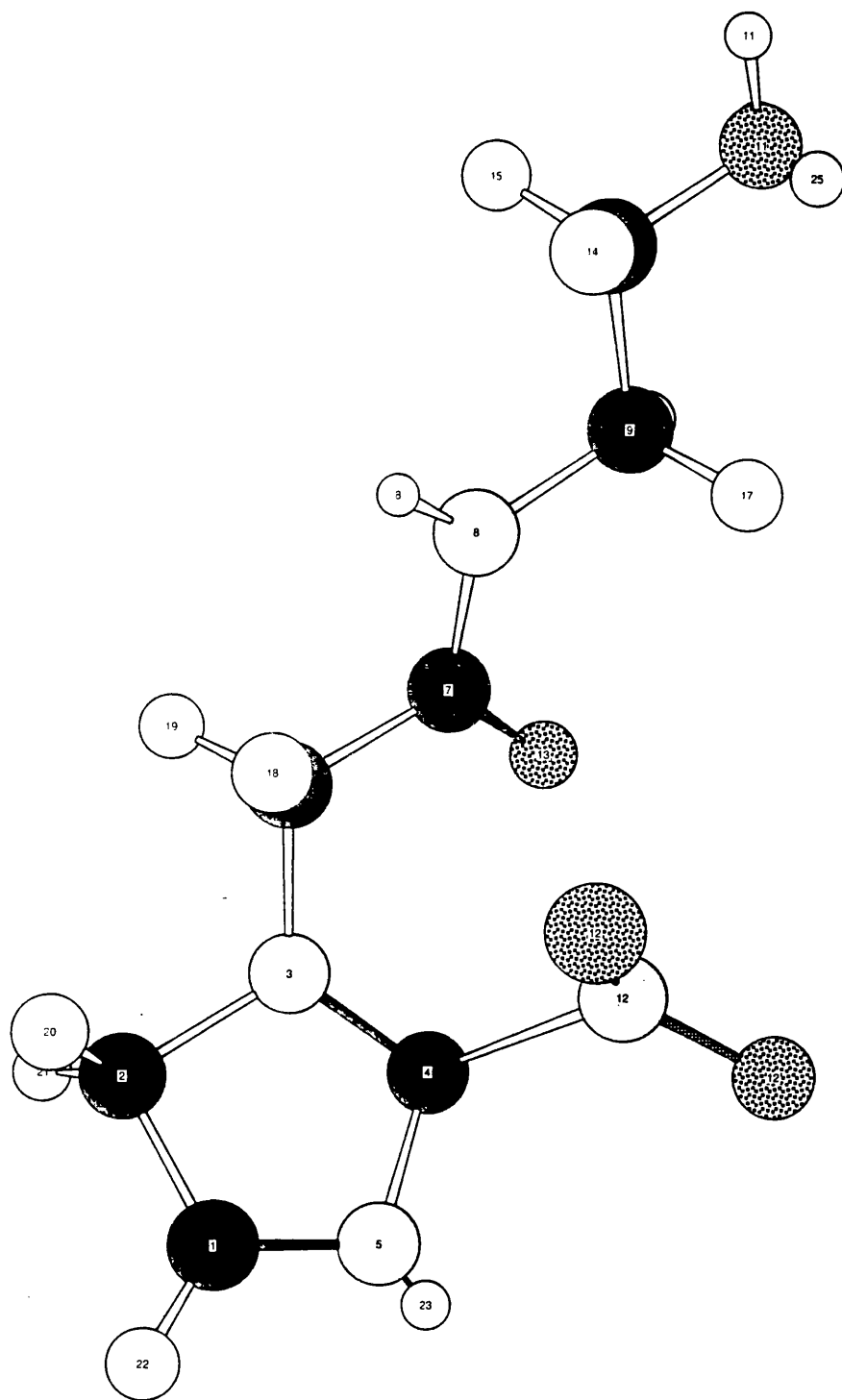
The molecular models of SR-4554, etanidazole and misonidazole. The models were derived using a computer generated minimisation programme (CSC Chem 3D, Cambridge Scientific Computing Inc., MA, USA).

The minimised steric energies in all the models ranged between 6 and 9 kcal/mole. Stippled circles represent oxygen atoms, circles with stripes represent fluorine atoms, white circles represent hydrogen atoms or lone pairs of electrons, black circles represent carbon atoms, and yellow coloured circles represent nitrogen atoms. The imidazole ring, C-NO₂ bond and the side chain were all planar. It should be noted that due to rotation about single bonds, other conformations are possible. In SR-4554 and etanidazole, the side chain bends further into the ring than in misonidazole. In addition, hydrogen bonding between the terminal hydroxyl group and the carboxyl group or amide nitrogen in SR-4554 and etanidazole stabilises these compounds, increases their hydrophilic character and decreases their resemblance to lipid-like molecules. Such hydrogen bonding is not possible in misonidazole.

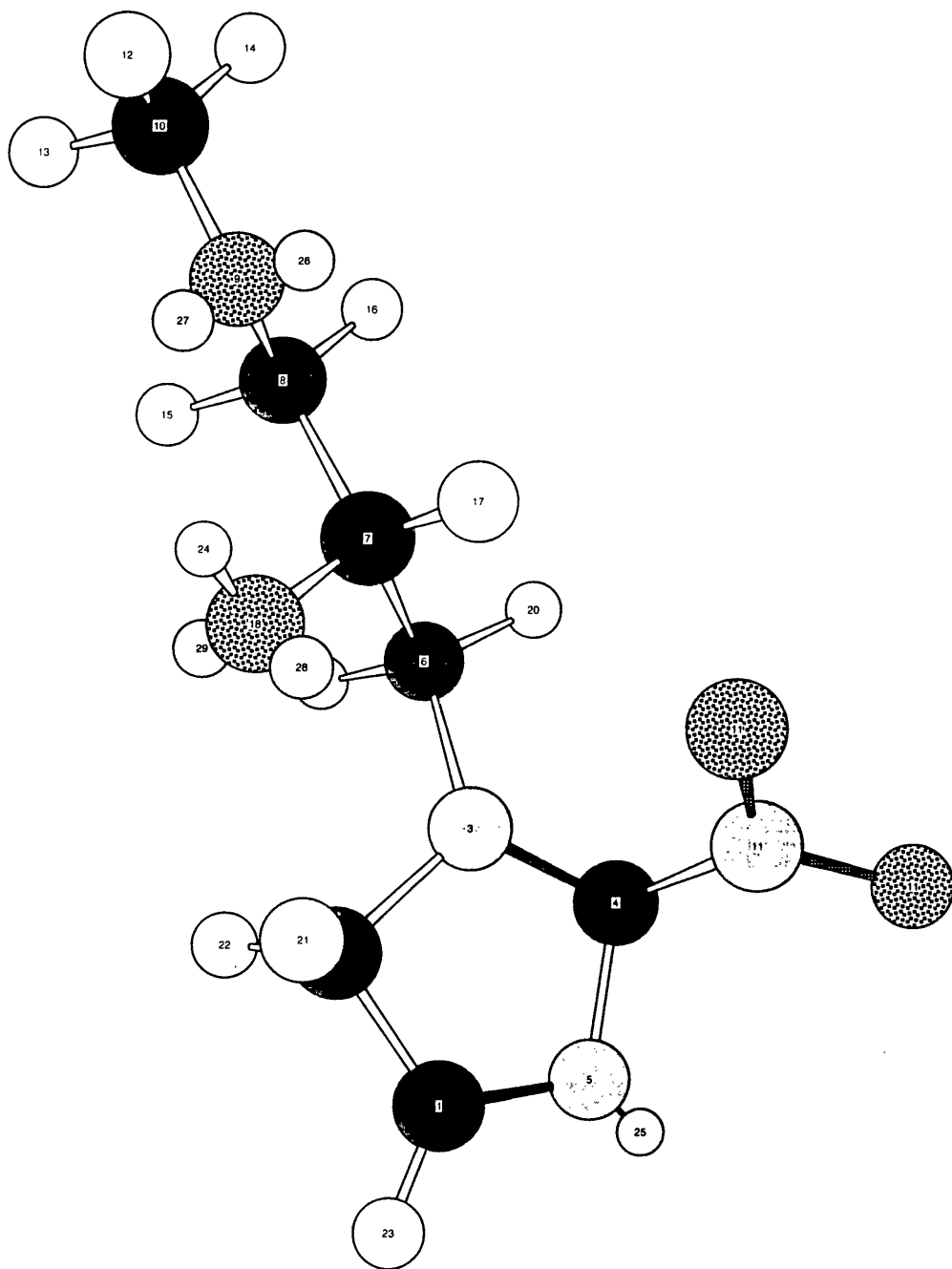
B1. Molecular model of SR-4554.



B2. Molecular model of etanidazole.



B3. Molecular model of misonidazole.



APPENDIX C

Publications arising from this thesis

Abstracts and presentations

1. Aboagye, E.O., McCoy, C.L., Maxwell, R.J., Tracy, M., Workman, P. & Griffiths, J.R. (1994). Assessment of tumour hypoxia by quantitative ^{19}F magnetic resonance spectroscopy. Proceedings of the Society for Magnetic Resonance, San Francisco, 3, 1349.
2. Aboagye, E.O., Graham, M.A., Lewis, A.D., Kelson, A.B., Tracy, M. & Workman, P. (1994). Pharmacokinetics and metabolism of a novel fluorinated 2-nitroimidazole SR-4554. Proceedings of the International Conference on Bioreductive Drug Activation, Lake Tahoe, Session 1.
3. Aboagye, E.O., Maxwell, R.J., Lewis, Workman, P., Tracy, M. & Griffiths, J.R. (1995). Evaluation of SR-4554 as a probe for tumour hypoxia. British Association for Cancer Research Annual Meeting, Nottingham, Session 7.6.
(Published abstract: Br. J. Cancer, 71, Suppl XXIV, 20).
4. Huxham, I.M., Aboagye, E.O., Gaze, M.N., Johnson, A.D., Lewis, A.D., Mairs, R.J. & Plumb, J.A. (1995). Intracellular localisation of anti-cancer therapeutic compounds using electron spectroscopic imaging as a tool to investigate mechanisms of drug targeted cancer therapy. British Association for Cancer Research Annual Meeting, Nottingham, Session 4.4.
(Published abstract: Br. J. Cancer, 71, Suppl XXIV, 12).
5. Aboagye, E.O., Maxwell, R.J., Lewis, A.D., Horsman, M.R., Workman, P., Tracy, M. & Griffiths, J.R. (1995). SR-4554: A non-invasive marker for hypoxic cells. Proceedings of the Ninth International Conference on Chemical Modifiers of Cancer Treatment, Oxford, Session IV-12.

Papers

1. Aboagye, E.O., Lewis, A.D., Johnson, A. Workman, P., Tracy, M. & Huxham, I.M. (1995). The novel fluorinated 2-nitroimidazole hypoxic probe SR-4554: reductive metabolism and semi-quantitative localisation in human ovarian cancer multicellular spheroids as measured by electron energy loss spectroscopic analysis. *Br. J. Cancer*, **72**, 312-318.
2. Aboagye, E.O., Lewis, A.D., Graham, M.A., Kelson, A.B., Tracy, M. & Workman, P. (1995). Development and validation of a solid phase extraction and high performance liquid chromatographic assay for a novel fluorinated 2-nitroimidazole hypoxia probe SR-4554 in Balb/c mouse plasma. *J. Chromatogr.: Biomed. Appl.*, **672**, 125-132.
3. Aboagye, E.O., Graham M.A., Lewis, A.D., Kelson, A.B., Ryan, K.J., Tracy, M. & Workman, P. (1995). Pharmacokinetics, bioavailability and biodistribution in mice of the novel fluorinated 2-nitroimidazole SR-4554. *Anti-Cancer Drug Design*, (in press).

Patent

1. Tracy, M., Kelson, A.B., Workman, P., Lewis, A.D. & Aboagye, E.O. (1995). Novel fluorinated 2-nitroimidazole analogues for imaging hypoxic tumour cells *in vivo*. United States Patent U.S.S.N. 08/286,477 (Filed, August 1994; CIP, August 1995).

